MODIFICATION OF THE GANGLIOSIDE GM1 TO FACILITATE IMAGING AND FUNCTIONAL STUDIES

A dissertation

submitted by

Zhao Liu

In partial fulfillment of the requirements
for the degree of

Doctor of Philosophy

in

Chemistry

TUFTS UNIVERSITY

Date

February
2012

ADVISOR: Krishna Kumar

Abstract

Since 1997, the lipid rafts model has been proposed to describe the structure and functions of cell membranes. Many efforts have been made to visualize the lipid rafts in living cells using various techniques, and revealed the lipid rafts have small size (20-200 nm) and short lifetime (<1 s). Nonetheless, the direct evidence remains lacking due to limitation of available techniques. We have designed a new detecting system using fluorinated ganglioside GM1 to probe lipid rafts by nanoSIMS imaging.

We have synthesized a series of fluorinated ganglioside GM1 analogues (F-GM1s) by modification of natural GM1 that derived from bovine brain tissues using fluorinated fatty acid substitution on the lipid tails. (Chapter 2) Mono- and tri-fluorinated GM1 analogues have been obtained with fluorine atoms at different positions of the lipid tail. Higher order fluorination (–C6F13) of GM1 has also been accomplished either on the fatty acid chain or both the fatty acid (C6F13-GM1) and the sphingosine chains (Di-C6F13-GM1). This is the first report of modification of the sphingosine chain on ganglioside analogues.

We have evaluated the biophysical properties of F-GM1s using multiple techniques, including FACS, AFM and calcium signaling assay. (Chapter 3) As a result, the terminal mono-fluorinated version (18-F-GM1) exhibited the highest similarity to the native GM1 and could be potentially used as a probe to study its behaviors in membranes. The mono-fluorinated GM1 analogues have been employed to study phase behaviors in a quaternary mixture of supported lipid bilayers using SIMS imaging. By isotopic labeling, domains rich in F-GM1 and cholesterol have been observed. Additionally, 18-F-GM1

formed larger domains than 12-F-GM1 in bilayers, which was attributed to their different phase transition temperature revealed by a DSC assay.

We have designed and synthesized a NBD labeled GM1 analogue to study its endocytic pathway in cells. The GM1 analogue was incorporated in Hela cells and analyzed by confocal fluorescence microscopy. The fluorescently labeld GM1 was found accumulated in lysosomes, Golgi, and ER, thus provided a potential method for drug delivery and functional studies.

Acknowledgement

The road to the PhD degree is full of challenges and can hardly be accomplished by individual. I am truly fortunate that I have joined a warm group and obtained a good deal of help and cooperation from lots of people.

First of all, I would like to thank my advisor, Professor Krishna Kumar, for accepting me to come and pursue my PhD degree, allowing me to work on the projects I am interested in, and encouraging me to put my proposal into practice. His scientific sense and strict manner will always light up in my life.

I would also thank Professor Clay Bennett, Elena Rybak-Akimova, and Jianmin Gao to serve as my academic committee members. The same thank to my previous committee members, Professor Marc D'Alarcao and Professor David Lee, who have given me very helpful suggestions in my research when they were working in Chemistry Department.

The work described here was done by cooperation with many researchers from different labs. Professor Andreas Janshoff and Eva Sunnick from Gottingen University in Germany have given me a great help to run AFM imaging experiments on the lipid bilayers containing GM1 analogues (Chapter 3), their advice has been really helpful and I have learned the most knowledge about AFM I have during my stay in Germany. Professor Steven Boxer and Dr. Monica Lozano from Stanford University have worked on the secondary ion mass spectrometry, and I have to thank Monica for her expertise to obtain nice the nano-SIMS images of fluorinated GM1 in model membranes (Chapter 4). I could not thank Subrahmanian Tarakkad Krishnaji enough in Kumar lab not only for his direct contribution to the confocal imaging of fluorescently labeled GM1 in mammalian

cells (Chapter 5), but also for his helpful discussions and constructive suggestions on my research including synthesis and analysis.

Thanks to Dr. David Wilbur in Chemistry Department, Tufts University, for instrumental support in my research, including NMR, ESI-MS, and MALDI-TOF, especially for helping me to obtain 19F-NMR spectra of my fluorinated compounds. Thanks to Mr. Marek Domin from Mass Spectrometry Center, Boston College, for analyzing my synthetic products by HRMS. I have sent my samples of GM1 analogues to several Mass Spec labs for HRMS analysis, however, only Mr. Domin was able to obtain the HRMS spectra of my samples nicely. I would like to thank Mr. Stephen Kwok from Tufts Medical School for training me to use flow cytometry. And I also thank Sreevidhya Tarakkad Krishnaji from Tufts University for helping me to set up DSC experiments.

I need to thank all the members of Kumer group, particularly He Meng and Deniz Yuksel, as well as Nicholas Yoder, Ginevra Clark, Laila Dafik, Yulia Ivanova, Venkateshwarlu Kalsani, Gizem Akcay, Venkat Raman, Cristina Zamora, Emel Adaligil, and Sophia Wei-En Lin. Thank all of you for sharing your rich knowledge and sparkling ideas with me not only in science, but in culture, art, and many other fields as well, which have contributed to one of the most important part of the degree of doctor of philosophy.

Thanks to the staff in Chemistry Department for their daily support to facilitate my research.

A big thank to Dr. Vijay M Krishna Murthy for his kind suggestions during the thesis writing.

I would like to give my special thanks to my parents and my wife Wei Huang for their endless support at all times.

TABLE OF CONTENTS

LIST OF TABLES

LIST OF SCHEMES

LIST OF FIGURES

Chapter 1

Introduction

Plasma membranes that enclose the mammalian cells insulate and protect them from the environment. The membranes consist of lipids, proteins, sugars and other ancillary molecules. Apart from the diversity of proteins and sugars, lipodomics has recently revealed an unprecedented variety of membrane lipids, such as phospholipids, sphingolipids, glycolipids, and steroids.[1,2] Cells interact with each other, and selectively exchange substances with their environment mainly through the plasma membrane. Membrane proteins and lipids are involved in a variety of cell-cell interactions and signaling processes, bacteria and viruses usually attach and infect host cells by recognizing cell receptors on the plasma membrane.[3] Understanding the structure and functions of cell membranes will help us to control and adjust these biological processes. For many years, scientists have employed biochemical and biophysical techniques to study the properties and behavior of cell membranes. The mostly used techniques are atomic force microscopy (AFM)[4,5], fluorescence resonance energy transfer (FRET)[6], imaging mass spectrometry (IMS)[7], stochastic optical reconstruction microscopy (STORM)[8], and stimulated Emission Depletion (STED)[9,10]. These experimental techniques have revealed the lateral heterogeneity of lipid bilayers, an important discovery of cell membranes, which shows some lipid molecules can form domains in the membrane.[11] This property is believed to dominate cell-cell recognition and signal transduction and play an important role in a variety of biological processes and viral infection. The goal of the work in this thesis is to provide a new detecting system to investigate the structure and functions of cell membranes.

1.1 Lipid rafts in cell membranes

Since the discovery of the cell membrane as a physical structure by Plowe[12] in 1931, Numerous techniques have been developed to study it and several models have been proposed to describe the nature of cell membranes. Besides the lipid-protein model[13] and fluid mosaic model[14], the most recent and widely accepted model is the lipid rafts model[15]. Nonetheless, the hypothesis remains controversial,[16] mainly due to the limitation of current available detecting techniques.

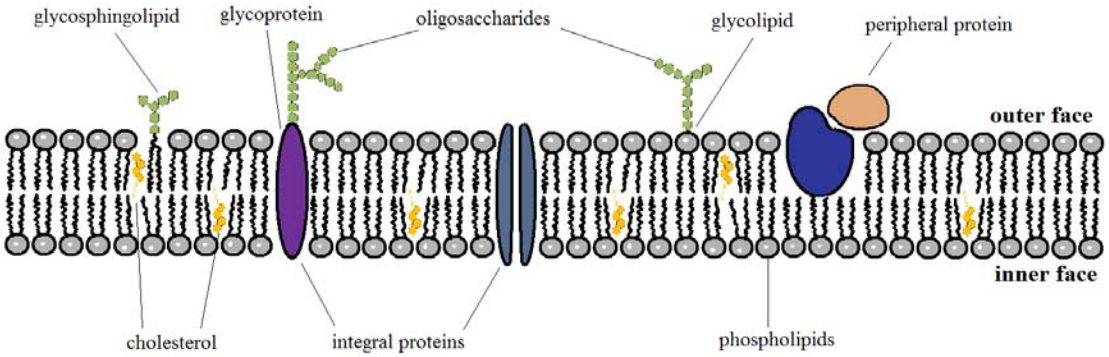

Fig. 1.1 Schematic representatives of plasma membranes in a cut view.

1.1.1 Lipid-protein sandwich model

In 1935, Danielli and Davson[13] proposed the first model of cell membranes involving lipid bilayers and proteins in the architecture. (Fig 1.2) In this model, proteins are adsorbed on both surfaces of lipid bilayers. The lipid molecules in the membrane, usually phospholipids, are amphiphilic and point their hydrophilic head groups towards the aqueous phase. Since proteins were thought to be hydrophobic at the inner core and hydrophilic at the outer part, they attach onto the hydrophilic surface of lipid bilayers.

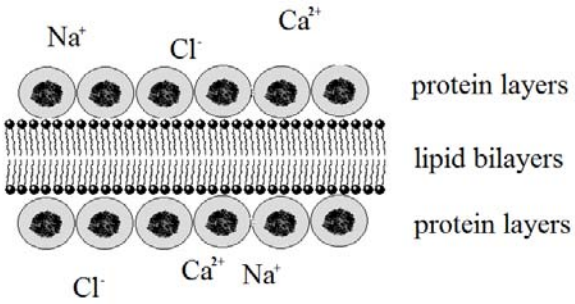

Fig 1.2 The lipid-protein sandwich model of cell membranes by Danielli and Davson[13].

The lipid bilayers and proteins form a sandwich structure to fulfill the observed cell membrane functions: charged solutes, such as ions, can penetrate the membrane through water soluble part of proteins but not through the lipid membrane that contains bivalent cations, such as calcium ions. Hydrophobic molecules can penetrate the membrane through the lipophilic lipid bilayer region. Danielli and Davson's model explained the permeability based on the physio-chemical properties of hydrophilic and lipophilic regions of the membranes. This model predicted the participation of proteins in mass transport through the cell membranes. However, it could not describe the detailed structure due to the limited available experimental technologies. After nearly half a century, the "protein layers" was shown to be ion channel proteins embedded in plasma membranes that selectively transport ions and other solutes across the membrane.

1.1.2 Fluid mosaic model

In the 1960s, biological membranes from mammalian cells were extensively studied to understand their structure and functions. At that time, techniques for protein investigation have already been developed, such as X-ray crystallography and other physical methods.[17-19] Proteins have been visualized in plasma membranes as isolated dots by labeled antibodies using electron microscopy.[20] Based on experimental observations,

Singer and Nicolson[14] proposed a two-dimensional fluid mosaic model for mammalian cell membranes. In this model, the cell membrane is "an oriented, two-dimentional, viscous solution of amphipathic proteins and lipids in instantaneous thermodynamic equilibrium". (Fig 1.3) Phospholipids form lipid bilayers by the lipid tails facing each other and ionic phosphate groups towards aqueous solutions. Integral proteins, such as cytochrome c on mitochondrial membranes, are embedded in the lipid bilayers. Peripheral proteins are loosely attached to the bilayers and can easily dissociate from the membrane. The proteins interact with each other and the neighboring lipid molecules surrounding to form mosaic structures interspersed in the membrane. The mosaic structure has no long-range order at tens of micrometer scale or higher, but the short-range order that can form aggregates by protein-protein or protein-lipid interactions was not ruled out.

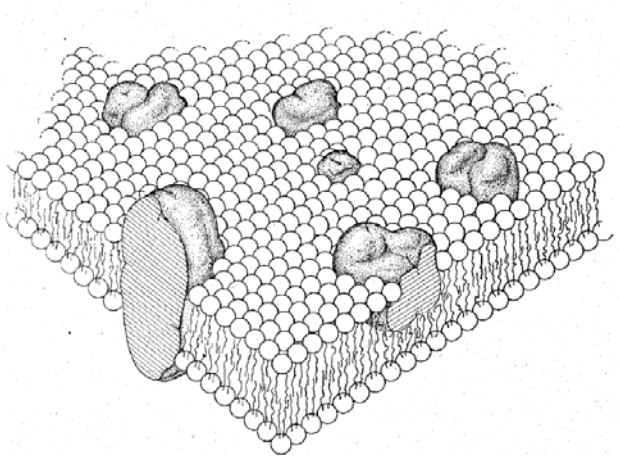

Fig 1.3 The fluid mosaic model by Singer. From reference 14. Reprinted with permission from AAAS.

The fluid mosaic model has successfully explained experimental observation on a certain level. For example, it predicted the mosaic membrane structure is in a fluid state

and the integral proteins can freely float in the plane of membrane to lead to a random distribution. Indeed, the homogenous distribution of proteins in membranes was observed by Frye and Edidin's experiment[21], in which human and mouse cells in culture were fused with each other, and their antigen proteins were found to be distributed evenly in both cells. In addition, the membrane was postulated to be asymmetric, in which the outer and inner surfaces were not identical, due to the asymmetric distribution of oligosaccharides on the two surfaces. Several lectin binding experiments[22,23] supported this prediction, in which lectins were observed to bind to the outer surface but not the inner surface of plasma membranes. In most recent years, the oligosaccharides on the outer surface have been confirmed to be the glycocalyx[24] and other glycoproteins and glycolipids.

The fluid mosaic model had been accepted for decades. It successfully predicted protein-protein and protein-lipid interactions and their biophysical properties within the membranes. However, the homogeneity of lipid bilayers was soon challenged by the observation that some proteins preferentially resided in a certain area of plasma membranes. Further studies of this phenomenon lead to the most recent lipid rafts model.

1.1.3 The lipid rafts model

Not long after the postulation of fluid mosaic model, biologists observed cell membrane behaviors that it could not explain. Many membrane proteins and lipids showed much smaller diffusion coefficients in cell membranes than in artificial membranes, in spite of their same phospholipids compositions (the fluid mosaic model proposed cell membranes were formed by phospholipid bilayers), suggesting the existence of more complicated interactions in cell membranes.[25-27] In addition, GPI-anchored protein receptors labeled

with gold exhibited clustering and temporary immobilization, indicating its higher affinity to a certain area in the membrane. Furthermore, the movement of membrane proteins and lipids in the plasma membrane was found not to be a simple Brownian diffusion in two dimensions. Thus, the homogeneity of cell membranes by the fluid mosaic model has been challenged and several models have been proposed to explain these observations. Of these emerging models, the lipid raft model is the most widely accepted one.

The concept of lipid rafts originated from the discovery of differential transport of lipids to the membrane of epithelial cells. In epithelial cells, the apical membranes are rich in glycosphingolipids and the basolateral membranes are rich in glycerolipids. Simons and coworkers have found that in epithelial Madin-Darby canine kidney (MDCK) cells, the newly synthesized glucosylceramide in the Golgi complex was preferentially delivered to apical membranes, whereas the glycerolipid phosphatidylcholine was delivered to the basolateral membranes, suggesting lipids could not pass the tight junction between apical and basolateral membranes in either direction.[28,29] in addition, the newly synthesized surface glycoproteins in epithelial cells are also differentially transported to apical and basolateral membranes. The sorting of these glycoproteins appeared to be at the *trans*-Golgi network, the same region where lipid sorting take place.[30] Therefore, it was proposed that: (1) the homogeneity of cell membranes was not true; (2) the transport of lipids and glycoproteins were carried out by the same vesicles from the Golgi complex to either apical or basolateral membranes; (3) the lipid sorting was related to the protein sorting.

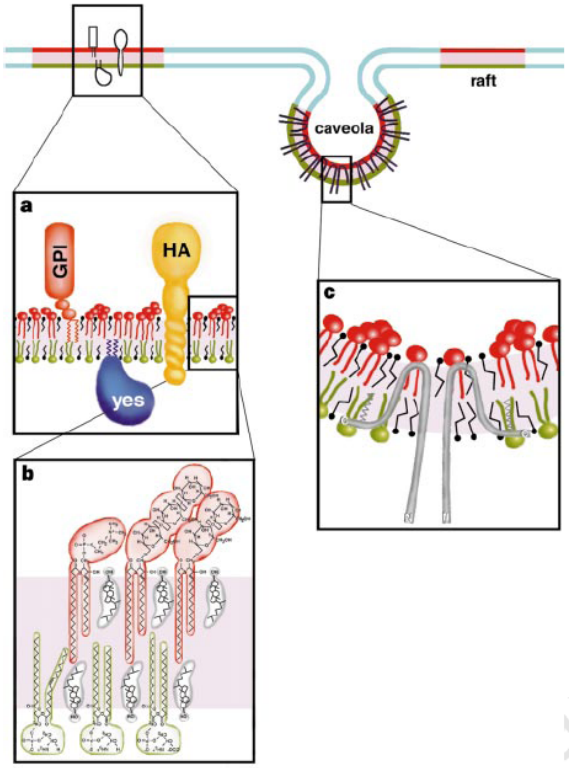

Fig.1.4 The model of lipid rafts and caveolae in the plasma membrane by Simons. Reprinted by permission from Macmillan Publishers Ltd: NATURE (reference 15), copyright (1997)

In the 1970's, It was observed that glycosphingolipids, sphingomylin, and cholesterol were not soluble in the non-ionic detergent Triton X-100, and could be isolated from other cell membrane components by a Triton wash.[31,32] The insoluble residue was therefore called detergent-resistant materials (DRM). The detergent-insoluble lipids were studied in model membranes, which showed that DRM form liquid ordered phases and detergent-soluble lipids form liquid disordered phases at 37 °C,[33,34] suggesting that DRM are phase related and different phases may also exist on cell membranes. Brown[35] used Triton X-100 treatment to exploit the DRM in MDCK cells, and found that GPI-anchored proteins were not extracted with detergent (residing in DRM instead of in the detergent formed micelles), whereas basolateral marker proteins were soluble in the detergent. This observation supported Simons' hypothesis that

membrane proteins were sorted by the same processes as lipid sorting, indicating the potential co-localization of GPI-anchored proteins with sphingolipids and cholesterol in the membranes. Recently, this hypothesis was further supported by cholesterol-depletion studies in plasma membranes. By removing cholesterol in living cells with methyl-β-cyclodextrin[36] treatment, the function of some membrane proteins could be disrupted, such as Ca^{2+} signaling in T cells[37] and GPI-anchored protein clustering[38], suggesting the localization of membrane proteins is cholesterol dependent.

In 1997, Simons[15] proposed the lipid raft model, which described glycoproteins residing in sphingolipid rich domains as functional complexes in cell membranes. These domains—lipid rafts—are formed by detergent-resistant lipids and glycoproteins, and are localized on the exoplasmic leaflet (the outer layer; whereas the inner layer is defined as the endoplasmic leaflet) of cell membranes. The raft lipids, as well as glycoproteins, are preferentially delivered to the exoplasmic membrane by the *trans*-Golgi network, and differentiated from phosphatidylcholines that are transported to basolateral membranes. Combined with cholesterol, sphingolipids can form self-aggregates and separate from more fluid phosphatidylcholines, thus providing a region for GPI-anchored proteins to form functional clusters. Lipid rafts are not only involved in sorting of newly produced proteins, but also in endocytic pathways that transport proteins and other materials from the cell surface to inside the cells.

The lipid rafts theory has been extensively studied in model membranes, such as giant unilamellar vesicles (GUV) [39-43] and solid-supported lipid membranes[44-46], phase separation, and domain formation has been observed in various sizes depending on lipid compositions. However, when the plasma membrane was studied in living cells, lipid

rafts are generally much smaller in size with shorter lifetimes than in model membranes. In the last decade, many efforts have been made to detect the lipid rafts on living cells (see details in Section 1.2), yet the direct evidence is still lacking.

1.1.4 Other cell membrane models

The existence of microdomains in cell membranes has been widely accepted, but how such domains are formed is still under debate.[47] Apart from the lipid rafts model, several other models have been proposed to explain the microdomain formation, mainly based on protein-protein and/or protein-lipid interactions. Some models disagree with the lipid rafts model; some can be viewed as the supplementary of the lipid rafts model.

The protein-protein interaction model[48] proposed that membrane domains are created by the interactions among membrane proteins, without assistance of membrane lipids, called the protein-protein interaction model. This model was raised based on the following observations. Membrane protein receptors on T cells can cluster and self-aggregate without actin participation. The clustered membrane proteins can form a network in plasma membranes to trap signaling complexes, such as CD2/ Lck/ LAT. However, mutation of proteins that interfered with protein binding perturbed the clustering, but membrane anchoring mutated proteins did not,[48] indicating that sphingolipids were not associated with the clustered protein networks. It was thus proposed that the membrane domains were created by protein-protein interactions rather than lipid rafts or actin cytoskeletons.

The protein corralling model proposed that the cytoskeleton form networks as a barrier to diffusion of membrane proteins and lipids. The long-range restriction of the

membrane diffusion by the cytoskeleton has been well documented.[49] Participation of the cytoskeleton in membrane domain formation was proposed by providing a track for the motion of membrane proteins. In some cases, disruption of the cytoskeleton perturbed the lateral movement of membrane proteins and lipids. Therefore, it was proposed that the signaling protein receptors were constrained in the corral regions to form signaling complexes in domain area. Recently, it was revealed that the aggregation of the GPI-anchored protein, CD59, was dependent on cholesterol, the actin skeleton network, and Gαi2-dependent Src-family kinase activation.[50] Another example was that the cell adhesion process, which required cell surface protein recognition, was also found to require participation of the cytoskeleton network.[51]

The lipid shell model proposes that membrane proteins form thermodynamiclly stable complexes with sphingolipids and cholesterol (lipid shells) surrounding them.[52] The protein-lipid shell complexes are laterally mobile and can wander between sphingolipid-cholesterol lipid rafts in the membrane, depending on the affinity of the sphingolipid self-association. The shell structure is formed by lipid-lipid, glycan-lipid, and protein-lipid interactions. The lipid shells can also associate with caveolae in the membrane. Protein-lipid shell complexes move along the membrane and stay in lipid rafts and/or caveolae, but require no lipid phase generation to enter and exit the raft structures. A GPI-anchored protein, Thy-1, has been used as an example of lipid shell model. Thy-1 (25 kDa) was found associated with 80 molecules of sphingolipid and cholesterol, forming a lipid shell of ~7 nm in thickness. The lipid shell model can be viewed as a supplementary part of the lipid rafts model, by suggesting detailed membrane domain structures and interactions between proteins and lipid rafts. Recently, the

transient clustering of Thy-1 proteins was found to be mediated by a transmembrane protein CBP, indicating the potential interactions between the protein-lipid shell complexes and other proteins in cell membranes.[53,54]

1.2 Visualization of lipid rafts

The discovery of membrane microdomains has attracted many scientific efforts, but its study soon met the bottleneck of current techniques to visualize lipid rafts on cell membranes.[55] Traditional light microscopy and electron microscopy are limited by their resolutions and require chemical modifications that may interfere with functions of membrane components. A variety of new techniques have been developed and applied to cell membrane studies in the last two decades. However, the lipid raft theory remains controversial because of the lack of unambiguous experimental evidence.[47,56]

1.2.1 Current technologies to study lipid rafts

The investigation of lipid rafts has advanced dramatically during the last twenty years based on the development of techniques and instruments. Since the 1960s, cell membranes have been studied extensively by electron microscopy at nanometer scale.[57,58] The requirement of high vacuum and modification of samples with heavy metals hampered the use of electron microscopy to investigate living cell membranes rafts. During the 1990s, the discovery of detergent-resistant material in cell membranes revived the clustering hypothesis once more. Various biophysical and biochemical methods have been applied to investigate lipid rafts. Nonpolar detergent extraction at 4 °C combined with cholesterol extraction has been used to figure out membrane protein association and interactions with lipid rafts.[59,60] The solubility of a protein in a detergent resistant

membrane after cholesterol extraction indicates its potential association with lipid rafts. In other words, if a protein becomes soluble after a methyl-β-cyclodextrin wash, which can remove cholesterol from membranes, it will be residing in lipid rafts.[61] Labeled antibodies have been used widely to visualize the pattern of protein receptors and sphingolipids in cell membranes.[62,63] However, the indirect observation of interaction between protein receptors and lipid rafts is complicated by use of antibody probes, considering their relatively large size compared to lipid molecules.[56,64] During the last ten years, new techniques have been used to study lipid rafts in artificial and living cell membranes.

Atomic force microscopy (AFM) is used to scan surfaces of non-conducting samples with high resolution by using a cantilever that is equipped with a nanometer scale tip and can apply force onto the sample surface.[65] The position and angle of the cantilever is governed by a laser beam system on the back surface of the cantilever. By detecting the deflected laser during the scanning processes, AFM reveals the surface properties of the sample. AFM can be done in contact mode, tapping mode or phase imaging mode. Compared to its forerunner STM, the major advantage of AFM is the samples can be scanned in aqueous media with lateral resolution at the nanometer scale, and the height resolution of 0.1 nm. Soon after its invention in 1986[66], AFM has been widely used to study biomembranes, such as membrane phase separation, domain nucleation and growth.[67,68] Distribution of ganglioside GM1 in model membrane bilayers has been studied by AFM, and revealed that the formation of GM1-cholesterol rich domains of 40-100 nm in diameter.[69,70] The ganglioside GM1 was also found to induce oligomerization and aggregation of amyloid beta peptide (Aβ), which accumulates in the

brain during Alzheimer's disease.[71] By modification of the tip on cantilevers with peptide and other types of ligands, AFM has been used to investigate protein-ligand interactions.[72-75] Binding affinity were inferred by the atomic force applied onto the cantilever to disassociate ligands from their protein receptors. AFM has also been used to study ligand-receptor interactions directly on bacteria or cell membranes.[76]

Fluorescence microscopy has been used for decades in cell membrane phase separation studies. Various modified markers, such as fluorescently labeled ganglioside GM1, and cross linked GPI-anchored proteins, have been used to label the lipid rafts in cell membranes. These methods are suitable for dynamics and singl-molecule investigations in both artificial and living cell membranes.[43,77-79] However, the resolution of fluorescence microscopy was limited by inevitable background due to light diffracting and scattering and only achieved 0.1 μm. In the last two decades, new light microscopy techniques have been developed and applied to study lipid rafts, and to image membrane molecules at high resolution, and in three dimensions.

Fluorescence resonance energy transfer (FRET) studies revealed localization of lipid modified proteins in membrane microdomains in living cells.[80-84] High resolution FRET has shown co-localization of GPI-anchored proteins and ganglioside GM1 within 10 nm range. Using high-spatial and temporal resolution FRET microscopy, Goswami and others have observed stable clustering of GPI-anchored proteins on the nanometer scale in CHO cell membranes, which could be perturbed by depletion of cholesterol.[38] Many other protein-protein interactions in mammalian cell membranes have been investigated by FRET microscopy using fluorescently labeled proteins, such as cholera toxin[85], lipid anchored GFP[86], and fibroblast growth factor receptor[87]. Single-molecule

tracking techniques[49], such as immunogold labeling[88,89], single fluorephore video imaging[90], have also been applied to investigate protein distributions on cell membranes by FRET.

Fluorescence correlation spectroscopy (FCS) measures the fluorescence fluctuations of fluorescent active molecules or particles in a well defined area, thus provides with information about the molecules or particles such as average concentration, and diffusion rate (mobility). Dual color labeled *Fluorescence cross-correlation spectroscopy (FCCS)* has been used in biochemical reactions to study reaction rates, kinetics, and other interactions between two fluorescently labeled molecules. FCS and FCCS open a window to detect interactions between molecules in the 10 to 200 nm range, and have been used to study lipid rafts.[91] Hetereogeneity of DPPC/DLPC/cholesterol ternary lipid membrane was observed by dual-color FCCS on giant unilamellar vesicles (GUVs). Their phase separation was found to be dependent on the ratio of ternary lipid mixture.[92] Burns[93] studied the mobility of fluorescently labeled ganglioside GM1 and phospholipid using FCS in the mixture of DPPC and DOPC on solid supported lipid bilayers. Fluorescenctly labeled GM1 showed significantly different mobility in the gel and disordered liquid phases, whereas the fluorescently labeled phospholipid showed unexpected mobility in the gel phase. The author attributed the unexpected mobility of phospholipids to the influence by the fluorophore. Furthermore, the relationship between membrane protein partitioning and lipid phase separation has been studied by FCS. For example, Caveolin-1 scaffolding domain peptides showed preferential binding to the liquid disordered (l_d) phase in GUVs. Fluorescently labeled tumor necrosis factor (TNF) showed differential distribution in membrane domains by FCS, which was interpreted as

potential aggregation of TNF receptors in lipid rafts.[94] The diffusion, transport and organization of sphingolipid-binding domains of amyloid peptide Aβ has been studied by FCCS on cell membranes, and its behaviors exhibited dependence on cholesterol, indicating Aβ peptide interacting with cholesterol rich domains.[95]

To overcome the limitation of traditional fluorescence microscopy due to light diffraction and obtain high resolution in the nanometer range, in the last ten years, several new techniques have been developed and successfully deployed to visualize in the 10 nm range.[96] These new techniques include STORM and STED.

Stochastic optical reconstruction microscopy (STORM) uses photo-switchable probes containing two or more different fluorophores for single molecule detection.[97] Each probe molecule is labeled with one activator and one reporter fluorophore to generate a photo-switchable probe. The laser beam at the activator wavelength can turn on the reporter (the excited state); the laser beam at the reporter wavelength (longer than the activation wavelength) can switch the reporter fluorophore off (the ground state).[98] By switching individual fluorophore on and off, each time only one type of fluorophore can be excited and generate an optically resolvable fluorescence image. This process could be repeated many times until figure out the accurate position of the probe from distribution analysis, which has been achieved the lateral resolution of 20 nm. STORM has been employed to analyze the morphology of synapses in the brain.[99]

Stimulated Emission Depletion (STED) uses a focused laser beam to excite a fluorophore, followed by a ring-shaped depletion laser beam surrounding the excitation spot to suppress the light diffraction and bring the surrounding fluorescent molecules to the ground state before they emit light.[100] The depletion process, which was called

stimulated emission, reduces the fluorescence emission area of the fluorophore and increased the accuracy in finding the correct position in the sample.[101] STED has been used in direct observations and fast mapping of lipid molecules in living cell membranes with a lateral resolution of 20 nm on the <1 ms time scale.[102,103]

Secondary ion mass spectrometry (SIMS) provides a powerful non-optical tool to study cell membranes. Nano-SIMS and TOF-SIMS, two variants of the SIMS technology, both use a focused primary ion beam to break up molecules on the sample surface, and detect the generated secondary ions containing chemical information of the sample surface. The well defined focusing system enables distinguishing differences in a sample surface in the 100 nm range.[104] Nano-SIMS has been used to study phase separation in isotopic labeled mixture of $^{13}C_{18}$-DSPC or ^{15}N-DLPC on supported lipid bilayers.[104] TOF-SIMS has been used to study living cells and revealed the biological molecular details geographically at the 3-D level.[105]

1.2.2 Regulation of lipid rafts in living cells

The investigation of living cell membranes remains difficult due to its extremely diverse components. In artificial membranes, ordered and disordered lipid phase separation has been observed and studied extensively in supported lipid bilayers and GUVs.[106] The sizes of lipid domains ranged from tens to hundreds of nanometers and the lifetime from minutes to hours. So far, direct observation of lipid rafts *in vivo* has still not been possible by available techniques. Indirect evidence, including recent STED and STORM studies of fluorescently labeled membrane proteins and lipids, indicate that lipid microdomains in living cell membranes are in the range of 20-200 nm in scales area[107] with lifetimes of 10 ms to 10 s, depending on cell type.[54,108,109] Compared to artificial membranes, living

cell membranes have far more diverse compositions and are subject to myriad environments.[110] Lipid molecules in cell membranes are involved in thermodynamic fluctuation equilibrium including the lipid flip-flop motion between two leaflets of the bilayer.[111] In cell membranes, lipid molecules and membrane proteins can form protein-lipid complexes which may influence raft formation, whereas artificial membranes that have shown large domains do not contain proteins except for probes that may disturb the lipid self-assembly.[112,113] In addition, F-actin has been found localized in membrane microdomains[114] and the actin cytoskeleton enhances aggregation of the rafts.[115] Furthermore, Lipid rafts existing in cell membranes are dynamically coupled to intracellular lipid reservoirs or vesicle trafficking processes, such as endocytosis, thus restrict their size and lifetime in the membrane.[116] Therefore, direct investigation of lipid rafts in cell membranes is limited by their small size and short lifetime.

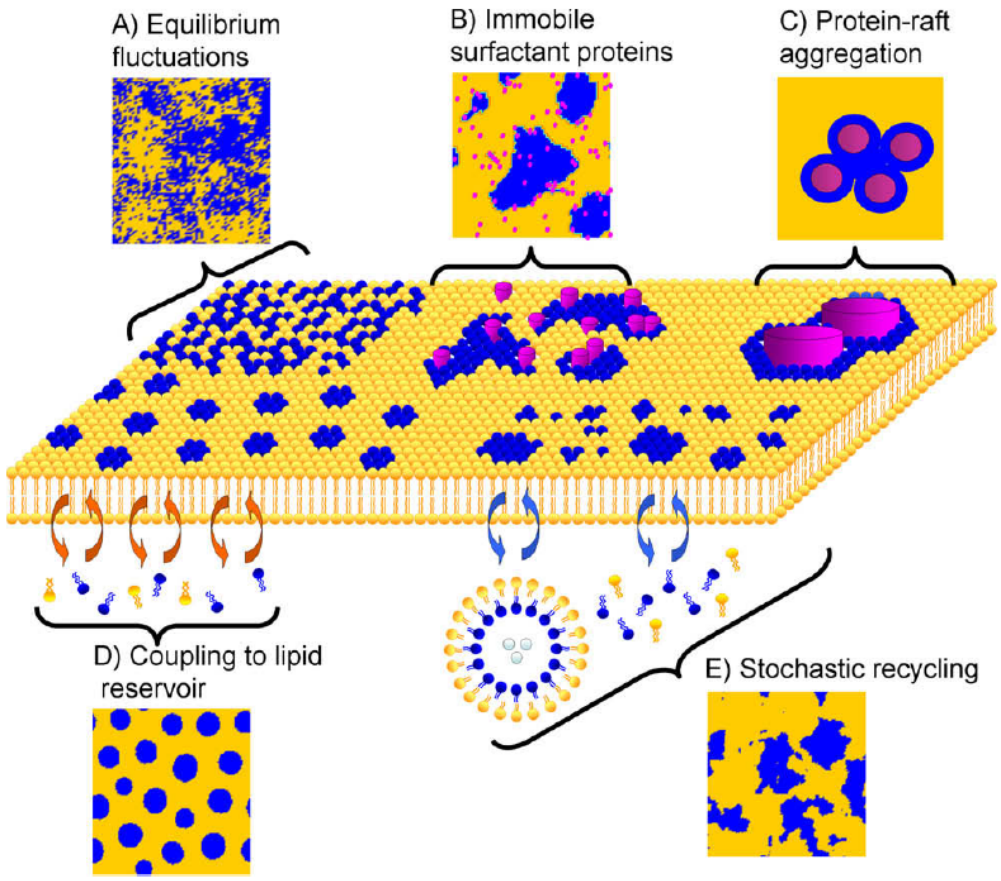

Fig. 1.5 Schematic representative of current model for lipid raft formation: A) thermal equilibrium fluctuation of plasma membrane leads to formation of rafts with small size and short lifetimes; B) immobile surfactant membrane proteins pin compositional lipid interfaces to form finite-sized rafts; C) protein-lipid interaction induces clustering of rafts to form stable rafts; D) the plasma membrane is coupled to internal lipid reservoir to suppress formation of large lipid domains; E) vesicular and non-vesicular lipid recycling results in suppression of macroscopic phase separation and microdomains. Reprinted from reference 110, Copyright (2010), with permission from Elsevier.

1.3 Organofluorine compounds

Organofluorine compounds are closely related to both scientific research and our daily life.[117] Elemental fluorine is abundant on earth but organofluorine compounds are scarce in nature. Fluorine chemistry has been developed to synthesize and investigate organofluorine compounds. Fluorine substitution regulates the activity of biologically related molecules, and has been used as an important tool for biological cycle modulation and drug design.[118] Fluorine chemistry has become a broad subject overlapping with material science, environmental science, and biology.[119]

1.3.1 The properties of organofluorine compounds

Table 1.1. Physiochemical properties of CH_2-X bond.[120]

Element	Electro-negativity	Bond length (CH_2X, Å)	Van der Waals radius (Å)	Bond energy (kcal/mol)
H	2.1	1.09	1.20	99
F	4.0	1.39	1.35	116
O(OH)	3.5	1.43	1.40	85

Organofluorine compounds are organic molecules containing one or more fluorine atoms. Although the length of C-F bond (1.39 Å) is larger than the C-H bond (1.09 Å), C-F exhibits similar steric demand as C-H.[120] Single substitution of hydrogen with fluorine (CH for CF) has been reported to give very small influences on steric and geometric properties.[121] Monofluorinated substrate analogues usually fit the active sites of enzymes well and retain the biological activities of their native counterparts, for instance, fluoroacetyl-CoA, fluoropyruvate, and β-fluorinated amino acids mimic their hydrocarbon counterparts and showed high affinity to enzymes. [122-125] Double

substitution of hydrogen with fluorine (CH_2 for CF_2), however, leads to dramatic change of physical properties compared to single substitution. Dasaradhi[126] and co-workers have exploited the fluorinated tristearins on C-12 position, and found that the di-fluorination significantly lowered the m.p. from 72 to 58 °C, whereas the mono-fluorination only changed the m.p. from 72 to 73 °C. The similar fluorination induced m.p. lowering has been observed in di-fluorinated diacylphosphatidylcholines, indicating this is a general phenomenon in organofluorine compounds.[127,128] Crystallographic studies revealed a larger C-CX_2-C angle than the ideal sp^3 tetrahedral angle (109.5°). For example, the C-CH_2-P, C-CHF-P, and C-CF_2-P phosphates exhibit bond angles of 112°, 113°, and 116°, respectively.[129,130] The larger bond angle leads to a distorted structure of the hydrocarbon chain, thus results in a larger molecular free volume and significant conformational disorder. In fact, 12-fluorostearic acid has shown to form as stable a supported monolayer in aqueous solution as stearic acid, whereas the monolayer formed by 12,12-difluorostearic acid is relatively unstable.[126] CF_3 displays more steric requirement than CH_3, by comparing molar volumes of many corresponding analogues, the size of CF_3 group is found to be similar to an isopropyl group. The van der Waals hemisphere volume of CF_3 was reported by Seebach[131] to be 42.6 Å, and that of CH_3 was 16.8 Å. Fluorine element has the highest electronegativity (3.98) and lowest polarizability (0.56×10^{-24} cm^3) in element periodic table. C-F bond (488 kJ/mol) is one of the strongest covalent bonds in chemistry. Therefore organofluorine compounds are usually more stable and more resistant to biological degradations, suggesting their potential application in enzyme inhibition and drug design.[132]

1.3.2 The synthetic development and applications of organofluorine compounds

Elemental fluorine (F_2) has been known as an extremely toxic gas for more than a century, and there was no available safe fluorination method before 1970s. Not until recently, the development in fluorine chemistry confers a variety of convenient and selective fluorination reagents for organofluorine compound production.[117,133] The nucleophilic reagents *diethylaminosulfer trifluoride* (DAST), *2,2-difluoro-1,3-dimethylimidazolidine* (DFI), are able to convert alcohol to monofluoride, and *bis(2-methoxyethyl)aminosulfur trifluoride* (Deoxofluor) can substituent the oxygen of carbonyl group with -CF_2- efficiently. The high negativity of fluorine makes common fluoride compounds usually nucleophilic, but recently the safe electrophilic fluorination reagents are also commercially available instead of toxic F_2 gas. These reagents provide "F^+" in organic synthesis, such as *1-Chloromethyl-4-fluoro-1,4-diazoniabicyclo[2.2.2]octane bis(tetrafluoroborate)* (Selectflour) and *N-fluorobenzene-sulfonimide* (NFSI). The trifluoromethyl analogues can be obtained readily using *trimethyl(trifluoromethyl silane* (Ruppert-Prakash reagent) or trifluoroacetamides.[134]

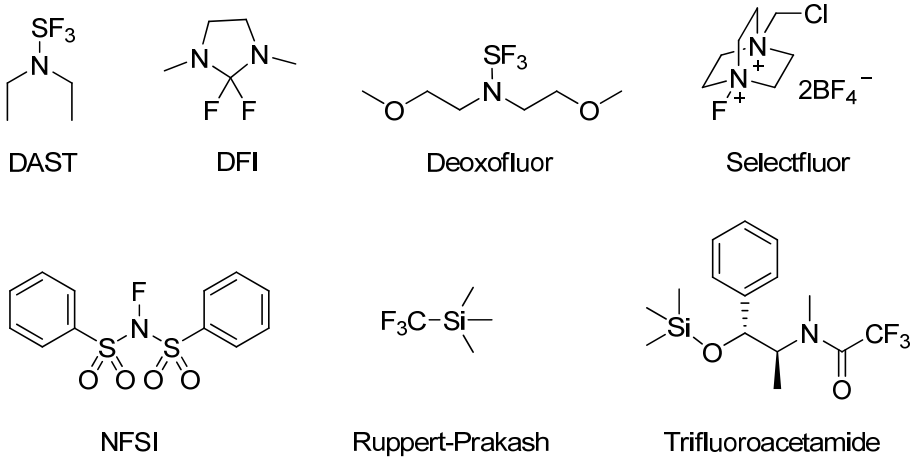

Fig. 1.6 Examples of current fluorination reagents.

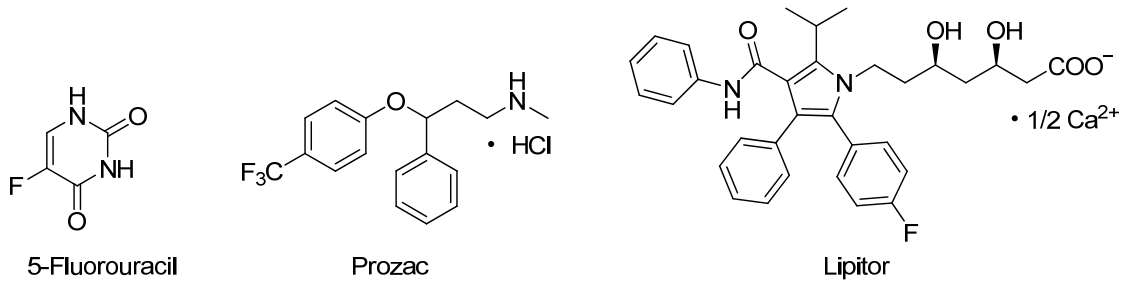

Fig. 1.7 Schematic examples of fluorinated drug molecules.

Organofluorine compounds are an important and diverse subset in drug discovery and therapeutics. Since the first fluorine containing drug 5-fluorouracil was approved in 1957, over 220 fluorinated drugs are now on the market and have taken a significantly increased percentage of total approved drugs annually in the last ten years.[135,136] For example, the anticancer drug 5-fluorouracil blocks DNA and RNA synthesis by inhibiting thymidylate synthase. Haloperidol is a type of long-documented antipsychotic drug, for which the detailed mechanism remains unknown, but so far the effective non-fluorinated analogue has not been found. The best known fluorinated antipsychotic agent fluoxetine (Prozac), as an antidepressant, is a trifluoromethyl modified derivative. [117] Atorvastatin (Lipitor) is able to lower cholesterol level by competitively inhibiting HMG-CoA reductase, which catalyzes the rate limiting step in cholesterol biosynthesis, and is now one of the top-selling pharmaceuticals in the world.

1.3.3 The self-assembly of fluorocarbons and fluorous chemistry

The heterogeneous phase behavior of biological membranes has been well documented, and many models have been constructed to mimic the phase separation of biological membranes. Recently, the fluorous phase separation from the hydrocarbon environment

has drawn attention.[137] The immiscibility of fluorocarbons and hydrocarbons leads to the separation of the mixture, and provides a potential method to control the phase separation in biological membranes. Fluorocarbon substituted lipids and polymers have been applied to liposomes, solid support lipid bilayers, and mammalian cells to investigate their properties and behaviors in the membranes.

The fluorocarbon amphiphilic lipids form bilayer membranes, emulsions and vesicles in aqueous solution, which exhibit better stability and less permeability than hydrocarbon membranes.[138,139] The vesicles formed by fluorocarbon analogues are strikingly stable, which could be sterilized by heating, even with only one fatty acid chain perfluorinated.[104] When mixed with hydrocarbon lipids, such as the natural lipid DMPC, the fluorocarbon lipids self-assemble and result in phase separation.[140] Webb and coworkers reported a synthetic fluorocarbon amphiphilic lipid that can cause phase separation from the phopholipid gel phase at 1 mol % concentration.[141,142] Schmidt synthesized a perfluorinated glycolipid that can form membrane domains to modulate cell adhesion and rolling.[143,144]

Recent studies showed that the semifluoro ($-C_6F_{13}$) substituted phospholipid (F6PC) segregated from DPPC and exhibited a 50 nm scale strip-patterned phase separation in solid support bilayers, in spite of their similar structures and close transition temperatures.[145] AFM examination showed that the microdomain structure depended on the composition ratio of fluorocarbon and hydrocarbon phospholipids. Attenuated total reflectance infrared spectroscopy (ATR-IR) revealed the tilt angle difference between DPPC and F6PC[146], which lead to the height difference between the distinct phases in AFM studies.[132] In mammalian cells, ligand conjugated F6PC lipids were able to insert

into cell membranes, followed by internalization of the conjugates to deliver the ligands into the cells. The higher permeability of F6PC than DPPC conferred more efficient delivery of cargo into the cytoplasm, indicating the potential application of fluorocarbon lipids in drug delivery.[147]

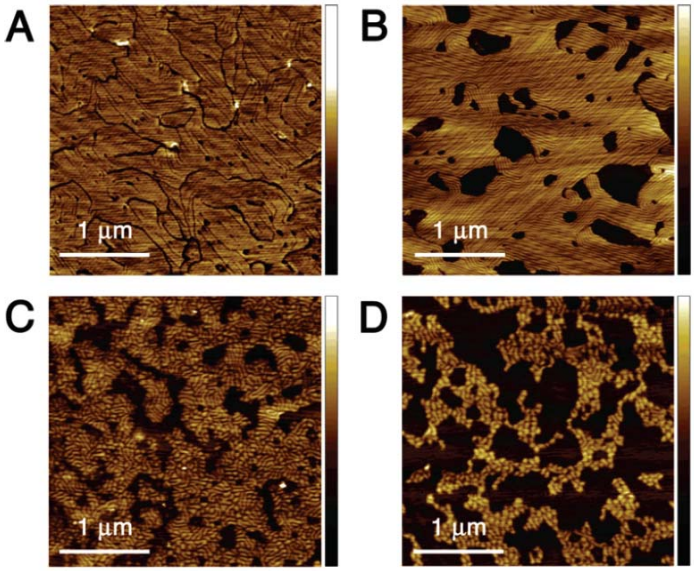

Fig 1.8 AFM images of supported lipid bilayers composed of various DPPC: F6PC ratios: (A) 85:15 (1.1 nm Z scale); (B) 65:35 (2.6 nm Z scale); (C) 45:55 (2.1 nm Z scale); (D) 25:75 (2.2 nm Z scale). F6PC: -C_6F_{13} substituted phospholipid. Reprinted with permission from reference 145. Copyright (2007) American Chemical Society.

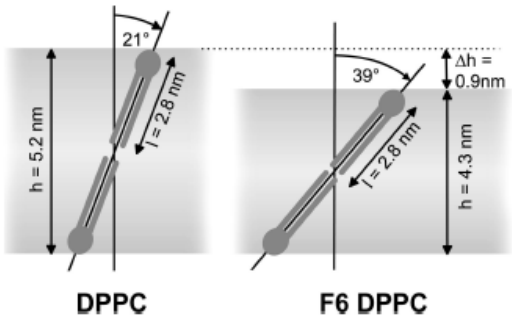

Fig 1.9 Simplified geometric model to relate the bilayer thickness *h* of DPPC and F6 DPPC with the apparent tilt angle Θ. By assuming the same empirical linear length *l* of 2.8 nm for both the DPPC and F6-DPPC lipid molecules, the bilayer thickness *h* is calculated in this simplified model as 2*l* cos Θ. F6 DPPC: -C_6F_{13} substituted phospholipid. Reprinted with permission from reference 139. Copyright (2008) American Chemical Society.

The immiscibility of perfluorocarbon and semifluorocarbon compounds against both aqueous and organic phases forms a distinct "fluorous phase". The unique property of high degree fluorocarbon leads to a fluorous chemistry and quickly developed in both lab research and industry.[148] In 1994, Horváth[149] reported a convenient method to separate a fluorocarbon modified catalyst from organic reaction mixture using a "fluorous biphase system". The fundamental theory of fluorous chemistry has been studied for decades. The hydrophobicity of fluorous compounds has been described by Mukerjee[150], who found that the perfluorocarbons were even more hydrophobic than hydrocarbons, leading to their immiscibility against water. The solubility of fluorocarbons in organic solvents was described by Scott's simplified model.[151] In this model, the partial molal free energy of mixing of two non-electrolyte solvents is expressed as the sum of the entropy of mixing and the heat of mixing at temperature T, where x_1 and x_2 are the respective mole fractions, v_1 and v_2 are the molal volumes of each solvent, and ϕ_1 and ϕ_2 are the volume fractions. In this model, the solubility parameters δ_1 and δ_2 are defined as $\delta = (\Delta E^v/v)^{1/2}$, where ΔE^v is the energy of vaporization of pure solvent and v is molal volume, and the miscibility of the two nonpolar solvents is determined by δ_1 and δ_2, since the difference between δ_1 and δ_2 determines the heat of mixing. If $\delta_1 = \delta_2$, the heat of mixing will be zero and two solvent will be miscible at any conditions; if the difference between δ_1 and δ_2 is so large that the entropy of mixing ($RT\ln x$) is negligible, the two solvents will be completely immiscible; under conditions in between the two solvents will be partially soluble. Experimental results revealed perfluorocarbons with significantly low δ values, conferring their weak interactions with water and all other organic molecules.[152,153]

$$\overline{\Delta F_1} = RT\ln x_1 + v_1(\delta_1-\delta_2)^2\phi_2^2 \quad (1a)$$

$$\overline{\Delta F_2} = RT\ln x_2 + v_2(\delta_1-\delta_2)^2\phi_1^2 \quad (1b)$$

Nowadays, perfluorocarbon compounds have become an essential part of both industry and our daily life.[154] The most common example is the polytetrafluoroethylene (Teflon), which is used due to its resistance to both water and oil, and stability in various harsh conditions.[136] Perfluoronated alkanes are used as blood substitute as they are great oxygen carriers and metabolically stable in the human body. The fluorocarbon-tag (FC-tag) has been employed in purification in a variety of biological materials, including peptides, oligosaccharides, and oligonucleotides.[155-159] The fluorous phase modified cartridges are commercially available to facilitate isolation of FC-tagged molecules by solid phase extraction.[160,161]

In the following chapters, a series of fluorinated ganglioside GM1 will be synthesized to study lipid rafts in biological membranes. The synthesis of semi-fluorinated GM1 analogue will be exploited to facilitate future investigations of phase separation modulation.

1.4 Reference

(1) Shevchenko, A.; Simons, K., Lipidomics: coming to grips with lipid diversity. *Nature Rev. Mol. Cell Biol.* **2010**, *11*, 593-598.
(2) Dennis, E. A., Lipidomics joins the omics evolution *Proc. Natl Acad. Sci. USA* **2009**, *106*, 2089-2090.
(3) Brügger, B.; Glass, B.; Haberkant, P.; Leibrecht, I.; Wieland, F. T.; Kräusslich, H.-G., The HIV lipidome: A raft with an unusual composition *Proc. Natl Acad. Sci. USA* **2006**, *103*, 2641–2646.
(4) Hinterdorfer, P.; Schütz, G.; Kienberger, F.; Schindler, H., Detection and characterization of single biomolecules at surfaces. *Reviews in Molecular Biotechnology* **2001**, *82*, 25-35.
(5) Gaiduk, A.; Kühnemuth, R.; Antonik, M.; Seidel, C. A. M., Optical Characteristics of Atomic Force Microscopy Tips for Single-Molecule Fluorescence Applications. *ChemPhysChem* **2005**, *6*, 976-983.
(6) Zacharias, D. A.; Violin, J. D.; Newton, A. C.; Tsien, R. Y., Partitioning of Lipid-Modified Monomeric GFPs into Membrane Microdomains of Live Cells *Science* **2002**, *296*, 913-916.
(7) Becker, J. S.; Jakubowski, N., The synergy of elemental and biomolecular mass spectrometry: new analytical strategies in life sciences *Chem. Soc. Rev.* **2009**, *38*, 1969-1983
(8) Rust, M. J.; Bates, M.; Zhuang, X., Sub-diffraction-limit imaging by stochastic optical reconstruction microscopy (STORM). *Nat. Methods* **2006**, *3*, 793-796.
(9) Hell, S. W., Far-Field Optical Nanoscopy *Science* **2007**, *316*, 1153-1158.
(10) Eggeling, C.; Ringemann, C.; Medda, R.; Schwarzmann, G.; Sandhoff, K.; Polyakova, S.; Belov, V. N.; Hein, B.; Middendorff, C. v.; Schönle, A.; Hell, S. W., Direct observation of the nanoscale dynamics of membrane lipids in a living cell. *Nature* **2009**, *457*, 1159-1162.
(11) Lajoielow, P.; Nabi, I. R., Lipid Rafts, Caveolae, and Their Endocytosis *International Review of Cell and Molecular Biology* **2010**, *282*, 135-163
(12) Plowe, J. Q., Membranes in the plant cell *Protoplasma* **1931**, *12*, 196-240.
(13) Danielli, J. F.; Davson, H., A contribution to the theory of permeability of thin films. . *J. Cell. Comp. Phys.* **1935**, *5*, 495.
(14) Singer, S. J.; Nicolson, G. L., The Fluid Mosaic Model of the Structure of Cell Membranes *Science* **1972**, *175*, 720-731
(15) Simons, K.; Ikonen, E., Functional rafts in cell membranes. *Nature* **1997**, *387*, 569-572.
(16) Kenworthy, A. K., Have we become overly reliant on lipid rafts? Talking Point on the involvement of lipid rafts in T-cell activation. *EMBO Rep.* **2008**, *9*, 531-535.
(17) Wallach, D. F.; Zahler, P. H., Protein conformations in cellular membranes *Proc. Natl. Acad. Sci. U. S. A.* **1966**, *56*, 1552-1559.
(18) Steim, J. M.; Fleischer, S., Aggregation-induced red shift of the Cotton effect of mitochondrial structural protein *Proc. Natl. Acad. Sci. U. S. A.* **1967**, *58*, 1292-1298.
(19) David M. Neville, J., Circular dichroism of liver cell membrane organ specific protein *Biochem. Biophys. Res. Commun.* **1969**, *34*, 60-64.

(20) Nicolson, G. L.; Hyman, R.; Singer, S. J., THE TWO-DIMENSIONAL TOPOGRAPHIC DISTRIBUTION OF H-2 HISTOCOMPATIBILITY ALLOANTIGENS ON MOUSE RED BLOOD CELL MEMBRANES *J. Cell Biol.* **1971**, *5*, 905-910.
(21) Frye, C. D.; Edidin, M. *J. Cell Sci.* **1970**, *7*, 313.
(22) Drysdale, R. G.; Herrick, P. R.; Franks, D. *Vox Sang* **1968**, *15*, 194.
(23) Nicolson, G. L.; Singer, S. J. *Proc Nat Acad Sci USA* **1971**, *68*, 942.
(24) Luft, J. H., Fine structures of capillary and endocapillary layer as revealed by ruthenium red. *Fed Proc* **1966**, *25*, 1773-1783.
(25) Peters, R.; Cherry, R. J., Lateral and rotational diffusion of bacteriorhodopsin in lipid bilayers: experimental test of the Saffman-Delbruick equations. *Proc. Natl. Acad. Sci. U. S. A.* **1982**, *79*, 4317-4321.
(26) Minton, A. P., Lateral diffusion of membrane proteins in protein-rich membranes. *Biophys. J.* **1989**, *55*, 805-808.
(27) Tilton, R. D.; Gast, A. P.; Robertson, C. R., Surface diffusion of interacting proteins. *Biophys. J.* **1990**, *58*, 1321-1326.
(28) van Meer G.; Stelzer, E. H. K.; Wijnaendts-van-Resandt, R. W.; Simons, K., Sorting of Sphingolipids in Epithelial (Madin-Darby Canine Kidney) Cells. *J. Cell Biol.* **1987**, *105*, 1623-1635.
(29) Simons, K.; van Meer G., Lipid Sorting in Epithelial Cells. *Biochemistry* **1988**, *27*, 6197-6202.
(30) van Meer G., Lipid traffic in animal cells. *Annu. Rev. Cell Biol.* **1989**, *5*, 247-275.
(31) Vitetta, E. S.; Boyse, E. A.; Uhr, J. W., Isolation and Characterization of a Molecular Complex Containing Thy-1 Antigen from Surface of Murine Thymocytes and T Cells. *Eur. J. Immunol.* **1973**, *3*, 446-453.
(32) Letartem.M; Acton, R. T.; Williams, A. F., Preliminary Characterization of Thy-1.1 and Ag-B Antigens from Rat Tissues Solubilized in Detergents. *Biochem. J.* **1974**, *143*, 51-61.
(33) Ahmed, S. N.; Brown, D. A.; London, E., On the origin of sphingolipid/cholesterol-rich detergent-insoluble cell membranes: Physiological concentrations of cholesterol and sphingolipid induce formation of a detergent-insoluble, liquid-ordered lipid phase in model membranes. *Biochemistry* **1997**, *36*, 10944-10953.
(34) Silvius, J. R., Fluorescence energy transfer reveals microdomain formation at physiological temperatures in lipid mixtures modeling the outer leaflet of the plasma membrane. *Biophys. J.* **2003**, *85*, 1034-1045.
(35) Brown, D.; Rose, J., Sorting of GPI-anchored proteins to glycolipid-enriched membrane subdomains during transport to the apical cell surface. *Cell* **1992**, *68*, 533-544.
(36) Christian, A. E.; Haynes, M. P.; Phillips, M. C.; Rothblat, G. H., Use of cyclodextrins for manipulating cellular cholesterol content. *J. Lipid Res.* **1997**, *38*, 2264-2272.
(37) Pizzo, P.; Giurisato, E.; Tassi, M.; Benedetti, A.; Pozzan, T.; Viola, A., Lipid rafts and T cell receptor signaling: a critical re-evaluation. *Eur. J. Immunol.* **2002**, *32*, 3082-3091.
(38) Goswami, D.; Gowrishankar, K.; Bilgrami, S.; Ghosh, S.; Raghupathy, R.; Chadda, R.; Vishwakarma, R.; Rao, M.; Mayor, S., Nanoclusters of GPI-anchored proteins are formed by cortical actin-driven activity. *Cell* **2008**, *135*, 1085-97.

(39) Feigenson, G. W., Giant unilamellar vesicles (GUV) used to study phase behavior of lipid mixtures. *Biophys. J.* **2001**, *80*, 514a-514a.
(40) Kahya, N.; Schwille, P., Fluorescence correlation studies of lipid domains in model membranes. *Mol. Membr. Biol.* **2006**, *23*, 29-39.
(41) Feigenson, G. W.; Buboltz, J. T., Ternary phase diagram of dipalmitoyl-PC/dilauroyl-PC/cholesterol: Nanoscopic domain formation driven by cholesterol. *Biophys. J.* **2001**, *80*, 2775-2788.
(42) Veatch, S. L.; Keller, S. L., Separation of liquid phases in giant vesicles of ternary mixtures of phospholipids and cholesterol. *Biophys. J.* **2003**, *85*, 3074-3083.
(43) Veatch, S. L.; Keller, S. L., Miscibility phase diagrams of giant vesicles containing sphingomyelin. *Phys. Rev. Lett.* **2005**, *94*, -.
(44) Johnston, L. J., Nanoscale imaging of domains in supported lipid membranes. *Langmuir* **2007**, *23*, 5886-95.
(45) Shang, Z.; Mao, Y.; Tero, R.; Liu, X.; Hoshino, T.; Tanaka, M.; Urisu, T., Clustering effects of GM1 and formation mechanisms of interdigitated liquid disordered domains in GM1/SM/CHOL-supported planar bilayers on mica surfaces. *Chem. Phys. Lett.* **2010**, *497*, 108-114.
(46) Dietrich, C.; Volovyk, Z. N.; Levi, M.; Thompson, N. L.; Jacobson, K., Partitioning of Thy-1, GM1, and cross-linked phospholipid analogs into lipid rafts reconstituted in supported model membrane monolayers. *Proc. Natl. Acad. Sci. U. S. A.* **2001**, *98*, 10642-7.
(47) Munro, S., Lipid rafts: Elusive or illusive? *Cell* **2003**, *115*, 377-388.
(48) Douglass, A. D.; Vale, R. D., Single-molecule microscopy reveals plasma membrane microdomains created by protein–protein networks that exclude or trap signalling molecules in T cells. *Cell* **2005**, *121*, 937-950.
(49) Kusumi, A.; Nakada, C.; Ritchie, K.; Murase, K.; Suzuki, K.; Murakoshi, H.; Kasai, R. S.; Kondo, J.; Fujiwara, T., Paradigm shift of the plasma membrane concept from the two-dimensional continuum fluid to the partitioned fluid: high-speed single-molecule tracking of membrane molecules. *Annu. Rev. Biophys. Biomol. Struct.* **2005**, *34*, 351-78.
(50) Suzuki, K. G. N.; Fujiwara, T. K.; Sanematsu, F.; Iino, R.; Edidin, M.; Kusumi, A., GPI-anchored receptor clusters transiently recruit Lyn and Gα for temporary cluster immobilization and Lyn activation: single-molecule tracking study 1. *J. Cell. Biol.* **2007**, *177*, 717-730.
(51) van Zanten TS; A, C.; M, K.; B, J.; CG, F.; MF, G.-P., Hotspots of GPI-anchored proteins and integrin nanoclusters function as nucleation sites for cell adhesion. *Proc. Nat. Acad. Sci. USA* **2009**, *106*, 18557-11862.
(52) Anderson, R. G. W.; Jacobson, K., A role for lipid shells in targeting proteins to caveolae, rafts, and other lipid domains. *Science* **2002**, *296*, 1821-1825.
(53) Chen, Y.; Veracini, L.; Benistant, C.; Jacobson, K., The transmembrane protein CBP plays a role in transiently anchoring small clusters of Thy-1, a GPI-anchored protein, to the cytoskeleton. *J. Cell Sci.* **2009**, *122*, 3966-3972.
(54) Jacobson, K.; Mouritsen, O. G.; Anderson, R. G. W., Lipid rafts: at a crossroad between cell biology and physics. *Nat. Cell Biol.* **2007**, *9*, 7-14.
(55) Lichtenberg, D.; Goni, F. M.; Heerklotz, H., Detergent-resistant membranes should not be identified with membrane rafts. *Trends Biochem. Sci.* **2005**, *30*, 430-436.

(56) Kenworthy, A. K., Have we become overly reliant on lipid rafts? *EMBO Rep.* **2008**, *9*, 531-535.
(57) Singer, G. L. N. S. J., Ferritin-Conjugated Plant Agglutinins as Specific Saccharide Stains for Electron Microscopy: Application to Saccharides Bound to Cell Membranes. *Proc. Natl. Acad. Sci. U. S. A.* **1971**, *68*, 942-945.
(58) Nicolson, G. L., DIFFERENCE IN TOPOLOGY OF NORMAL AND TUMOUR CELL MEMBRANES SHOWN BY DIFFERENT SURFACE DISTRIBUTIONS OF FERRITIN-CONJUGATED CONCANAVALIN-A. *Nature-New Biology* **1971**, *233*, 244.
(59) Brown, D. A.; London, E., FUNCTIONS OF LIPID RAFTS IN BIOLOGICAL MEMBRANES. *Annu. Rev. Cell Dev. Biol.* **1998**, *14*, 111-136.
(60) Brown, D. A.; London, E., Structure and Origin of Ordered Lipid Domains in Biological Membranes. *J. Membr. Biol.* **1998**, *164*, 103-114.
(61) Simons, K.; J. Gerl, M., Revitalizing membrane rafts: new tools and insights. *Nat. Rev. Mol. Cell Biol.* **2010**, *11*, 688-699.
(62) Thomas, S.; Kumar, R. S.; Casares, S.; Brumeanu, T.-D., Sensitive detection of GM1 lipid rafts and TCR partitioning in the T cell membrane. *J. Immunol. Methods* **2003**, *275*, 161-168.
(63) Örtegren, U.; Karlsson, M.; Blazic, N.; Blomqvist, M.; Nystrom, F. H.; Gustavsson, J.; Fredman, P.; Strålfors, P., Lipids and glycosphingolipids in caveolae and surrounding plasma membrane of primary rat adipocytes. *Eur. J. Biochem.* **2004**, *271*, 2028-2036.
(64) Ueda, A.; Shima, S.; Miyashita, T.; Ito, S.; Ueda, M.; Kusunoki, S.; Asakura, K.; Mutoh, T., Anti-GM1 antibodies affect the integrity of lipid rafts. *Mol. Cell. Neurosci.* **2010**, *45*, 355-362.
(65) Binnig, G.; Rohrer, H., Scanning tunneling microscopy-from birth to adolescence. *Rev. Mod. Phys.* **1987**, *59*, 615–625.
(66) Binnig, G.; Quate, C. F.; Ch. Gerber, Atomic Force Microscope. *Phys. Rev. Lett.* **1986**, *56*, 930-933.
(67) Blanchette, C. D.; Lin, W.-C.; Orme, C. A.; Ratto, T. V.; Longo, M. L., Using Nucleation Rates to Determine the Interfacial Line Tension of Symmetric and Asymmetric Lipid Bilayer Domains. *Langmuir* **2007**, *23*, 5875–5877.
(68) Giocondi, M.-C.; Vié, V.; Lesniewska, E.; Milhiet, P.-E.; Zinke-Allmang, M.; Grimellec, C. L., Phase Topology and Growth of Single Domains in Lipid Bilayers. *Langmuir* **2001**, *17*, 1653–1659.
(69) Yuan, C.; Johnston, L. J., Distribution of Ganglioside GM1 in l-α-Dipalmitoylphosphatidylcholine/Cholesterol Monolayers: A Model for Lipid Rafts. *Biophys. J.* **2000**, *79*, 2768 - 2781
(70) Yuan, C.; Furlong, J.; Burgos, P.; Johnston, L. J., The Size of Lipid Rafts: An Atomic Force Microscopy Study of Ganglioside GM1 Domains in Sphingomyelin/DOPC/Cholesterol Membranes. *Biophys. J.* **2002**, *82*, 2526 - 2535
(71) Mao, Y.; Shang, Z.; Imai, Y.; Hoshino, T.; Tero, R.; Tanaka, M.; Yamamoto, N.; Yanagisawa, K.; Urisu, T., Surface-induced phase separation of a sphingomyelin/cholesterol/ganglioside GM1-planar bilayer on mica surfaces and microdomain molecular conformation that accelerates Aβ oligomerization. *Biochimica et Biophysica Acta (BBA) - Biomembranes* **2010**, *1798*, 1090-1099.

(72) Goksu, E. I.; Vanegas, J. M.; Blanchette, C. D.; Lin, W. C.; Longo, M. L., AFM for structure and dynamics of biomembranes. *Biochimica Et Biophysica Acta-Biomembranes* **2009**, *1788*, 254-266.
(73) Carneiro, F. A.; Lapido-Loureiro, P. A.; Cordo, S. M.; Stauffer, F.; Weissmuller, G.; Bianconi, M. L.; Juliano, M. A.; Juliano, L.; Bisch, P. M.; Da Poian, A. T., Probing the interaction between vesicular stomatitis virus and phosphatidylserine (vol 35, pg 145, 2006). *European Biophysics Journal with Biophysics Letters* **2006**, *35*, 451-451.
(74) Andre, G.; Brasseur, R.; Dufrene, Y. F., Probing the interaction forces between hydrophobic peptides and supported lipid bilayers using AFM. *J. Mol. Recognit.* **2007**, *20*, 538-545.
(75) El Kirat, K.; Dufrene, Y. F.; Lins, L.; Brasseur, R., The SIV tilted peptide induces cylindrical reverse micelles in supported lipid bilayers. *Biochemistry* **2006**, *45*, 9336-9341.
(76) Canetta, E.; Adya, A. K.; Walker, G. M., Atomic force microscopic study of the effects of ethanol on yeast cell surface morphology. *FEMS Microbiol. Lett.* **2006**, *255*, 308-15.
(77) Zhao, J.; Wu, J.; Heberle, F. A.; Mills, T. T.; Klawitter, P.; Huang, G.; Costanza, G.; Feigenson, G. W., Phase studies of model biomembranes: complex behavior of DSPC/DOPC/cholesterol. *Biochim. Biophys. Acta* **2007**, *1768*, 2764-76.
(78) Zhao, J.; Wu, J.; Shao, H.; Kong, F.; Jain, N.; Hunt, G.; Feigenson, G., Phase studies of model biomembranes: macroscopic coexistence of Lalpha+Lbeta, with light-induced coexistence of Lalpha+Lo Phases. *Biochim. Biophys. Acta* **2007**, *1768*, 2777-86.
(79) Klose, C.; Ejsing, C. S.; Garcia-Saez, A. J.; Kaiser, H. J.; Sampaio, J. L.; Surma, M. A.; Shevchenko, A.; Schwille, P.; Simons, K., Yeast lipids can phase-separate into micrometer-scale membrane domains. *J. Biol. Chem.* **2010**, *285*, 30224-32.
(80) Varma, R.; Mayor, S., GPI-anchored proteins are organized in submicron domains at the cell surface. *Nature* **1998**, *394*, 798-801.
(81) Sharma, P.; Varma, R.; Sarasij, R. C.; Ira; Gousset, K.; Krishnamoorthy, G.; Rao, M.; Mayor, S., Nanoscale organization of multiple GPI-anchored proteins in living cell membranes. *Cell* **2004**, *116*, 577-589.
(82) Friedrichson, T.; Kurzchalia, T. V., Microdomains of GPI-anchored proteins in living cells revealed by crosslinking. *Nature* **1998**, *394*, 802-805.
(83) van Zanten, T. S.; Cambi, A.; Koopman, M.; Joosten, B.; Figdor, C. G.; Garcia-Parajo, M. F., Hotspots of GPI-anchored proteins and integrin nanoclusters function as nucleation sites for cell adhesion. *Proc. Natl. Acad. Sci. U. S. A.* **2009**, *106*, 18557-18562.
(84) Sheets, E. D.; Lee, G. M.; Simson, R.; Jacobson, K., Transient confinement of a glycosylphosphatidylinositol-anchored protein in the plasma membrane. *Biochemistry* **1997**, *36*, 12449-12458.
(85) Kenworthy, A. K.; Petranova, N.; Edidin, M., High-resolution FRET microscopy of cholera toxin B-subunit and GPI-anchored proteins in cell plasma membranes. *Mol. Biol. Cell* **2000**, *11*, 1645-55.
(86) Zacharias, D. A.; Violin, J. D.; Newton, A. C.; Tsien, R. Y., Partitioning of lipid-modified monomeric GFPs into membrane microdomains of live cells. *Science* **2002**, *296*, 913-6.

(87) You, M.; Li, E.; Wimley, W. C.; Hristova, K., Forster resonance energy transfer in liposomes: measurements of transmembrane helix dimerization in the native bilayer environment. *Anal. Biochem.* **2005**, *340*, 154-64.
(88) Suzuki, K. G.; Fujiwara, T. K.; Sanematsu, F.; Iino, R.; Edidin, M.; Kusumi, A., GPI-anchored receptor clusters transiently recruit Lyn and G alpha for temporary cluster immobilization and Lyn activation: single-molecule tracking study 1. *J. Cell Biol.* **2007**, *177*, 717-30.
(89) Suzuki, K. G. N.; Fujiwara, T. K.; Edidin, M.; Kusumi, A., Dynamic recruitment of phospholipase C gamma at transiently immobilized GPI- anchored receptor clusters induces IP3-Ca2+ signaling: single-molecule tracking study 2. *J. Cell Biol.* **2007**, *177*, 731-742.
(90) Murase, K.; Fujiwara, T.; Umemura, Y.; Suzuki, K.; Iino, R.; Yamashita, H.; Saito, M.; Murakoshi, H.; Ritchie, K.; Kusumi, A., Ultrafine membrane compartments for molecular diffusion as revealed by single molecule techniques. *Biophys. J.* **2004**, *86*, 4075-4093.
(91) Lenne, P. F.; Wawrezinieck, L.; Conchonaud, F.; Wurtz, O.; Boned, A.; Guo, X. J.; Rigneault, H.; He, H. T.; Marguet, D., Dynamic molecular confinement in the plasma membrane by microdomains and the cytoskeleton meshwork. *EMBO J.* **2006**, *25*, 3245-56.
(92) Korlach, J.; Baumgart, T.; Webb, W. W.; Feigenson, G. W., Detection of motional heterogeneities in lipid bilayer membranes by dual probe fluorescence correlation spectroscopy. *Biochimica Et Biophysica Acta-Biomembranes* **2005**, *1668*, 158-163.
(93) Burns, A. R.; Frankel, D. J.; Buranda, T., Local mobility in lipid domains of supported bilayers characterized by atomic force microscopy and fluorescence correlation spectroscopy. *Biophys. J.* **2005**, *89*, 1081-1093.
(94) Gerken, M.; Krippner-Heidenreich, A.; Steinert, S.; Willi, S.; Neugart, F.; Zappe, A.; Wrachtrup, J.; Tietz, C.; Scheurich, P., Fluorescence correlation spectroscopy reveals topological segregation of the two tumor necrosis factor membrane receptors. *Biochim. Biophys. Acta* **2010**, *1798*, 1081-9.
(95) Sankaran, J.; Manna, M.; Guo, L.; Kraut, R.; Wohland, T., Diffusion, transport, and cell membrane organization investigated by imaging fluorescence cross-correlation spectroscopy. *Biophys. J.* **2009**, *97*, 2630-9.
(96) Huang, B.; Babcock, H.; Zhuang, X., Breaking the diffraction barrier: super-resolution imaging of cells. *Cell* **2010**, *143*, 1047-58.
(97) Rust, M. J.; Bates, M.; Zhuang, X. W., Sub-diffraction-limit imaging by stochastic optical reconstruction microscopy (STORM). *Nat. Methods* **2006**, *3*, 793-795.
(98) Bates, M.; Huang, B.; Dempsey, G. T.; Zhuang, X. W., Multicolor super-resolution imaging with photo-switchable fluorescent probes. *Science* **2007**, *317*, 1749-1753.
(99) Dani, A.; Huang, B.; Bergan, J.; Dulac, C.; Zhuang, X., Super-resolution imaging of chemical synapses in the brain. *Neuron* **2010**, *68*, 843-856.
(100) Hell, S. W.; Wichmann, J., Breaking the diffraction resolution limit by stimulated emission: stimulated-emission-depletion fluorescence microscopy. *Opt. Lett.* **1994**, *19*, 780-2.
(101) Hell, S. W., Far-field optical nanoscopy. *Science* **2007**, *316*, 1153-8.
(102) Eggeling, C.; Ringemann, C.; Medda, R.; Schwarzmann, G.; Sandhoff, K.; Polyakova, S.; Belov, V. N.; Hein, B.; von Middendorff, C.; Schonle, A.; Hell, S. W.,

Direct observation of the nanoscale dynamics of membrane lipids in a living cell. *Nature* **2009**, *457*, 1159-62.
(103) Sahl, S. J.; Leutenegger, M.; Hilbert, M.; Hell, S. W.; Eggeling, C., Fast molecular tracking maps nanoscale dynamics of plasma membrane lipids. *Proc. Natl. Acad. Sci. U. S. A.* **2010**, *107*, 6829-34.
(104) Kraft, M. L.; Weber, P. K.; Longo, M. L.; Hutcheon, I. D.; Boxer, S. G., Phase separation of lipid membranes analyzed with high-resolution secondary ion mass spectrometry. *Science* **2006**, *313*, 1948-51.
(105) Breitenstein, D.; Rommel, C. E.; Mollers, R.; Wegener, J.; Hagenhoff, B., The chemical composition of animal cells and their intracellular compartments reconstructed from 3D mass spectrometry. *Angew Chem Int Ed Engl* **2007**, *46*, 5332-5.
(106) Lingwood, D.; Simons, K., Lipid Rafts As a Membrane-Organizing Principle. *Science* **2010**, *327*, 46-50.
(107) Pike, L. J., Rafts defined: a report on the Keystone Symposium on Lipid Rafts and Cell Function. *J. Lipid Res.* **2006**, *47*, 1597-8.
(108) Schutz, G. J.; Kada, G.; Pastushenko, V. P.; Schindler, H., Properties of lipid microdomains in a muscle cell membrane visualized by single molecule microscopy. *EMBO J.* **2000**, *19*, 892-901.
(109) Hemler, M. E., Tetraspanin functions and associated microdomains. *Nat. Rev. Mol. Cell Biol.* **2005**, *6*, 801-11.
(110) Fan, J.; Sammalkorpi, M.; Haataja, M., Formation and regulation of lipid microdomains in cell membranes: Theory, modeling, and speculation. *FEBS Lett.* **2010**, *584*, 1678-1684.
(111) Pomorski, T.; Hrafnsdottir, S.; Devaux, P. F.; van Meer, G., Lipid distribution and transport across cellular membranes. *Seminars in Cell & Developmental Biology* **2001**, *12*, 139-148.
(112) Hammond, A. T.; Heberle, F. A.; Baumgart, T.; Holowka, D.; Baird, B.; Feigenson, G. W., Crosslinking a lipid raft component triggers liquid ordered-liquid disordered phase separation in model plasma membranes. *Proc. Natl. Acad. Sci. U. S. A.* **2005**, *102*, 6320-6325.
(113) Lingwood, D.; Ries, J.; Schwille, P.; Simons, K., Plasma membranes are poised for activation of raft phase coalescence at physiological temperature. *Proc. Natl. Acad. Sci. U. S. A.* **2008**, *105*, 10005-10010.
(114) Harder, T.; Simons, K., Clusters of glycolipid and glycosylphosphatidylinositol-anchored proteins in lymphoid cells: accumulation of actin regulated by local tyrosine phosphorylation. *Eur. J. Immunol.* **1999**, *29*, 556-562.
(115) Valensin, S.; Paccani, S. R.; Ulivieri, C.; Mercati, D.; Pacini, S.; Patrussi, L.; Hirst, T.; Lupetti, P.; Baldari, C. T., F-actin dynamics control segregation of the TCR signaling cascade to clustered lipid rafts. *Eur. J. Immunol.* **2002**, *32*, 435-446.
(116) Besterman, J. M.; Low, R. B., Endocytosis - a Review of Mechanisms and Plasma-Membrane Dynamics. *Biochem. J.* **1983**, *210*, 1-13.
(117) Muller, K.; Faeh, C.; Diederich, F., Fluorine in pharmaceuticals: Looking beyond intuition. *Science* **2007**, *317*, 1881-1886.
(118) Berger, R.; Resnati, G.; Metrangolo, P.; Weber, E.; Hulliger, J., Organic fluorine compounds: a great opportunity for enhanced materials properties. *Chem. Soc. Rev.* **2011**, *40*, 3496-3508.

(119) Okazoe, T., Overview on the history of organofluorine chemistry from the viewpoint of material industry. *Proceedings of the Japan Academy Series B-Physical and Biological Sciences* **2009**, *85*, 276-289.
(120) Park, B. K.; Kitteringham, N. R.; O'Neill, P. M., Metabolism of fluorine-containing drugs. *Annu. Rev. Pharmacol. Toxicol.* **2001**, *41*, 443-470.
(121) Stabel, A.; Dasaradhi, L.; Ohagan, D.; Rabe, J. P., Scanning-Tunneling-Microscopy Imaging of Single Fluorine Atom Substitution in Stearic-Acid. *Langmuir* **1995**, *11*, 1427-1430.
(122) Wang, E. A.; Walsh, C., Characteristics of Beta, Beta-Difluoroalanine and Beta, Beta, Beta-Trifluoroalanine as Suicide Substrates for Escherichia-Coli-B Alanine Racemase. *Biochemistry* **1981**, *20*, 7539-7546.
(123) Walsh, C., Suicide Substrates - Mechanism-Based Enzyme Inactivators. *Tetrahedron* **1982**, *38*, 871-909.
(124) Chambers, S. E.; Lau, E. Y.; Gerig, J. T., Origins of Fluorine Chemical-Shifts in Proteins. *J. Am. Chem. Soc.* **1994**, *116*, 3603-3604.
(125) Gregory, D. H.; Gerig, J. T., Prediction of Fluorine Chemical-Shifts in Proteins. *Biopolymers* **1991**, *31*, 845-858.
(126) Dasaradhi, L.; Ohagan, D.; Petty, M. C.; Pearson, C., Synthesis and Characterization of Selectively Fluorinated Stearic Acids (Octadecanoic Acids) and Their Tristearins - the Effect of Introducing One and 2 Fluorine-Atoms into a Hydrocarbon Chain. *Journal of the Chemical Society-Perkin Transactions 2* **1995**, 221-225.
(127) Longmuir, K. J.; Capaldi, R. A.; Dahlquist, F. W., Nuclear Magnetic-Resonance Studies of Lipid-Protein Interactions - Model of Dynamics and Energetics of Phosphatidylcholine Bilayers That Contain Cytochrome-C Oxidase. *Biochemistry* **1977**, *16*, 5746-5755.
(128) Mcdonough, B.; Macdonald, P. M.; Sykes, B. D.; Mcelhaney, R. N., F-19 Nuclear Magnetic-Resonance Studies of Lipid Fatty Acyl Chain Order and Dynamics in Acholeplasma-Laidlawii B Membranes - a Physical, Biochemical, and Biological Evaluation of Monofluoropalmitic Acids as Membrane Probes. *Biochemistry* **1983**, *22*, 5097-5103.
(129) Chambers, R. D.; Ohagan, D.; Lamont, R. B.; Jain, S. C., The Difluoromethylenephosphonate Moiety as a Phosphate Mimic - X-Ray Structure of 2-Amino-1,1-Difluoroethylphosphonic Acid. *Journal of the Chemical Society-Chemical Communications* **1990**, 1053-1054.
(130) Nieschalk, J.; Batsanov, A. S.; OHagan, D.; Howard, J. A. K., Synthesis of monofluoro- and difluoro- methylenephosphonate analogues of sn-glycerol-3-phosphate as substrates for glycerol-3-phosphate dehydrogenase and the X-ray structure of the fluoromethylenephosphonate moiety. *Tetrahedron* **1996**, *52*, 165-176.
(131) Seebach, D., Organic-Synthesis - Where Now. *Angewandte Chemie-International Edition in English* **1990**, *29*, 1320-1367.
(132) Yoder, N. C.; Yuksel, D.; Dafik, L.; Kumar, K., Bioorthogonal noncovalent chemistry: fluorous phases in chemical biology. *Curr. Opin. Chem. Biol.* **2006**, *10*, 576-583.
(133) Ritter, T., Catalysis: Fluorination made easier. *Nature* **2010**, *466*, 447-448.
(134) Kirsch, P. *Modern fluoroorganic chemistry : synthesis, reactivity, applications*; Wiley-VCH: Weinheim, 2004.

(135) Kirk, K. L., Fluorinated pharmaceuticals. *Abstracts of Papers of the American Chemical Society* **2000**, *219*, U662-U662.
(136) Hagmann, W. K., The many roles for fluorine in medicinal chemistry. *J. Med. Chem.* **2008**, *51*, 4359-4369.
(137) Riess, J. G., Fluorous micro- and nanophases with a biomedical perspective. *Tetrahedron* **2002**, *58*, 4113-4131.
(138) Kunitake, T.; Okahata, Y.; Yasunami, S., Formation and Enhanced Stability of Fluoroalkyl Bilayer-Membranes. *J. Am. Chem. Soc.* **1982**, *104*, 5547-5549.
(139) Riess, J. G.; Krafft, M. P., Fluorinated Phosphocholine-Based Amphiphiles as Components of Fluorocarbon Emulsions and Fluorinated Vesicles. *Chem. Phys. Lipids* **1995**, *75*, 1-14.
(140) Elbert, R.; Folda, T.; Ringsdorf, H., Saturated and Polymerizable Amphiphiles with Fluorocarbon Chains - Investigation in Monolayers and Liposomes. *J. Am. Chem. Soc.* **1984**, *106*, 7687-7692.
(141) Webb, S. J.; Greenaway, K.; Bayati, M.; Trembleau, L., Lipid fluorination enables phase separation from fluid phospholipid bilayers. *Org. Biomol. Chem.* **2006**, *4*, 2399-2407.
(142) Mart, R. J.; Liem, K. P.; Wang, X.; Webb, S. J., The effect of receptor clustering on vesicle - Vesicle adhesion. *J. Am. Chem. Soc.* **2006**, *128*, 14462-14463.
(143) Gege, C.; Schneider, M. F.; Schumacher, G.; Limozin, L.; Rothe, U.; Bendas, G.; Tanaka, M.; Schmidt, R. R., Functional microdomains of glycolipids with partially fluorinated membrane anchors: Impact on cell adhesion. *ChemPhysChem* **2004**, *5*, 216-224.
(144) Schumacher, G.; Bakowsky, U.; Gege, C.; Schmidt, R. R.; Rothe, U.; Bendas, G., Lessons learned from clustering of fluorinated glycolipids on selectin ligand function in cell rolling. *Biochemistry* **2006**, *45*, 2894-2903.
(145) Yoder, N. C.; Kalsani, V.; Schuy, S.; Vogel, R.; Janshoff, A.; Kumar, K., Nanoscale patterning in mixed fluorocarbon-hydrocarbon phospholipid bilayers. *J. Am. Chem. Soc.* **2007**, *129*, 9037-9043.
(146) Schuy, S.; Faiss, S.; Yoder, N. C.; Kalsani, V.; Kumar, K.; Janshoff, A.; Vogel, R., Structure and thermotropic phase behavior of fluorinated phospholipid bilayers: A combined attenuated total reflection FTIR spectroscopy and imaging ellipsometry study. *J. Phys. Chem. B* **2008**, *112*, 8250-8256.
(147) Dafik, L.; Kalsani, V.; Leung, A. K. L.; Kumar, K., Fluorinated Lipid Constructs Permit Facile Passage of Molecular Cargo into Living Cells. *J. Am. Chem. Soc.* **2009**, *131*, 12091-93.
(148) Dunitz, J. D., Organic fluorine: Odd man out. *ChemBioChem* **2004**, *5*, 614-621.
(149) Horvath, I. T.; Rabai, J., Facile Catalyst Separation without Water - Fluorous Biphase Hydroformylation of Olefins. *Science* **1994**, *266*, 72-75.
(150) Mukerjee, P.; Handa, T., Adsorption of Fluorocarbon and Hydrocarbon Surfactants to Air-Water, Hexane-Water, and Perfluorohexane-Water Interfaces - Relative Affinities and Fluorocarbon-Hydrocarbon Nonideality Effects. *J. Phys. Chem.* **1981**, *85*, 2298-2303.
(151) Scott, R. L., The Solubility of Fluorocarbons. *J. Am. Chem. Soc.* **1948**, *70*, 4090-4093.

(152) Hildebrand, J. H.; Fisher, B. B.; Benesi, H. A., Solubility of Perfluoro-Normal-Heptane with Benzene, Carbon Tetrachloride, Chloroform, Normal-Heptane and 2,2,4-Trimethylpentane. *J. Am. Chem. Soc.* **1950**, *72*, 4348-4351.
(153) Jolley, J. E.; Hildebrand, J. H., The Liquid-Liquid Solubility of Octamethyl-Cyclotetrasiloxane with Perfluoromethylcyclohexane and Perfluoro-N-Heptane. *J. Phys. Chem.* **1957**, *61*, 791-793.
(154) Dobbs, A. P.; Kimberley, M. R., Fluorous phase chemistry: a new industrial technology. *J. Fluorine Chem.* **2002**, *118*, 3-17.
(155) Montanari, V.; Kumar, K., Just add water: A new fluorous capping reagent for facile purification of peptides synthesized on the solid phase. *J. Am. Chem. Soc.* **2004**, *126*, 9528-9529.
(156) Montanari, V.; Kumar, K., A fluorous capping strategy for Fmoc-based automated and manual solid-phase peptide synthesis. *Eur. J. Org. Chem.* **2006**, 874-877.
(157) Pearson, W. H.; Berry, D. A.; Stoy, P.; Jung, K. Y.; Sercel, A. D., Fluorous affinity purification of oligonucleotides. *J. Org. Chem.* **2005**, *70*, 7114-7122.
(158) Goto, K.; Miura, T.; Hosaka, D.; Matsumoto, H.; Mizuno, M.; Ishida, H. K.; Inazu, T., Rapid oligosaccharide synthesis on a fluorous support. *Tetrahedron* **2004**, *60*, 8845-8854.
(159) Miura, T.; Goto, K. T.; Hosaka, D.; Inazu, T., Oligosaccharide synthesis on a fluorous support. *Angew. Chem., Int. Ed.* **2003**, *42*, 2047-2051.
(160) Park, G.; Ko, K. S.; Zakharova, A.; Pohl, N. L., Mono- vs. di-fluorous-tagged glucosamines for iterative oligosaccharide synthesis. *J. Fluorine Chem.* **2008**, *129*, 978-982.
(161) Asuya, M. C. Z.; Tojino, M.; Mizuno, M.; Hatanaka, K., Fluorous tag method for the simultaneous synthesis of different kinds of glycolipids. *J. Fluorine Chem.* **2010**, *131*, 655-659.

Chapter 2

Isolation, purification and fluorination of ganglioside GM1

2.1 Background and motivation

The lipid rafts theory has become a basic concept of the heterogeneity of mammalian cell membrane, which is crucial in a variety of biological processes involving signal transduction, cellular recognition, and internalized trafficking.[1] However, the investigation of lipid rafts remains indirect mainly because of the inevitable perturbation of probing reporters and limitation of current available technologies.[2-5] Light microscopy plays an important role in cellular moiety studies, such as cell machineries and some proteins, but the resolution is restrained by light diffraction.[6] The most recent STORM and STED provided a new method to break the diffraction barrier, they still require fluorescence labeling though.[6-8] The common fluorescently active probes had premier performance in protein studies but are not suitable for membrane lipid interactions, mainly due to the ineligible steric and electronic effects on lipid molecules, which might interfere with the native affinity and patterning in the membranes.[9] Electron microscope and AFM have high resolution at nm scale, however, the former needs metallic labeling and the latter provides physical properties other than chemistry composition.[10,11] Therefore, new probes and new technologies are in need to investigate more detailed membrane structures.

In the lipid rafts theory, the plasma membrane microdomains are formed by clustering of detergent resistant membranes that are rich in glycosphingolipids and cholesterol. To examine the membrane phase behavior, we have designed and synthesized a series of fluorinated ganglioside GM1, ranging from mono-, tri- to semi-fluorocabon substitution of the hydrocarbon chains. The fluorinated gangliosides are suitable to analyze using the platform of nano-SIMS, in which the fluorine atom highly

increases the sensitivity of the secondary ions and facilitate the detection of gangliosides. The self-assembly of gangliosides was found dependent on hydrogen bonding of the sugar moiety, thus the substitution on the hydrocarbon chains will not disturb their aggregation in the membranes. Minimal substitutions of fluorine atoms will not change the physical properties of gangliosides, so that their phase behavior in the membranes should not change. The segregation property of perfluorocarbons will facilitate the clustering of gangliosides in the membranes, therefore provides a potential method to control the lipid rafts formation and regulate the signal transduction and cell recognition. In this chapter, the synthesis of F-GM1 analogues will be discussed.

2.2 Isolation and purification of GM1 from bovine brain tissues

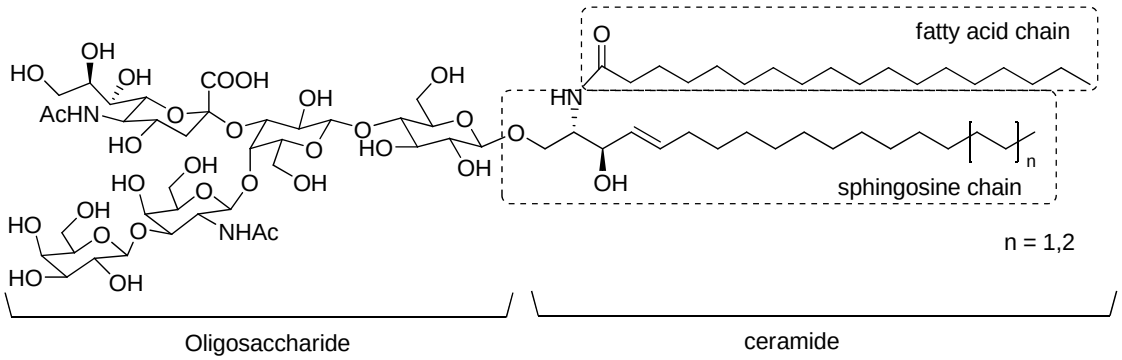

Scheme 2.1 The structure of natural ganglioside GM1.

Ganglioside GM1 is a member of ganglioside family that contains an oligosaccharide head and a ceramide tail.[12] GM1 is expressed in the outer leaflet of the plasma membrane and rich in the nervous system and almostly found in every vertebrate tissue.[13] GM1 participates in the physiological activities in brain and neuron, and has important impacts in Guillain-Barré syndrome[14,15], alzheimer's disease[16], Neuroplasticity

and healing[17]. GM1 is also the receptor of bacterial toxins[18] and antibodies in autoimmunity[19]. GM1 was found to be abundant in detergent resistant membrane and believed to play an important role in lipid rafts formation. In our work, GM1 was obtained by isolation and purification from fresh bovin brain tissues. The processing method was derived from Folch's reported scheme[20] with modification, so that it will be suitable for large quantity raw material processes. By using this method, gram scales of ganglioside GM1 is available for synthetic and biological application.

a. Brain acetone powder preparation

Fresh bovine brain samples 30 lbs, after removing bone debris, brain membrane and blood vessels, were weighed and added 10 times ice cold acetone, then homogenized for 30 min. The mixture was filtered. Residues were combined and dried under reduced pressure at 40 °C to afford bovine brain acetone powder ~ 3 lbs.

b. Extraction of total lipids

Bovine brain acetone powder was added 10 times in volume chloroform: methanol: water (50:50:10) and stirred for 1 h. The solution was collected. Residue was added 5 volume s of chloroform: methanol: water (50:50:10) and stirred for 1 h to collect the solution, and repeat twice. All the solutions were combined and added 1/2 volume 50 mmol/l NaCl solution, stirred for 2 h, and leave the two layers to settle after mixing extensively. Finally the lower layer was collected and dried under reduced pressure at 40 °C afford the total lipids.

c. GM1 isolation from total lipids by flash column chromatography

The flash column chromatography required several times of silica gel column purification. Firstly, the sample was loaded on the silica gel column under solvent C, and eluted with solvent C to remove most of cholesterol and phospholipids, then eluted with solvent D to roughly separate the gangliosides from other lipids. The crude gangliosides was collected and further purified by flash column chromatography with solvent D and finally afford 1.3 g pure GM1.

Solvent A: chloroform: methanol = 5: 1 (v: v)

Solvent B: chloroform: methanol: water = 60: 40: 9

Solvent C: dichloromethane: methanol = 5: 1 (v: v)

Solvent D: dichloromethane: methanol: water = 60: 40: 9

d. TLC

TLC plate: Silica gel 60 F_{254}

Stain: Resorcinol/HCl or p-anisaldehyde

Solvent: Chloroform: methanol: 0.02% $CaCl_2$ = 60: 40: 9

e. ESI-MS

ESI-MS was taken under negative mode.

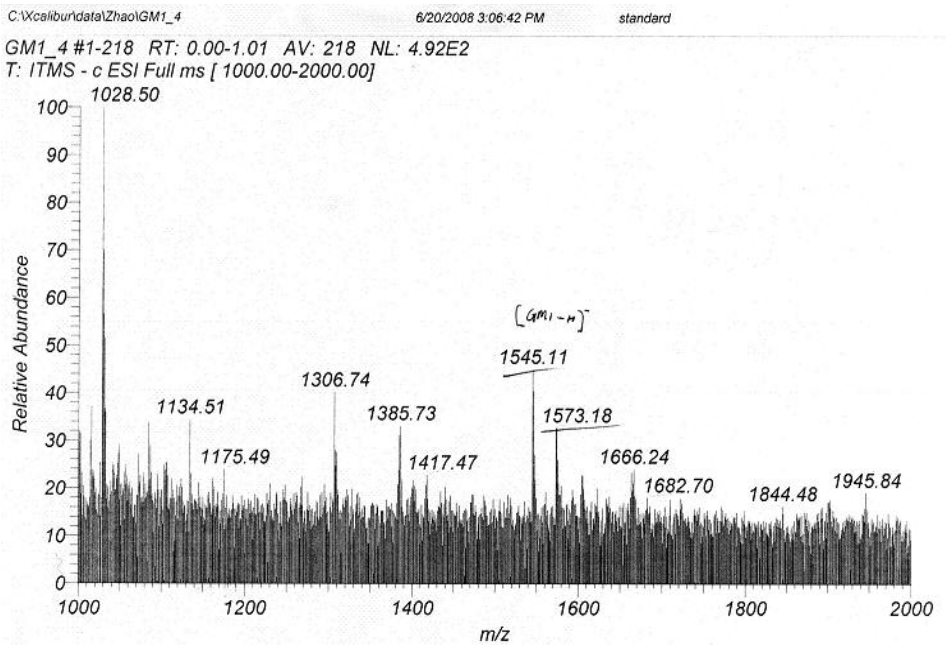

Figure 2.1 ESI-MS of GM1 standard.

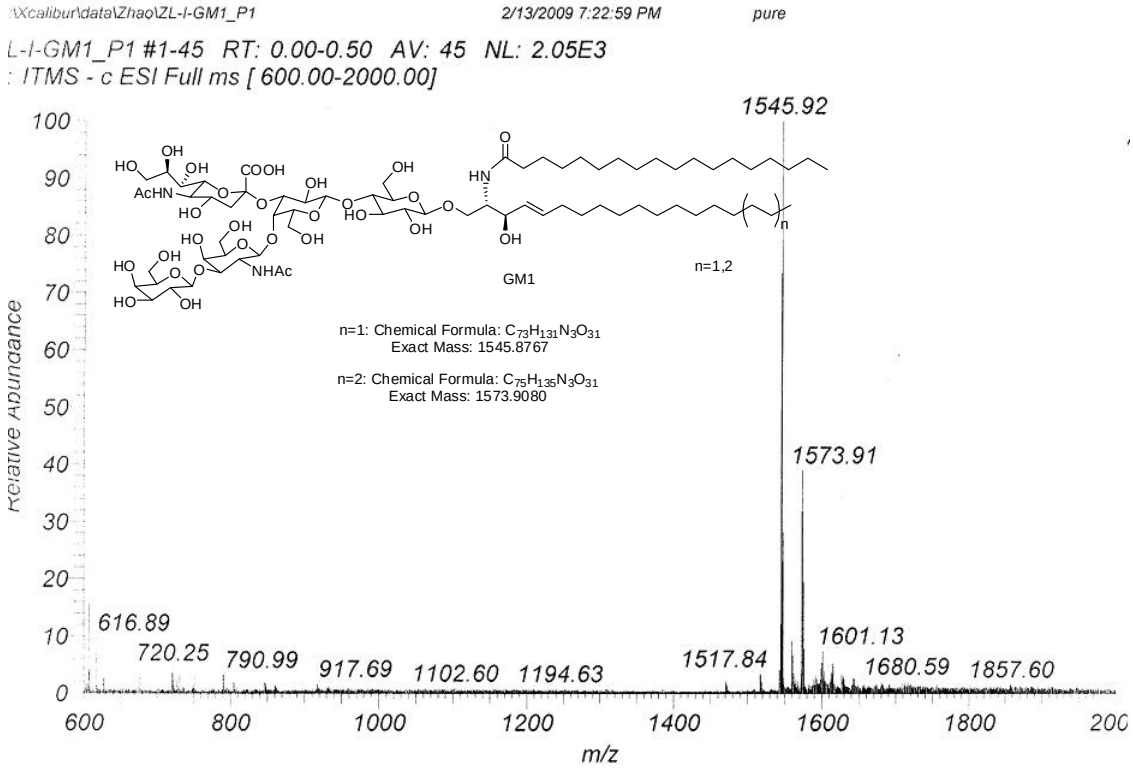

Figure 2.2 ESI-MS of GM1 isolated from bovine brain samples.

f. HPLC analysis of GM1

Column: Zorbax C8, analt, 4.6 mm × 150 mm, 5 μm

Solvent A: MeOH / H_2O (10:90, v:v)

Solvent B: AcCN

Flow: 1 ml / min

Gradient: Solvent A / Solvent B: 20 to 80%

(The HPLC data is shown in the appendix)

2.3 Synthesis of fluorinated GM1 derivatives

Ganglioside GM1 is an amphaphilic molecule containing a hydrophilic oligosaccharide head and a hydrophobic ceramide moiety. To facilitate detection of GM1 in biological systems, derivatization on the acetyl group of sialic acid and the fatty acid chain has been employed to generate radioactive[21,22], paramagneticly[23] or fluorescently[24-28] active analogues. In our approach to fluorinated GM1, the fatty acid chain is used for fluorine substitution since the fluorocarbon does not change hydrophobicity of the aliphatic chain and the oligosaccharide will not be disturbed for hydrogen bonding to retain the self-assembly property of GM1.

In the synthetic scheme, ganglioside GM1 was first hydrolyzed by alkaline hydrolysis followed by selectively protection and deprotection of amine group to obtain lyso-GM1, which has only one free amine on the sphinosine group. Fluorinated fatty acids, including monofluoro at different positon, trifluoro, and semiperfluoro versions,

were synthesized separately and activated by *N*-hydroxysuccinimide. The activated fluoro-fatty acid was then coupled to lyso-GM1 under anhydrous condition to give the fluorinated derivatives of GM1. To obtain the semiperfluoro substituent on both aliphatic chains, we modified unsaturated sphingosine chain by ozonolysis to cleave the double bond and generate an aldehyde intermediate, followed by wittig coupling with a ylide to replace the sphingosine with semifluorocarbon substituted chain. This is the first reported functional modification of the sphingosine chain on gangliosides.

2.3.1 Synthesis of lyso-GM1

The natural ganglioside GM1, derived from bovine brain tissue, was hydrolyzed in KOH/MeOH solution under high pressure in a sealed thick-walled reaction tube at 100 °C for 2 days. The hydrolysis process upon time has been well established by Sonnino[29]. Both of the amide bonds on the ceramide and the sialic acid were cleaved, whereas the acetyl amide bond on the GalNAc was more stable and remained uncleaved. After removal of solvent, the residue was neutralized carefully with 1 M acetic acid and dialyzed against water to get rid of the salts. The crude materials was then lyophilized and purified through silica gel column by the reported method[26]. The amine group on the sphingosine chain of DeAc-lysoGM1 was selectively protected with Fmoc by a dual-phase reaction at 0 °C under kinetic control, and then the more steric hindered amine group on sialic acid was subsequently acetylated by excess acetic anhydride. Finally, the Fmoc group was deprotected readily in ammonia hydroxide solution to give lyso-GM1 for further modification.

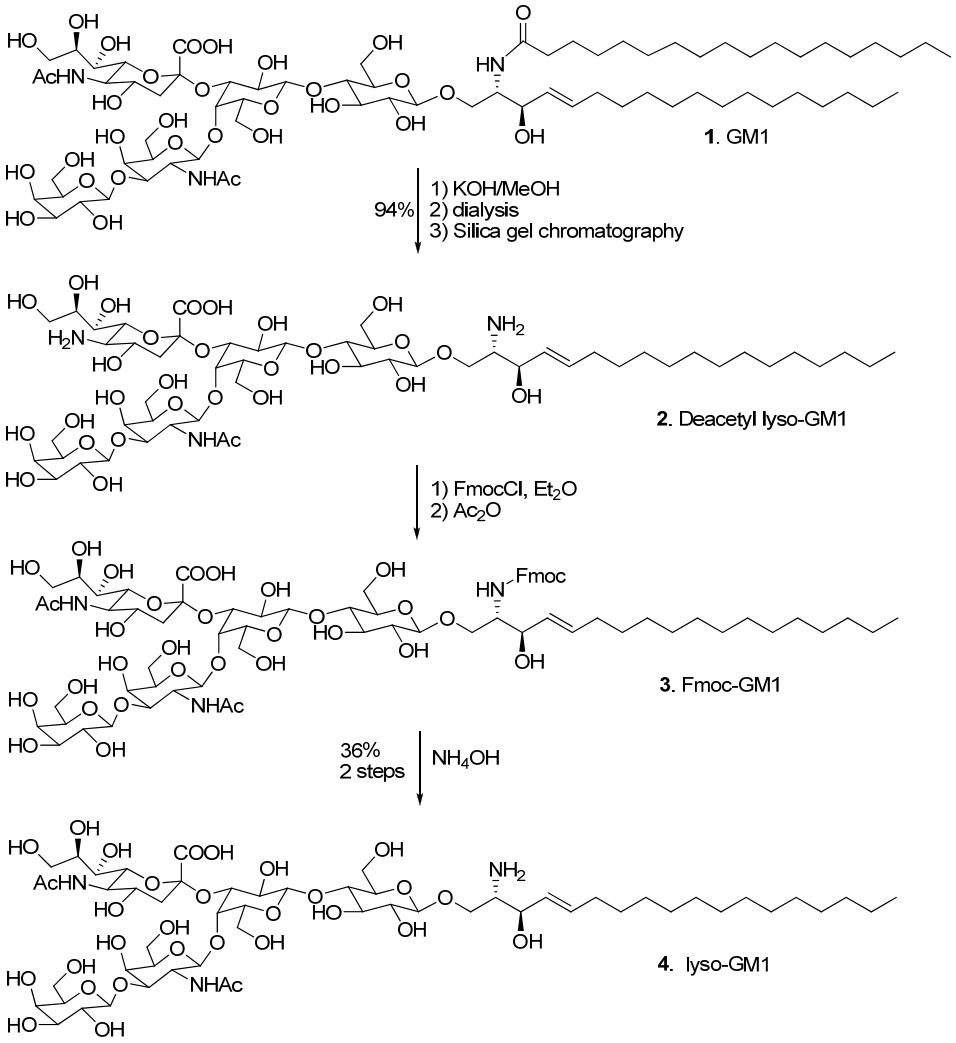

Scheme 2.2 Synthetic scheme of lyso-GM1

2.3.2 Synthesis of 18-F3-GM1

The trifluoromethyl substituted stearic acid was achieved using a [3+15] wittig coupling reaction[30], followed by hydrogenation and hydrolysis to give the product. Briefly, the synthesis of 18,18,18-trifluorooctadecanoic acid (**10**) commenced from methyl 15-oxopentadecanoate (**6**) by elongation of the fatty acid chain with triphenyl(3,3,3-trifluoropropyl) phosphonium iodide (**7**) using wittig chemistry. Methyl 15-oxopentadecanoate (**6**) was obtained from 15-pentadecanolide via an acid catalyzed ring opening in methanol to give methyl 15-hydroxypentadecanoate (**5**), followed by oxidation of the alcohol with pyridinium dichromate (PDC). The yield over these two steps was 55%. Triphenyl(3,3,3-trifluoropropyl)phosphonium iodide (**7**) was readily obtained from 3,3,3-trifluoropropyl iodide by reflux in CH_3CN with PPh_3 with 65% yield. The phosphonium salt was treated with n-BuLi to obtain the corresponding ylide, and then reacted with aldehyde **6** at room temperature for 36 h to give methyl 18,18,18-trifluorooctadec-15-enoate (**8**) with 42% yield. Hydrogenation and subsequent hydrolysis of **8** proceeded without event to afford the trifluoromethylated fatty acid with 83% yield over two steps. CF_3-stearic acid was activated as *N*-succinimidyl 18,18,18-trifluorostearate (**11**) for coupling with lyso-GM1 (Scheme 2.3). The NHS ester **11** was then conjugated with lyso-GM1 to afford the trifluoromethyl GM1 (Scheme 2.4).

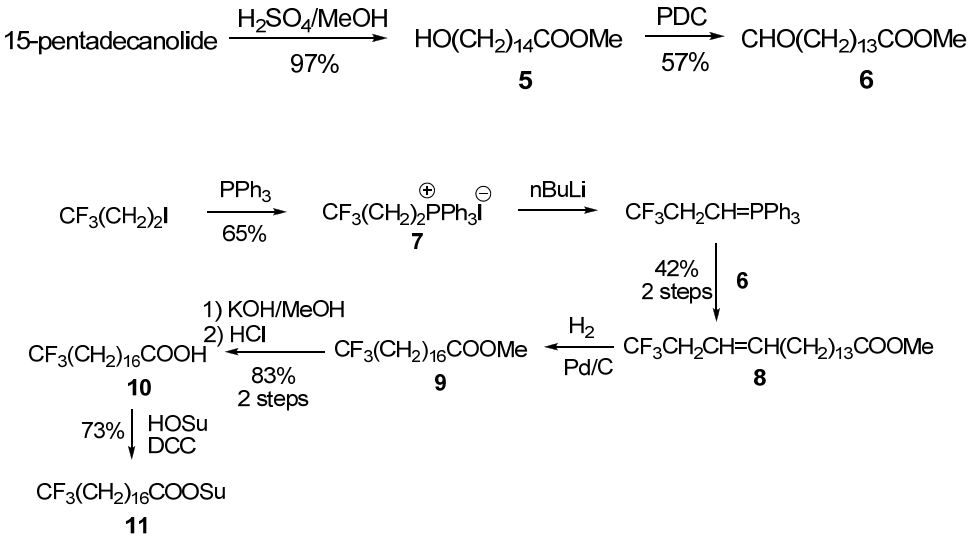

Scheme 2.3 Synthesis of NHS-activated 18,18,18-trifluorostearic acid

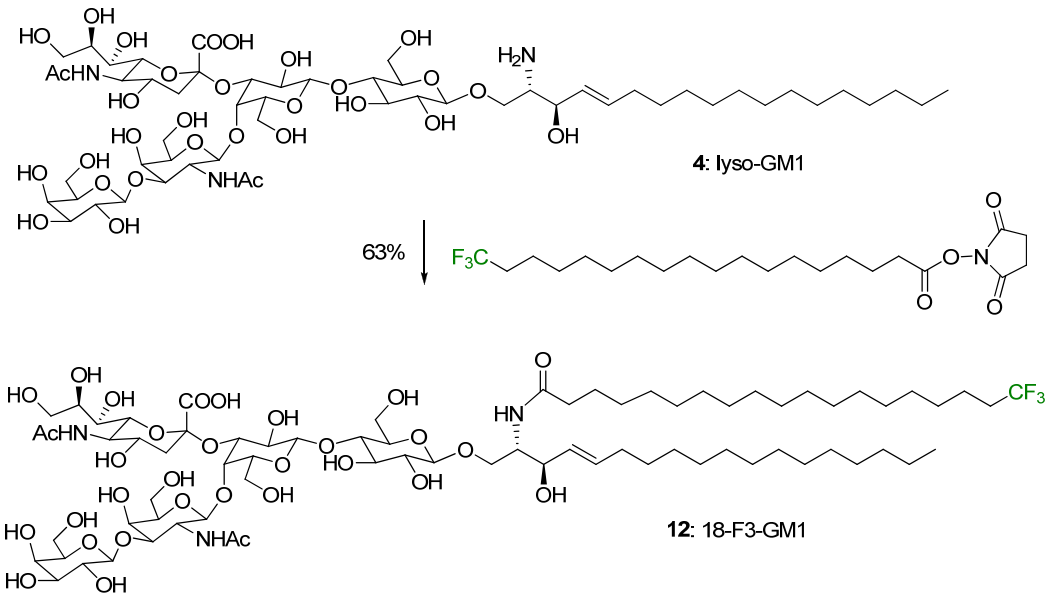

Scheme 2.4 Synthesis of 18-F3-GM1

2.3.3 Synthesis of 18-F-GM1

The monofluorinated stearic acid was synthesized using a [3+15] Wittig coupling for hydrocarbon chain elongation. The synthesis started with a benzyl protected Wittig reagent and the aldehyde **6** coupled using Wittig chemistry to give stearic acid analog **13** with 33% yield.[31] The hydrogenation and deprotection of benzyl group of **13** were completed in one step, followed by fluorine substitution of terminal hydroxyl group to afford the terminal fluoro-stearic acid methyl ester **15** with 77% yield over two steps. After hydrolysis deprotection of methyl ester, the terminal fluoro-stearic acid **16** was activated by *N*-hydorxysuccinimidate and DCC and successively conjugated with lyso-GM1 to afford the terminal monofluoro-GM1 **18** with 19% yield for three steps (Scheme 2.5 & 2.6).

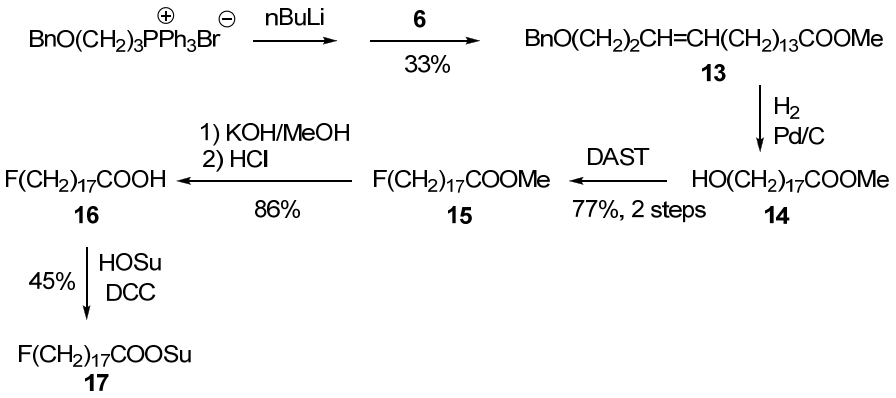

Scheme 2.5 Synthesis of NHS-activated 18-fluorostearic acid

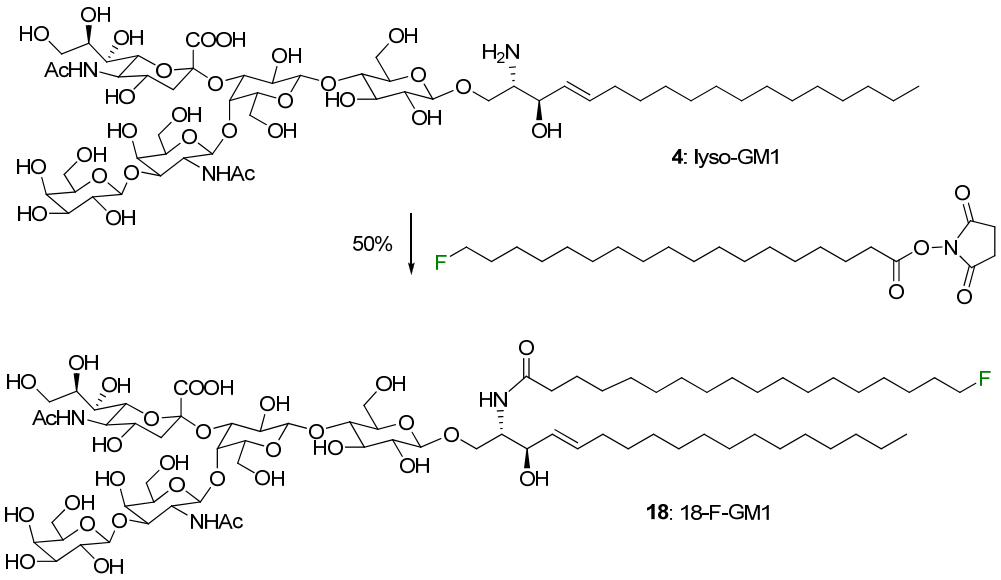

Scheme 2.6 Synthesis of 18-F-GM1

2.3.4 Synthesis of 12-F-GM1

Since the 12-hydroxylstearic acid is commercially available, the 12-fluoro-stearic acid **21** is readily obtained by introducing a fluorine atom to substitute the OH with DAST reagent following a methyl ester protection step with 52% yield for two steps. Starting with the racemic mixture 12-hydroxylstearic acid resulted in racemic product after the S_N2 substitution. The methyl deprotection of followed by *N*-hydroxysuccinimidate activation provided the activated 12-F-stearic acid succinimidyl ester **22** with 74% yield for two steps. The ester **22** was finally coupled with lyso-GM1 to afford the 12-fluorinated GM1 **23** (Scheme 2.7 & 2.8). Proton decoupled ^{19}F-NMR revealed the product of 12-F-GM1 was a mixture of two diastereomers (δ = -182.045 and -182.052).

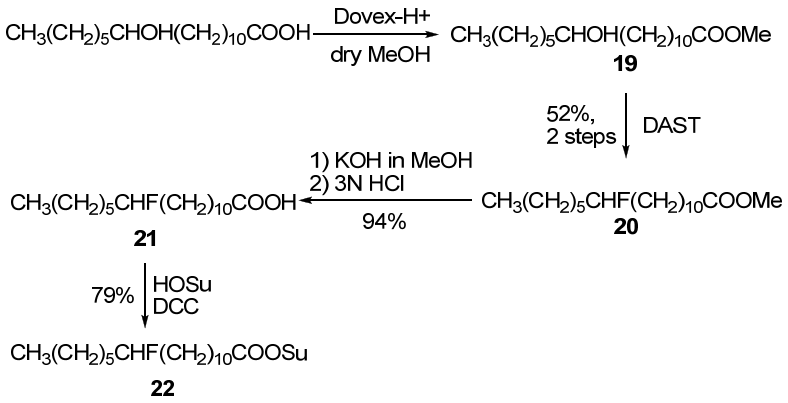

Scheme 2.7 Synthesis of 12-fluorostearic acid

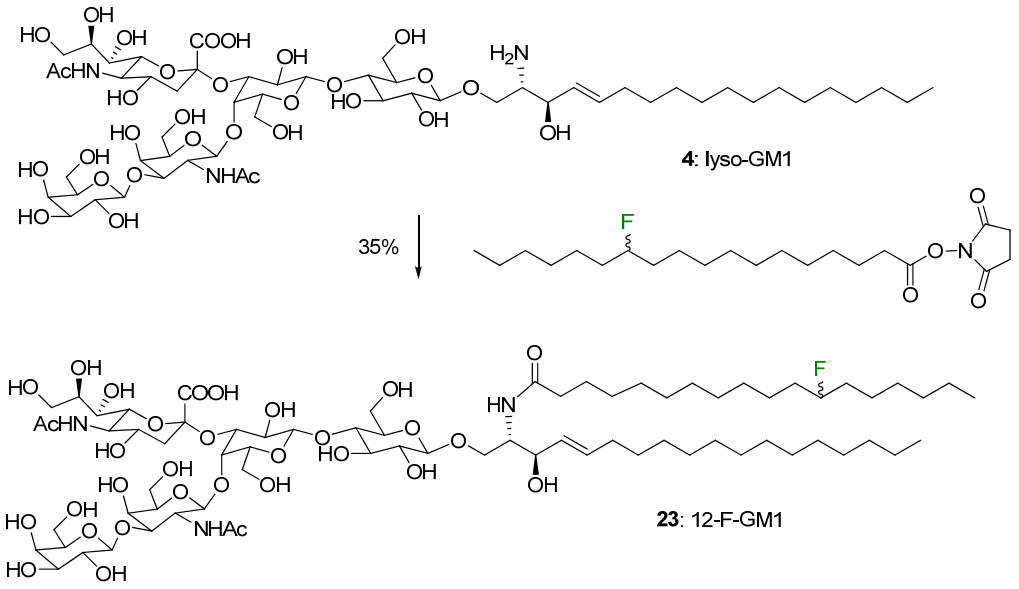

Scheme 2.8 Synthesis of 12-F-GM1

2.3.5 Synthesis of C6F13 modified GM1

The two lipid tails of GM1 were modified with C6F13 in two steps successively. The C6F13 substituted stearic acid is available in our lab.[32] The C6F13 substituted GM1 on fatty acid chain was simply obtained by NHS activation of C6F13 stearic acid and coupling with lyso-GM1 to give C6F13-GM1 **24** with 67% yield. (Scheme 2.9)

The modification of sphingosine hydrocarbon chain was accomplished using ozonolysis cleavage followed by coupling of the aldehyde product with a Wittig reagent containing terminal C6F13. The synthesis of C6F13 Wittig reagent started from a semi-perfluorinated olefin **25**, which was generated by a radical induced coupling with perfluorocarbon iodide and octadiene with 30% yield.[33] The selective hydroboration of olefin **25** followed by oxidation with hydrogen peroxide in basic condition afforded semiperfluoro terminated alcohol **26** with 64% yield.[34] Bromination reaction converted the terminal alcohol **26** to the bromide **27** with 47% yield, which is resistant to any TLC stains and had to be analyzed by NMR for flash chromatography fractions. The bromide **27** was then treated with triphenylphosphine in acetonitrile at reflex to give the salt of Wittig reagent **28**, which was easily purified by washing with anhydrous ether to get rid of non-polar starting materials and leave the pure product as a white solid with 74% yield. (Scheme 2.10)

To cleave the sphingosine chain at the double bond position, the C6F13-GM1 was treated with ozone at -78 °C followed by treatment with triphenylphosphine for ring opening to afford the GM1 aldehyde **29** with 71% yield. Ozonolysis at low temperature efficient prevented the oligosaccharide cleavage from the ceramide.[35] The trioxolane

intermediate of C6F13-GM1 required 3 days to open the ring, whereas that of natural GM1 needed no more than 24 h (data not shown), presumably due to stabilizing effect of fluorocarbons. The aldehyde **29** was fully protected by acetyl groups using acetic anhydride to give the peracetylated C6F13-GM1 aldehyde **30** with 77% yield. Previous study revealed that Wittig coupling directly on the unprotected aldehyde **29** was impossible, which only yielded hydrolyzed products (data not shown). The peracetylated aldehyde **30** was reacted with the *n*-Buli treated ylide **28** for two days then quenched with methanol to afford the Di-C6F13-GM1 **31** with 20% yield for two steps. The acetyl groups were deprotected during the methanol quenching step under the basic condition. (Scheme 2.11) It turned out that the unreacted C6F13-GM1 ran in the same fractions as the product on flash chromatography, and the flash column is not able to separate them. Thus the flourous phase cartridge was employed to separate these two analogues using their different affinity to the solid flourous phase due to their varied fluorocarbon chains.

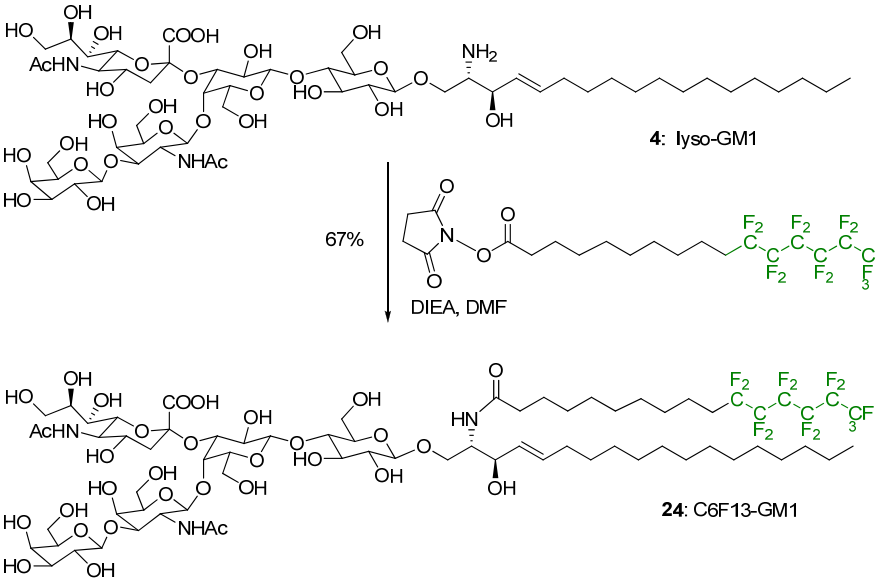

Scheme 2.9 Synthesis of C6F13-GM1

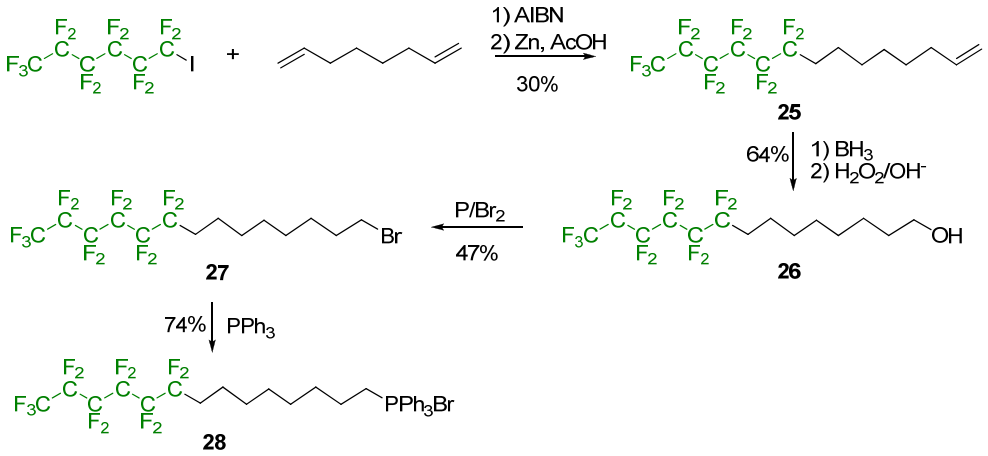

Scheme 2.10 Synthesis of C6F13 substituted triphenylphosphine bromide

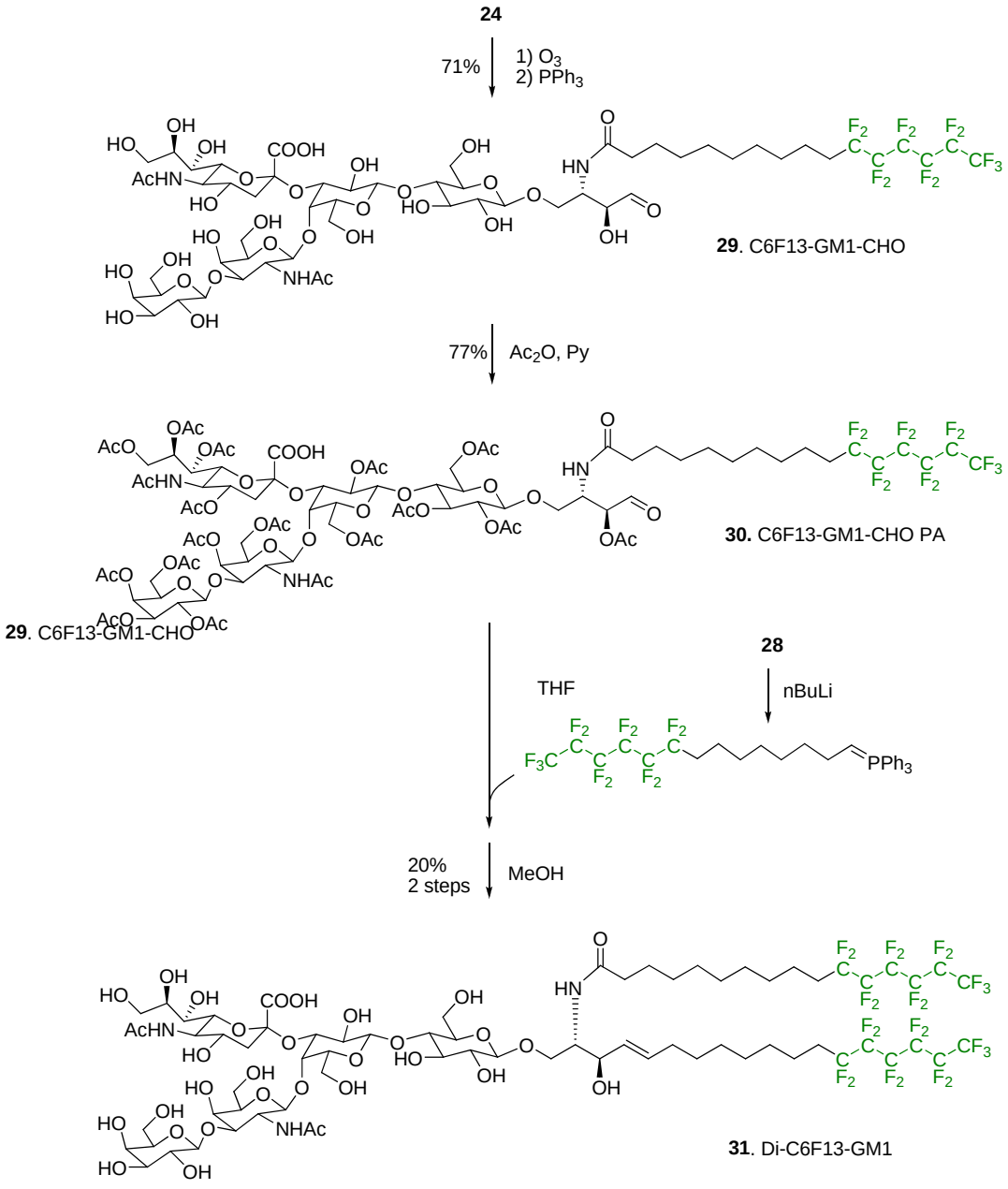

Scheme 2.11 Synthesis of Di-C6F13-GM1

2.3.6 Olefin metathesis to substitute sphinogosine with fluorocarbon chain lead to a mixture of alkenes.

The synthesis of Di-C6F13-GM1 was also tested using catalyzed olefin cross-metathesis due to its mild reaction condition. The synthesis of C6F13 substituted olefin started with C6F13 substituted ethylene iodide, which was converted to Wittig reagent **34** and elongated by Wittig coupling. Caprolactone was treated with sulfuric acid in methanol to give methyl 6-hydroxy-hexonoate **32**, followed by PDC oxidation to provide with methyl 6-oxohexanoate **33** with 40% for two steps. The Wittig reagent **34** was treated with *n*-BuLi and aldehyde **33**, successively, to complete the chain elongation in two days with 50% yield. Hydrogenation of the coupling product **35** gave C6F13 substituted methyl ester **36**, followed by DIBAL reduction provided with C6F13 substituted aldehyde **37** with 86% yield for two steps. The Wittig coupling of the aldehyde **37** with ethyl ylide afforded the (*E*)-olefin **38** with 52% yield, which configuration was confirmed by NMR. (Scheme 2.12)

The C6F13-GM1 **24** was modified using catalyzed olefin metathesis to truncate the sphingosine chain and facilitate the further metathesis with C6F13-olefin. By Grubbs-Hoveyda II catalysis and microwave assistance, C6F13-GM1 was truncated at the double bond to generate 2-alkene tethered product **39**. (Scheme 2.13, Fig 2.3) The C6F13 substituted 2-alkene **38** was used for cross metathesis with truncated C6F13-GM1 **39** with by Grubbs-Hoveyda II catalyst. The olefins were capped with methyl groups in order to avoid reported migration of terminal alkenes in catalyzed cross metathesis reactions.[36] (Scheme 2.14) However, by-products were observed with one or two more

methylene groups that cannot be separated from the product. (Fig 2.4) These unprecedented results are involved in the thesis to facilitate further studies in future.

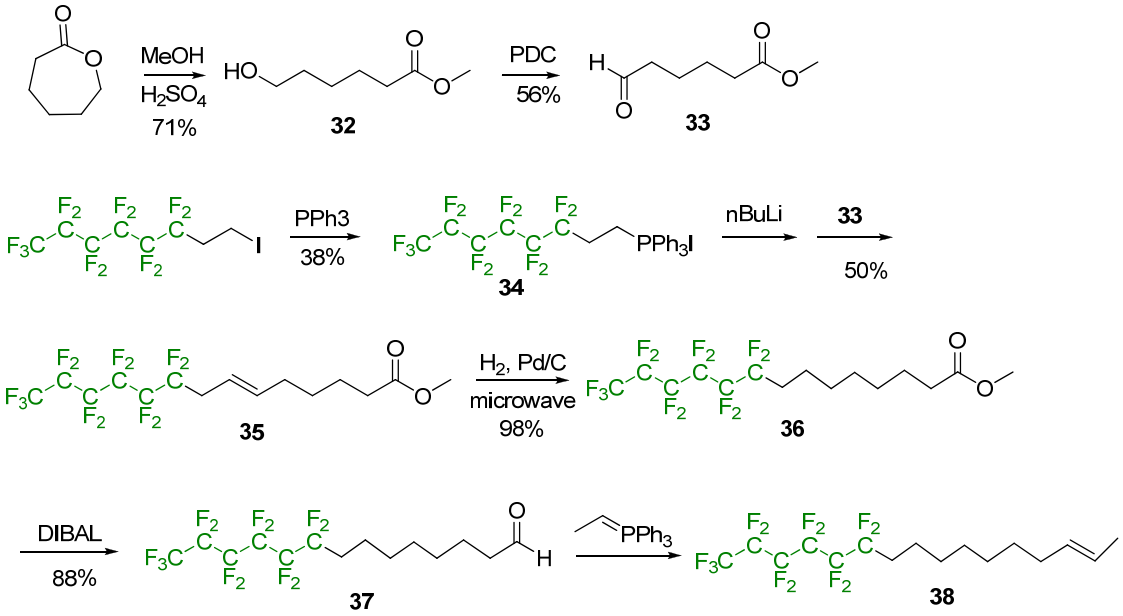

Scheme 2.12 Synthesis of C6F13 substituted olefin

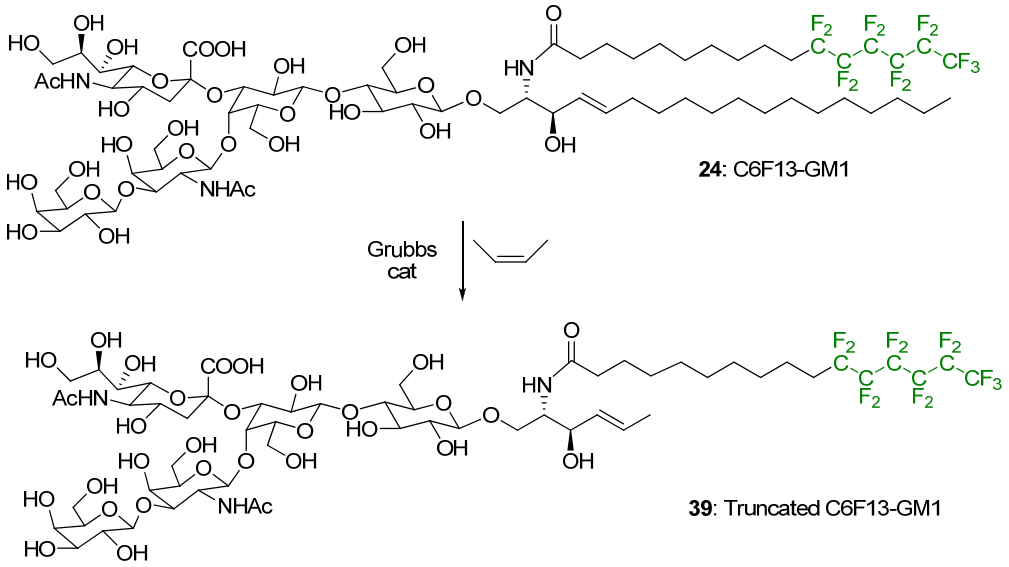

Scheme 2.13 Synthesis of truncated C6F13-GM1 olefin

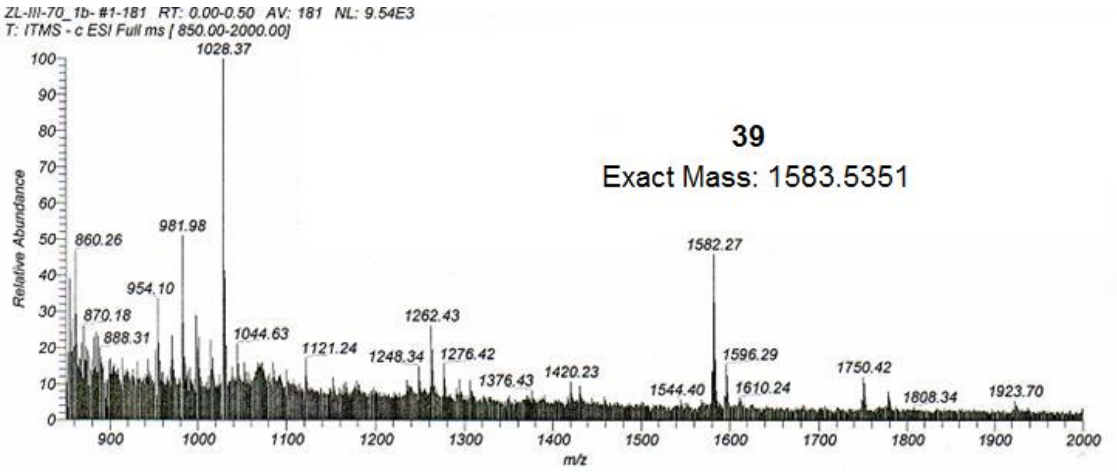

Fig. 2.3 ESI-MS of Truncated C6F13-GM1

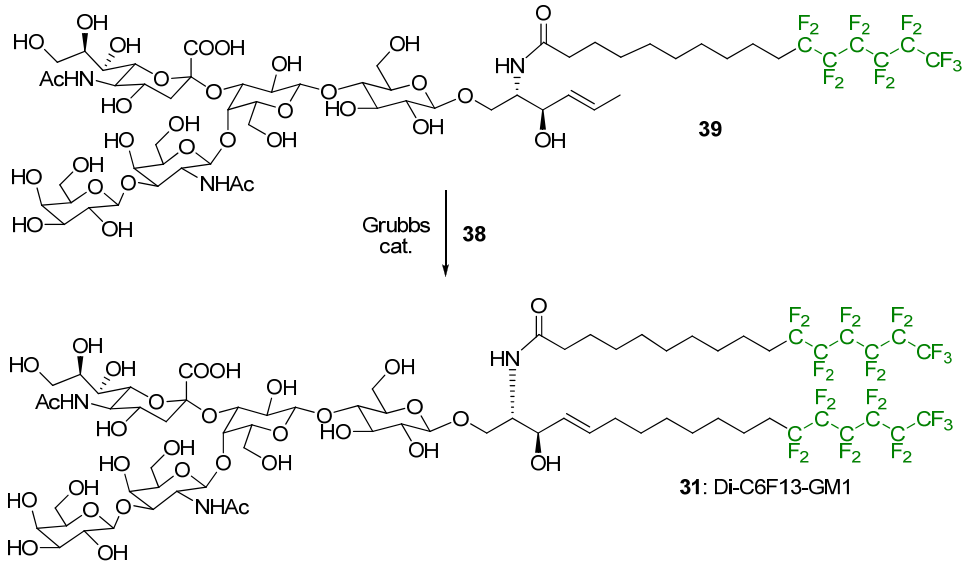

Scheme 2.14 Synthetic route of Di-C6F13-GM1

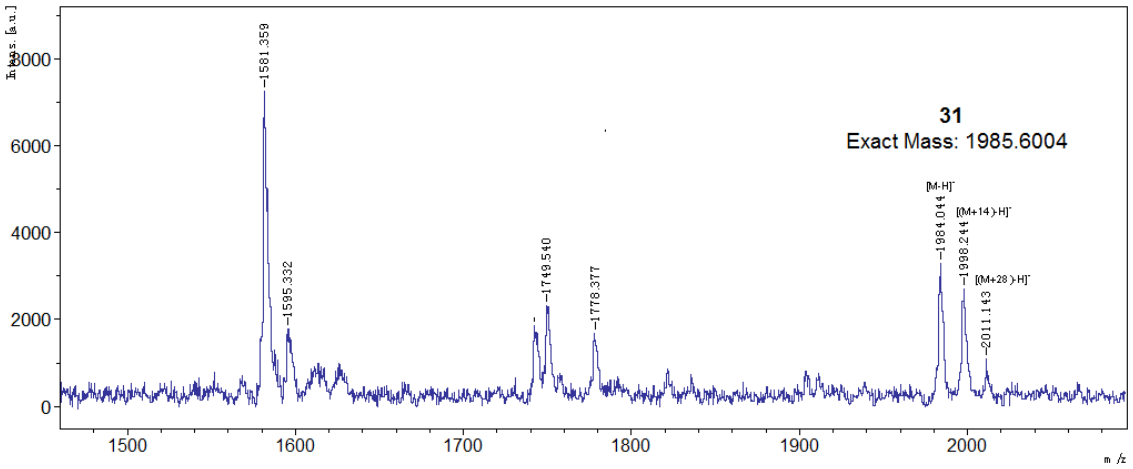

Fig. 2.4 ESI-MS spectrum of Di-C6F13-GM1 products by olefin metathesis

2.4 Experimental section

Materials and instruments. The fluoro-reagents were purchased from SynQuest Labs Inc. (Alachua, FL, USA), and other reagents were from Sigma-Aldrich, USA. The dialysis membrane 3,500 MWCO was from Thermo Scientific Inc. (Rockford, IL, USA). Silica gel 60A 230-400 mesh for column chromatography was from Whatman Inc. (Piscataway, NJ, USA). Routine NMR spectra were obtained from Bruker DPX-300 NMR and Bruker Avance III 500 MHz NMR instruments. The low resolution mass spectra were obtained from Finnigan LTQ Mass Spectrometer, and the GM1 derivatives were analyzed under negative mode. HRMS spectra were obtained by Agilent 6210 Time-of-Flight LC/MS in The Center for Mass Spectrometry (CMS) facility at The Merkert Chemistry Center in Boston College.

Deacetyl-lyso-GM1 (2): G_{M1} (208 mg, 0.13 mmol) was dissolved in KOH in MeOH (0.8 M, 50 mL) in a thick-walled reaction tube, and stirred at 100 ˚C for 2 d. The solvent was removed under *vacuo* and the resulting residue was neutralized slowly with 1 M acetic acid to pH 7.0, and then dialyzed against H_2O (2 × 1.0 L). The solution in the dialysis bag after freeze-drying, yielded the crude product (160 mg, 94%).

ESI-MS: *m*/*z* $[C_{53}H_{94}N_3O_{29} - H]^-$ calcd: 1236.6, found: 1236.7; *m*/*z* $[C_{55}H_{98}N_3O_{29} - H]^-$ calcd: 1264.6, found: 1264.7.

N-Fmoc-lyso-GM1 (3): Deacetyl-lyso-GM1 (160 mg, 0.13 mmol) was partitioned in 12 mL of a 1:1 mixture of aq. $NaHCO_3$ (0.1 M) and Et_2O and cooled on a dry ice bath until the aqueous phase froze. Fmoc-Cl (40 mg, 0.16 mmol) was added and the mixture was stirred at 4 ˚C for 24 h. TLC and ESI-MS showed disappearance of the starting materials.

Acetic anhydride (40 μL) was added and the mixture was stirred at 4 ˚C for 12 h. After removal of solvent under *vacuo*, the residue was purified by flash column chromatography ($CHCl_3$-MeOH-H_2O, 60:40:5, v/v/v) to give the crude product (164 mg, 84%).

ESI-MS: *m*/*z* $[C_{70}H_{106}N_3O_{32} - H]^-$ calcd: 1500.6, found: 1500.6; *m*/*z* $[C_{72}H_{110}N_3O_{32} - H]^-$ calcd: 1528.7, found: 1528.7.

Lyso-GM1 (4): *N*-Fmoc-lyso-GM_1 (164 mg, 0.11 mmol) was treated with sat. NH_4OH (5.0 mL) and stirred at r.t. for 6 h. TLC and ESI-MS showed complete conversion of the starting material. Upon removal of solvents under reduced pressure, the resultant residue was purified by flash column chromatography ($CHCl_3$-MeOH-2M ammonia, 60:40:5, v/v/v) to afford the pure product (60 mg, 43%).

ESI-MS: *m*/*z* $[C_{55}H_{96}N_3O_{30} - H]^-$ calcd: 1278.6, found: 1278.7; *m*/*z* $[C_{57}H_{100}N_3O_{30} - H]^-$ calcd: 1306.6, found: 1306.7.

Methyl 15-Hydroxypentadecanoate (5): To 5% H_2SO_4 in MeOH (20 mL) was added 15-pentadecanolide (2.0 g, 8.3 mmol). The reaction mixture was heated at reflux for 2 h, and then cooled to room temperature. Et_2O (50 mL) was added to the mixture and the organic layer was washed with H_2O (40 mL), sat. $NaHCO_3$ (2 × 20 mL), H_2O (2 × 20 mL), and brine (2 × 20 mL), then dried over anhyd. Na_2SO_4. Upon removal of solvent and drying under *vacuo*, the desired product was obtained as a white solid (2.2 g, 97%).

^{1}H NMR ($CDCl_3$, 500 MHz): δ = 3.67 (s, 3 H), 3.64 (t, *J* = 6.5 Hz, 2 H), 2.30 (t, *J* = 7.5 Hz, 2 H), 1.64-1.48 (m, 4 H), 1.25 (s, 20 H).

^{13}C NMR ($CDCl_3$, 125 MHz): δ = 174.32, 63.09, 51.40, 34.12, 32.82, 29.59, 29.55, 29.42, 29.23, 29.14, 25.73, 24.96.

Methyl 15-Oxopentadecanoate (6): A 250-mL round-bottomed flask was charged with methyl 15-hydroxypentadecanotate (1.0 g, 3.68 mmol) and anhyd. CH_2Cl_2 (200 mL). To this solution was added PDC (2.76 g, 7.34 mmol) with stirring at r.t., to give a dark-brown solution. The mixture was further stirred for 12 h, then the solvent was removed and the resultant residue was washed with EtOAc-hexane (10%, 200 mL). The organic layers were combined and the solvent removed. The residue was purified by flash column chromatography (EtOAc-hexane, 10%) to give the product as a white powder (0.57 g, 57%).

^{1}H NMR ($CDCl_3$, 500 MHz): δ = 9.76 (s, 1 H), 3.66 (s, 3 H), 2.42 (dt, *J* = 34, 7.5 Hz, 2 H), 2.30 (t, *J* = 7.5 Hz, 2 H), 1.62 (m, 4 H), 1.25 (s, 18 H).

^{13}C NMR ($CDCl_3$, 125 MHz): δ = 202.90, 174.35, 51.42, 43.91, 34.12, 33.66, 29.53, 29.39, 29.33, 29.23, 29.14, 29.03, 24.95, 24.70, 22.10.

Triphenyl(3,3,3-trifluoropropyl)phosphonium Iodide (7): To a solution of 3,3,3-trifluoropropyl iodide (348 mg, 1.55 mmol) in anhyd. acetonitrile (10 mL), Ph_3P (560 mg, 2.14 mmol) was added with stirring. The mixture was heated at reflux for 24 h. Solvent was removed and the residue was washed with Et_2O (3 × 10 mL). The solid residue was collected and dried under *vacuo* to give the pure product (495 mg, 65%).

^{1}H NMR ($CDCl_3$, 500 MHz): δ = 7.87 (m, 9 H), 7.74 (m, 6 H), 4.08 (m, 2 H), 2.65 (m, 2 H).

^{19}F NMR ($CDCl_3$, 470 MHz): δ = -68.73 (t, *J* = 7.0 Hz).

Methyl 18,18,18-Trifluorooctadec-15-enoate (8): Triphenyl(3,3,3-trifluoropropyl) phosphonium iodide (330 mg, 0.68 mmol) was suspended in anhyd. THF (3 mL). To this mixture was added *n*-BuLi (1.6 M in THF, 0.66 mL) at r.t. When the solids dissolved to give a brown solution, methyl 15-oxopentadecanoate **6** (164 mg, 0.61 mmol) in anhyd. THF (3 mL) was added at 0 ˚C. The mixture was allowed to reach r.t. and stirred for 36 h. The solvent was removed and the resultant residue was purified by flash column chromatography (EtOAc-hexane, 10%) to afford the pure product as a white powder (90 mg, 42%).

^{1}H NMR ($CDCl_3$, 500 MHz): δ = 5.70 (m, 1 H), 5.37 (m, 1 H), 3.66 (s, 3 H), 2.84 (m, 2 H), 2.29 (m, 2 H), 2.05 (t, *J* = 6.0 Hz, 2 H), 1.60 (m, 2 H), 1.37 (m, 2 H), 1.26 (s, 18 H).

^{13}C NMR ($CDCl_3$, 125 MHz): δ = 174.35, 132.13, 113.35, 118.14, 51.43, 43.12, 34.15, 33.68, 29.55, 29.41, 29.35, 29.25, 19.17, 29.05, 24.89, 24.75, 22.14.

Methyl 18,18,18-Trifluorooctadecanoate (9): To a solution of methyl 18,18,18-trifluorooctadec-15-enoate (90 mg, 0.26 mmol) in toluene (1.0 mL), was added 10% Pd/C (10 mg). The mixture was irradiated under H_2 gas in a microwave reactor (50 W) with stirring at 80 ˚C, for 1 h. The solvent was removed, and ^{1}H NMR confirmed that the hydrogenation was complete. The material was directly used in the hydrolysis reaction.

18,18,18-Trifluorostearic Acid (10): Methyl 18,18,18-trifluorooctadec-15-enoate obtained above was treated with KOH in MeOH (0.9 M, 1 mL) at r.t. for 1 h, then diluted with H_2O (3 mL) and acidified with 1 M HCl to pH 2. The solution was extracted with

Et_2O (3 × 5 mL), washed with H_2O (2 × 5 mL) and brine (2 × 5 mL), dried over anhyd. Na_2SO_4 and the solvent was removed under *vacuo*. The crude material was purified using flash column chromatography (EtOAc-hexane, 25%) to afford the pure product (72 mg, 83% over the two steps).

^{1}H NMR ($CDCl_3$, 500 MHz): δ = 2.38 (t, *J* = 8.0 Hz, 2 H), 2.08 (m, 2 H), 1.67 (m, 2 H), 1.36 (m, 2 H), 1.28 (s, 24 H).

^{13}C NMR ($CDCl_3$, 125 MHz): δ = 178.65, 127.32, 36.45, 33.84, 30.89, 29.62, 29.59, 29.53, 29.34, 29.17, 29.07, 28.79, 28.70, 24.37, 21.83.

N-Succinimidyl 18,18,18-Trifluorostearate (11): To a solution of *N*-hydroxysuccinimide (34.5 mg, 0.30 mmol) and 18,18,18-trifluorostearic acid (72 mg, 0.21 mmol) in anhyd. dioxane (5 mL), was added DCC (103 mg, 0.50 mmol) at r.t., and the mixture was stirred overnight to allow the completion of the reaction. The precipitate was removed by filtration and the solvent was evaporated. The residue was purified by flash column chromatography (EtOAc-hexane, 15%) to give the product as a white powder (68 mg, 73%).

^{1}H NMR ($CDCl_3$, 500 MHz): δ = 2.83 (s, 4 H), 2.60 (t, *J* = 8.0 Hz, 2 H), 2.06 (m, 2 H), 1.74 (m, 2 H), 1.54 (s, 4 H), 1.26 (s, 22 H).

^{13}C NMR ($CDCl_3$, 125 MHz): δ = 169.11, 168.67, 127.32, 33.85, 33.62, 30.96, 29.62, 29.59, 29.53, 29.34, 29.17, 29.07, 28.79, 28.70, 25.59, 24.58, 21.85.

^{19}F NMR ($CDCl_3$, 470 MHz): δ = -69.59 (t, *J* = 11.0 Hz).

18-F3-GM1 (12): To a solution of *N*-succinimidyl 18,18,18-trifluorostearate (18 mg, 41 μmol) and lyso-GM1 (27 mg, 21 μmol) in anhyd. DMF (2 mL), was added DIPEA (10 μL). The mixture was stirred at r.t. for 4 h, then the solvent was evaporated and the residue was purified using flash column chromatography ($CHCl_3$-MeOH-H_2O, 60:40:5, v/v/v) to give trifluoro-GM1 **12** as a white powder (28 mg, 63%).

^{1}H NMR ($CDCl_3$, 500 MHz) δ= 5.67 (d of t, 1H), 5.44 (d of d, 1H), 4.92, (d, 1H), 4.44 (d, 1H), 4.40 (d, 1H), 4.29 (d, 1H), 4.15 (b, 3H), 4.07 (m, 1H), 4.01 (m, 2H), 3.96 (m, 1H), 3.86 (m, 7H), 3.76 (m, 2H), 3.69 (m, 8H), 3.52 (m, 7H), 3.40 (m, 4H), 3.27 (m, 1H), 2.71 (m, 2H), 2.11 (m, 4H), 2.00 (m, 8H), 1.90 (t, 1H), 1.55 (m, 4H), 1.28 (m, 50H), 0.89 (m, 3H)

^{19}F NMR ($CDCl_3$, 470 MHz): δ = -67.81 (t, *J* = 11.2 Hz).

ESI-MS: *m*/*z* $[C_{73}H_{128}F_3N_3O_{31} - H]^-$ calcd: 1598.8, found: 1599.1; *m*/*z* $[C_{75}H_{132}F_3N_3O_{31} - H]^-$ calcd: 1626.8, found: 1627.1.

HRMS-ESI: *m*/*z* $[C_{73}H_{128}F_3N_3O_{31} + Na]^+$ calcd: 1622.8381, found: 1622.8344.

Methyl 18-(benzyloxy)octadec-15-enoate (13). The 3-benzyloxypropyl triphosphonium bromide (1.98 g, 4.0 mmol) was suspended in 20 ml dry THF and cooled to -78 °C, then added *n*-butyl lithium 3.6 ml (1.6M in hexane, 5.8 mmol). The mixture was allowed to reach r.t. and stirred for 20 min. Methyl Methyl 15-Oxopentadecanoate (1.0 g, 3.7 mmol) in 1 ml dry THF was added dropwise at -78 °C to give a dark red solution. The mixture was stirred at r.t. for 48 h. After the reaction was complete, methanol (2 ml) was added to quench the reaction. Solvent was removed under *vacuo*, residue was purified flash

column chromatography (EtOAc-hexane, 3%) to afford 480 mg product as a white solid with 33% yield.

^{1}H NMR ($CDCl_3$, 500MHz) δ= 7.35 (d, J=4.5 Hz, 4H), 7.28 (m, 1H), 5.46 (m, 1H), 5.40 (m, 1H), 4.53 (s, 2H), 3.67 (s, 3 H), 3.48 (t, J=7 Hz, 2H), 2.35 (m, 3H), 2.02 (m, 2H), 1.62 (m, 2.27H), 1.26 (s, 21H)

^{13}C NMR ($CDCl_3$, 125 MHz) δ= 174.30, 138.60, 132.69, 132.10, 128.33, 127.60, 127.48, 126.16, 125.37, 72.85, 70.33, 70.08, 51.39, 34.12, 33.10, 32.66, 29.64, 29.31,29.57, 29.46, 29.26, 29.17, 27.99, 27.36, 24.97

Methyl 18-hydroxyoctadecanoate (14). Methyl 18-(benzyloxy)octadec-15-enoate (480 mg, 1.2 mmol) was dissolved in toluene 10mL and added Pd/C 100 mg. The mixture was stirred under hydrogen gas at r.t. for 24 h. Pd/C was filtered out. Solvent was removed under *vacuo*, residue was purified by flash column chromatography (EtOAc-hexane, 10%) to afford 460 mg product with 96% yield.

^{1}H NMR ($CDCl_3$, 500 MHz) δ= 3.67 (s, 3H), 3.64 (t, J=7 Hz, 2H), 2.302 (t, J=7.5 Hz, 2H), 2.59 (m, 4. H), 1.25 (s, 28H)

^{13}C NMR ($CDCl_3$, 125 MHz) δ= 174.33, 63.07, 51.40, 34.12, 32.82, 29.64, 29.62, 29.60, 29.58, 29.43, 29.24, 29.15, 25.74, 24.96

Methyl 18-fluorooctadecanoate (15). Methyl 18-hydroxyoctadecanoate (460 mg, 1.2 mmol) was dissolved in dry THF and cooled to -78 °C. Diethylaminosulfur trifluoride (DAST, 280 mg, 1.75 mmol) was added dropwise. The mixture was stirred at -78 °C for 2 h and allowed to reach r.t. and stirred overnight. After the reaction was complete, methanol 2 ml was added to quench. Solvent was removed and residue was purified by

flash column chromatography (EtOAc-hexane, 5 %) to give 292 mg product with 77 % yield.

^{1}H NMR ($CDCl_3$, 500 MHz) δ= 4.44 (d of t, J_1=48 Hz, J_2=6 Hz, 2H), 3.67 (s, 3H), 2.30 (t, J=8 Hz, 2H), 1.66 (m, 4H), 1.25 (s, 30H)

^{13}C NMR ($CDCl_3$, 125 MHz) δ= 174.28, 84.83, 83.56, 51.37, 34.10, 31.57, 30.49, 30.33, 29.64, 29.62, 29.54, 29.44, 29.24, 29.15, 25.16, 25.12, 24.96, 22.63, 14.07

^{19}F NMR ($CDCl_3$, 470 MHz) δ= -218.4 (t of t, J_1=48 Hz, J_2=24 Hz)

18-fluorooctadecanoic acid (16). Methyl 18-fluorooctadecanoate (188 mg, 0.59 mmol) was treated with KOH in MeOH (2 M, 5 mL) and stirred at r.t. overnight. Solvent was evaporated. The residue was acidified with 1 M HCl to pH 2. The precipitate was collected by vacuum filtration and dried under *vacuo* and afforded 153 mg product (86%). The product was confirmed pure by NMR and directly used for next step.

^{1}H NMR ($CDCl_3$, 500 MHz) δ= 4.44 (d of t, J_1=47 Hz, J_2=7 Hz, 2H), 2.35 (t, J=8 Hz, 2H), 1.67 (m, 5H), 1.26 (s, 29H)

^{19}F NMR ($CDCl_3$, 470 MHz) δ= -218.4

N-succinimidyl 18-fluorostearate (17). Hydroxysuccinimide (75 mg, 0.65 mmol) and 18-fluorostearic acid (153 mg, 0.50 mmol) was dissolved in 5 ml anhydrous THF and added DCC (207 mg, 1.0 mmol) at 0 °C, then stirred at r.t. overnight. The precipitate was removed by filtration. Solvent was removed under *vacuo*, and residue was purified by flash column chromatography (EtOAc-hexane, 15 to 20%). The product was collected as a white powder, with a yield of 90 mg (45 %).

^{1}H NMR ($CDCl_3$, 500 MHz) δ= 4.44 (d of t, J_1=48 Hz, J_2=6 Hz, 2H), 2.83 (s, 4H), 2.60 (t, *J*=8 Hz, 2H), 1.70 (m, 4H), 1.39 (t, *J*=7 Hz, 4H), 1.26 (s, 21H)

^{13}C NMR ($CDCl_3$, 125 MHz) δ= 169.13, 168.67, 84.88, 83.58, 30.95, 30.49, 30.34, 29.64, 29.61, 29.54, 29.51, 29.34, 29.24, 29.08, 28.79, 25.59, 25.16, 25.12, 24.58

^{19}F NMR ($CDCl_3$, 470 MHz) δ= -218.4

18-F-GM1 (18). N-succinimidyl 18-trifluorostearate (35 mg, 87 μmol) and lysoGM1 **4** (60 mg, 48 μmol) was suspended in 8 ml dry DMF and added 10 μl diisopropylethyl amine. The mixture was stirred at r.t. for 12 h. Solvent was removed under *vacuo* and residue was purified using flash column chromatography ($CHCl_3$-MeOH-H_2O, 60:40:5, v/v/v) to give 18-fluoro-GM1 as a white powder (38 mg, 52%).

ESI-MS: *m*/*z* $[C_{73}H_{130}FN_3O_{31}\text{-}H]^-$ calcd: 1562.9, found: 1562.6; *m*/*z* $[C_{75}H_{134}FN_3O_{31}\text{-}H]^-$ calcd: 1590.9, found: 1590.6.

HRMS-ESI: *m*/*z* $[C_{73}H_{130}FN_3O_{31}+Na]^+$ calcd: 1586.8565, found: 1586.8460; *m*/*z* $[C_{75}H_{134}FN_3O_{31}+Na]^+$ calcd: 1614.8883, found: 1614.8820.

^{1}H NMR ($CDCl_3$, 500 MHz) δ= 5.68 (d of t, 1H), 5.44 (d of d, 1H), 4.92 (d, 1H), 4.45 (d, 1H), 4.41 (d, 1H), 4.35 (t, 1H), 4.29 (d, 1H), 4.19 (d, 1H), 4.15 (s, 1H), 4.07 (t, 1H), 4.00 (s, 2H), 3.97 (m, 1H), 3.87 (m, 5H), 3.76 (m, 2H), 3.69 (m, 6H), 3.53 (m, 5H), 3.40 (m, 3H), 3.27 (s, 1H), 2.74 (m, 1H), 2.17 (t, 1H), 2.00 (s, 3H), 1.99 (s, 3H), 1.91 (t, 1H), 1.69 (m, 2H), 1.57 (b, 2H), 1.38 (b, 3H), 1.29 (b, 35H), 0.90 (t, 3H)

^{19}F NMR ($CDCl_3$, 470 MHz) δ= -218.4 (m)

Methyl 12-hydroxyloctadecanoate (19). The 12-hydroxyloctadecanoic acid (0.60 g, 2.0 mmol) was treated with Dovex-H^+ (100 mg) in 10 ml anhydrous methanol. After the reaction was complete, Dovex-H^+ resin were filtered, and solvent was removed under *vacuo*. The product was directly used for the next step.

^{1}H NMR ($CDCl_3$, 500 MHz) δ = 3.66 (s, 3H), 3.58 (s, 1H), 2.30 (m, 2H), 2.02 (s, 1H), 1.61 (m, 2H), 1.42 (m, 4H), 1.27 (b, 22H), 0.88 (t, 3H)

^{13}C NMR ($CDCl_3$, 125 MHz) δ = 174.34, 72.07, 51.41, 37.49, 37.47, 31.11, 31.84, 29.68, 29.57, 29.49, 29.40, 29.37, 29.22, 29.13, 25.63, 25.61, 24.95, 22.61, 14.06

Methyl 12-fluorooctadecanoate (20). Methyl 12-hydroxyloctadecanoate obtained above was dissolved in 30 mL dry THF and cooled down to -78 °C. DAST (0.36g, 2.2 mmol) was added dropwise at the same temperature. The mixture was stirred at -78 °C for 2 h and allowed to reach r.t. for 12 h. Methanol 5 ml was added to quench the reaction. Solvent was removed under *vacuo* and residue was purified by flash column chromatography (EtOAc-hexane, 5 %) to give 310 mg product with 52 % yield for 2 steps.

^{1}H NMR ($CDCl_3$, 500 MHz) δ= 4.45 (m, 1H), 3.67 (s, 3H), 2.30 (t, 2H, J = 8 Hz), 1.62 (m, 4H), 1.53 (m, 2H), 1.46 (m, 2H), 1.28 (b, 20H), 0.89 (t, 3H)

^{13}C NMR ($CDCl_3$, 125 MHz) δ= 174.31, 94.59 (d, J = 33 Hz), 51.41, 35.26, 35.09, 34.11, 31.75, 29.50, 29.40, 29.23, 29.18, 29.14, 25.14, 25.11, 25.08, 24.95, 22.58, 14.05

^{19}F NMR ($CDCl_3$, 470 MHz) δ= -180.46

12-fluorooctadecanoic acid (21). Methyl 12-fluorooctadecanoate (250 mg, 0.79 mmol) was treated with KOH in MeOH (2 M, 5 mL) and stirred at r.t. overnight. Solvent was evaporated. The residue was acidified with 1 M HCl to pH 2. The precipitate was collected by vacuum filtration and dried under *vacuo* and afforded 225 mg product (94 %). The product was confirmed pure by NMR and directly used for next step.

^{1}H NMR ($CDCl_3$, 500 MHz) δ= 4.45 (m, 1H), 2.35 (t, 2H), 1.7-1.4 (m, 8H), 1.28 (b, 20H), 0.89 (t, 3H)

^{13}C NMR ($CDCl_3$, 125 MHz) δ= 179.37, 94.61, 35.26, 35.10, 33.92, 31.75, 29.49, 29.38, 29.21, 29.18, 29.05, 25.14, 25.11, 25.08, 24.68, 22.58, 14.05

^{19}F NMR ($CDCl_3$, 470 MHz) δ= -180.40

N-succinimidyl 12-fluorooctadecanoate (22). Hydroxysuccinimide (123 mg, 1.07 mmol) and 12-fluorooctadecanoic acid (215 mg, 0.71 mmol) was dissolved in 2 ml anhydrous THF and added DCC (293 mg, 1.42 mmol) at 0 °C, then stirred at r.t. overnight. The precipitate was filtered. Solvent was removed under *vacuo*, and residue was purified by flash column chromatography (EtOAc-hexane, 15 to 20%). The product was collected as a white powder, with a yield of 225 mg (79 %).

^{1}H NMR ($CDCl_3$, 500 MHz) δ = 4.55-4.37 (m, 1H), 2.83 (s, 4H), 2.60 (m, 2H), 1.75 (m, 2H), 1.60 (m, 2H), 1.52-1.37 (m, 6H), 1.28 (b, 18H), 0.89 (t, 3H)

^{13}C NMR ($CDCl_3$, 125 MHz) δ = 169.13, 168.67, 94.61, 35.26, 35.10, 31.75, 30.95, 29.49, 29.47, 29.42, 29.30, 29.18, 29.05, 28.77, 25.60, 25.11, 24.58, 22.58, 14.05

^{19}F NMR ($CDCl_3$, 470 MHz) δ = -180.42

12-F-GM1 (23). N-succinimidyl 12-fluoroctadecanoate (20 mg, 50 μmol) and lysoGM1 **4** (32 mg, 25 μmol) was suspended in 0.5 ml dry DMF and added 10 ml diisopropylethyl amine. The mixture was stirred at r.t. for 12 hrs. Solvent was removed under *vacuo* and residue was purified using flash column chromatography ($CHCl_3$-MeOH-H_2O, 60:40:5, v/v/v) to give 12-F-GM1 as a white powder (18 mg, 35%).

1H-NMR (CD_3OD, 500MHz) δ= 5.68 (d of t, 1H), 5.44 (d of d, 1H), 4.92 (d, 1H), 4.55-4.37 (m, CHF, 1H), 4.44 (d, 1H), 4.42 (d, 1H), 4.29 (d, 1H), 4.18 (m, 3H), 4.04 (t, 1H), 4.01 (t, 2H), 3.39 (m, 1H), 3.87 (m, 6H), 3.77 (m, 2H), 3.71 (t, 3H), 3.68 (m, 3H), 3.53 (m, 7H), 3.41 (m, 4H), 3.34 (d, 1H), 3.27 (m, 1H), 2.73 (m, 1H), 2.17 (t, 2H), 2.01 (s, 3H), 1.99 (s, 3H), 1.91 (t, 1H), 1.57 (m, 5H), 1.46 (m, 3H), 1.31 (b, 46H), 0.90 (m, 6H)

^{19}F NMR ($CDCl_3$, 470 MHz) δ= -182.045, -182.052

ESI-MS: *m/z* $[C_{73}H_{130}FN_3O_{31} + H]^+$ calcd: 1564.9, found: 1565.0; *m/z* $[C_{75}H_{134}FN_3O_{31} + H]^+$ calcd: 1592.9, found: 1593.0.

HRMS-ESI: *m/z* $[C_{73}H_{130}FN_3O_{31} + Na]^+$ calcd: 1586.8565, found: 1586.8490; *m/z* $[C_{75}H_{134}FN_3O_{31} + Na]^+$ calcd: 1614.8878, found: 1614.8793.

C6F13-GM1 (24). LysoGM1 **4** (120 mg, 94 μmol) and NHS activated C6F13-containing stearic acid (83 mg, 141μmol) were suspended in 5 ml dry DMF, and added DIEA 0.10 ml at 0 °C to give a clear solution. The mixture was stirred at r.t. overnight. Solvent was removed under *vacuo*. The residue was purified by flash column chromatography ($CHCl_3$-MeOH-H_2O, 60:40:5, v/v/v) to give 110 mg (67%) of pure product.

1H-NMR (CD_3OD, 500MHz) δ= 5.68 (d of t, 1H), 5.44 (d of d, 1H), 4.92 (d, 1H), 4.59 (s, 0.5H), 4.44 (d, 1H), 4.41 (d, 1H), 4.29 (d, 1H), 4.42 (s, 0.5H), 4.15 (m, 2H), 4.07 (t, 1H), 4.00 (s, 2H), 3.96 (m, 1H), 3.89 (m, 3H), 3.83 (m, 3H), 3.76 (m, 2H), 3.68 (m, 6H), 3.53 (m, 7H), 3.40 (m, 3H), 3.35 (s, 3H), 2.71 (m, 1H), 2.67 (s, 1H), 2.17 (t, 2H), 2.10 (m, 1H), 2.00 (s, 3H), 1.99 (s, 3H), 1.91 (t, 1H), 1.58 (m, 3H), 1.28 (b, 30 H), 0.90 (t, 3H)

^{19}F NMR ($CDCl_3$, 470 MHz) δ = -82.88, -115.83, -123.43, -124.38, -124.98, -127.80

ESI-MS: *m/z* $[C_{71}H_{114}F_{13}N_3O_{31} - H]^-$ calcd: 1750.7, found: 1750.5; *m/z* $[C_{73}H_{118}F_{13}N_3O_{31} - H]^-$ calcd: 1778.8, found: 1778.6.

HRMS-ESI: *m/z* $[C_{71}H_{114}F_{13}N_3O_{31} + Na]^+$ calcd: 1774.7121, found: 1774.7063; *m/z* $[C_{73}H_{118}F_{13}N_3O_{31} + Na]^+$ calcd: 1802.7439, found: 1802.7372.

9,9,10,10,11,11,12,12,13,13,14,14,14-tridecafluorotetradec-1-ene (25). Octadiene (4.4 g, 0.4 mol) and tridecafluorohexyl iodide (8.8 g, 0.2 mol) were mixed with AIBN (0.2 g, 1.2 mmol) in a thick-walled flask and purged with argon and heated at 70°C for 24 h. The mixture was then transferred to a round bottom flask charged with 40 mL glacial acetic acid and 4.0 g zinc powder and stirred at rt for 24 h. Zinc powder was removed through celite. Solvent was removed under *vacuo* and residue was distilled under reduced pressure. The crude product was collected between 45-55°C and further purified through flash column chromatography with pentane to give a colorless liquid (4.1g, 30%).

^1H NMR ($CDCl_3$, 500 MHz): δ = 5.80 (m, 1H), 4.98 (m, 2H), 2.04 (m, 4H), 1.61 (m, 2H), 1.41 (m. 6H)

^{13}C NMR ($CDCl_3$, 125 MHz): δ = 138.80, 118.46, 117.24, 114.42, 111.11, 110.30, 108.59, 108.43, 33.60, 30.89, 28.94, 28.64, 28.60, 20.06

^{19}F NMR ($CDCl_3$, 470 MHz): δ = -81.26, -114.87, -122.43, -123.36, -124.05, -126.61

9,9,10,10,11,11,12,12,13,13,14,14,14-tridecafluorotetradecan-1-ol (26): Tridecafluorotetradec-1-ene **25** (4.0 g, 9.3 mmol) was dissolved in 50 mL ah. THF and cooled to 0 °C. Borane in THF (1.03 M, 3.1 mL, 3.1 mmol) was added dropwise and the reaction was allowed to warm up to r.t. and stirred for 2 h. The mixture was cooled to 0°C again and added MeOH 5 mL, NaOH (20%) 5 mL and H_2O_2 (30%) 5 mL. The mixture was stirred at r.t. for 2 h and acidified with 1 M HCl to pH 3~4 and diluted with water, then extracted with ether (30 mL × 3), washed with water, brine, dried on ah. Na_2SO_4. After removal of the solvent, the residue was purified through flash column chromatography (EtOAc-Hexane 5% to 15% to 20%) to afford the pure product as a colorless liquid (2.65g, 64%).

^{1}H NMR ($CDCl_3$, 500 MHz): δ = 3.64 (q, 2H), 2.05 (m, 2H), 1.59 (m, 4H), 1.35 (b, 8H)

^{13}C NMR ($CDCl_3$, 125 MHz): δ = 118.46, 117.22, 111.11, 110.29, 108.58, 108.42, 62.97, 32.70, 30.87, 29.16, 29.14, 29.02, 25.64, 20.07

^{19}F NMR ($CDCl_3$, 470 MHz): δ = -81.25 (t), -114.87 (t), -122.43 (s), -123.37 (s), -124.05 (s), -126.62 (s)

14-bromo-1,1,1,2,2,3,3,4,4,5,5,6,6-tridecafluorotetradecane (27). Tridecafluorotetradecanol (1.54 g, 3.44 mmol) and red phosphorus (200 mg, 6.45 mmol) was suspended in 25 mL dry dichloromethane and added bromine (1.0 g, 6.25 mmol) dropwise at 0 °C. The

mixture was allowed to stir at r.t. for 24 h. The reaction was quenched with aq. Na_2CO_3 (1 M, 5 mL), extracted with ether (30 mL× 3), washed with water, brine, dried on ah. Na_2SO_4. After solvent removed, the residue was purified through flash column chromatography with hexane to give the pure product as a colorless liquid (0.82 g, 47%).

^{1}H NMR ($CDCl_3$, 500 MHz): δ = 3.41 (t, 2H, *J* = 6.8 Hz), 2.05 (m, 2H), 1.86 (m, 2H), 1.60 (m, 2H), 1.35 (m, 8H)

^{13}C NMR ($CDCl_3$, 125 MHz): δ = 118.44, 117.23, 111.11, 110.23, 108.56, 108.42, 33.80, 32.71, 30.88, 29.02, 28.98, 28.49, 28.04, 20.07

^{19}F NMR ($CDCl_3$, 470 MHz): δ = -81.25, -114.87, -122.42, -123.36, -124.04, -126.62

9,9,10,10,11,11,12,12,13,13,14,14,14-tridecafluorotetradecanyl triphenylphosphorium bromide (28). Tridecafluorotetradecanyl bromide **27** (0.82g, 1.60 mmol) and triphenylphosphine (1.40g, 5.34mmol) were dissolved in 50 mL dry acetonitrile and heated at reflux for 24 h. Solvent was removed under *vacuo* and residue was washed with dry ether (15 mL × 3) to give pure product as a white solid (0.92 g, 74%).

^{1}H NMR ($CDCl_3$, 500 MHz): δ = 7.87 (m, 6H), 7.79 (m, 3H), 7.70 (m, 6H), 3.91 (t, 2H), 2.00 (m, 2H), 1.67 (m, 4H), 1.53 (m, 2H), 1.28 (m, 6H)

^{13}C NMR ($CDCl_3$, 125 MHz): δ = 134.87, 133.75, 130.42, 128.50, 118.96, 118.28, 30.29, 30.16, 28.96, 28.90, 28.79, 22.69

^{19}F NMR ($CDCl_3$, 470 MHz): δ = -81.25 (t), -114.87 (m), -122.42 (s), -123.36(s), -124.04(s), -126.61 (m)

C6F13-GM1-CHO (29). C6F13-GM1 **24** (250 mg, 0.14 mmol) was dissolved in $CHCl_3$/MeOH (1:1) 30 mL and cooled to -78°C. The solution was bubbled with ozone for 10 min to give a blue solution, followed by oxygen bubbling to remove the remaining ozone until blue color disappeared completely. Triphenylphosphine (370 mg, 1.4 mmol) was added and stirred at r.t. for 48 h. Solvent was removed under *vacuo*. The residue was purified by flash chromatography ($CHCl_3$-MeOH-H_2O, 60:40:9) to give 160 mg product with 71% yield.

^{19}F NMR ($CDCl_3$, 470 MHz) δ = - -81.25, -114.85, -122.41, -123.36, -124.03, -126.61

ESI-MS: *m*/*z* $[C_{57}H_{86}F_{13}N_3O_{32} - H]^-$ calcd: 1570.5, found: 1569.1

HRMS-ESI: *m*/*z* $[C_{57}H_{86}F_{13}N_3O_{32} + Na]^+$ calcd: 1594.4879, found: 1594.4804

C6F13-GM1-CHO Peracetate (30). C6F13-GM1 aldehyde **29** (35 mg, 22 μmol) was dissolved in 20 mL 25% acetic anhydride in pyridine and stirred at r.t. for 24 h. Solvent was removed under *vacuo* and residue was purified by preparative TLC plate with ethyl acetate. The yield was 35 mg (77%).

^{19}F NMR ($CDCl_3$, 470 MHz) δ = -81.24, -114.86, -122.41, -123.35, -124.03, -126.59

ESI-MS: *m*/*z* $[C_{89}H_{11}8F_{13}N_3O_{48} - H]^-$ calcd: 2242.7, found: 2242.0

Di-C6F13-GM1 (31). Tridecafluorotetradecanyl triphenylphosphorium bromide **28** (80 mg, 100 μmol) was suspended in 5 mL freshly dried THF and added nBuLi (1.6 M, 200 μL, 280 μmol) dropwise at -78 °C, then stirred at r.t. for 0.5 h. C6F13-GM1-CHO Peracetate **30** (35 mg, 15 μmol) was added at -78 °C and the mixture was stirred at r.t.

for 48 h. The mixture was quenched with 1 mL MeOH for 2 h. Solvent was removed under *vacuo*. The residue was purified through flash column chromatography ($CHCl_3$-MeOH-H_2O 60:40:5 v/v/v) to give 6 mg product with 20% yield. However, the product still contained trace amount of C6F13-GM1, which will be further purified through Fluorous SPE cartridge.

FPE cartridge purification. The new FPE cartridge was rinsed with 2 mL DMF and then washed with 10 mL MeOH/H2O (80%) and 10 mL MeOH/H2O (20%). Di-C6F13GM1 crude mixture was loaded to column with 0.5 mL DMF then washed with 10 mL 20% MeOH/H_2O to elute all non-fluorous compounds. The column was then washed with 80% MeOH/H_2O 10 mL to elute C6F13-GM1, and finally MeOH 10 mL to get Di-C6F13-GM1. The Di-C6F13-GM1 was obtained as a whit solid of 4 mg (67% recovery).

^{19}F NMR ($CDCl_3$, 470 MHz) δ = --82.90, -115.83, -123.42, -124.38, -124.99, -127.80

ESI-MS: *m*/*z* $[C_{71}H_{101}N_3O_{31}F_{26} - H]^-$ calcd: 1984.6, found: 1984.2

HRMS-ESI: *m*/*z* $[C_{71}H_{101}N_3O_{31}F_{26} + Na]^+$ calcd: 2008.5896, found: 2008.5879

Methyl 6-hydroxy-hexnoate (32). Caprolactone (5.0 g, 44 mmol) was dissolved in 40 mL dry methanol and added sulfuric acid 2.5 mL dropwise. The solution was heated at reflux for 2 h and cooled to rt. Ether 70 mL was added to the mixture and washed with brine, sat. $NaHCO_3$, brine, and dried over dry Na_2SO_4. Solvent was removed under *vacuo* to give 4.5 g of product as a colorless oil (70% yield), which was used directly in the next step.

^{1}H NMR ($CDCl_3$, 500 MHz): δ = 3.68 (s, 3H), 3.65 (t, 2H), 2.24 (t, 2H), 1.65 (m, 4H), 1.40 (m, 2H)

Methyl 6-oxohexanoate (33). Methyl 6-hydroxy-hexnoate (2.0 g, 13.7 mmol) was dissolved in 150 mL of dry dichloromethane and added pyridium dichromate (10.2 g, 27.1 mmol) and stirred at r.t. for 24 h. The solid was removed by centrifugation and solvent removed under *vacuo*. The residue was purified by flash column chromatography (EtOAc-Hexane 15%) to give 1.12 g pure product (yield of 56%) as colorless oil.

^{1}H NMR ($CDCl_3$, 500 MHz): δ = 9.77 (s, 1H), 3.67 (s, 3H), 2.47 (t, 2H), 2.35 (t, 2H), 1.67 (m, 4H)

^{13}C NMR ($CDCl_3$, 125 MHz): δ = 202.17, 173.88, 51.77, 43.71, 33.91, 24.59, 21.75

3,3,4,4,5,5,6,6,7,7,8,8,8-tridecafluorooctyl triphenylphosphium iodide (34). 3,3,4,4,5,5,6,6,7,7,8,8,8-tridecafluorooctyl iodide (0.95 g, 2.0 mmol) and triphenylphosphine (1.05 g, 4.0 mmol) was dissolved in 15 mL dry acetonitrile and heated at reflex for 24 h. Solvent was removed under *vacuo* and residue was washed with dry ether (10 mL × 3) to give pure product 0.76 g (38% yield), which was used directly for next step.

^{1}H NMR ($CDCl_3$, 500 MHz): δ = 7.89 (m, 9H), 7.76 (m, 6H), 4.14 (m, 2H), 2.59 (m, 2H)

^{13}C NMR ($CDCl_3$, 125 MHz) δ = 137.46, 137.37, 135.90, 135.88, 134.11, 134.03, 133.99, 133.84, 131.09, 130.99, 128.88, 128.69, 128.63, 117.40, 116.70, 24.94, 16.46

^{19}F NMR ($CDCl_3$, 470 MHz) δ = -80.78, -114.24, -121.91, -122.84, -123.53, -126.11

Methyl 9,9,10,10,11,11,12,12,13,13,14,14,14-tridecafluorotetradec-6-enoate (35). Tridecafluorooctyl triphenylphosphium iodide **34** (0.74 g, 1.0 mmol) was dissolved in 20 mL dry THF and added *n*-BuLi in hexane (1.6M, 0.62 mL, 2.0 mmol) dropwise at -78 °C. The mixture was stirred for 20 min at r.t. to give a dark red solution and added methyl 6-oxohexanoate **33** (158 mg, 1.1 mmol) and stirred at r.t. for 48 h. The mixture was quenched with methanol (2 ml). Solvent was removed under *vacuo* and residue was purified by flash column chromatography (EtOAc-hexane 2.5%) to give 235 mg of product (50% yield) as a colorless oil.

^{1}H NMR ($CDCl_3$, 500 MHz): δ = 5.74 (m, 1H), 5.43 (m, 1H), 3.67 (s, 3H), 2.54 (d of t, 2H), 2.32 (t, 2H), 2.09 (t, 2H), 1.65 (m, 2H), 1.42 (m, 2H)

^{13}C NMR ($CDCl_3$, 125 MHz): δ = 173.92, 136.54, 115.97, 51.45, 33.83, 29.46, 28.58, 27.04, 24.45

^{19}F NMR ($CDCl_3$, 470 MHz): δ = -81.27, -113.61, -122.43, -123.37, -123.57, -126.63

Methyl 9,9,10,10,11,11,12,12,13,13,14,14,14-tridecafluorotetradecanoate (36). Methyl tridecafluorotetradec-6-enoate **35** (235 mg, 0.49 mmol) was dissolved in 15 mL toluene and added Pd/C 50 mg. The solution was purged with H_2 gas and irrigated with microwave (80 °C, 250 Watts) under H_2 gas for 2 h. Solvent was removed under *vacuo* and residue was filtered through a short silica gel column to give 217 mg pure product (92%) as colorless oil.

^{1}H NMR ($CDCl_3$, 500 MHz): δ = 3.67 (s, 3H), 2.31 (m, 2H), 2.05 (m, 2H), 1.62 (m, 4H), 1.35 (b, 6H)

^{13}C NMR ($CDCl_3$, 125 MHz): δ = 174.36, 51.67, 34.22, 31.11, 29.11, 29.07, 25.02, 20.28

^{19}F NMR ($CDCl_3$, 470 MHz): δ = -81.27, -114.87, -122.43, -123.36, -124.49, -126.61

9,9,10,10,11,11,12,12,13,13,14,14,14-tridecafluorotetradecanal (37). Methyl tridecafluorotetradecanoate **36** (217 mg, 0.46 mmol) was dissolved in 10 mL dry toluene and cooled to -78 °C. DIBAL (1.2M in toluene, 0.53 ml, 0.64 mmol) was added dropwise and stirred at -78 °C for 10 min. The mixture was quenched with 2 ml methanol. Sodium hydroxide (1 M, 5 mL) was added to give a clear solution. The solution was extracted with ether (10 ml × 3) and washed with brine, dried on dry sodium sulfate. Solvent was removed under *vacuo* and residue was purified by flash column chromatography (EtOAc-hexane 10%) to give 182 mg product (88% yield) as colorless oil.

^{1}H NMR ($CDCl_3$, 500 MHz): δ = 9.77 (s, 1H), 2.44 (m, 2H), 2.05 (m, 2H), 1.63 (m, 4H), 1.36 (b, 6H)

^{13}C NMR ($CDCl_3$, 125 MHz): δ = 202.72, 44.04, 31.11, 29.20, 29.11, 22.16, 20.30

^{19}F NMR ($CDCl_3$, 470 MHz): δ = -81.26, -114.88, -122.43, -123.37, -124.05, -126.61

(*E*)-11,11,12,12,13,13,14,14,15,15,16,16,16-tridecafluorohexadec-2-ene (38). Ethyl triphenylphosphium (257 mg, 0.61 mmol) was suspended in 8 ml dry THF and cooled to -78 °C. *N*-butyl lithium in hexane (1.6 M, 0.44 mL, 0.7 mmol) was added dropwise and stirred at r.t. for 20 min to give a dark red solution. Then 9,9,10,10,11,11,12,12,13,13,14,14,14-tridecafluorotetradecanal **37** (182 mg, 0.41 mmol) in 2 ml dry THF was added dropwise at -78 °C and the mixture was stirred at r.t. for 48 h. Methanol 2 ml was added to quench the reaction. Diethyl ether 10 mL was added into the

mixture, and washed with water and brine, dried on sodium sulfate. Solvent was removed under *vacuo* and residue was purified by flash column chromatography with hexane to give 103 mg product (52% yield) as a colorless oil.

^{1}H NMR ($CDCl_3$, 500 MHz): δ = 5.41 (m, 2H), 2.03 (m, 4H), 1.61 (m, 5H), 1.33 (b, 8H)

^{13}C NMR ($CDCl_3$, 125 MHz): δ = 131.67, 130.88, 124.98, 124.03, 32.71, 31.14, 29.66, 29.31, 26.97, 20.32, 18.10, 12.94

^{19}F NMR ($CDCl_3$, 470 MHz): δ = -81.26, -114.88, -122.43, -123.37, -124.06, -126.61

Truncated C6F13-GM1 (39). C6F13-GM1 **24** (1.0 mg, 0.57 μmol) and Grubbs-Hoveyda catalyst 2nd generation 1.0 mg was dissolved in 1 mL methanol-toluene (1:1) and purged with cis-2-butene gas until saturation. The mixture was irrigated with microwave under cis-2-butene (40 °C, 10 Watts, 200 psi) for 2 h. Truncated C6F13-GM1 **39** was confirmed by ESI-MS as a major product.

Di-C6F13-GM1 (31, by olefin metathesis**)**: Truncated C6F13-GM1 **39** (1.0 mg, 0.63 μmol) and Grubbs-Hoveyda II catalyst 1.0 mg was dissolved in 1 mL methanol/toluene (1:1), then added C6F13-olefin **38** (1.0 mg, 2.2 μmol). The mixture was irrigated with microwave (40 °C, 10 Watts, 200 psi) for 12 h. Di-C6F13-GM1 was confirmed by MALDI-TOF as a major product. However, a by-product with an additional CH_2 group was observed and it was proven impossible to avoid in the reaction or purified after the reaction.

2.5 Conclusions

The lipid rafts model has been widely accepted to describe the formation of microdomains on the plasma membranes. However, the investigation of lipid rafts is asking for breakthrough in detecting probes and technologies. We have developed a new method to study lipid interactions and dynamic behavior of lipid molecules in the membrane, by using a fluorinated ganglioside GM1 marker to increase the sensitivity in SIMS profile.

The ganglioside GM1 was derived from bovine brain tissues by modified purification procedure of extraction and flash column chromatography, and gram scale of GM1 for synthetic labeling. The modification of fluorinated GM1 focused on the fatty acid chain and sphingosine chain in order to avoid disturbing hydrophilicity of oligosaccharide and self-assembly of GM1. The amide bond of fatty acid chain was cleaved by alkaline hydrolysis followed by selective protection and deprotection to expose only one free amine for coupling. Coupling of NHS activated F-stearic acid with lyso-GM1 readily produced a series of F-GM1 analogues. The steric difference between oligosaccharide and sphingosine was employed to obtain the selectivity in Fmoc protection. Direct coupling of NHS activated stearic acid (or F-stearic acid) to DeAc-lysoGM1 exhibited similar selectivity as Fmoc and yielded more coupling product on the sphinosine amine position than on the sialic acid. The data is not shown here, but the synthetic route to modify the fatty acid chain could be further improved. To make the terminal fluorinated stearic acid, Wittig coupling has been proven the best way for hydrocarbon chain elongation, whereas Grignard reaction failed to conjugate terminal fluorocarbon chain with protected fatty acid analogues. Availability of 12-hydroxystearic

acid made fluorination of stearic acid convenient. The 12-F-GM1 has undefined stereochemistry on the fluorocarbon due to the racemic starting material, but this will not interfere with the patterning of lipid rafts and the product was still useful for activity assay.

The perfluorocarbon substitution of the fatty acid chain on GM1 was achieved by hydrolysis and selectively protection followed by coupling with NHS activated perfluorocarbon substituted fatty acid. The modification of the sphingosine chain was firstly accomplished by Wittig coupling following ozonolysis cleavage of the double bond. The protection for hydroxyl groups was proven essential for wittig coupling under anhydrous condition, which can be easily uncapped by methanol quench in the workup step under basic condition. Purification of Di-C6F13-GM1 from C6F13-GM1 became convenient by using fluorous phase cartridge depending on the fluorous phase affinity. This was the first reported modification of GM1 on the sphingosine chain and will lead to more different labeled gangliosides possible for function and activity studies.

2.6 References

(1) Simons, K.; Ikonen, E., Functional rafts in cell membranes. *Nature* **1997**, *387*, 569-572.
(2) Lichtenberg, D.; Goni, F. M.; Heerklotz, H., Detergent-resistant membranes should not be identified with membrane rafts. *Trends Biochem. Sci.* **2005**, *30*, 430-6.
(3) Kenworthy, A. K., Have we become overly reliant on lipid rafts? Talking Point on the involvement of lipid rafts in T-cell activation. *EMBO Rep.* **2008**, *9*, 531-5.
(4) Munro, S., Lipid rafts: Elusive or illusive? *Cell* **2003**, *115*, 377-388.
(5) Hancock, J. F., Lipid rafts: contentious only from simplistic standpoints. *Nat. Rev. Mol. Cell Biol.* **2006**, *7*, 456-462.
(6) Huang, B.; Babcock, H.; Zhuang, X., Breaking the diffraction barrier: super-resolution imaging of cells. *Cell* **2010**, *143*, 1047-58.
(7) Rust, M. J.; Bates, M.; Zhuang, X. W., Sub-diffraction-limit imaging by stochastic optical reconstruction microscopy (STORM). *Nat. Methods* **2006**, *3*, 793-795.
(8) Eggeling, C.; Ringemann, C.; Medda, R.; Schwarzmann, G.; Sandhoff, K.; Polyakova, S.; Belov, V. N.; Hein, B.; von Middendorff, C.; Schonle, A.; Hell, S. W., Direct observation of the nanoscale dynamics of membrane lipids in a living cell. *Nature* **2009**, *457*, 1159-62.
(9) Lingwood, D.; Simons, K., Lipid rafts as a membrane-organizing principle. *Science* **2010**, *327*, 46-50.
(10) Parton, R. G.; Molero, J. C.; Floetenmeyer, M.; Green, K. M.; James, D. E., Characterization of a distinct plasma membrane macrodomain in differentiated adipocytes. *J. Biol. Chem.* **2002**, *277*, 46769-46778.
(11) Schiavo, G.; Deinhardt, K.; Berninghausen, O.; Willison, H. J.; Hopkins, C. R., Tetanus toxin is internalized by a sequential clathrin-dependent mechanism initiated within lipid microdomains and independent of epsin 1. *J. Cell Biol.* **2006**, *174*, 459-471.
(12) Overkleeft, H. S.; Wennekes, T.; van den Berg, R. J. B. H. N.; Boot, R. G.; van der Marel, G. A.; Aerts, J. M. F. G., Glycosphingolipids-Nature, Function, and Pharmacological Modulation. *Angew. Chem., Int. Ed.* **2009**, *48*, 8848-8869.
(13) Zeller, C. B.; Marchase, R. B., Gangliosides as Modulators of Cell-Function. *Am. J. Physiol.* **1992**, *262*, C1341-C1355.
(14) Nobileorazio, E.; Carpo, M.; Meucci, N.; Grassi, M. P.; Capitani, E.; Sciacco, M.; Mangoni, A.; Scarlato, G., Guillain-Barre-Syndrome Associated with High Titers of Anti-Gm1 Antibodies. *Journal of the Neurological Sciences* **1992**, *109*, 200-206.
(15) Kaida, K.; Morita, D.; Kanzaki, M.; Kamakura, K.; Motoyoshi, K.; Hirakawa, M.; Kusunoki, S., Ganglioside complexes as new target antigens in Guillain-Barre syndrome. *Ann Neurol* **2004**, *56*, 567-71.
(16) Rajendran, L.; Schneider, A.; Schlechtingen, G.; Weidlich, S.; Ries, J.; Braxmeier, T.; Schwille, P.; Schulz, J. B.; Schroeder, C.; Simons, M.; Jennings, G.; Knolker, H. J.; Simons, K., Efficient inhibition of the Alzheimer's disease beta-secretase by membrane targeting. *Science* **2008**, *320*, 520-3.
(17) Schneider, J. S.; Sendek, S.; Daskalakis, C.; Cambi, F., GM1 ganglioside in Parkinson's disease: Results of a five year open study. *Journal of the Neurological Sciences* **2010**, *292*, 45-51.

(18) Vanheyni.S, Cholera Toxin - Interaction of Subunits with Ganglioside Gm1. *Science* **1974**, *183*, 656-657.
(19) Niebroj-Dobosz, I.; Janik, P.; Kwiecinski, H., Serum IgM anti-GM1 ganglioside antibodies in lower motor neuron syndromes. *European Journal of Neurology* **2004**, *11*, 13-16.
(20) Folch, J.; Lees, M.; Stanley, G. H. S., A SIMPLE METHOD FOR THE ISOLATION AND PURIFICATION OF TOTAL LIPIDES FROM ANIMAL TISSUES. *J. Biol. Chem.* **1957**, *226*, 497-509.
(21) Pacuszka, T.; Fishman, P. H., Synthesis of a Photoreactive, Radiolabeled Derivative of the Oligosaccharide of Gm1 Ganglioside. *Glycobiology* **1992**, *2*, 251-255.
(22) Sonnino, S.; Chigorno, V.; Acquotti, D.; Pitto, M.; Kirschner, G.; Tettamanti, G., A Photoreactive Derivative of Radiolabeled Gm1 Ganglioside - Preparation and Use to Establish the Involvement of Specific Proteins in Gm1 Uptake by Human-Fibroblasts in Culture. *Biochemistry* **1989**, *28*, 77-84.
(23) Acquotti, D.; Sonnino, S.; Masserini, M.; Casella, L.; Fronza, G.; Tettamanti, G., A New Chemical Procedure for the Preparation of Gangliosides Carrying Fluorescent or Paramagnetic Probes on the Lipid Moiety. *Chem. Phys. Lipids* **1986**, *40*, 71-86.
(24) Schwarzmann, G.; Sandhoff, K., Lysogangliosides - Synthesis and Use in Preparing Labeled Gangliosides. *Methods Enzymol.* **1987**, *138*, 319-341.
(25) Nakagawa, T.; Tani, M.; Kita, K.; Ito, M., Preparation of fluorescence-labeled GM1 and sphingomyelin by the reverse hydrolysis reaction of sphingolipid ceramide N-deacylase as substrates for assay of sphingolipid-degrading enzymes and for detection of sphingolipid-binding proteins. *Journal of Biochemistry* **1999**, *126*, 604-611.
(26) Schwarzmann, G.; Wendeler, M.; Sandhoff, K., Synthesis of novel NBD-GM1 and NBD-GM2 for the transfer activity of GM2-activator protein by a FRET-based assay system. *Glycobiology* **2005**, *15*, 1302-11.
(27) Mobius, W.; Herzog, V.; Sandhoff, K.; Schwarzmann, G., Intracellular distribution of a biotin-labeled ganglioside, GM1, by immunoelectron microscopy after endocytosis in fibroblasts. *J. Histochem. Cytochem.* **1999**, *47*, 1005-14.
(28) Belov, V. N.; Polyakova, S. M.; Yan, S. F.; Eggeling, C.; Ringemann, C.; Schwarzmann, G.; de Meijere, A.; Hell, S. W., New GM1 Ganglioside Derivatives for Selective Single and Double Labelling of the Natural Glycosphingolipid Skeleton. *Eur. J. Org. Chem.* **2009**, 5162-5177.
(29) Sonnino, S.; Acquotti, D.; Kirschner, G.; Uguaglianza, A.; Zecca, L.; Rubino, F.; Tettamanti, G., Preparation of Lyso-Gm1 (Ii(3)Neu5acggose(4)-Long Chain Bases) by a One-Pot Reaction. *J. Lipid Res.* **1992**, *33*, 1221-1226.
(30) Muller, S.; Schmidt, R. R., Synthesis of Unique Ceramides and Cerebrosides Occurring in Human Epidermis. *Helv. Chim. Acta* **1993**, *76*, 616-630.
(31) Nagatsugi, F.; Sasaki, S.; Maeda, M., Synthesis of Omega-Fluorinated Octanoic-Acid and Its Beta-Substituted Derivatives. *J. Fluorine Chem.* **1992**, *56*, 373-383.
(32) Yoder, N. C.; Kalsani, V.; Schuy, S.; Vogel, R.; Janshoff, A.; Kumar, K., Nanoscale patterning in mixed fluorocarbon-hydrocarbon phospholipid bilayers. *J. Am. Chem. Soc.* **2007**, *129*, 9037-9043.
(33) Brace, N. O.; Albain, K.; Mayforth, R. D.; Miller, J. A., The Effect of Conjugation on Hydrogen Iodide and Hydrogen-Fluoride Elimination from 1-(F-Alkyl)-2-Iodoalkenes

- from 5-(F-Butyl)-4-Iodo-1-Pentene to 5-(F-Butyl)Pentadienes and Further to 1-Fluoro-1-(F-Propyl)-1,3,5-Hexatrienes. *J. Org. Chem.* **1990**, *55*, 5252-5259.
(34) Ramachandran, P. V.; Jennings, M. P., Investigation of the factors controlling the regioselectivity of the hydroboration of fluoroolefins. *Chem. Commun.* **2002**, 386-387.
(35) Pacuszka, T.; Fishman, P. H., Generation of Cell-Surface Neoganglioproteins - Gm1-Neoganglioproteins Are Non-Functional Receptors for Cholera-Toxin. *J. Biol. Chem.* **1990**, *265*, 7673-7678.
(36) Wan, Q.; Cho, Y. S.; Lambert, T. H.; Danishefsky, S. J., Olefin cross-metathesis: A powerful tool for constructing vaccines composed of multimeric antigens. *J. Carbohydr. Chem.* **2005**, *24*, 425-440.

Chapter 3

Biophysical and biological properties of Fluorinated GM1

3.1 Evaluation of F-GM1 incorporation onto living cells

Ganglioside GM1 is an important component of plasma membranes.[1] GM1 is rich in brain and neuron cells with the percentage of up to 5%, but has been found in almost all the vertebrate cells. The concentration of GM1 in plasma membranes can be easily increased by incubating the cells with supplemented GM1 the cell culture. In this section, the incorporation of fluorinated GM1 analogues onto cell surface has been studied using flow cytometry. Fluorescence tagged cholera toxin B subunit (CTB) was employed as a probe for the detection of F-GM1 analogues, taking advantage of the high affinity and selectivity of CTB binding to GM1.[2] The binding site of GM1 to CTB is the oligosaccharide moiety[3], therefore the modification of fluorocarbon on hydrophobic tails should not influence their binding affinity. Chinese hamster ovarian K1 (CHO-K1)[4] cell line that is devoid of GM1 on their surface was used to test the F-GM1 incorporation. By using fluorescence assisted cell analysis, the incorporation activities of F-GM1 analogues onto multiple mammalian cell lines have been evaluated to verify any influences of fluorination on GM1 properties.

3.1.1 Fluorescence assisted cell sorting and analysis

Fluorescence assisted cell sorting (FACS) is a type of flow cytometry that can analyze and separate cells and other small particles based on fluorescence signal of the particles[5]. The flow cytometry has been invented in 1965 and widely used in research and industry.[6,7] As shown in Fig 3.1, cells are carried by an ultra-thin water stream to form a flow of cells that each time only one cell passes through the tubing. The flow of cells is then broken up by ultrasonic to form uniform droplets, and each droplet contains no more

than one cell. When the cells pass through the analyzer, fluorescence labels on the cells are excited by a laser beam and generate fluorescent signals. Depending on different fluorescent signals, a feedback-voltage control system adjusts the electrostatic field along the cell flow, thus separate the cells of interest individually from the mixture and achieve the “cell sorting”. The fluorescence assisted cell sorter is used to separate cells, whereas the FACS analysis only detect and analyze the fluorescence signals on the cells. Currently, FACS sorter can separate thousands of cells per minute, and FACS analysis could reach the rate at tens of thousands of cells per minute. Equipped with a variety of excitation laser generators, FACS has become a powerful high throughput screening (HTS) tool in biochemistry, molecular biology, and pharmaceutical studies. In our work, we just utilized the FACS to analyze the cells and the term “FACS” only refers to the FACS analysis.

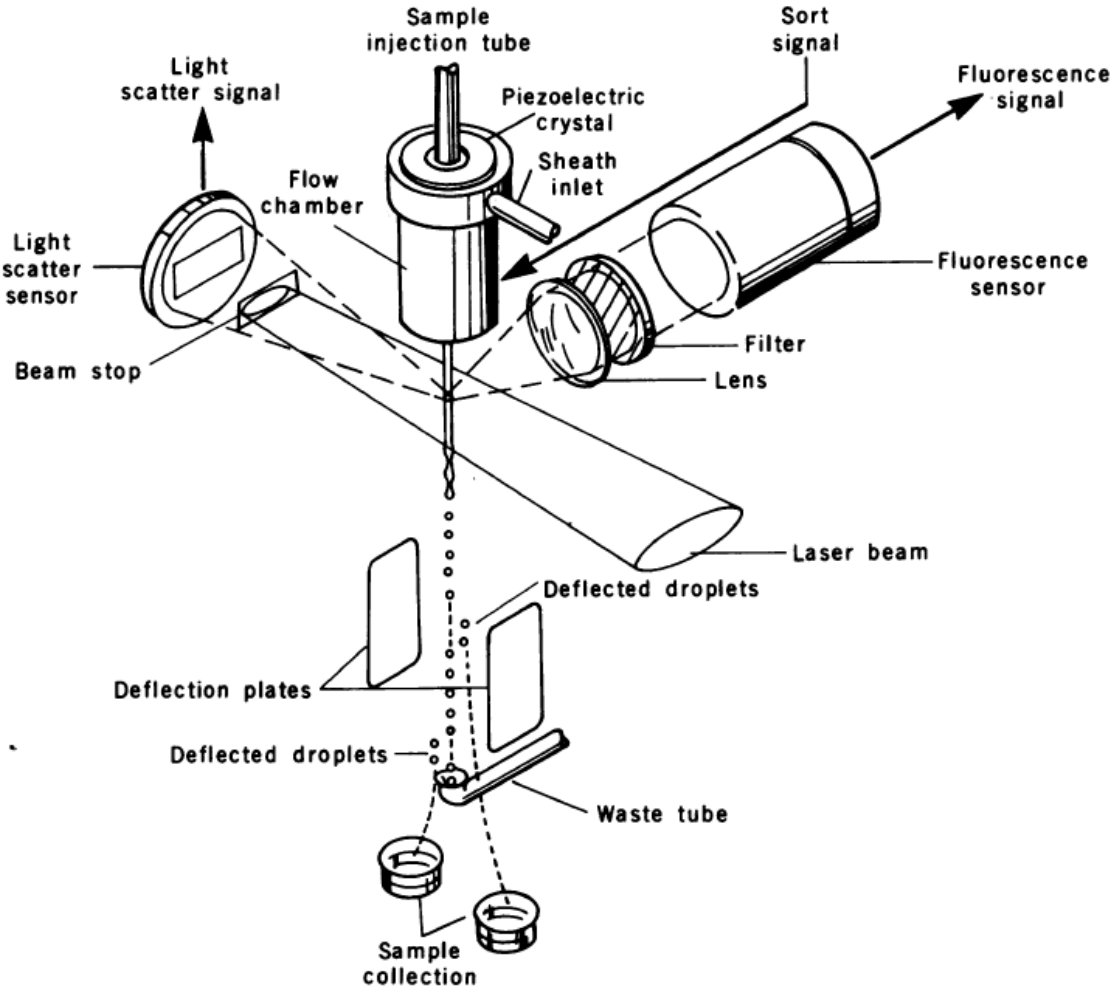

Fig 3.1 Schematic representative of flow cytometry.[7] The stream of cell samples forms uniform small droplets, and each droplet contains no more than one cell. The fluorescence signals from labeled cells are collected and generate feedback to control the electrostatic field along the stream. The cells in droplets are separated and collected individually at high speed for screening and sorting. From reference 7. reprinted with permission from AAAS.

3.1.2 Results and Discussion

3.1.2.1 Fluorinated GM1 can be incorporated onto cell surface as natural GM1

The CHO-K1 cells were used as a platform to test the incorporation of F-GM1 analogues. GM1, 18-F-GM1, and 18-F3-GM1 were incubated with CHO-K1 cells at 25 µM, followed by stain with FITC-CTB (250 ng/mL) that recognize the external GM1 analogues on the cells. The FACS analysis revealed incorporation of both 18-F-GM1 and 18-F3-GM1 onto CHO-K1 cells at the same level of that of natural GM1, in which the incorporation efficacy was in order of 18-F-GM1 >18-F3-GM1>GM1 with slight differences. (Fig 3.2) The negative control of CHO-K1 cells with no external GM1 displayed the lacking of native GM1 by FITC-CTB stain.

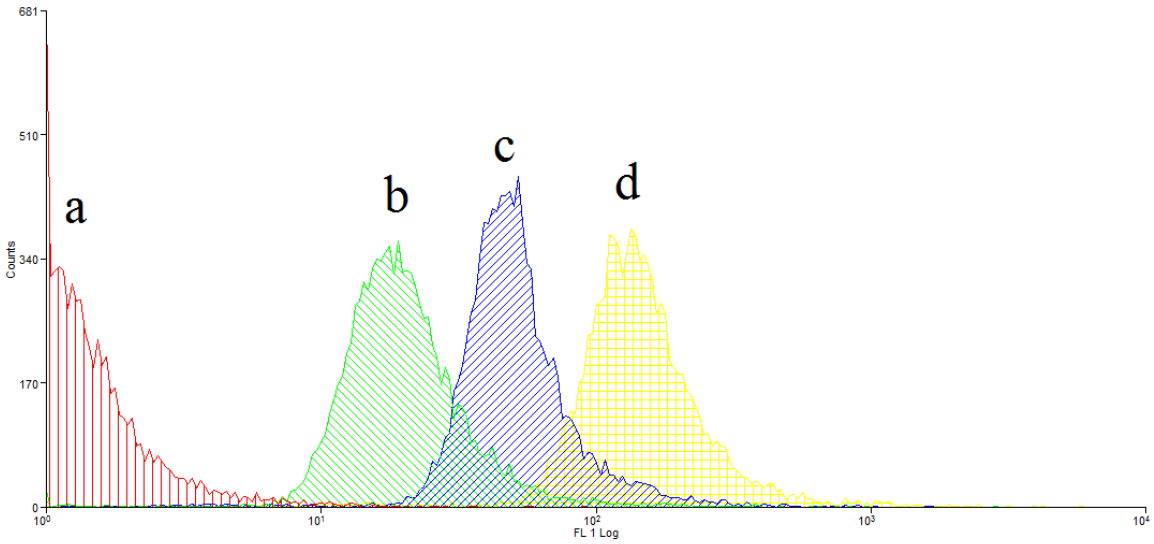

Fig 3.2 FACS histogram of CHO-K1 incubated with GM1 and derivatives. From left to right: (a) CHO-K1, (b) CHO-K1 + GM1 (25 µM), (c) CHO-K1 + 18-F3-GM1 (25 µM), (d) CHO-K1 + 18-F-GM1 (25 µM)

3.1.2.2 The incorporation of F-GM1 on CHO-K1 were concentration dependent

The CHO-K1 cells were incubated with F-GM1 analogues (18-F3-GM1 and 18-F-GM1) for 2 h, in the concentration of 2.5 µM, 7.5 µM, and 25 µM. After staining with FITC-CTB (250 ng/mL), cells showed increasing incorporation of F-GM1 at the concentration dependent manner. (Fig 3.3 and 3.4)

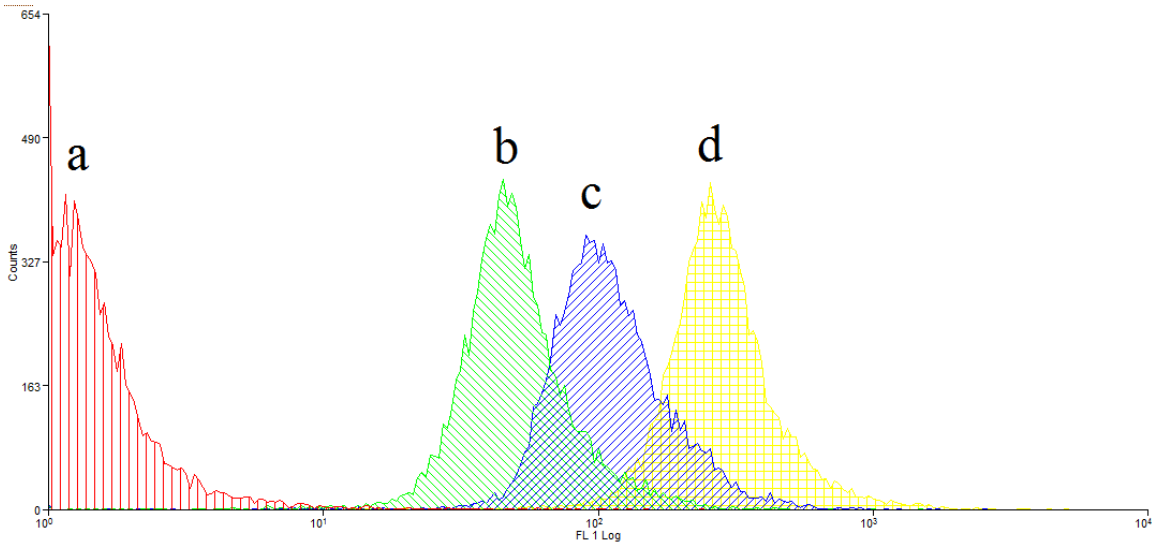

Fig 3.3 FACS histogram of CHO-K1 incubated with different concentrations of 18-F-GM1. From left to right: (a) CHO-K1, (b) CHO-K1 + 18-F-GM1 (2.5 µM), (c) CHO-K1 + 18-F-GM1 (7.5 µM), (d) CHO-K1 + 18-F-GM1 (25 µM)

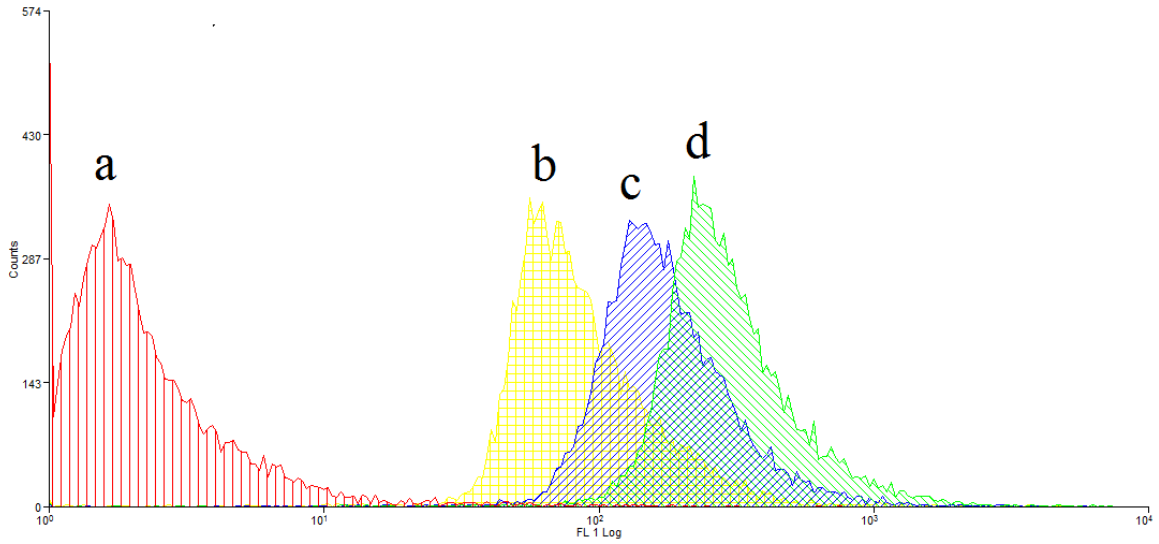

Fig 3.4 FACS histogram of CHO-K1 incubated with different concentrations of 18-F3-GM1. From left to right: (a) CHO-K1, (b) CHO-K1 + 18-F3-GM1 (2.5 µM), (c) CHO-K1 + 18-F3-GM1 (7.5 µM), (d) CHO-K1 + 18-F3-GM1 (25 µM)

3.1.2.3 The incorporation of F-GM1 on CHO and Jurkat cells

CHO cells were reported to be expressing GM1 on their surface.[8] However, when we stained CHO cells (Sigma-aldrich: 85050302) with FITC-CTB, they displayed negative results by FACS analysis. The external 18-F3-GM1 displayed significant incorporation onto CHO cells, but without external GM1 or F-GM1, the wild type CHO cells showed FITC-CTB signal at the same level of as negative control after stain. (Fig 3.5) The negative control has no FITC-CTB stain step. The Jurkat cell line, which was originally derived from immune system, has been shown to display GM1 on the surface. [9] We used Jurkat cell line as positive control for external F-GM1 incorporation. FACS histogram (Fig 3.6) showed significant amount of GM1 on wild type Jurkat cells after FITC-CTB stain, and the incorporation of external 18-F3-GM1 exhibited additional signal to that of wild type Jurkat cells.

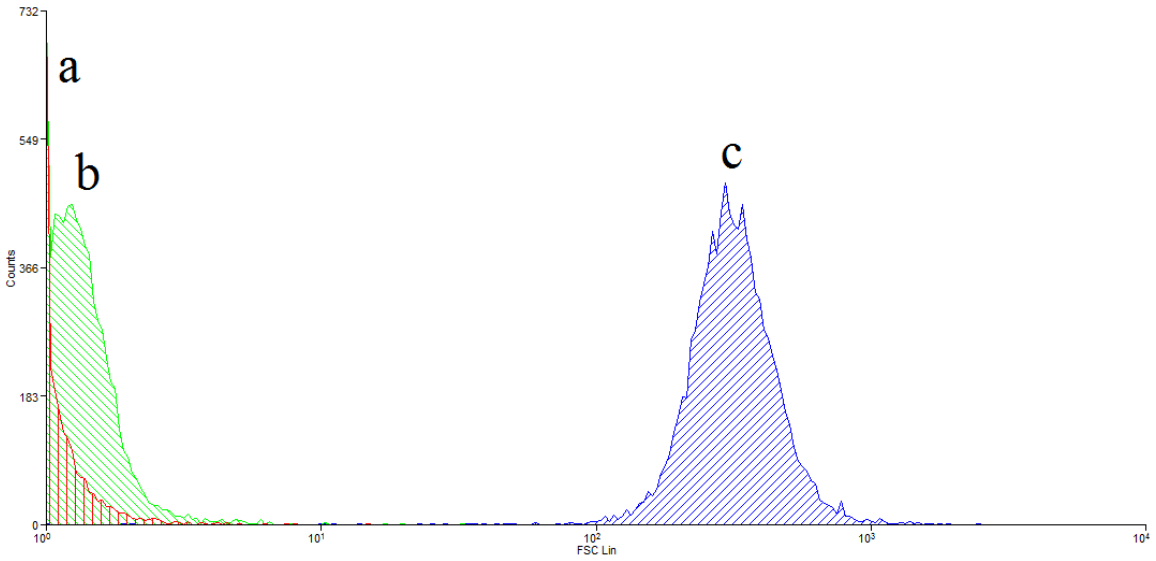

Fig 3.5 FACS histogram of incubated with external GM1 followed by FITC-CTB stain. From left to right: (1) CHO (2) CHO + FITC-CTB (3) CHO + 18-F3-GM1 (25 µM) + FITC-CTB

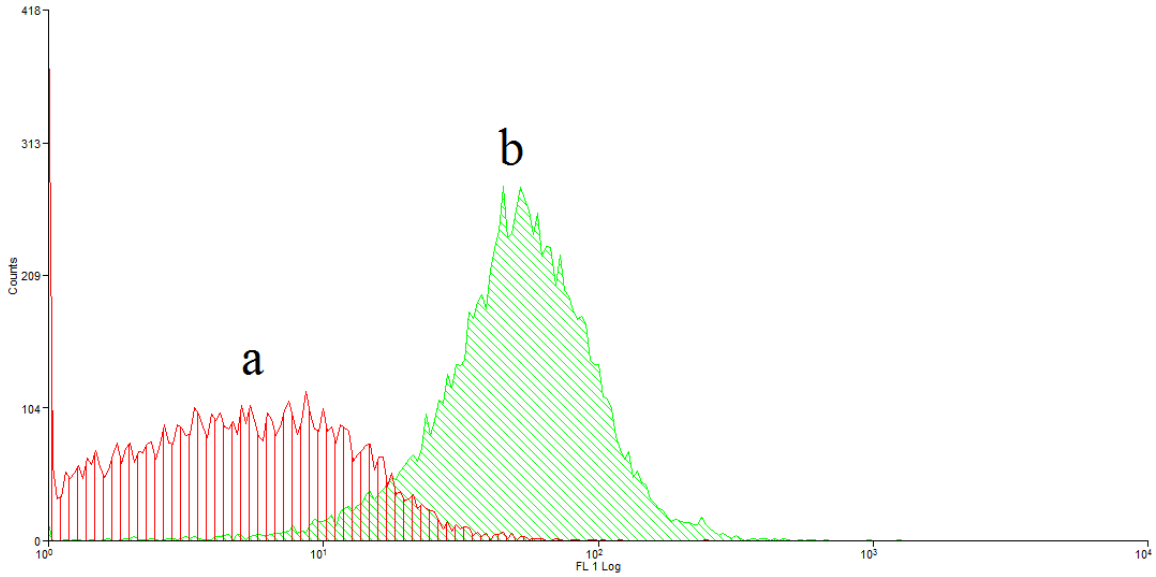

Fig 3.6 FACS histogram of Jurkat cells stained with FITC-CTB. From left to right: (a) Jurkat (b) Jurkat + FITC-CTB

3.1.3 Conclusions

FACS analysis has been used to exploit the incorporation of fluorinated GM1 analogues on living cells, including CHO-K1, CHO and Jurkat cell lines. CHO-K1 is a mutant type of CHO cell line that devoid of GM1 on the surface. Incubation of CHO-K1 cells with external wild type GM1, 18-F-GM1, 18-F3-GM1 in cell culture medium resulted in significant incorporation of GM1 analogues on the cells, revealed by FACS analysis with FITC-CTB stain. The amount of F-GM1 analogues incorporated on cells exhibited dependence on their concentrations in the cell culture medium. In addition, FACS analysis showed that the wild type CHO cells was devoid of GM1 and could also be incorporated with external F-GM1. Furthermore, F-GM1 analogues were introduced the Jurkat cells that express native GM1 on their surfaces, and lead to elevated GM1 signals than wild type Jurkat cells. Therefore, FACS analysis has shown to be a powerful tool for F-GM1 incorporation assay, and confirmed incorporation of external F-GM1 analogues onto multiple cell lines to facilitate further studies on living cells.

3.1.4 Experimental section

Materials and instruments. CHO, CHO-K1, and Jurkat cells were from ATCC. CTB, FITC-CTB and other common buffers and chemicals were from Sigma. The cell growth media were from Cancer Center, Tufts Medical Center. The instrument for FACS analysis was a BD FACS Calibur model from Tufts medical school.

Cell culture: CHO and CHO-K1 were cultured in HAM-F12 supplemented with 10% fetal bovine serum. Jurkat cells were cultured in complete medium of RPMI 1640 with

10% fetal bovine serum. The cells were cultured for at least 48 h in 12 cm plastic cell culture plates.

GM1 incorporation and staining on cells. The cells were incubate in 6 well plate (1 $\times 10^6$ cells per well) with 2 mL complete medium for 12 h. Medium was changed and cells were suspended in fresh medium with 25 μM GM1 (or F-GM1) incubate at 37°C for 2 h. The cells were washed twice with fresh medium, and incubated for 1 h in the medium containing 250 ng/mL FITC-CTB. The cells were washed with 1× PBS (-Ca, -Mg) buffer twice and suspend in 1× PBS (-Ca, -Mg) buffer for FACS analysis. For adhesion cells, the cells were trypsinized if needed.

FACS analysis. The cells (~10^6 cells/ml) were placed in Falcon 2054 (polystyrene, 5 ml round bottom) tubes after stain. The excitation laser was set on 488 nm; and the detection was on 530 nm (FITC). Before each run of sample, the instrument was washed until 15 events /min was obtained as blank. The cell flow rate was 35 μL/min and each sample has a total count of 10,000 events. The data was processed on the software of *Summit* (Dako).

3.2. AFM studies of F-GM1 on solid supported lipid bilayers

Atomic force microscopy (AFM) is a type of scanning probe microscopy that uses an ultra fine tip to scan the sample and study its surface properties. AFM is specialized in the high resolution and mild working conditions, and has been widely used in the surface science and biological membrane studies.[10-14] One important application of AFM is to investigate the biological membrane phase separation and the lipid rafts paradigm.[15-17] Ganglioside GM1, as a common molecule in lipid rafts, has been studied using AFM for its biophysical properties and phase behaviors in a variety of model membranes.[18,19] Here we report the AFM studies of fluorinated GM1 in solid supported lipid bilayers. By comparing with natural GM1, the results can give information about structure-property relationship that is useful in function studies.

3.2.1 AFM in membrane bilayer studies

AFM is equipped with a cantilever that has a very sharp tip on the end. The cantilever scans laterally on the sample surface and its vertical motion is monitored by a laser beam reflection to reveal local physical properties and generates a map of the sample surface. AFM has been widely used to detect solid support lipid membranes with very high resolution (1 nm laterally and 0.1 nm vertically) under mild conditions.[20-22] The hydrophilic surfaces, such as mica, glass, and quartz, have been employed as solid supports to form lipid bilayers, where the hydrophilic head groups face out and hydrophobic lipid tails toward inside, thus provide a way to mimic plasma membranes. For example, AFM revealed the temperature dependent phase separation in phospholipid bilayer membranes to form gel phase and liquid disordered phase,[23] and with assistance

of cholesterol a distinct liquid ordered phase was formed as a transition state between the gel phase and liquid disordered phase.[24] (Fig 3.7) AFM has also been used to image protein patterning[25-27], plasma membranes[28,29], and bacteria surfaces[30].

The lipid rafts theory, which proposes the lipid sorting and phase separation determines the protein receptor clustering, has been also examined by AFM in model membranes. For instance, a variety of binary and ternary membrane bilayers, with or without protein receptors, have been investigated for their phase separation and receptor distribution behaviors.[17,31-34] Ganglioside GM1 has been found rich in detergent resistant membranes and considered to be a typical lipid rafts component, thus was extensively used in lipid rafts formation studies. Introduction of GM1 in lipid membranes induces formation of microdomains at nanometer scale in size.[35] By using AFM, the domains containing GM1 could be revealed by its height difference from phospholipids and sphingomyelin. With cholesterol participation, the coalescence of GM1 and cholesterol has been observed in microdomains.[36-38] GM1 has been found preferentially localized in the gel phase[37,39], and slightly lowered its transition temperature T_m.[40] Fluorescently labeled ganglioside GM1 was used in lipid bilayers to visualize lipid microdomains, and the fluoroscence label on the oligosaccharide moiety did not perturb the domain formation properties.[41]

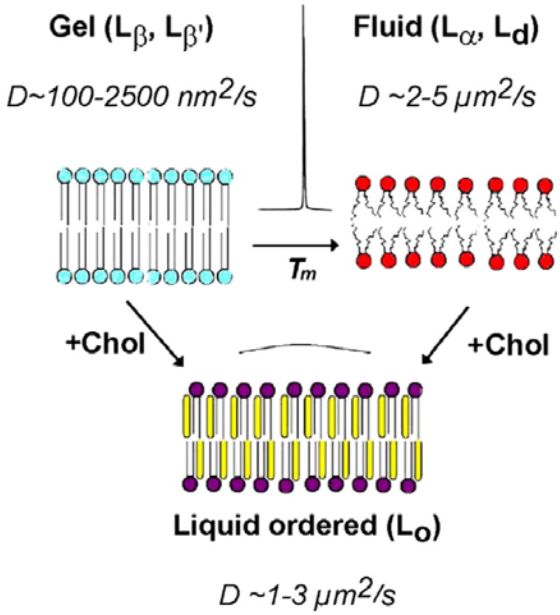

Fig 3.7 Phase properties of phospholipids. The transition between gel phase and fluid phase was characterized by a sharp peak of T_m in differential scanning calorimetry. By adding cholesterol, the sharp peaks became broader depending on concentration and the lipid bialyer exhibited a liquid ordered phase. Reprinted from reference 24. Copyright (2010), with permission from Elsevier.

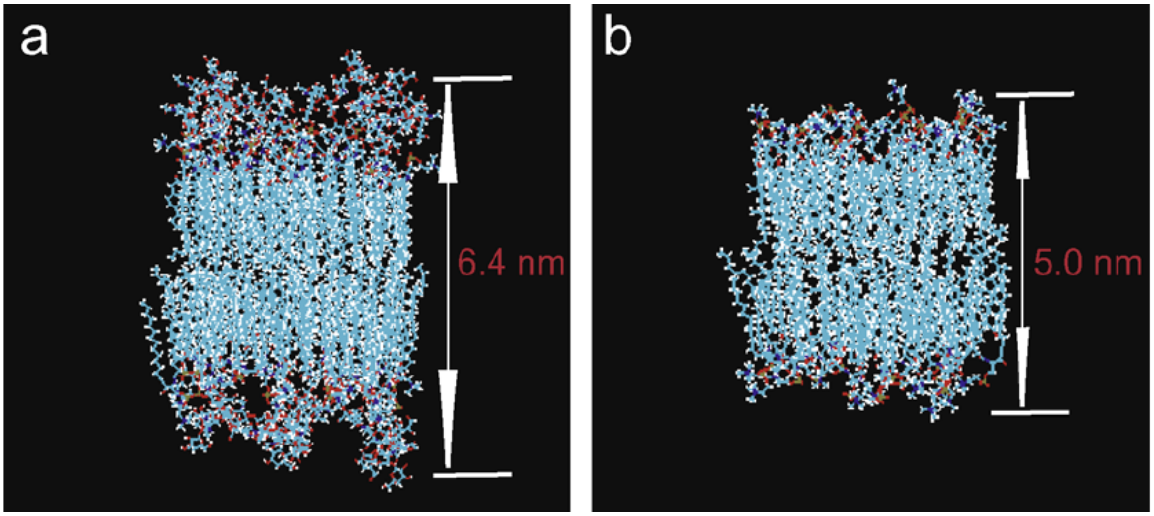

Fig 3.8 Molecular modeling simulation revealed the lipid bilayers structural differences between (a) GM1/SM/Chol (1:2:2) and (b) SM/Chol (1:1). Reprinted from reference 42. Copyright (2008), with permission from Elsevier.

3.2.2Results and Discussion

3.2.2.1 DPPC/POPC (1:1) with 1 % natural GM1

In the lipid bilayer formed by a mixture of DPPC/POPC (1:1 molar ratio), phase separation was observed to form a gel phase and a liquid disordered (l_d) phase with roughly 1:1 ratio. DPPC has saturated fatty acid tails and localized in the gel phase, whereas POPC has one unsaturated tail and resided in l_d phase. The height difference between the gel phase and the l_d phase was about 2 nm. (Fig 3.9) After adding 1 % natural GM1 into the mixture, the ratio of two phases in the bilayers was still around 1:1, and GM1 was found at the boundary of two phases. (Fig 3.10) The height difference between GM1 patches and the gel phase was shown to be ~1.5 nm[42]. The immiscibility of GM1 with gel phase did not interfere with the phase separation of DPPC/POPC mixture. These results agreed with the reported GM1 topography on lipid bilayers. [37]

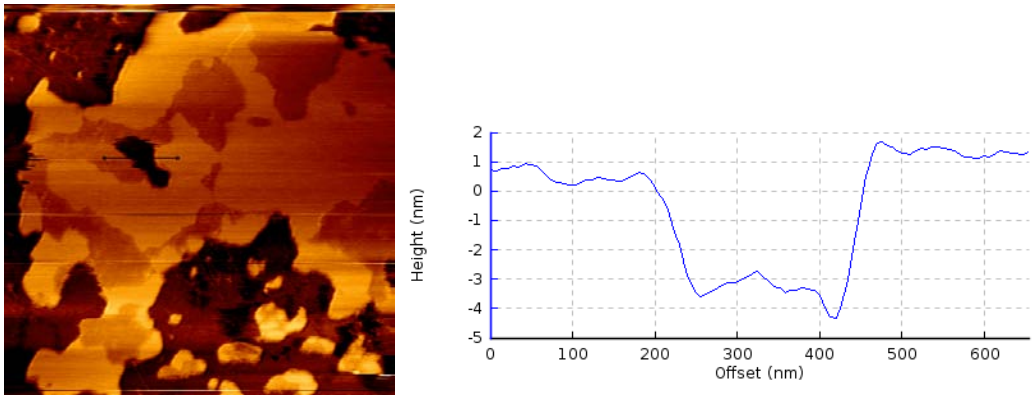

Fig 3.9 Height image of DPPC/POPC (1:1) mixture

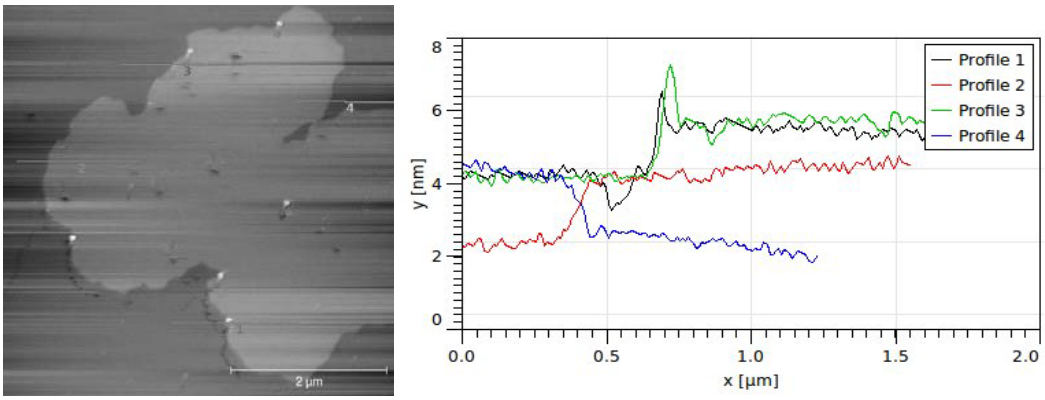

Fig 3.10 Height image of DPPC/POPC (1:1) mixture with 1 % natural GM1

3.2.2.2 DPPC/POPC (1:1) with 1% 18-F-GM1

The mixture of DPPC/POPC (1:1) with 1% 18-F-GM1 formed of lipid bilayers on mica surface. Phase separation was observed with a gel phase and a l_d phase at about 1:1 ratio. (Fig 3.11) By measuring the height profile, the self-assembly of 18-F-GM1 was found at the boundary between the gel phase and the l_d phase forming small patches that are 1.5 nm higher than the gel phase. Other than the boundary GM1 patches, a type of microdomains were observed at 10 nm scale in diameter in the gel phases. The height measurement revealed the existence of GM1 in these microdomains. These results are consistent with phase behaviors of natural GM1 in lipid bilayers, indicating the high similarity of terminal mono-fluorinated GM1 to its native version.

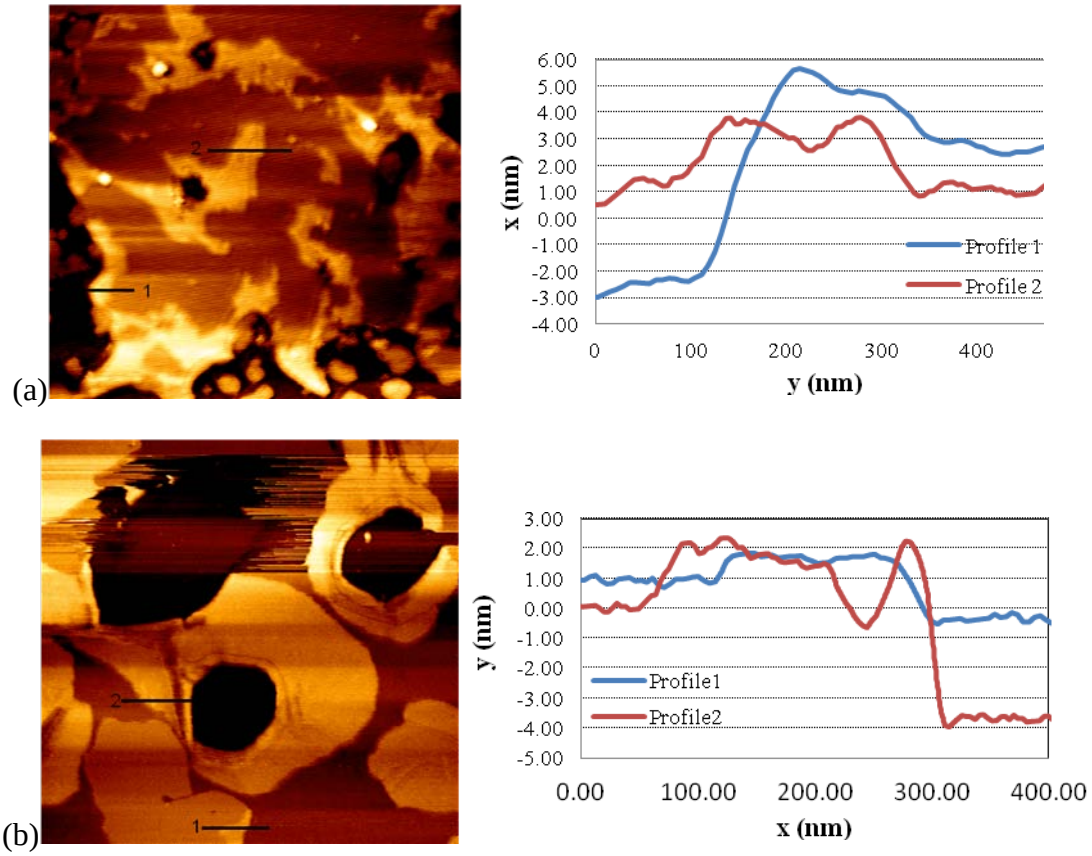

Fig 3.11 Height images of DPPC/POPC (1:1) mixture with 1% 18-F-GM1. (a) 3.5μm × 3.5 μm. (b) 2.5μm × 2.5 μm.

3.2.2.3 DPPC/POPC (1:1) with 1% 12-F-GM1

The lipid bilayers of DPPC/POPC (1:1) supplemented with 1% 12-F-GM1 exhibited quite different phase behaviors from natural GM1. The gel phase and l_d phase showed significantly different ratio of area. The gel phase occupied much larger area than the l_d phase revealed by AFM height imaging. (Fig 3.12) Some small patches of 12-F-GM1 were observed, at ~10 nm scale in diameter, to form in the gel phase. But the occurrence of 12-F-GM1 patches was less than that of native version.

3.2.2.4 DPPC/POPC (1:1) with 1% 18-F3-GM1

The membrane formed by DPPC/POPC (1:1) w/ 1% 18-F3-GM1 also exhibited different phase separation from natural GM1. The gel phase was much smaller than l_d phase by AFM height imaging. (Fig 3.13) Small patches of 18-F3-GM1 were found in the gel phase, at ~10 nm scale in diameter. Boundary 18-F3-GM1 elongated patches were also observed.

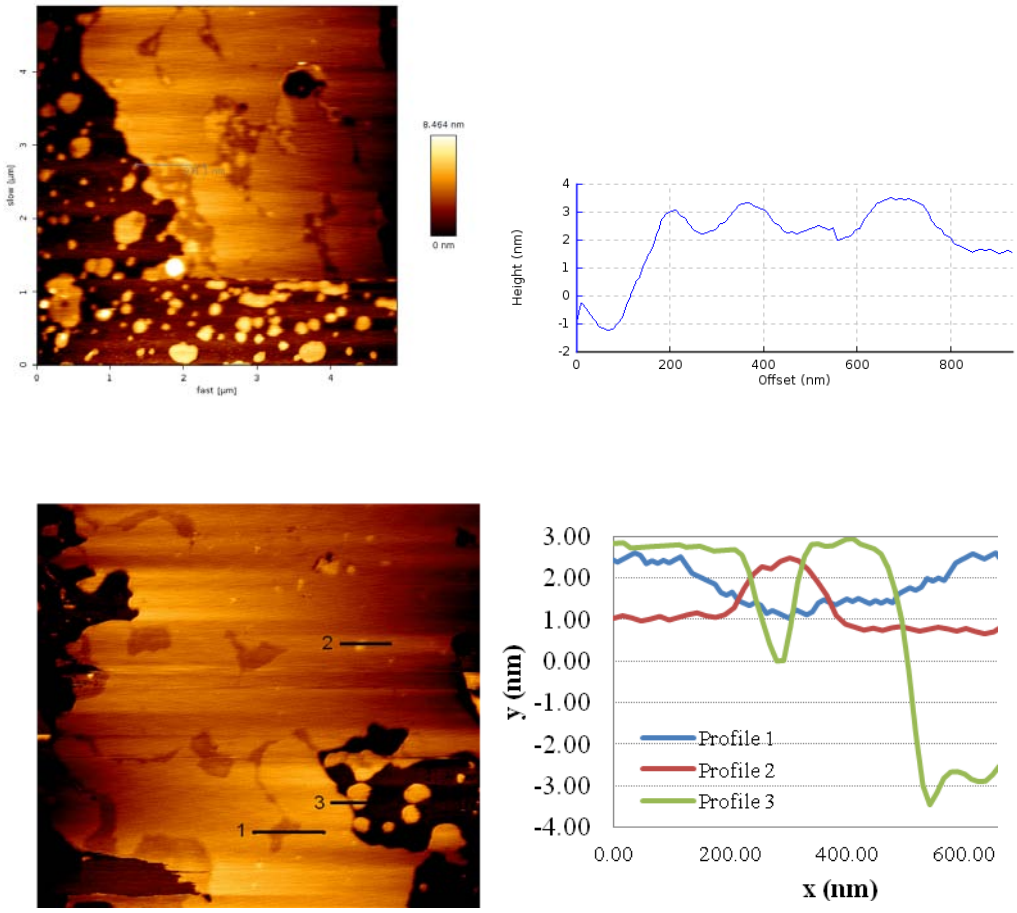

Fig 3.12. Height images of DPPC/POPC (1:1) mixture with 1% 12-F-GM1. (5µm × 5µm)

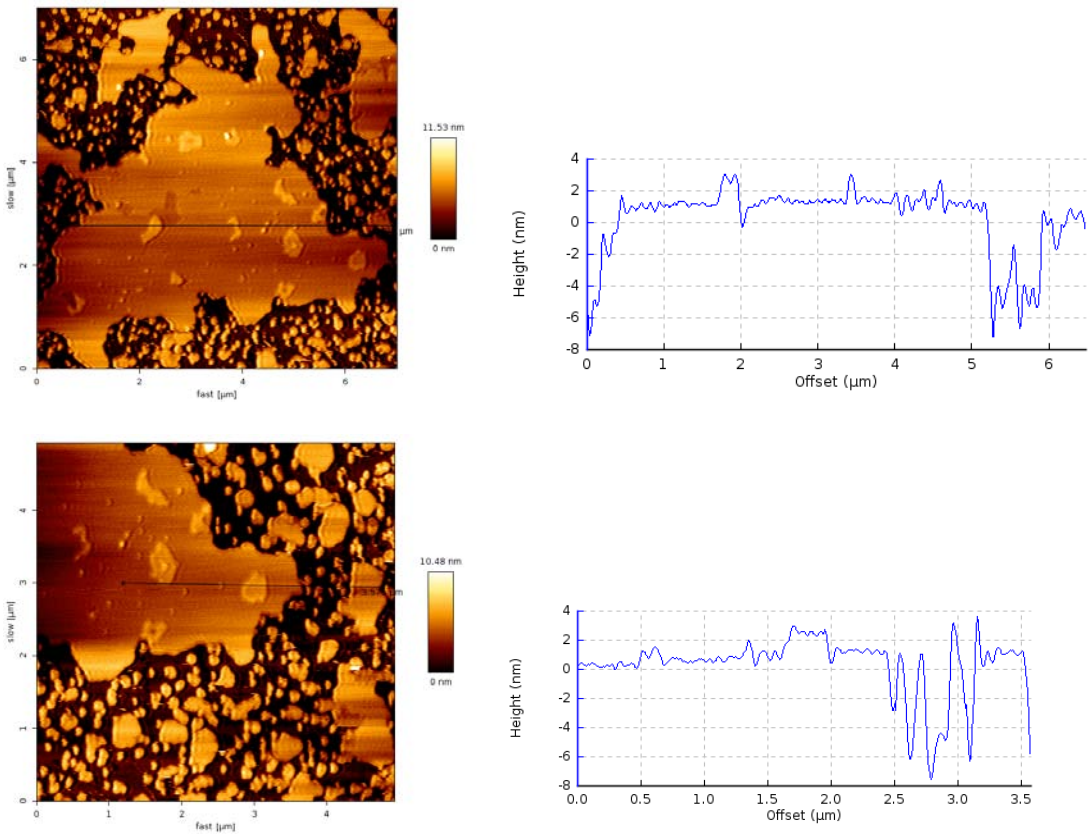

Fig 3.13 Height images of DPPC/POPC (1:1) mixture with 1% 18-F3-GM1

3.2.2.5 DPPC/POPC (1:1) with 1% C6F13-GM1

The mixture of DPPC/POPC (1:1) with 1% C6F13-GM1 formed lipid bilayers. However, C6F13-GM1 did not show significant height difference and was not clearly observed as microdomains by AFM height imaging. CTB (3μg) was added on the bilayers to label the C6F13-GM1 and revealed that it localized on the edge of gel phase. These observations suggested that fluorocarbon substitution significantly changed the phase behavior of GM1 in the membranes. (Fig 3.14)

3.2.2.6 The phase behaviors of GM1 analogues in SPM/POPC mixture

The mixture of POPC and 10% natural GM1 was subject to mica surface and formed the lipid bilayers. At room temperature, POPC (T_m = -2°C) forms l_d phase and GM1 self-assembed to form isolated patches with height difference of (2.5 ± 0.2) nm. (Fig 3.15) To study the phase behavior of F-GM1 analogues in SPM/POPC mixture, the lipid bilayers were prepared with SPM/POPC (1:1) supplemented with 1 to 5 % of GM1 analogues. In a control experiment, SPM/POPC (1:1) mixture showed phase separation with height difference of (1.3± 0.2) nm between the gel phase and the l_d phase. (Fig. 3.16) When natural GM1 (1%) was added to the SPM/POPC (1:1) mixture, a type of scattered microdomains was observed in the bilayers on the boundary of the two phases, at nanometer scale in diameter. (Fig 3.17) Phase separation was also observed in the lipid bilayers of SPM/POPC (1:1) supplemented with 5% 18-F-GM1 and C6F13-GM1, respectively. However, the microdomains of GM1 analogues were found both in the gel phase and l_d phase. (Fig 3.18 and 3.19) Indeed, the mixture of SPM/POPC did not form very large bilayers, compared to that of DPPC/POPC, which was also observed by other

researchers. Additionally, the AFM height imaging elucidated the height difference between phases in the bilayers but it could not tell the chemical composition of the membrane. Therefore, further investigation of the lipid bilayers requires other techniques for more details.

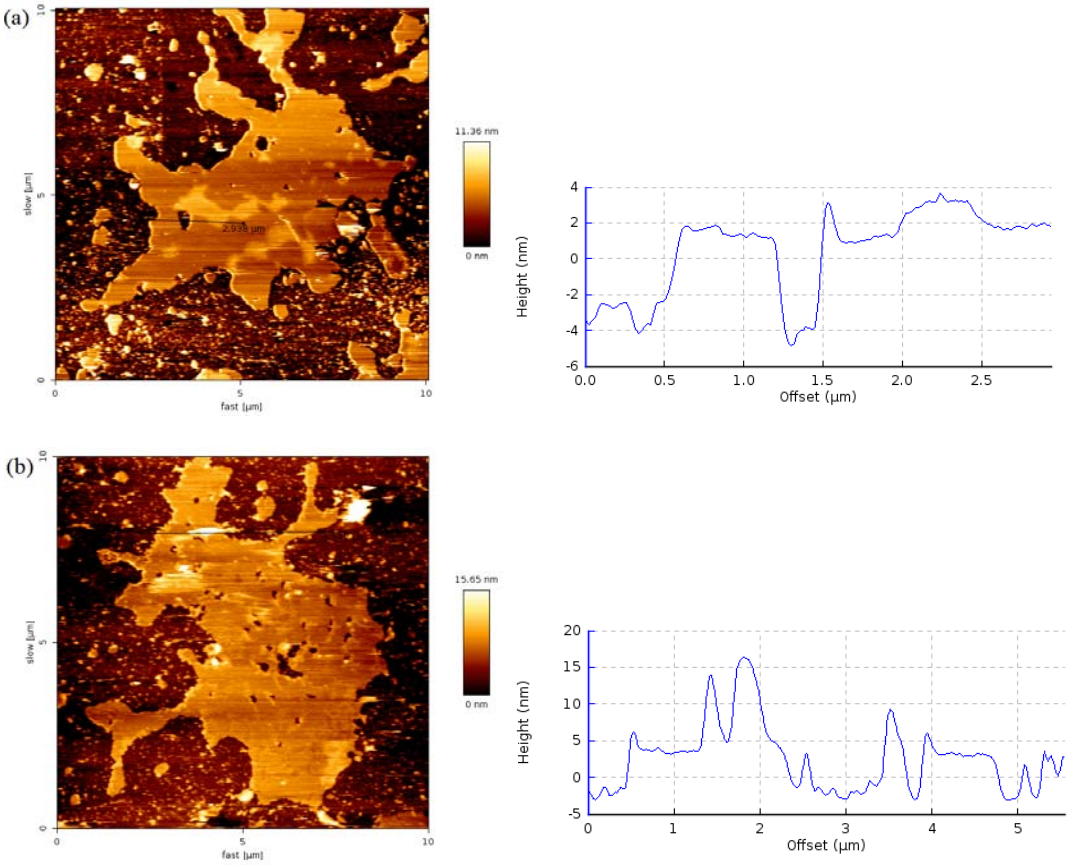

Fig 3.14 Height image of DPPC/POPC (1:1) with (a) 1% C6F13-GM1 and (b) 1% C6F13-GM1 followed by addition of 3 µg CTB.

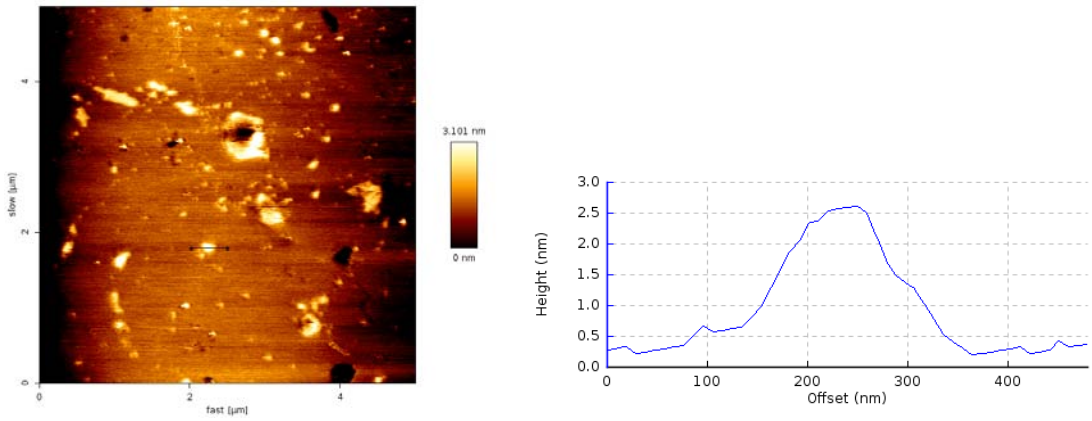

Fig 3.15 Height image of POPC with 10% GM1

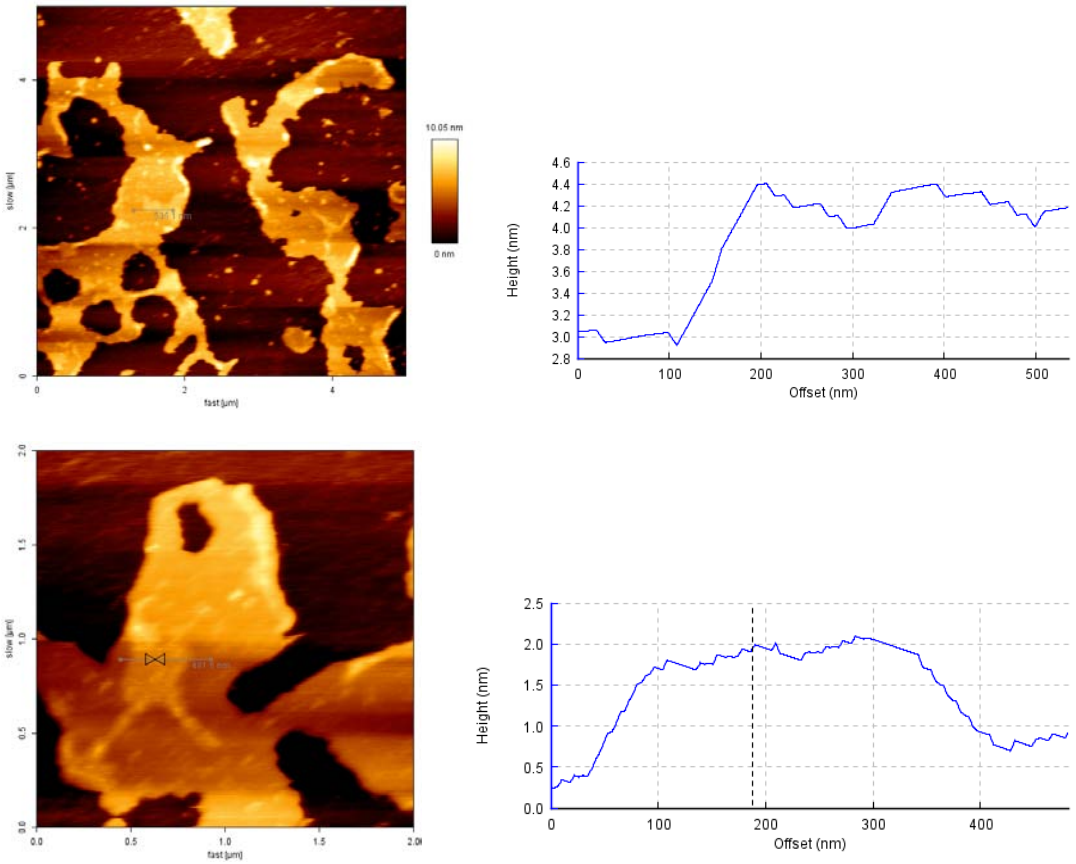

Fig 3.16 Height images of SPM /POPC (1:1)

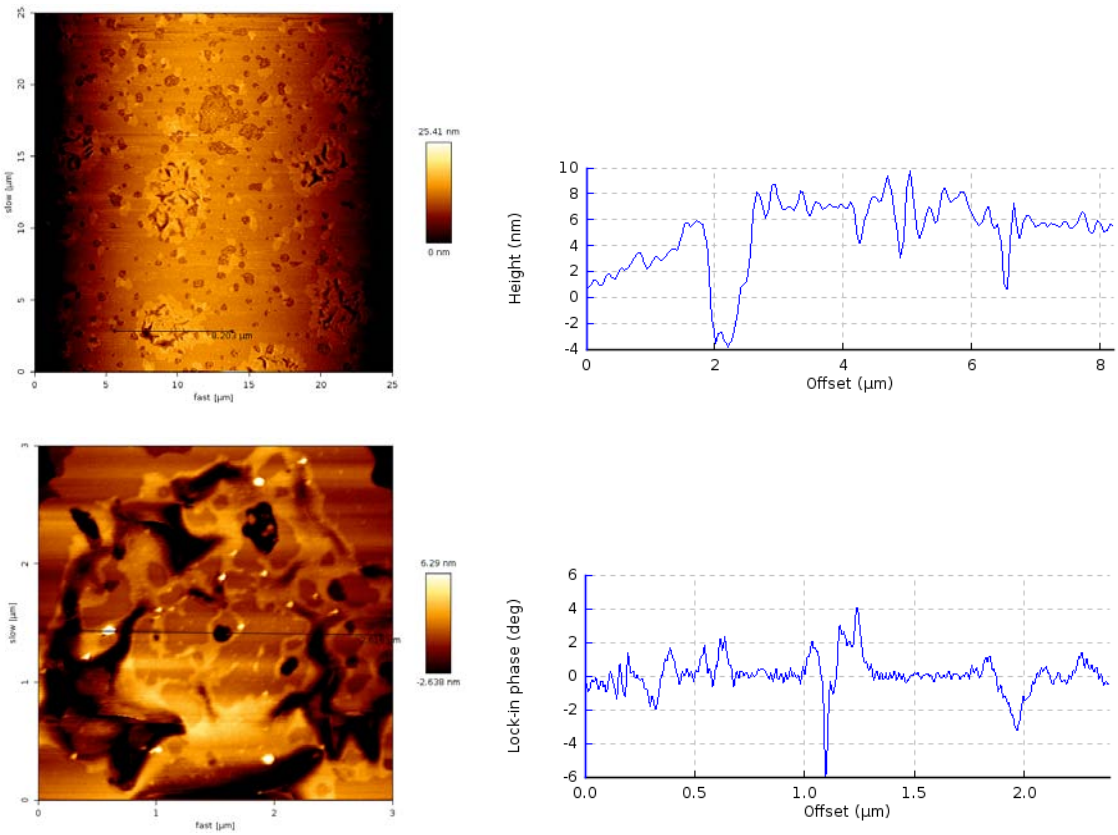

Fig 3.17 Height images of SPM /POPC (1:1) with 1% GM1

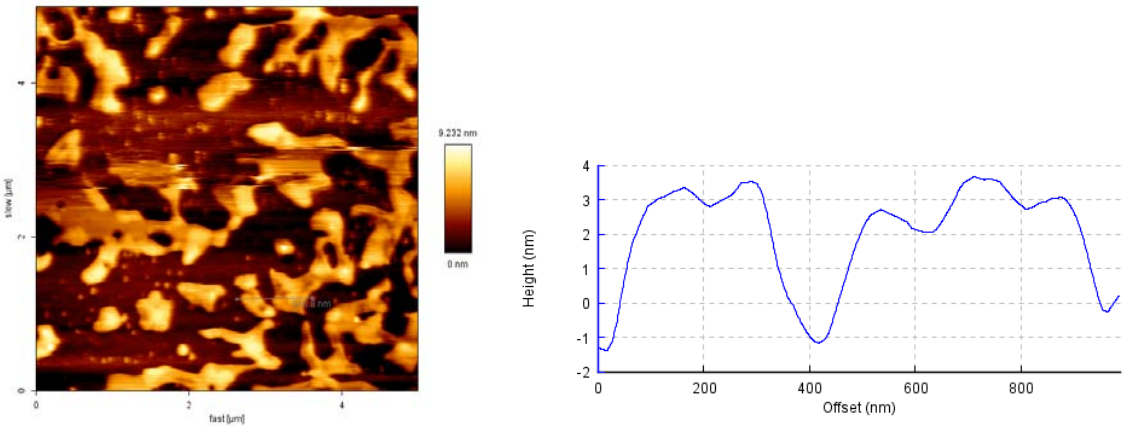

Fig 3.18 Height image of SPM /POPC (1:1) with 5% 18-F-GM1

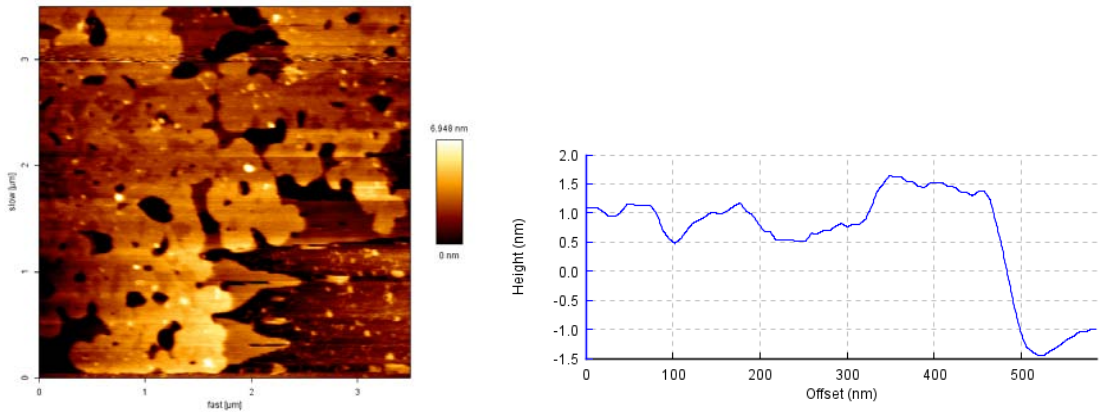

Fig 3.19 Height image of SPM /POPC (1:1) with 5% C6F13-GM1

3.2.3 Conclusions

Fluorinated ganglioside GM1 analogues (18-F-GM1, 12-F-GM1, 18-F3-GM1, and C6F13-GM1) have been analyzed by AFM in supported lipid bilayers to study their phase behaviors. In the bilayers of DPPC/POPC (1:1) with 1% 18-F-GM1, the gel phase and l_d phase showed roughly 1:1 ratio and GM1 localized in between as a boundary. The 12-F-GM1 (1%) changed the phase separation behavior dramatically in the same mixture, which exhibited much larger gel phase than the l_d phase. Interestingly, 18-F3-GM1 played an opposite role and the 1% 18-F3-GM1 significantly decreased the area of gel phase compared to the l_d phase. C6F13-GM1 did not change the phase separation of DPPC/POPC very much, but the C6F13-GM1 microdomains were not observed in height images. By labeling the GM1 analogue using CTB, the C6F13-GM1 microdomains were revealed to exist between two phases, indicating the height of C6F13-GM1 patches was probably similar as that of the gel phase. Therefore, 18-F-GM1 exhibited the highest similarity to native GM1 in phase behaviors.

The phase behavior of F-GM1 analogues was also analyzed in SPM/POPC bilayers by AFM imaging. Microdomains formed by F-GM1 analogues have been observed in the membrane, indicating the immiscibility of GM1, SPM and POPC. Interestingly, GM1 and SPM have been identified as signaling receptors with different locations and functions on the plasma membrane of mammalian cells.[43] Our AFM results provided with further evidence in the biophysical aspect and gave potential support on cell signaling and functional studies.

3.2.4 Experimental section

Materials. 1-palmitoyl-2-oleoyl-sn-glycero-3-phosphocholine (POPC), 1,2-dipalmitoyl-sn-glycero-3-phosphocholine (DPPC), cholesterol (Chol), *N*-palmitoyl-$_D$-sphingomyelin (SPM) and cholera toxin B subunit (CTB) were from Sigma-aldrich. Analytical-grade chloroform and methanol were purchased from FisherScientific.

AFM sample preparation. The support lipid bilayers were prepared by transporting liposomes onto mica surfaces in aqueous solution. All glasswares were washed with chloroform before use. The mixture of lipids were measured at desired ratio and transferred into test tubes and blowed to dry with argon to form lipid films. The lipid films were added Tris buffer (250 µL, pH=7.4) and warmed up at 55 ºC for 30 min with vertex occasionally to give clear solutions. The fresh mica surface was added 0.5 mL same buffer and 15 µL 0.1 M $CaCl_2$ solution. The samples were sonicated for 30 min at room temperature and 125 µL of each sample was loaded onto mica surface followed by equilibrating overnight. Before AFM imaging, the samples on mica were heated up at 55 ºC for 30 min and cooled down to room temperature. The lipid bilayers were rinsed with Tris buffer (2 mL × 3, pH=7.4) and added 1 mL same buffer for AFM assay.

Atomic force microscope. AFM was performed in aqueous solutions using NanoWizard II ® (JPK Instruments AG, Bouchéstrasse 12, 12435 Berlin, Germany), equipped with a fluid cell, using a silicon nitride cantilever (Olympus OTR8, Asylum Research, Santa Barbara, CA) with a nominal spring constant of 0.61 N/m. The setpoint was at ~ 0.7 V and Igain (30 Hz), Pgain (0.002) were optimized accordingly. The acquired data was processed using JPK SPM software release 3.3a.

3.3. Calcium signaling induced by F-GM1 analogues on the cell surface

Calcium signaling is an important biological process in mammalian cell life cycles.[44] Calcium ion is one of the most common secondary messengers and regulates a wide range of cell functions including enzyme activities, cell morphology, stickiness, motility, apoptosis and proliferation.[45] Ganglioside GM1 is found to be a promoter of intracellular calcium signaling. GM1 is able to induce calcium ion influx released from both extracellular sources and intracellular calcium ion reservoirs.[46] In this section, the synthetic F-GM1 analogues have been exerted in multiple cell lines to evaluate their activities in calcium signaling processes.

3.3.1 Calcium signaling and lipid rafts

Eukaryote cells maintain a very steep gradient of calcium ions from cytoplasm to the extracellular milieu. At the resting status, the cytosolic free calcium ion concentration is kept at ~100 nM while the extracellular concentration is usually at mM scale. When triggered to the exited state, the extracellular calcium ions were imported down through the 20,000 fold gradient (E_{Ca}~+150 mV) across the plasma membrane by ion channels.[44] Inside the cells, endoplasmic reticulum (ER) and mitochondria are the common storages of calcium ions to keep the cytosolic calcium ion concentration at a certain level. As a secondary messenger, calcium ions play an important role in cell signaling and regulation. To date, several signaling pathways have been confirmed to utilize the calcium gradient for functioning, including Na^+/Ca^{2+} exchange, the Na^+/Ca^{2+}-K^- exchange, GPCR/PIP_2-Ca^{2+}, IP_3/Ca^{2+} pathways.

Calcium signaling pathway has been proposed to be related to lipid rafts based on the following experiments. Jurkat cells were incubated with external ganglioside GM1 to obtain a high concentration of GM1 on the cell surface. The "high-GM1" cells were then incubated with cholera toxin B subunits (CTB) and anti-CTB antibodies, a calcium ion influx was triggered and cytosolic calcium ion concentration was elevated by several folds.[46] This phenomenon was attributed to the clustering of cell surface GM1 by pentavalent CTB followed by the clustering of CTB by divalent anti-CTB antibodies. The clustering of GM1 by cross-linking with CTB and anti-CTB antibody was confirmed by BODIBY-GM1 labeling on Jurkat cells.[47] Multiple cell lines have been studied and exhibited the same calcium ion influx triggering, which was proven to be independent from cAMP, protein kinase C, phosphoinositides turnover, or CD3 receptors. [48-50] Therefore, it was proposed that calcium signaling occurs by aggregation of receptors in lipid rafts.[51]

The synthetic F-GM1 analogues have been subjected to the calcium signaling triggering on living cells to evaluate their activities. Mono- and tri-fluorinated GM1 analogues were compared with native GM1 to elucidate the structure-function relationship. Di-C6F13-GM1 was designed for self-assembly by using fluorous phase aggregation property, thus provide with a potential way to modulate the lipid rafts formation and cell signaling pathway.

3.3.2 Results and Discussion

3.3.2.1 Mono-fluorinated GM1 induced calcium signaling in Jurkat cells

Jurkat T cells can express ganglioside GM1 on the cell surface. Without external ganglioside GM1, Jurkat cells treated with cholera toxin B subunits followed by anti-CTB antibodies have shown the triggered calcium ion influx. (Fig 3.20 a and b) After introducing with external natural GM1 (25 μM), the triggered calcium ion influx has increased significantly, confirmed that the calcium signaling was dependent on GM1. (Fig 3.20 c and d) Similarly, the mono-fluorinated 18-F-GM1 (25 μM) triggered the cytosolic calcium ion concentration increase at the same level. (Fig 3.20 e and f) However, when Jurkat cells were treated with 18-F3-GM1, the triggered calcium ion influx was at the same level as wild type Jurkat cells with no external GM1, suggesting that the tri-fluorinated GM1 has no significant influence on calcium signaling pathway. (Fig 3.20 g and h) The anti-CD3 antibody has been used as a positive control for calcium signaling measurement (data not shown).

Compared to the mono-fluorinated GM1, the trifluoromethyl group in 18-F3-GM1 has a much larger size than the methyl group, and potentially results in extra influences on membrane patterning, clustering, and cholera toxin binding. One possibility could be the trifluorination dramatically changed the phase behavior of GM1 in plasma membranes and it no longer participates in the raft formation, thus the lipid rafts induced calcium signaling was not affected by the external trifluoro-GM1. The mono-fluorinated GM1 has similar steric demand as the hydrocarbon version (native GM1), so that it enhances in the lipid raft formation and triggers the rafts related cell signaling pathway as

efficient as the native GM1 does. These results are consistent to what we have observed in AFM study that 18-F-GM1 has similar phase behavior in lipid bilayers, whereas the 18-F3-GM1 caused significant change in the phase separation (see section 3.2 for details).

3.3.2.2 Neither natural GM1 nor F-GM1 induced calcium signaling in CHO-K1 cells.

CHO-K1 cells are devoid of ganglioside GM1 on the cell surface, which has been approved by FACS analysis in previous sections. F-GM1 analogues have been evaluated on CHO-K1 cells to trigger calcium ion influx as above. The incorporation of F-GM1 analogues on CHO-K1 cells and their binding to CTB have been verified by FACS analysis. However, not only the four fluorinated GM1 analogues (12-F-GM1, 18-F-GM1, 18-F3-GM1, and Di-C6F13-GM1) but the native GM1 as well showed no calcium ion influx triggered by CTB and anti-B antibody. (Fig 3.21 a-e) It probably because the calcium signaling pathway in CHO-K1 cells is not related to ganglioside GM1, or lipid rafts, as the original CHO-K1 cells lack GM1 on their surface. But other possibilities are not ruled out and further investigation is required to confirm the function of external GM1 on CHO-K1 cells.

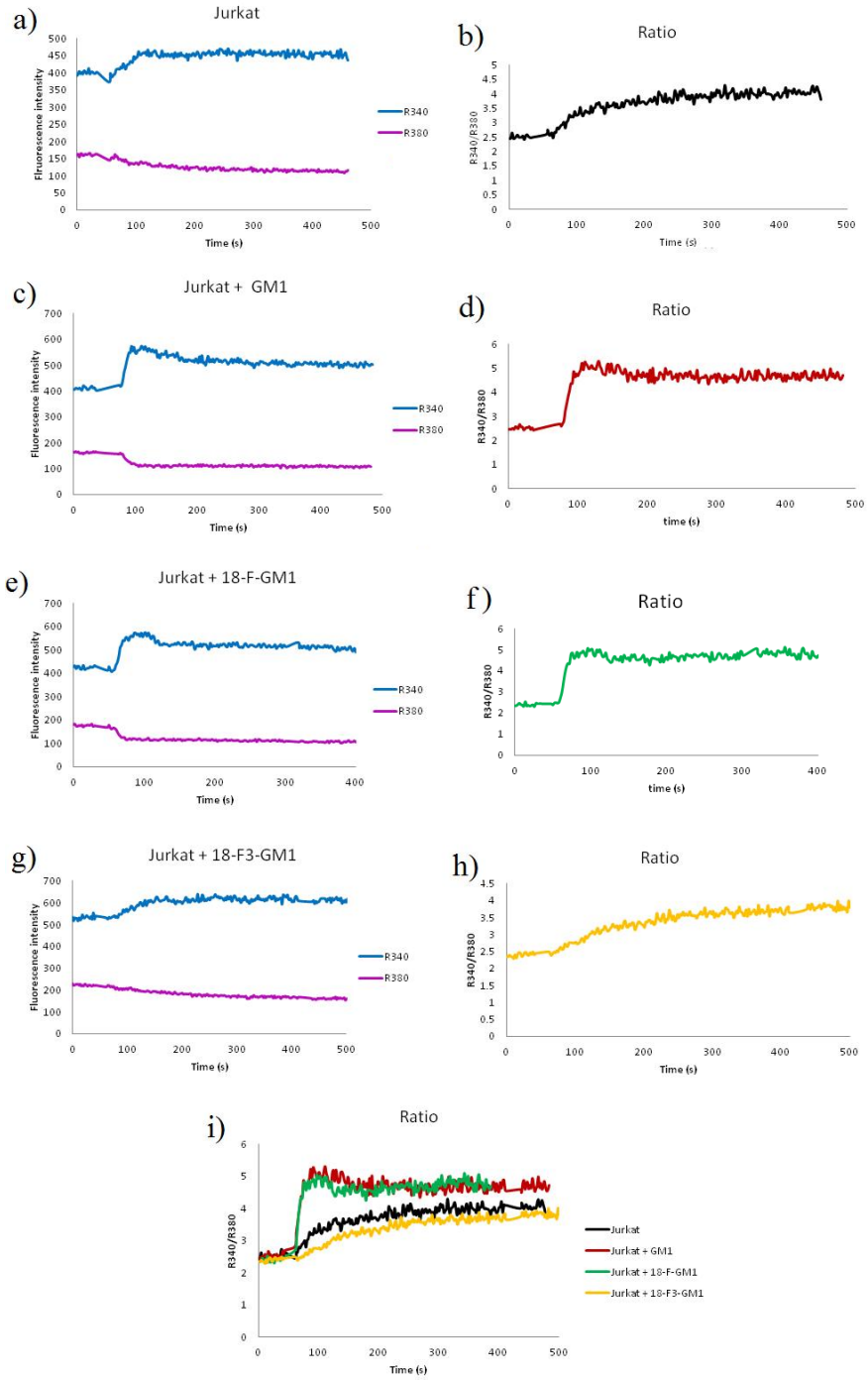

Fig 3.20 Induction of calcium concentration by GM1 and F-GM1 in Jurkat cells. a, c, e, g showed Jurkat cells incubated with buffer, natural GM1, 18-F-GM1, or 18-F3-GM1 followed by CTB, anti-B antibody, and fura-2/AM to evaluate the fluorescence change by calcium concentration at excitation 340 and 380 nm and excitation 510 nm. b, d, f, h are the ratio of fluorescence exited at 340 and 380 nm. i represented the ratios in one graph to compare them.

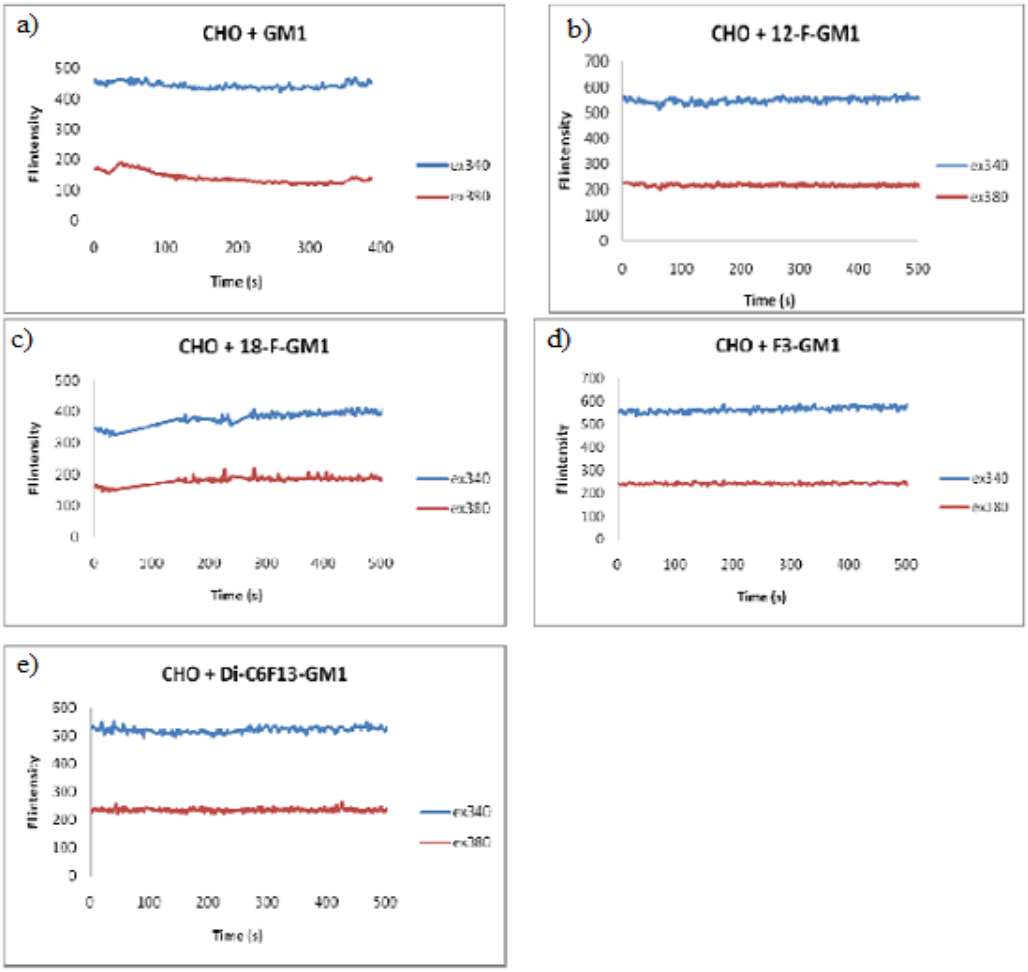

Fig 3.21 GM1 and F-GM1 did not induce calcium concentration change in CHO-K1 cells. CHO-K1 cells incubated with (a) natural GM1, (b) 12-F-GM1, (c) 18-F-GM1, (d) 18-F3-GM1, or (e) C6F13-GM1 followed by CTB, anti-B antibody, and fura-2/AM to evaluate the fluorescence change by calcium concentration at excitation 340 and 380 nm and excitation 510 nm.

3.3.3 Conclusions

The synthetic F-GM1 analogues have been incorporated onto mammalian cells to evaluate their ability of triggering calcium signaling. In Jurkat T cells, 18-F-GM1 induced calcium ion influx at the same level as the natural GM1, whereas 18-F3-GM1 did not induce significant change of cytosolic calcium ion concentration compared to the wild type Jurkat cells. The tri-fluorinated GM1 requires more steric demand than the mono-fluorinated analogue, thus may cause change of their phase properties and membrane behaviors in lipid raft formation, and result in different influences on cell signaling pathways. Since wild type Jurkat cells express natural GM1 on their surfaces, the calcium signaling assay always showed a large background. If the GM1 knock-out mutant of Jurkat cells is available, the F-GM1 induced calcium signaling could be more accurately analyzed.

CHO-K1 cells have been tested for calcium signaling with F-GM1 analogues, but none of them showed significant calcium ion concentration change including natural GM1, indicating that the calcium signaling pathway in CHO-K1 is not closely related to the GM1 concentration on cell surfaces. Better cell line platforms are required to test the F-GM1/cellular calcium signaling pathway relationship. In addition, as various cell signaling pathways are proven to be related to lipid raft formation, other cell signaling parhways such as protein phosphorylation[52,53] can be used to study lipid raft functions in living cells.

3.3.4 Experimental section

Materials. Human T cell leukemia Jurkat clone E6.1 (ATCC number: TIB-152) and CHO-K1 celsl (ATCC number: CCL-61) are from ATCC. CT B subunit is purchased from Sigma Aldrich. Anti-CTB antibody was from Meridian Life Science (Saco, ME). Anti-CD3 antibody is from Biolegend (San Diego, CA). Fura-2 acetoxymethyl ester (Fura-2/AM) is from AXXORA (San Diego, CA). The cell culture medium and buffer are from Invitrogen (Cambridge, MA). Other common reagents are from Sigma Aldrich.

Cell culture. Jurkat T cells (clone E6.1) were cultured in complete culture medium of RPMI 1640 medium supplemented with 10% FBS and antibiotics, and CHO-K1 cells were cultured in HAM-F12 medium with 10% FBS and antibiotics. The medium was changed 2-3 times a week, and cells with passage number 3-8 were used for calcium signaling assay. The cells were incubated at 37 °C under 5% CO_2 for 24 h before use. When indicated the cells were incubated in culture medium (10 % FBS) with exogenous 25 μM ganglioside GM1 (or F-GM1) for 2 h followed by incubation with 250 ng/mL CTB for 1 h after wash.

Ca^{2+} signaling measurement. Jurkat T cells were washed with 50 mM HEPES buffer (pH 7.2, supplemented with 120 mM NaCl, 1 mM $CaCl_2$, 0.5 mM $MgCl_2$, 5 mM KCl, 1 mM Na_2HPO_4, and 1 mg/mL of glucose) 3 times with 2 mL each, and incubated with 400 μL fura-2/AM[54] (5 mM in HEPES buffer) for 20 min, then add 7 mL of HEPES buffer and incubated for 20 min. The cells were washed once with HEPES buffer and resuspended in 2 mL of HEPES buffer in cuvettes for calcium assay. The cuvette of cells were prewarmed to 37 °C for 5 min, and fluorescence was measured with excitation at

340 and 380 nm and emission at 510 nm (10 nM slit widths for both em and ex). Calcium signaling in cells was triggered by adding anti-CTB antibody (40 μg/mL) and CTB (5μM) successively. Anti-CD3 antibody triggered calcium signaling was used for positive control. The fluorescence was monitored at 37 °C for 10 min.

3.4 References

(1) Zeller, C. B.; Marchase, R. B., Gangliosides as Modulators of Cell-Function. *Am. J. Physiol.* **1992**, *262*, C1341-C1355.

(2) Jenkins, A. T. A.; Williams, T. L., Measurement of the binding of cholera toxin to GM1 gangliosides on solid supported lipid bilayer vesicles and inhibition by europium (III) chloride. *J. Am. Chem. Soc.* **2008**, *130*, 6438-6443.

(3) Merritt, E. A.; Sarfaty, S.; Vandenakker, F.; Lhoir, C.; Martial, J. A.; Hol, W. G. J., Crystal-Structure of Cholera-Toxin B-Pentamer Bound to Receptor G(M1) Pentasaccharide. *Protein Sci.* **1994**, *3*, 166-175.

(4) Fritz, V. 1. M. R.; Daniotti, J.; Maccioni, H. J. F., Chinese hamster ovary cells lacking GM1 and GD1a synthesize gangliosides upon transfection with human GM2 synthase. *Biochim. Biophys. Acta* **1997**, *1354*, 153-158.

(5) Herzenberg, L. A.; Sweet, R. G.; Herzenberg, L. A., Fluorescence-activated Cell Sorting. *Sci Am* **1976**, *3*, 108-117.

(6) Fulwyler, M. J., Electronic Separation of Biological Cells by Volume. *Science* **1965**, *150*, 910-&.

(7) Horan, P. K.; Wheeless, L. L., Quantitative Single Cell Analysis and Sorting. *Science* **1977**, *198*, 149-157.

(8) Rusnati, M.; Urbinati, C.; Tanghetti, E.; Dell'Era, P.; Lortat-Jacob, H.; Presta, M., Cell membrane GM1 ganglioside is a functional coreceptor for fibroblast growth factor 2. *Proc. Natl. Acad. Sci. U. S. A.* **2002**, *99*, 4367-72.

(9) Bismuth, G.; Gouy, H.; Deterre, P., Signaling Via the Cell-Surface Ganglioside Gm1 in Human-T Cells - Induction of a Cell Calcium Mobilization and Influx by a Pathway Independent of Early Tyrosine Phosphorylations and of Inositol Phosphates Production. *J. Cell. Biochem.* **1993**, 283-283.

(10) Longo, M. L.; Goksu, E. I.; Vanegas, J. M.; Blanchette, C. D.; Lin, W. C., AFM for structure and dynamics of biomembranes. *Biochimica Et Biophysica Acta-Biomembranes* **2009**, *1788*, 254-266.

(11) Sahl, S. J.; Leutenegger, M.; Hilbert, M.; Hell, S. W.; Eggeling, C., Fast molecular tracking maps nanoscale dynamics of plasma membrane lipids. *Proc. Natl. Acad. Sci. U. S. A.* **2010**, *107*, 6829-34.

(12) Dufrene, Y. F.; Scheuring, S., Atomic force microscopy: probing the spatial organization, interactions and elasticity of microbial cell envelopes at molecular resolution. *Mol. Microbiol.* **2010**, *75*, 1327-1336.

(13) Gan, Y., Atomic and subnanometer resolution in ambient conditions by atomic force microscopy. *Surf. Sci. Rep.* **2009**, *64*, 99-121.

(14) Dufrene, Y. F., Towards nanomicrobiology using atomic force microscopy. *Nat. Rev. Microbiol.* **2008**, *6*, 674-680.

(15) Milhiet, P. E.; Seantier, B.; Giocondi, M. C.; Le Grimellec, C., Probing supported model and native membranes using AFM. *Curr. Opin. Colloid Interface Sci.* **2008**, *13*, 326-337.

(16) Engel, A.; Frederix, P. L. T. M.; Bosshart, P. D., Atomic Force Microscopy of Biological Membranes. *Biophys. J.* **2009**, *96*, 329-338.

(17) Longo, M. L.; Blanchette, C. D., Imaging cerebroside-rich domains for phase and shape characterization in binary and ternary mixtures. *Biochimica Et Biophysica Acta-Biomembranes* **2010**, *1798*, 1357-1367.

(18) Cremer, P. S.; Shi, J. J.; Yang, T. L.; Kataoka, S.; Zhang, Y. J.; Diaz, A. J., GM(1) clustering inhibits cholera toxin binding in supported phospholipid membranes. *J. Am. Chem. Soc.* **2007**, *129*, 5954-5961.
(19) Johnston, L. J.; Coban, O.; Burger, M.; Laliberte, M.; Ianoul, A., Ganglioside partitioning and aggregation in phase-separated monolayers characterized by bodipy GM1 monomer/dimer emission. *Langmuir* **2007**, *23*, 6704-6711.
(20) Zasadzinski, J. A. N.; Helm, C. A.; Longo, M. L.; Weisenhorn, A. L.; Gould, S. A. C.; Hansma, P. K., Atomic Force Microscopy of Hydrated Phosphatidylethanolamine Bilayers. *Biophys. J.* **1991**, *59*, 755-760.
(21) Meyer, E.; Howald, L.; Overney, R. M.; Heinzelmann, H.; Frommer, J.; Guntherodt, H. J.; Wagner, T.; Schier, H.; Roth, S., Molecular-Resolution Images of Langmuir-Blodgett-Films Using Atomic Force Microscopy. *Nature* **1991**, *349*, 398-400.
(22) Weisenhorn, A. L.; Egger, M.; Ohnesorge, F.; Gould, S. A. C.; Heyn, S. P.; Hansma, H. G.; Sinsheimer, R. L.; Gaub, H. E.; Hansma, P. K., Molecular-Resolution Images of Langmuir-Blodgett-Films and DNA by Atomic Force Microscopy. *Langmuir* **1991**, *7*, 8-12.
(23) Giocondi, M. C.; Le Grimellec, C., Temperature dependence of the surface topography in dimyristoylphosphatidylcholine/distearoylphosphatidylcholine multibilayers. *Biophys. J.* **2004**, *86*, 2218-2230.
(24) Le Grimellec, C.; Giocondi, M. C.; Yamamoto, D.; Lesniewska, E.; Milhiet, P. E.; Ando, T., Surface topography of membrane domains. *Biochimica Et Biophysica Acta-Biomembranes* **2010**, *1798*, 703-718.
(25) Muller, D. J.; Engel, A., Strategies to prepare and characterize native membrane proteins and protein membranes by AFM. *Curr. Opin. Colloid Interface Sci.* **2008**, *13*, 338-350.
(26) Ha, K. S.; Jung, S. H.; Park, D.; Park, J. H.; Kim, Y. M., Molecular imaging of membrane proteins and microfilaments using atomic force microscopy. *Exp. Mol. Med.* **2010**, *42*, 597-605.
(27) Le Grimellec, C.; Giocondi, M. C.; Seantier, B.; Dosset, P.; Milhiet, P. E., Characterizing the interactions between GPI-anchored alkaline phosphatases and membrane domains by AFM. *Pflugers Archiv-European Journal of Physiology* **2008**, *456*, 179-188.
(28) McPherson, A.; Kuznetsov, Y. G., Atomic Force Microscopy in Imaging of Viruses and Virus-Infected Cells. *Microbiology and Molecular Biology Reviews* **2011**, *75*, 268-285.
(29) Muller, D. J.; Krieg, M.; Alsteens, D.; Dufrene, Y. F., New frontiers in atomic force microscopy: analyzing interactions from single-molecules to cells. *Curr. Opin. Biotechnol.* **2009**, *20*, 4-13.
(30) Dufrene, Y. F., Nanoscale exploration of microbial surfaces using the atomic force microscope. *Future Microbiology* **2006**, *1*, 387-396.
(31) de Almeida, R. F. M.; Fedorov, A.; Prieto, M., Sphingomyelin/phosphatidylcholine/cholesterol phase diagram: Boundaries and composition of lipid rafts. *Biophys. J.* **2003**, *85*, 2406-2416.
(32) de Almeida, R. F. M.; Prieto, M., A model for raft/non-raft coexistence. Phosphatidylcholine/sphingomyelin/cholesterol ternary phase diagram. *Biophys. J.* **2003**, *84*, 325a-326a.

(33) Dufrene, Y. F.; Lee, G. U., Advances in the characterization of supported lipid films with the atomic force microscope. *Biochimica Et Biophysica Acta-Biomembranes* **2000**, *1509*, 14-41.
(34) Johnston, L. J.; Zou, S., Ceramide-enriched microdomains in planar membranes. *Curr. Opin. Colloid Interface Sci.* **2010**, *15*, 489-498.
(35) Yuan, C.; Furlong, J.; Burgos, P.; Johnston, L. J., The size of lipid rafts: an atomic force microscopy study of ganglioside GM1 domains in sphingomyelin/DOPC/cholesterol membranes. *Biophys. J.* **2002**, *82*, 2526-35.
(36) Yuan, C. B.; Johnston, L. J., Distribution of ganglioside GM1 in L-alpha-dipalmitoylphosphatidylcholine/cholesterol monolayers: A model for lipid rafts. *Biophys. J.* **2000**, *79*, 2768-2781.
(37) Vie, V.; Van Mau, N.; Lesniewska, E.; Goudonnet, J. P.; Heitz, F.; Le Grimellec, C., Distribution of ganglioside G(M1) between two-component, two-phase phosphatidylcholine monolayers. *Langmuir* **1998**, *14*, 4574-4583.
(38) Yuan, C.; Johnston, L. J., Atomic force microscopy studies of ganglioside GM1 domains in phosphatidylcholine and phosphatidylcholine/cholesterol bilayers. *Biophys. J.* **2001**, *81*, 1059-69.
(39) Palestini, P.; Allietta, M.; Sonnino, S.; Tettamanti, G.; Thompson, T. E.; Tillack, T. W., Gel Phase Preference of Ganglioside Gm1 at Low Concentration in 2-Component, 2-Phase Phosphatidylcholine Bilayers Depends Upon the Ceramide Moiety. *Biochimica Et Biophysica Acta-Biomembranes* **1995**, *1235*, 221-230.
(40) Reed, R. A.; Shipley, G. G., Properties of ganglioside G(M1) in phosphatidylcholine bilayer membranes. *Biophys. J.* **1996**, *70*, 1363-1372.
(41) Coban, O.; Burger, M.; Laliberte, M.; Ianoul, A.; Johnston, L. J., Ganglioside partitioning and aggregation in phase-separated monolayers characterized by bodipy GM1 monomer/dimer emission. *Langmuir* **2007**, *23*, 6704-11.
(42) Urisu, T.; Mao, Y.; Tero, R.; Imai, Y.; Hoshino, T., The morphology of GM1(x)/SM0.6-x/Chol(0.4) planar bilayers supported on SiO2 surfaces. *Chem. Phys. Lett.* **2008**, *460*, 289-294.
(43) Kiyokawa, E.; Baba, T.; Otsuka, N.; Makino, A.; Ohno, S.; Kobayashi, T., Spatial and functional heterogeneity of sphingolipid-rich membrane domains. *J. Biol. Chem.* **2005**, *280*, 24072-24084.
(44) Clapham, D. E., Calcium signaling. *Cell* **2007**, *131*, 1047-1058.
(45) Pozzan, T.; Rizzuto, R., Microdomains of intracellular Ca2+: Molecular determinants and functional consequences. *Physiological Reviews* **2006**, *86*, 369-408.
(46) Gouy, H.; Deterre, P.; Debre, P.; Bismuth, G., Calcium Signaling Via G(M1) Cell-Surface Gangliosides in the Human Jurkat T-Cell Line. *J. Immunol.* **1994**, *152*, 3271-3281.
(47) Ley, S. C.; Janes, P. W.; Magee, A. I., Aggregation of lipid rafts accompanies signaling via the T cell antigen receptor. *J. Cell Biol.* **1999**, *147*, 447-461.
(48) Spiegel, S.; Panagiotopoulos, C., Mitogenesis of 3t3 Fibroblasts Induced by Endogenous Ganglioside Is Not Mediated by Camp, Protein Kinase-C, or Phosphoinositides Turnover. *Exp. Cell Res.* **1988**, *177*, 414-427.
(49) Dixon, S. J.; Stewart, D.; Grinstein, S.; Spiegel, S., Transmembrane Signaling by the B-Subunit of Cholera-Toxin - Increased Cytoplasmic Free Calcium in Rat Lymphocytes. *J. Cell Biol.* **1987**, *105*, 1153-1161.

(50) Gouy, H.; Cefai, D.; Christensen, S. B.; Debre, P.; Bismuth, G., Cyclic Amp-Independent and Inositol Phosphate-Independent Inhibition of Ca2+ Influx by Cholera-Toxin in Cd3-Stimulated Jurkat T-Cells - a Study with a Cholera Toxin-Resistant Cell Variant and the Ca2+ Endoplasmic Reticulum-Atpase Inhibitor Thapsigargin. *J. Immunol.* **1991**, *147*, 757-766.
(51) Fang, Y.; Xie, X.; Ledeen, R. W.; Wu, G. S., Characterization of cholera toxin B subunit-induced Ca2+ influx in neuroblastoma cells: Evidence for a voltage-independent GM1 ganglioside-associated Ca2+ channel. *J. Neurosci. Res.* **2002**, *69*, 669-680.
(52) Kiyokawa, E.; Baba, T.; Otsuka, N.; Kobayashi, T., Spatial and functional heterogeneity of sphingolipid-rich membrane domains. *Cell Structure and Function* **2005**, *30*, 36-36.
(53) Duchemin, A. M.; Ren, Q.; Mo, L.; Neff, N. H.; Hadjiconstantinou, M., GM1 ganglioside induces phosphorylation and activation of Trk and Erk in brain. *J. Neurochem.* **2002**, *81*, 696-707.
(54) Malgaroli, A.; Milani, D.; Meldolesi, J.; Pozzan, T., Fura-2 Measurement of Cytosolic Free Ca-2+ in Monolayers and Suspensions of Various Types of Animal-Cells. *J. Cell Biol.* **1987**, *105*, 2145-2155.

Chapter 4

Phase behaviors of fluorinated GM1

NanoSIMS is a newly developed technique that image sample surface based on the secondary ion mass spectrometry (SIMS). Various biological samples, including biomembranes, have been analyzed on nanoSIMS to study their chemical composition. By using nano-SIMS, phase separation in supported lipid bilayers has been elucidated on a chemical composition manner.[1] We have employed the synthetic F-GM1 analogues in supported lipid bilayers to study their phase behaviors by nanoSIMS. Since fluorine is barely found in mammalian cells, the fluorine on F-GM1 analogues can be used to distinguish them from other molecules in nanoSIMS, as a distinct "F^-" secondary ion. Fluorine atoms are sensitive in nanoSIMS due to their high electron affinity, but their detailed influences on samples, such as minimum concentration request, fluorination level and region effects, interfering with neighbor molecules, have not been reported. Our purpose is to elucidate the distribution of fluorinated GM1 in the lipid bilayers using nano-SIMS scanning. The long-term goal is to develop a general platform to identify the distribution of bio-orthogonal labeled F-GM1 in plasma membrane and directly answer the question whether lipid rafts exist in living cells.

4.1 Secondary ion mass spectrometry

Mass spectrometry has been widely used to illustrate chemical compositions of complicated biological materials, such as the topological analysis of peptides,[2] proteins,[3,4] sugars[5] and nucleotides[6]. To date, there are two major methods of imaging mass spectrometry (IMS), the matrix-assisted laser desorption/ionization (MALDI) imaging and the SIMS imaging. MALDI imaging can analyze a small area of the sample surface by using a focused laser beam,[7] however, its resolution is restrained by the size of laser

spots and usually at micrometer scale.[8] SIMS imaging is a non-light excitation system and can generate secondary ions on the sample surface by a finely focused primary ion beam. Equipped with coaxial optics that enable copropagation of the primary and secondary ions, SIMS imaging has easily achieved the resolution of 100 nm.[9] SIMS was initially used in physics and materials science, and not until 2000 it has been applied to biological sample analysis.[9]

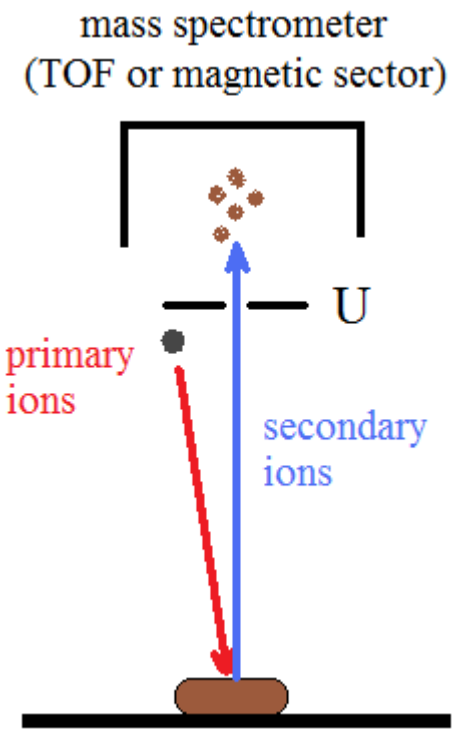

Fig 4.1 Schematic representative of secondary ion mass spectrometry (SIMS) instrument.

SIMS imaging uses a confined primary ion beam to scan across the sample surface and generate secondary ions that are analyzed by the mass spectrometer, either magnetic sector (nanoSIMS) or time of flight detector (TOF-SIMS).[9] (Fig 4.1) The NanoSIMS uses a continuous primary ion beam of either Cs (for negative secondary ions)

or O (for positive secondary ions), and can simultaneously analyze multiple secondary ions by using up to seven pre-selected m/z detectors. The TOF-SIMS analyze the secondary ions by using a time-of-flight mass spectrometer, thus can create a full mass spectrum of the materials at once.

SIMS imaging has been more and more used in analysis of biological sample in the last few years, such as plasma membranes[10,11], cell samples[12], and brain sections[13]. Using the nanoSIMS, the lipid or protein molecules are labeled with isotopes, including ^{2}H, ^{15}N, ^{13}C, ^{31}P, and ^{32}S, to distinguish the sample ions from the others.[14,15] The TOF-SIMS is able to detect up to m/z 1000, thus can recognize larger fragments to distinguish biological species and require no label of the samples.[16-18] A variety of solid supported lipid bilayers have been studied by SIMS imaging to illustrate their 2-D chemical compositions,[15,19-23] and phase separation has been observed in the membrane on both nano-SIMS[15] and TOF-SIMS[20,22,24]. For example, Kraft[15] and co-workers used isotopic label lipid probes successfully revealed the phase separation of lipid bilayers by high resolution nanoSIMS imaging. The 3-D imaging of cell samples has been achieved in TOF-SIMS by using C_{60}^{+} primary ions to bombard the sample surface and obtain SIMS images at different depths.[25,26] Recently, Fletcher[27] reported that the non-fixed frozen cell samples can gave more spatial information than chemically fixed frozen cell samples in both 2-D and 3-D TOF-SIMS imaging.

4.2 Results and discussion

4.2.1 Clustering of 12-F-GM1 in a quaternary mixture of lipid bilayers

The lipid bilayers containing 5% 12-F-GM1 has been analyzed by nanoSIMS to investigate the phase behavior in a quaternary mixture with SPM, DOPC, and cholesterol (2:2:1). Isotopic labeling of the lipid molecules and fluorination of GM1 enables distinguishing different substrates by their distinct secondary ions. It was not surprising that the mono-fluorination provides enough secondary F^- ions for nanoSIMS imaging, mainly due to the high electron affinity of fluorine atoms. NanoSIMS images revealed that 12-F-GM1 clustered with cholesterol to form microdomains, whereas SPM and DOPC coexist to fill out the major space of lipid bilayers. (Fig 4.2) The microdomains are in size of hundreds of nanometers to micron scales. This is the first nanoSIMS image of ganglioside GM1 residing in lipid domains in lipid bilayers. It confirmed the coalescence of GM1 and cholesterol to form lipid microdomains and SPM is away from these microdomains. The results fulfilled our goal to use F-GM1 as a tool to analyze the chemical compositions of lipid membranes and study lipid rafts by nanoSIMS.

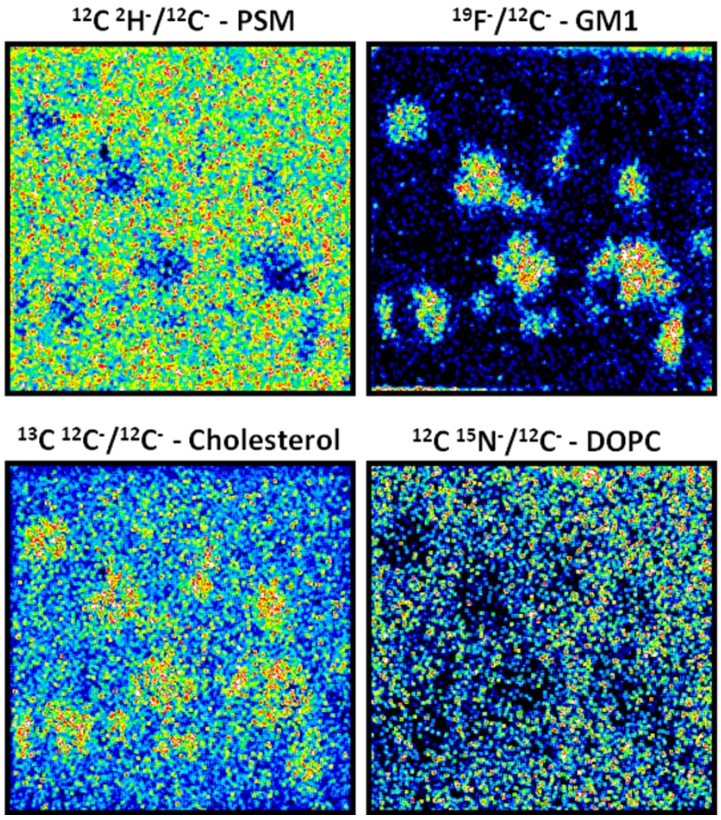

Fig 4.2 NanoSIMS imaging of 12-F-GM1 in lipid bilayers. (2:2:1 ^{2}H-SPM:^{15}N-DOPC:^{13}C-Cholesterol + 5mol% 12-^{19}F-GM1, raster size: 16×16 μm)

4.2.2 Clustering of 18-F-GM1 formed larger rafts in lipid bilayers

The 18-F-GM1 (5%) was applied to supported lipid bilayers (SPM/DOPC/cholesterol = 2:2:1) to analyze its phase behaviors by nanoSIMS. As a result, 18-F-GM1 and cholesterol rich microdomains have been observed, and interestingly, 18-F-GM1 formed much larger microdomains in lipid bilayers compared to that of 12-F-GM1. (Fig 4.3) The larger microdomains resulted in significant decrease of secondary ion signal intensity per unit area, which was not observed in 12-F-GM1 patches. In smaller patches by 12-F-GM1, the signal contrast between the GM1 rich and poor regions was clearer. Obviously,

the different behaviors between 18-F-GM1 and 12-F-GM1 were caused by their different fluorination positions. It is possible that compared to the terminal fluorination, the fluorine atom on the 12-position leads to a tilt angle in the lipid tail and results in a larger free volume of the molecule in lipid bilayer, thus decreases its ability to form large gel phases. This hypothesis can be easily verified by checking their phase transition temperatures (*T*m). In fact, an experiment of differential scanning calorimetry (DSC) test has been done and revealed the dramatically changed T_m of 12-F-GM1 (see details in section 4.2.3).

A type of tiny SPM-rich domains was also observed in the large cholesterol rich domains in the bilayers containing 18-F-GM1, and these tiny domains were immiscible with the cholesterol rich domains. A same image of the similar mixture (GM1 instead of 18-F-GM1) formed lipid bilayers was reported by Johnston[28], in which tiny domains were observed in large domains by AFM imaging. However, the AFM imaging only illustrated the height differences but not the chemical compositions, hence they interpret the tiny domains to be GM1 rich patches. Therefore, the nanoSIMS imaging is able to cover the backside of AFM imaging, and their combination provides a powerful tool to study biological membranes.

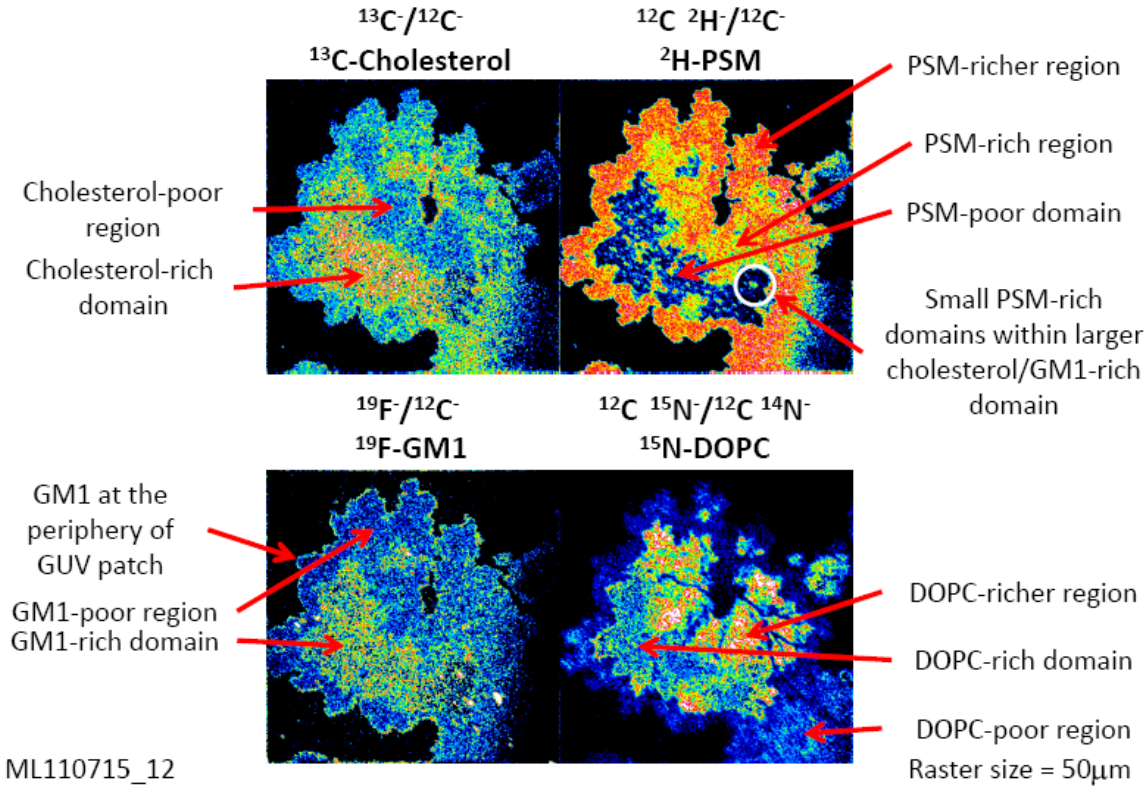

Fig 4.3 NanoSIMS imaging of 18-F-GM1 in lipid bilayers. (2:2:1 ^{2}H-SPM:^{15}N-DOPC:^{13}C-cholesterol + 5mol% 18-^{19}F-GM1, raster size: 50×50 μm)

4.2.3 Differential scanning calorimetry study on F-GM1 analogues

The phase transition temperature of GM1 analogues (2 mg/mL in water) were analyzed by differential scanning calorimetry (DSC) from 0 to 50 °C at 1 °C/min. These DSC scanning were cycled for at least 10 h incubation periods and perfect reproducible results were obtained. The native GM1 showed a broad peak of about 20 degrees, with maximum at 21 °C and 19 °C during heating and cooling scans, respectively. (Fig 4.4) This result is in agreement with previous report of phase transition temperature of hydrated GM1 by DSC scanning.[29] The terminal fluorinated GM1 showed similar

behavior in calorimetric scanning, in which 18-F-GM1 showed the T_m at 18 °C and 16 °C, whereas 18-F3-GM1 showed T_m at 17 °C and 15 °C during heating and cooling processes, respectively. (Fig 4.5 and 4.6) The slightly reduced T_m of terminal fluorinated GM1 could be explained by the reported T_m trend of fluorinated lipids that lipids with higher fluorination degree exhibits lower phase transition temperature.[30]

The 12-F-GM1 exhibited no obvious phase change peak within the calorimetric scanning temperature range, indicating a much lower T_m compared to other GM1 analogues. (Fig 4.7) The significant difference was proposed due to the tilted lipid tail of 12-F-GM1, thus resulted in a larger free volume of 12-F-GM1 molecule in lipid bilayers and lower T_m between ordered and disordered states. A simple reference could be DPPC (T_m = 41 °C) and POPC (T_m = -2 °C), in which the double bond in POPC causes a curved fatty acid chain and a larger free volume, hence dramatically reduces the phase transition temperatures. The DSC data explained our observation in nanoSIMS imaging that 18-F-GM1 and 12-F-GM1 formed different size of membrane domains in the lipid bilayers.

Overall, the DSC study of F-GM1 analogues revealed their phase behavior in membranes. Compared to native GM1, 18-F-GM1 and 18-F3-GM1 exhibited similar properties, whereas 12-F-GM1 exhibited a significant change. The 18-F-GM1 has the closest properties to the native GM1, suggesting its potential usage as a native GM1 mimic for biological and biophysical studies. The DSC studies strongly supported our investigation of F-GM1 behaviors in biological membranes.

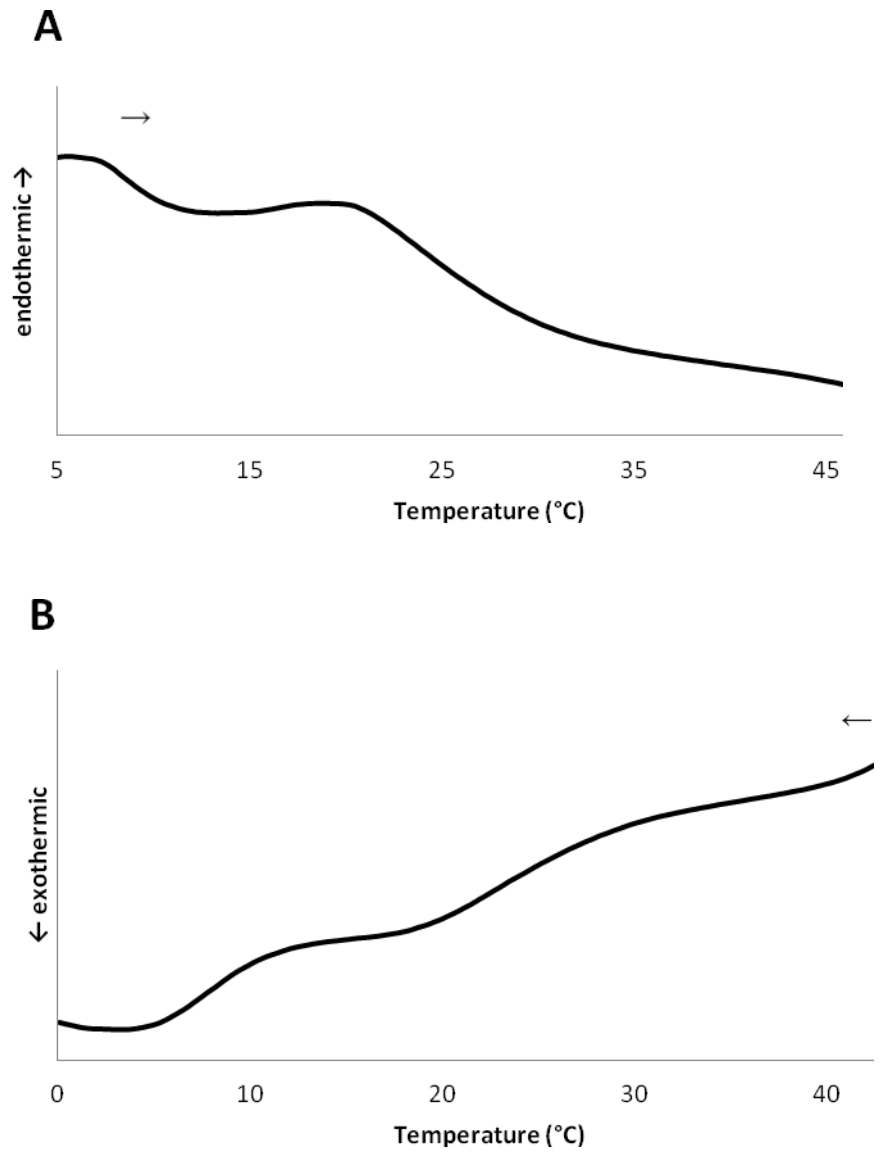

Figure 4.4 DSC heating/cooling scans of ganglioside GM1 in water (2 mg/mL) at scan rate of 1 °C/min. A. Heating scan, T_m= 21±1 °C. B. Cooling scan, T_m= 19±1 °C.

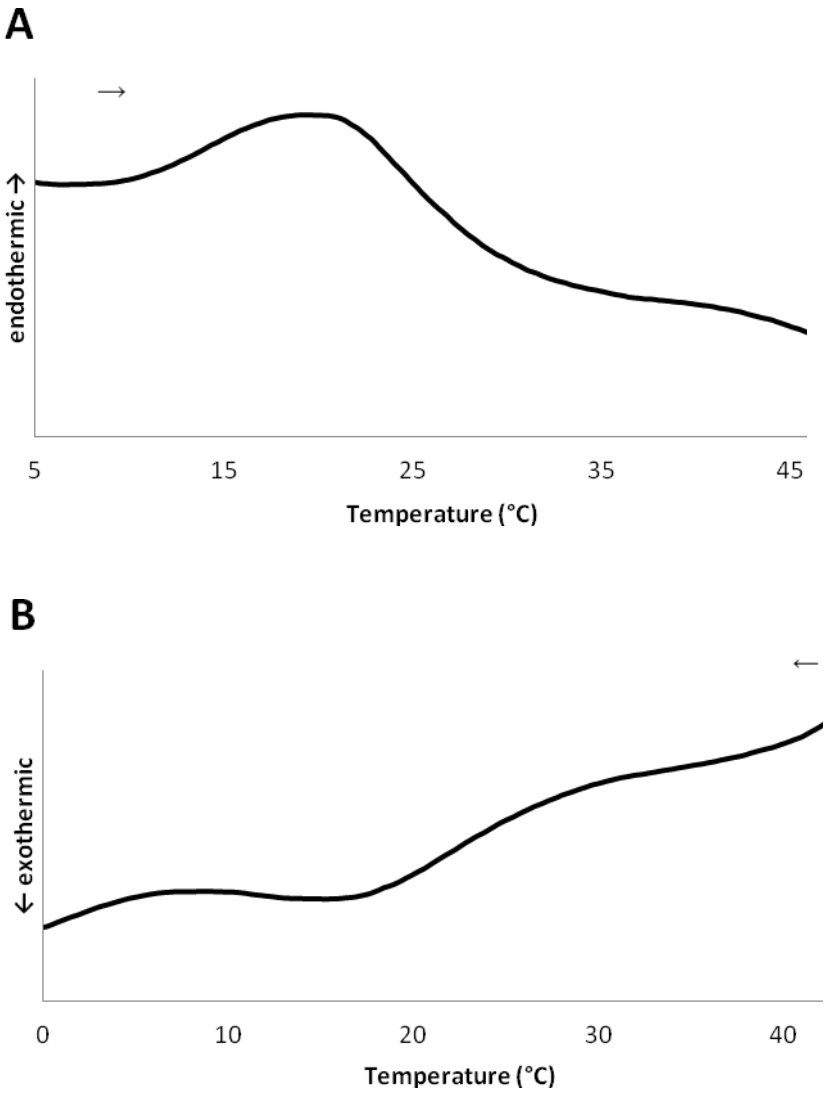

Figure 4.5 DSC scans of 18-F-GM1 in water (2 mg/mL) at scan rate of 1 °C/min. A. Heating scan, T_m= 18±2 °C. B. Cooling scan, T_m= 16±2 °C.

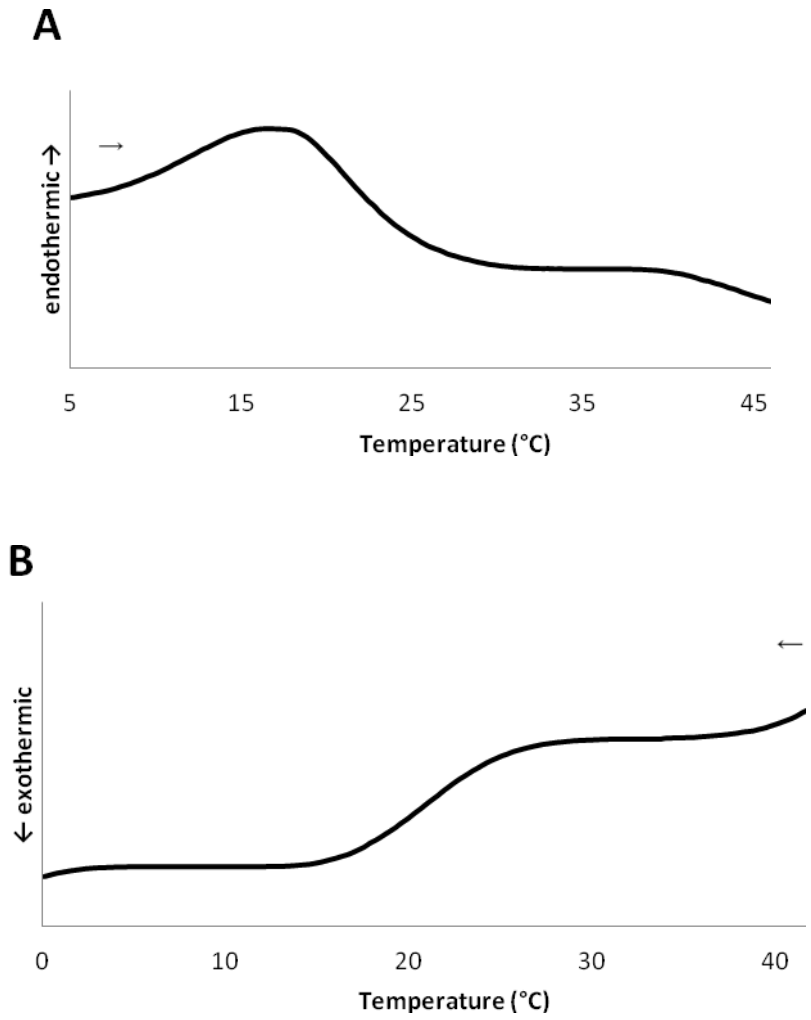

Figure 4.6 DSC scans of 18-F3-GM1 in water (2 mg/mL) at scan rate of 1 °C/min. A. Heating scan, T_m= 17±1 °C. B. Cooling scan, T_m= 15±1 °C.

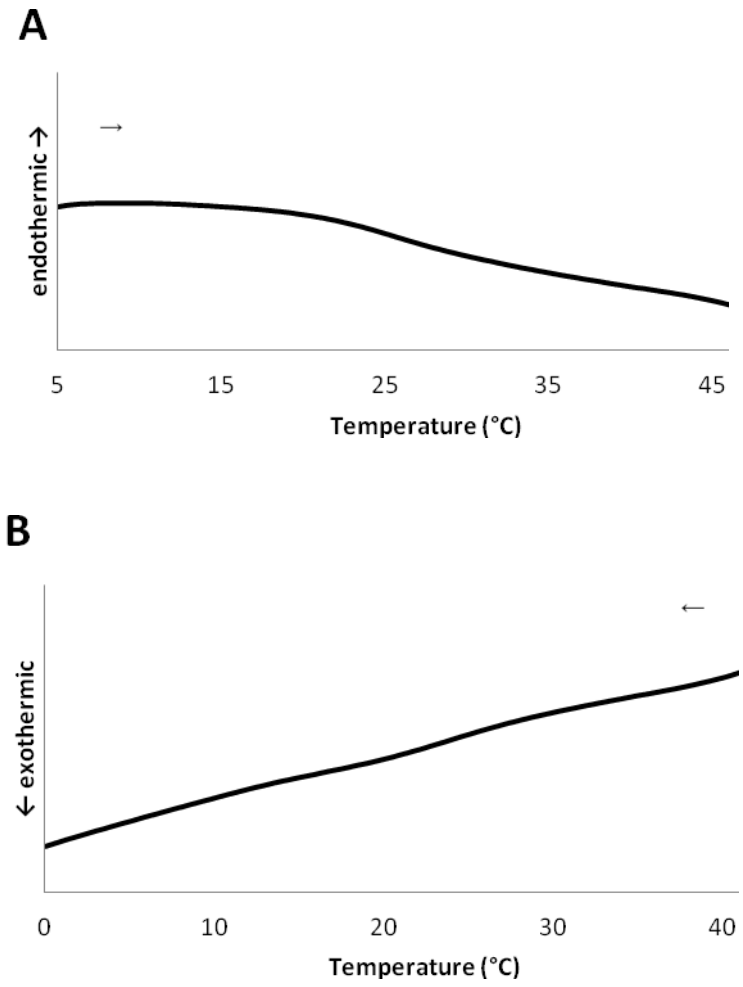

Figure 4.7 DSC scans of 12-F-GM1 in water (2 mg/mL) at scan rate of 1 °C/min, T_m was not observed within the temperature range. A. Heating scan. B. Cooling scan.

4.3 Conclusions

The F-GM1 analogues have been studied in a quaternary mixture of lipid bilayers and generated the first nanoSIMS image of F-GM1 and cholesterol rich lipid rafts. The mono-fluorination of GM1 generated sensitive and efficient secondary ion signal for nanoSIMS imaging. The different fluorination positions on GM1 resulted in different size of GM1-cholesterol rich domains in lipid bilayers. Further investigations by DSC scanning confirmed that 18-F-GM1 has similar phase properties as the native GM1, whereas 12-F-GM1 exhibited significant difference. Therefore, the 18-F-GM1 can be used in cell membrane to study the lipid rafts formation as an almost “label-free” GM1 probe. A type of tiny domains formed by SPM-DOPC was observed in the large GM1-cholesterol rich domains. Complemented with AFM and other cutting-edge analytical instruments, the nanoSIMS will definitely contribute an important role in cell membrane studies.

4.4 Experimental section

Preparation of the lipid bilayers. The lipid bilayers were prepared by fusing GUVs to a SiO_2/Si substrate forming lipid bilayer patches (the GUV ruptured into a dendritic patch as opposed to a close to circular patch) followed by thermal treatments to allow phase separation.

Nano-SIMS analysis of lipid bilayers. SIMS imaging was performed on the NanoSIMS 50L at Stanford University. The measurements were made with a ~2 pA $^{133}Cs^{+}$ primary ion beam focused on a ~100 nm diameter spot and rastered over sample areas that were 20 mm by 20 mm to 50 mm by 50 mm. The images consist of 10 replicate scans of 512 pixels by 512 pixels with a dwell time of 1 ms/pixel. Secondary ion intensities for $^{12}C^{-}$, $^{13}C^{-}$, $^{12}C^{2}H^{-}$, $^{19}F^{-}$, $^{12}C^{14}N^{-}$, and $^{12}C^{15}N^{-}$ were collected simultaneously in multi-collection mode. A mass resolving power of ~8900 and ~5600 were used to separate isobaric interferences $^{12}C^{2}H^{-}$ from $^{13}C^{1}H^{-}$ and $^{12}C^{1}H^{2-}$ at mass 14 and $^{12}C^{15}N^{-}$ from $^{13}C^{14}N^{-}$ at mass 27 respectively. Samples were also simultaneously imaged using secondary electrons.

Differential scanning calorimetry. The GM1 and F-GM1 analogues were dissolved in milliQ water (2 mg/mL) and injected to fill up the cell in calorimeter. Calorimetry scanning was performed on NanoDSC-II (Model 6100, Calorimetry Sciences Corporation, Provo, UT) and scanned at 1 °C/min from 0 to 50 °C after 1 h equilibrating.

4.5 References

(1) Kraft, M. L.; Weber, P. K.; Longo, M. L.; Hutcheon, I. D.; Boxer, S. G., Phase separation of lipid membranes analyzed with high-resolution secondary ion mass spectrometry. *Science* **2006**, *313*, 1948-51.
(2) Dorrestein, P. C.; Yang, Y. L.; Xu, Y. Q.; Straight, P., Translating metabolic exchange with imaging mass spectrometry. *Nat. Chem. Biol.* **2009**, *5*, 885-887.
(3) Yates, J. R.; Han, X. M.; Aslanian, A., Mass spectrometry for proteomics. *Curr. Opin. Chem. Biol.* **2008**, *12*, 483-490.
(4) Ahrens, C. H.; Brunner, E.; Qeli, E.; Basler, K.; Aebersold, R., Generating and navigating proteome maps using mass spectrometry. *Nat. Rev. Mol. Cell Biol.* **2010**, *11*, 789-801.
(5) Nana, K.; Satsuki, I.; Noritaka, H.; Akira, H.; Daisuke, T.; Teruhide, Y., Mass spectrometric analysis of carbohydrate heterogeneity for the characterization of glycoprotein-based products. *Trends in Glycoscience and Glycotechnology* **2008**, *20*, 97-116.
(6) Schurch, S.; Nyakas, A.; Stucki, S. R., Tandem Mass Spectrometry of Modified and Platinated Oligoribonucleotides. *J. Am. Soc. Mass Spectrom.* **2011**, *22*, 875-887.
(7) Jimenez, C. R.; Li, K. W.; Dreisewerd, K.; Spijker, S.; Kingston, R.; Bateman, R. H.; Burlingame, A. L.; Smit, A. B.; van Minnen, J.; Geraerts, W. P. M., Direct mass spectrometric peptide profiling and sequencing of single neurons reveals differential peptide patterns in a small neuronal network. *Biochemistry* **1998**, *37*, 2070-2076.
(8) Burnum, K. E.; Frappier, S. L.; Caprioli, R. M., Matrix-Assisted Laser Desorption/Ionization Imaging Mass Spectrometry for the Investigation of Proteins and Peptides. *Annual Review of Analytical Chemistry* **2008**, *1*, 689-705.
(9) Boxer, S. G.; Kraft, M. L.; Weber, P. K., Advances in Imaging Secondary Ion Mass Spectrometry for Biological Samples. *Annual Review of Biophysics* **2009**, *38*, 53-74.
(10) Nygren, H.; Borner, K.; Malmberg, P.; Mansson, J. E., Molecular imaging of lipids in cells and tissues. *Int. J. Mass Spectrom.* **2007**, *260*, 128-136.
(11) Johansson, B., ToF-SIMS imaging of lipids in cell membranes. *Surf. Interface Anal.* **2006**, *38*, 1401-1412.
(12) Fletcher, J. S.; Rabbani, S.; Henderson, A.; Blenkinsopp, P.; Thompson, S. P.; Lockyer, N. P.; Vickerman, J. C., A New Dynamic in Mass Spectral Imaging of Single Biological Cells. *Anal. Chem.* **2008**, *80*, 9058-9064.
(13) Clayton, D. F.; Amaya, K. R.; Monroe, E. B.; Sweedler, J. V., Lipid imaging in the zebra finch brain with secondary ion mass spectrometry. *Int. J. Mass Spectrom.* **2007**, *260*, 121-127.
(14) Boxer, S. G.; Marxer, C. G.; Kraft, M. L.; Weber, P. K.; Hutcheon, I. D., Supported membrane composition analysis by secondary ion mass spectrometry with high lateral resolution. *Biophys. J.* **2005**, *88*, 2965-2975.
(15) Boxer, S. G.; Kraft, M. L.; Weber, P. K.; Longo, M. L.; Hutcheon, I. D., Phase separation of lipid membranes analyzed with high-resolution secondary ion mass spectrometry. *Science* **2006**, *313*, 1948-1951.
(16) Heien, M. L.; Piehowski, P. D.; Davey, A. M.; Kurczy, M. E.; Sheets, E. D.; Winograd, N.; Ewing, A. G., Time-of-Flight Secondary Ion Mass Spectrometry Imaging

of Subcellular Lipid Heterogeneity: Poisson Counting and Spatial Resolution. *Anal. Chem.* **2009**, *81*, 5593-5602.
(17) Winograd, N.; Parry, S., High-resolution TOF-SIMS imaging of eukaryotic cells preserved in a trehalose matrix. *Anal. Chem.* **2005**, *77*, 7950-7957.
(18) Winograd, N.; Passarelli, M. K., Characterizing in situ Glycerophospholipids with SIMS and MALDI Methodologies. *Surf. Interface Anal.* **2011**, *43*, 269-271.
(19) Baker, M. J.; Zheng, L.; Winograd, N.; Lockyer, N. P.; Vickerman, J. C., Mass Spectral Imaging of Glycophospholipids, Cholesterol, and Glycophorin A in Model Cell Membranes. *Langmuir* **2008**, *24*, 11803-11810.
(20) Johnston, L. J.; Popov, J.; Vobornik, D.; Coban, O.; Keating, E.; Miller, D.; Francis, J.; Petersen, N. O., Chemical Mapping of Ceramide Distribution in Sphingomyelin-Rich Domains in Monolayers. *Langmuir* **2008**, *24*, 13502-13508.
(21) Heeren, R. M. A.; McDonnell, L. A.; de Lange, R. P. J.; Fletcher, I. W., Higher sensitivity secondary ion mass spectrometry of biological molecules for high resolution, chemically specific imaging. *J. Am. Soc. Mass Spectrom.* **2006**, *17*, 1195-1202.
(22) Winograd, N.; McQuaw, C. M.; Zheng, L. L.; Ewing, A. G., Localization of sphingomyelin in cholesterol domains by imaging mass spectrometry. *Langmuir* **2007**, *23*, 5645-5650.
(23) Ewing, A. G.; Piehowski, P. D.; Carado, A. J.; Kurczy, M. E.; Ostrowski, S. G.; Heien, M. L.; Winograd, N., MS/MS Methodology To Improve Subcellular Mapping of Cholesterol Using TOF-SIMS. *Anal. Chem.* **2008**, *80*, 8662-8667.
(24) Zheng, L.; McQuaw, C. M.; Baker, M. J.; Lockyer, N. P.; Vickerman, J. C.; Ewing, A. G.; Winograd, N., Investigating lipid-lipid and lipid-protein interactions in model membranes by ToF-SIMS. *Appl. Surf. Sci.* **2008**, *255*, 1190-1192.
(25) Wegener, J.; Breitenstein, D.; Rommel, C. E.; Mollers, R.; Hagenhoff, B., The chemical composition of animal cells and their intracellular compartments reconstructed from 3D mass spectrometry. *Angew. Chem., Int. Ed.* **2007**, *46*, 5332-5335.
(26) Mao, D.; Lu, C. Y.; Winograd, N., Molecular Depth Profiling by Wedged Crater Beveling. *Anal. Chem.* **2011**, *83*, 6410-6417.
(27) Fletcher, J. S.; Rabbani, S.; Henderson, A.; Lockyer, N. P.; Vickerman, J. C., Three-dimensional mass spectral imaging of HeLa-M cells - sample preparation, data interpretation and visualisation. *Rapid Commun. Mass Spectrom.* **2011**, *25*, 925-932.
(28) Yuan, C.; Furlong, J.; Burgos, P.; Johnston, L. J., The size of lipid rafts: an atomic force microscopy study of ganglioside GM1 domains in sphingomyelin/DOPC/cholesterol membranes. *Biophys. J.* **2002**, *82*, 2526-35.
(29) Reed, R. A.; Shipley, G. G., Properties of ganglioside GM1 in phosphatidylcholine bilayer membranes. *Biophys. J.* **1996**, *70*, 1363-72.
(30) Yoder, N. C.; Kalsani, V.; Schuy, S.; Vogel, R.; Janshoff, A.; Kumar, K., Nanoscale patterning in mixed fluorocarbon-hydrocarbon phospholipid bilayers. *J. Am. Chem. Soc.* **2007**, *129*, 9037-9043.

Chapter 5

Endocytic trafficking pathway of ganglioside GM1

Endocytosis has been an important strategy for drug delivery to the targets inside the cell. One of the endocytic pathways is the lipid rafts induced endocytosis, although its detailed mechanism is still unclear. Since ganglioside GM1 is a common molecule found in lipid rafts, modified GM1 could be a potential carrier to deliver cargos into the cells. However, the trafficking pathway of GM1 inside the cells remains under debate, mainly due to different probes used for GM1 tracking. In this chapter, we have designed a fluorescently labeled GM1 analogue to study the trafficking pathway of GM1 in mammalian cells, therefore provided with the theoretical basis for drug delivery using GM1 as a potential cargo carrier.

5.1 Background

Endocytosis is a controlled pathway for mammalian cells to take nutrients and essential materials from the environment into the cells.[1] The endocytosis process begins from the formation of vesicles with plasma membranes on the cell surface, followed by internalization and transport of the cargos inside the cells, and then the vesicles are sorted out in early endosomes and recycling endosomes, resulting in either degradation of cargos in lysosomes or back recycling to plasma membranes. To date, there are six endocytic pathways found in mammalian cells classified by different medias, such as clathrin, caveolae, CLIC/GEEC, IL2Rβ, Arf6, and flotillin, but mechanisms of most of them are still not clear.[2]

Glycosphingolipids, including ganglioside GM1, play an important role in the caveolar-type endocytosis pathway. Caveolae is consistently abundant in many cells, in a certain range, revealed by different endocytic markers, such as SV40 virions, cholera

toxin B subunit, and GPI-anchored proteins.[3,4] Caveolin1, the major caveolae forming membrane protein, can bind to the fatty acid tail of GM1 and co-localize with GM1 in cell membranes.[5] A clathrin independent endocytosis has also been observed in caveolin1 depleted cells with a cholesterol dependent manner, indicating the endocytic pathway is induced by a certain composition of lipids in plasma membranes. This endocytosis was then classified as lipid rafts induced endocytic pathway, and verified by many endocytic labels including CTB, GM1, SV40 virons, GPI-anchored proteins, and a variety of protein.[1,6]

Endocytosis is an important strategy to deliver macromolecules that are impermeable to plasma membranes into the cells.[7] In this strategy, the impermeable molecules are conjugated with a membrane permeable carrier that can be incorporated in to plasma membranes followed by internalization via endocytic pathways. A variety of hydrophobic or amphiphilic carriers have been designed to utilize endocytosis for delivery, such as lipids[8-10], peptides[11-13], and nano-particles[14-16]. As a common lipid rafts component in cell membranes, GM1 can construct a potential carrier that more efficiently via endocytic pathways, compared to other carriers that passively utilize endocytosis for delivery. With synthetic methods in hand to modify GM1, cargos can be easily conjugate to modified GM1 with a linker. Therefore, if we know the trafficking pathway of GM1 inside the cell, we can selectively deliver GM1 linked cargos to organelles.

The endocytic trafficking pathway of GM1 has been studied using different markers, such as CTB and anti-GM1 antibodies. However, different trafficking routes of GM1 have been observed using different markers.[17] For example, the fluorescently

labeled CTB was internalized by binding to cell surface GM1 and transported to early and recycling endosomes, trans-Golgi network (TGN), and endoplasmic reticulum (ER); whereas fluorescently labeled anti-GM1 antibodies were only found in early and recycling endosomes, followed by transporting back to plasma membranes but never reached golgi and ER. The differential trafficking of GM1 bound proteins suggested that proteins could influence the endocytic pathway and lead to different destinies. It was not surprising that CTB and antibodies can influence the GM1 tracking route, because both have much larger size than GM1 and could inevitably perturb the interactions between the bound GM1 and the surrounding molecules. In order to study the endocytic pathway of GM1, new GM1 tracking methods are required to reduce the steric effect, such as directly labeling of GM1 with fluorescent probes.

The fluorescently labeled GM1 was obtained in 1986, Acquotti[18] modified the natural GM1 by substituting the fatty acid chain with a pyrene labeled fatty acid. To date, a variety of GM1 derivatives with different fluorophores have been synthesized. Both the fatty acid tail and the 5-amidyl group on sialic acid have been employed as fluorescent modification sites.[19-24] These fluorescence active GM1 derivatives have been widely used to study biophysical properties and phase behaviors of GM1 both in artificial membranes and cell membranes.[23,25-28]

To study the endocytic trafficking pathway of GM1, we have designed to modify the 5-position of sialic acid with a NBD fluorophore. Since GM1 anchors into membranes with its lipid tails and leaves the oligosaccharide head group out in the aqueous solution, we modified the sialic acid residue with NBD to avoid affecting its

incorporation in membranes. In addition, the small size of NBD compared to other available fluorophores could minimize the potential influences on GM1 interaction with neighbors. In this chapter, the synthesis of NBD labeled GM1 and its trafficking pathway in Hela cells will be described.

5.2 Results and Discussions

5.2.1 Synthesis of NBD-GM1

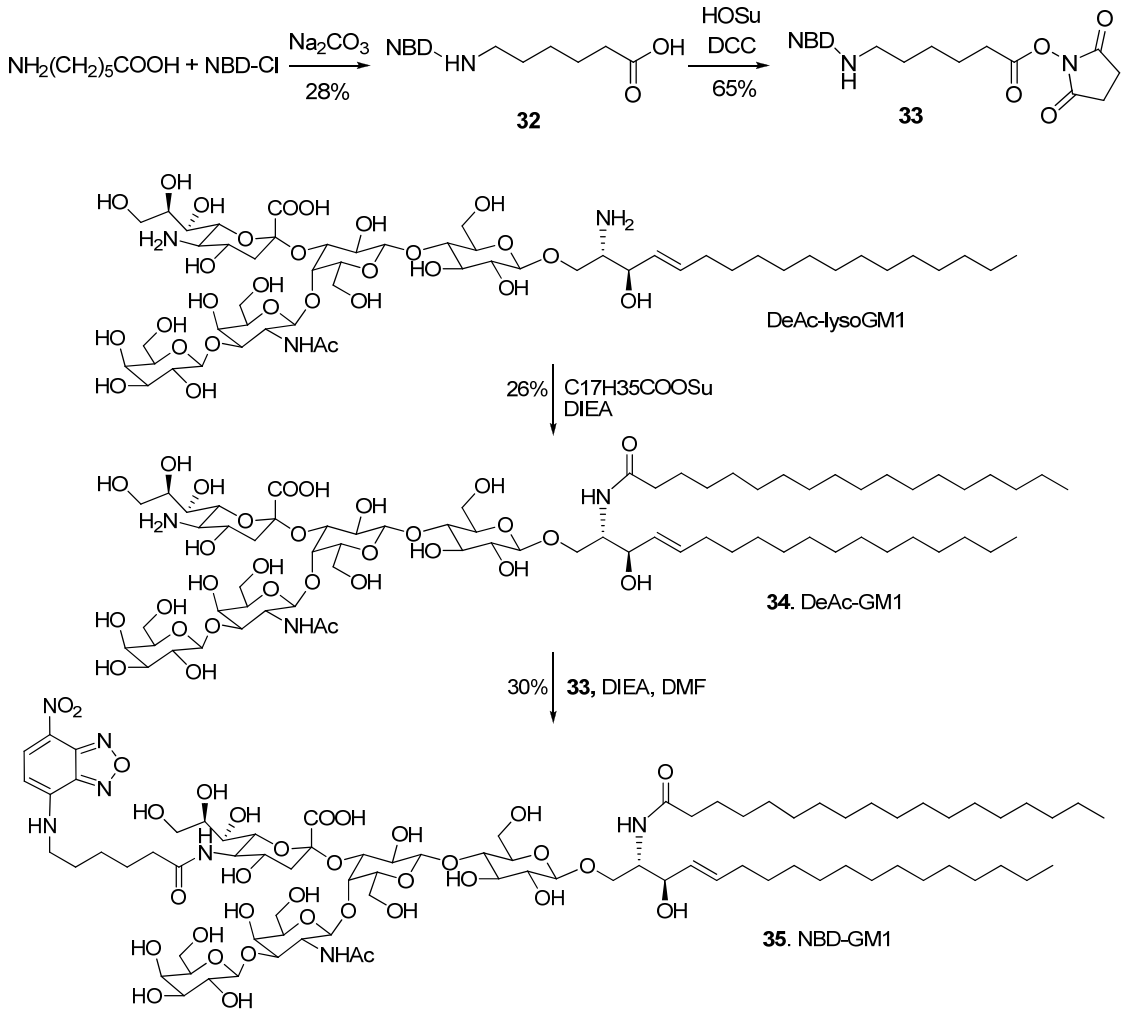

Scheme 5.1 Synthetic route to NBD labeled GM1 derivative **35**.

The NBD labeled of GM1 is achieved using deacetylated GM1 (DeAc-GM1) coupled with the NBD fluorophore. NBD-Cl was firstly tried to directly couple with DeAc-GM1 but the yield was found to be extremely low, mainly due to the steric hindrance on the oligosaccharide moiety. (data not shown) Therefore, NBD-Cl was coupled to a six carbon linker with a carboxylic acid terminal and treated with *N*-hydroxysuccinimidate and DCC to make an activated ester for coupling. DeAc-GM1 **34** was synthesized by selectively coupling of DeAc-lysoGM1 with NHS activated stearic acid on the sphingosine amine group under kinetic control. The steric hindrance of oligosaccharide moiety provided with a good selectivity on the sphingosine side, and hydrophobicity of stearic acid also potentially contributes to the same selectivity on the sphingosine. DeAc-GM1 was then coupled with NBD-linker-NHS ester togive NBD labeled GM1 derivative **35**.

5.2.2 Confocal imaging of NBD-GM1 in Hela cells

Hela cells that express GM1 on their surface were used to monitor the trafficking of GM1 inside the cells by confocal fluorescence microscopy. Briefly, Hela cells were incubated with NBD-GM1 **35** for 2 h to allow the internalization to occur. Cells were transfected with CellLight RFP agents to enable fluorescently labeling of ER or golgi complex by expressing RFP at corresponding organelles. Lysosomes, early endosomes, and recycling endosomes were labeled using lysotracker, Dextran-Texas Red, and Tf-Alex Fluor stain, respectively. Cell nuclei were stained by DRAQ.

The confocal imaging revealed a differential endocytic trafficking pathway of GM1 in Hela cells. (Fig 5.1) By comparing the co-localization with other dyes, NBD-GM1 was observed significantly accumulation in lysosomes, golgi, and ER, trace amount

in early endosomes and recycling endosomes, and none was observed in the nuclei. It can be, thus, suggested that the external GM1 will be mainly delivered to lysosomes, golgi, and ER by endocytic pathway. Drugs that have targets in lysosomes, golgi, or ER could be potentially delivered by GM1 carriers. Certainly, the actual design and application of GM1 assisted drug delivery require a lot of work to do. But the synthesized fluorescently labeled GM1 and cargo linked GM1 can also be used in detections and studies of interaction between the cargo and other molecules on a membrane platform. Additionally, the novel design of GM1 modification highlighted the application of lipid rafts theory on a broad way.

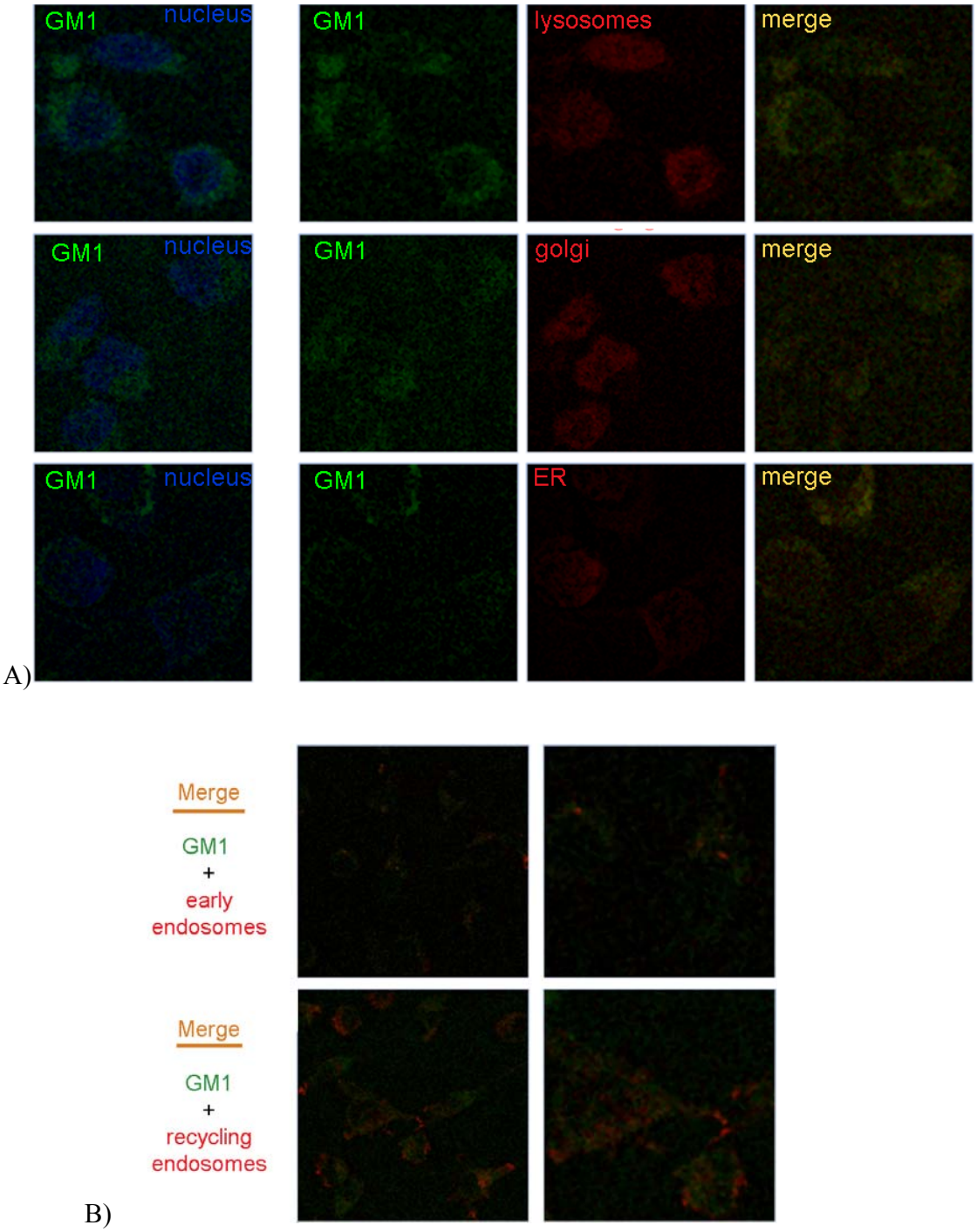

Fig 5.1 Confocal imaging of NBD labeled GM1 in Hela cells. A) Hela cells were incubated with 5 μM NBD-GM1 at 37 °C for 1 h followed by 100 ng/mL lysotracker stain for 30 min (1st row), or transfected Hela cells expressing RFP targeting golgi (2nd row) or ER (3rd row) incubated with 5 μM NBD-GM1 at 37 °C for 1 h. B) Hela cells were incubated with 5 μM NBD-GM1 at 37 °C for 1 h followed by 1 mg/mL Dextran-Texas Red (1st row) or 50 μg/mL Tf-Alex Fluor 647 stain (2nd row) for 30 min.

5.4 Conclusions

Ganglioside GM1 plays an important role in the clathrin independent endocytosis processes. However, the endocytic pathway of GM1 still remains unclear. Fluorescently modification of GM1 was synthesized to investigate its trafficking pathway in living cells. NBD labeling on the carbohydrate moiety was used in the design to minimize possible influence and interaction on the trafficking pathway. The external NBD labeled GM1 was incorporated onto Hela cells and analyzed using confocal fluorescence microscopy imaging. By comparing the localized positions of NBD-GM1 with other cell machinery stains, the external GM1 was found accumulated in lysosomes, golgi complex, and ER, whereas in the early endosomes, recycling endosomes and nuclei seldom or none of NBD-GM1 was observed. The results briefly described the endocytic GM1 trafficking pathway in Hela cells, provided with potential applications in further molecular probe design and drug delivery exertion.

5.5 Experimental section

Materials and instruments. The Hela cell line was obtained from Cancer center, Tufts Medical School. Common chemicals were purchased from Sigma-Aldrich, USA. CellLight^{TM} RFP BacMam 2.0 was purchased from Invitrogen, MA. Silica gel 60A 230-400 mesh for column chromatography was from Whatman Inc. (Piscataway, NJ, USA). Routine NMR spectra were obtained from Bruker DPX-300 NMR and Bruker Avance III 500 MHz NMR instruments. The low resolution mass spectra were obtained from Finnigan LTQ Mass Spectrometer, and the GM1 derivatives were analyzed under negative mode.

Synthesis of NBD labeled GM1 derivative.

6-(7-nitrobenzo[c][1,2,5]oxadiazol-4-ylamino)hexanoic acid 32. The 6-aminohexanoic acid (180 mg, 1.37 mmol) was dissolved in 2N aq. Na_2CO_3 (2 mL) and warmed up to 55 °C. NBD-Cl (140 mg, 0.7 mmol) was added and the mixture was stirred at same temperature for 2 h. The solution was cooled to r.t. and solvent was removed on lyophilizer. The residue was purified through flash column chromatography with 10% MeOH-$CHCl_3$ to afford 58 mg product (yield 28%).

^{1}H NMR ($CDCl_3$, 500 MHz): δ = 8.50 (d, 1H), 6.43 (s, 1H), 6.18 (d, 1H), 3.52 (t, 2H), 2.42 (t, 2H), 1.86 (p, 2H), 1.74 (p, 2H), 1.55 (m, 2H)

2,5-dioxopyrrolidin-1-yl 6-(7-nitrobenzo[c][1,2,5]oxadiazol-4-ylamino)hexanoate 33. The compound **32** (58 mg, 0.20 mmol) and N-hydroxysuccinimidate (45 mg, 0.40 mmol) were suspended in 2 mL anhydrous THF. The mixture was added DCC (162 mg, 0.80 mmol) and stirred at r.t. for 12 h. Solvent was removed under *vacuo* and the residue was purified through flash column chromatography with 5% EtOAc-hexane to give 50 mg product (yield 65%).

^{1}H NMR ($CDCl_3$, 500 MHz): δ = 8.50 (d, 1H), 6.43 (s, 1H), 6.19 (d, 1H), 3.54 (t, 2H), 2.87 (s, 4H), 2.67 (t, 2H), 1.87 (p, 4H), 1.64 (p, 2H)

DeAc-GM1 34. DeAc-LysoGM1 (32.6 mg, 26 μmol) and $C_{17}H_{35}COOSu$ (10.0 mg, 26 μmol) were suspended in 1 mL dry DMF and cooled to 0 °C, then added in DIEA 50 μL. The mixture was stirred at 4°C for 24 hrs. Solvent was removed under *vacuo*. Residue

was purified through preparative silica gel TLC with $CHCl_3$-MeOH-H_2O (v/v/v, 60:40:9) to give 9.2 mg product (23%).

MALDI-TOF: *m/z* $[C_{71}H_{129}N_3O_{30} - H]^-$ calc: 1502.9, found: 1502.5; *m/z* $[C_{73}H_{133}N_3O_{30} - H]^-$ calc: 1530.9, found: 1530.6

NBD-GM1 35. DeAc-GM1 **34** (4.2 mg, 2.8 μmol)) and compound **33** (3.4 μmol) were dissolved in 0.6 mL anhydrous DMF and added 50 μL DIEA. The mixture was stirred at r.t. 24 h. Solvent was removed under *vacuo*. Residue was purified through preparative silica gel TLC with $CHCl_3$-MeOH-H_2O (v/v/v, 60:40:5) to give 1.1 mg product (30%).

MALDI-TOF: *m/z* $[C_{83}H_{141}N_7O_{34} - H]^-$ calc: 1778.9, found: 1778.5; *m/z* $[C_{85}H_{145}N_7O_{34} - H]^-$ calc: 1806.9, found: 1806.5

Cell culture and fluorescent stain. Hela cells were cultured in DMEM cell culture medium supplemented with 10% fetal bovine serum and 1% penicillin sp. The cultured Hela cells were incubated in 24-well plate (20,000 cells /well) in 0.5 mL DMEM and allowed to adhere for 4-5 hrs. CellLight™ RFP that target ER and Golgi (10 μL, 50 PPC) was added to each well and incubate at 37 °C for 24 hrs. After wash with fresh medium (0.5 mL × 3) the cells were incubateded with 5 μM NBD-GM1 in DMEM medium for 1 hr. The cells were washed (0.5 mL × 3) and stained with lysotracker (100 ng/mL), Dextran-Texas Red (1 mg/mL) and Tf-Alex Fluor 647 (50 μg/mL) in 250 μL medium at 37 °C for 30 min. Then the cells were washed with PBS buffer and fixed with 4% Formaldehyde for 30 min @ 4°C, followed by washing off excess formaldehyde with PBS and stained with DRAQ5 in PBS (0.5 μM) for 10 min. Finally, the cells on

coverslips were mounted onto glass slides with 10 μL fluoromount and allowed to dry for 1 hr before analyzed by confocal fluorescence microscope imaging.

Confocal fluorescence microscopy. Imaging (CLSM) was performed on a Zeiss LSM510 Meta confocal microscope using the argon 458-nm excitation laser.

5.6 References

(1) Kirkham, M.; Parton, R. G., Clathrin-independent endocytosis: new insights into caveolae and non-caveolar lipid raft carriers. *Biochim. Biophys. Acta* **2005**, *1745*, 273-86.
(2) Doherty, G. J.; McMahon, H. T., Mechanisms of endocytosis. *Annu. Rev. Biochem.* **2009**, *78*, 857-902.
(3) Parton, R. G.; Simons, K., The multiple faces of caveolae. *Nat. Rev. Mol. Cell Biol.* **2007**, *8*, 185-94.
(4) Schmid, E. M.; Ford, M. G.; Burtey, A.; Praefcke, G. J.; Peak-Chew, S. Y.; Mills, I. G.; Benmerah, A.; McMahon, H. T., Role of the AP2 beta-appendage hub in recruiting partners for clathrin-coated vesicle assembly. *PLoS Biol.* **2006**, *4*, e262.
(5) Fra, A. M.; Masserini, M.; Palestini, P.; Sonnino, S.; Simons, K., A Photo-Reactive Derivative of Ganglioside Gm1 Specifically Cross-Links Vip21-Caveolin on the Cell-Surface. *FEBS Lett.* **1995**, *375*, 11-14.
(6) Helenius, A.; Damm, E. M.; Pelkmans, L.; Kartenbeck, J.; Mezzacasa, A.; Kurzckalia, T., Clathrin- and caveolin-1-independent endocytosis: entry of simian virus 40 into cells devoid of caveolae. *J. Cell Biol.* **2005**, *168*, 477-488.
(7) Smith, D. A.; van de Waterbeemd, H., Pharmacokinetics and metabolism in early drug discovery. *Curr. Opin. Chem. Biol.* **1999**, *3*, 373-378.
(8) Bildstein, L.; Dubernet, C.; Couvreur, P., Prodrug-based intracellular delivery of anticancer agents. *Adv. Drug Delivery Rev.* **2011**, *63*, 3-23.
(9) Schroeder, A.; Levins, C. G.; Cortez, C.; Langer, R.; Anderson, D. G., Lipid-based nanotherapeutics for siRNA delivery. *Journal of Internal Medicine* **2010**, *267*, 9-21.
(10) Boonyarattanakalin, S.; Hu, J. F.; Dykstra-Rummel, S. A.; August, A.; Peterson, B. R., Endocytic delivery of vancomycin mediated by a synthetic cell surface receptor: Rescue of bacterially infected mammalian cells and tissue targeting in vivo. *J. Am. Chem. Soc.* **2007**, *129*, 268-269.
(11) Morris, M. C.; Depollier, J.; Mery, J.; Heitz, F.; Divita, G., A peptide carrier for the delivery of biologically active proteins into mammalian cells. *Nat. Biotechnol.* **2001**, *19*, 1173-1176.
(12) Burlina, F.; Sagan, S.; Bolbach, G.; Chassaing, G., Quantification of the cellular uptake of cell-penetrating peptides by MALDI-TOF mass spectrometry. *Angew. Chem., Int. Ed.* **2005**, *44*, 4244-4247.
(13) Ron, G.; Glister, J.; Lee, B.; Allada, K.; Armstrong, W.; Arrington, J.; Beck, A.; Benmokhtar, F.; Berman, B. L.; Boeglin, W.; Brash, E.; Camsonne, A.; Calarco, J.; Chen, J. P.; Choi, S.; Chudakov, E.; Coman, L.; Craver, B.; Cusanno, F.; Dumas, J.; Dutta, C.; Feuerbach, R.; Freyberger, A.; Frullani, S.; Garibaldi, F.; Gilman, R.; Hansen, O.; Higinbotham, D. W.; Holmstrom, T.; Hyde, C. E.; Ibrahim, H.; Ilieva, Y.; De Jager, C. W.; Jiang, X.; Jones, M. K.; Kang, H.; Kelleher, A.; Khrosinkova, E.; Kuchina, E.; Kumbartzki, G.; LeRose, J. J.; Lindgren, R.; Markowitz, P.; Beck, S. M. T.; McCullough, E.; Meekins, D.; Meziane, M.; Meziani, Z. E.; Michaels, R.; Moffit, B.; Norum, B. E.; Oh, Y.; Olson, M.; Paolone, M.; Paschke, K.; Perdrisat, C. F.; Piasetzky, E.; Potokar, M.; Pomatsalyuk, R.; Pomerantz, I.; Puckett, A.; Punjabi, V.; Qian, X.; Qiang, Y.; Ransome, R.; Reyhan, M.; Roche, J.; Rousseau, Y.; Saha, A.; Sarty, A. J.; Sawatzky, B.; Schulte, E.; Shabestari, M.; Shahinyan, A.; Shneor, R.; Sirca, S.; Slifer, K.; Solvignon, P.; Song, J.; Sparks, R.; Subedi, R.; Strauch, S.; Urciuoli, G. M.; Wang, K.; Wojtsekhowski, B.; Yan,

X.; Yao, H.; Zhan, X.; Zhu, X., Measurements of the proton elastic-form-factor ratio mu(p)G(E)(p)/G(M)(p) at low momentum transfer. *Phys. Rev. Lett.* **2007**, *99*.
(14) Iversen, T.-G.; Skotland, T.; Sandvig, K., Endocytosis and intracellular transport of nanoparticles: Present knowledge and need for future studies. *Nano Today* **2011**, *6*, 176-185.
(15) Chen, X.; Tam, U. C.; Czlapinski, J. L.; Lee, G. S.; Rabuka, D.; Zettl, A.; Bertozzi, C. R., Interfacing carbon nanotubes with living cells. *J. Am. Chem. Soc.* **2006**, *128*, 6292-6293.
(16) Kam, N. W. S.; Liu, Z.; Dai, H. J., Functionalization of carbon nanotubes via cleavable disulfide bonds for efficient intracellular delivery of siRNA and potent gene silencing. *J. Am. Chem. Soc.* **2005**, *127*, 12492-12493.
(17) Daniotti, J. L.; Iglesias-Bartolome, R.; Trenchi, A.; Comin, R.; Moyano, A. L.; Nores, G. A., Differential endocytic trafficking of neuropathy-associated antibodies to GM1 ganglioside and cholera toxin in epithelial and neural cells. *Biochimica Et Biophysica Acta-Biomembranes* **2009**, *1788*, 2526-2540.
(18) Acquotti, D.; Sonnino, S.; Masserini, M.; Casella, L.; Fronza, G.; Tettamanti, G., A New Chemical Procedure for the Preparation of Gangliosides Carrying Fluorescent or Paramagnetic Probes on the Lipid Moiety. *Chem. Phys. Lipids* **1986**, *40*, 71-86.
(19) Song, W. X.; Rintoul, D. A., Synthesis and Characterization of N-Parinaroyl Ganglioside Gm1 - Effect of Choleragen Binding on Fluorescence Anisotropy in Model Membranes. *Biochemistry* **1989**, *28*, 4194-4200.
(20) Ito, M.; Nakagawa, T.; Tani, M.; Kita, K., Preparation of fluorescence-labeled GM1 and sphingomyelin by the reverse hydrolysis reaction of sphingolipid ceramide N-deacylase as substrates for assay of sphingolipid-degrading enzymes and for detection of sphingolipid-binding proteins. *Journal of Biochemistry* **1999**, *126*, 604-611.
(21) Schwarzmann, G.; Wendeler, M.; Sandhoff, K., Synthesis of novel NBD-GM1 and NBD-GM2 for the transfer activity of GM2-activator protein by a FRET-based assay system. *Glycobiology* **2005**, *15*, 1302-1311.
(22) Hindsgaul, O.; Larsson, E. A.; Olsson, U.; Whitmore, C. D.; Martins, R.; Tettamanti, G.; Schnaar, R. L.; Dovichi, N. J.; Palcic, M. M., Synthesis of reference standards to enable single cell metabolomic studies of tetramethylrhodamine-labeled ganglioside GM1. *Carbohydr. Res.* **2007**, *342*, 482-489.
(23) Johansson, L. B. A.; Mikhalyov, I.; Gretskaya, N., Fluorescent BODIPY-labelled G(M1) gangliosides designed for exploring lipid membrane properties and specific membrane-target interactions. *Chem. Phys. Lipids* **2009**, *159*, 38-44.
(24) Belov, V. N.; Polyakova, S. M.; Yan, S. F.; Eggeling, C.; Ringemann, C.; Schwarzmann, G.; de Meijere, A.; Hell, S. W., New GM1 Ganglioside Derivatives for Selective Single and Double Labelling of the Natural Glycosphingolipid Skeleton. *Eur. J. Org. Chem.* **2009**, 5162-5177.
(25) Johnston, L. J.; Coban, O.; Burger, M.; Laliberte, M.; Ianoul, A., Ganglioside partitioning and aggregation in phase-separated monolayers characterized by bodipy GM1 monomer/dimer emission. *Langmuir* **2007**, *23*, 6704-6711.
(26) Samsonov, A.; Mikhalyov, I., Lipid raft detecting in membranes of live erythrocytes. *Biochimica Et Biophysica Acta-Biomembranes* **2011**, *1808*, 1930-1939.

(27) Corbeil, D.; Freund, D.; Fonseca, A. V.; Janich, P.; Bornhauser, M., Differential expression of biofunctional GM1 and GM3 gangliosides within the plastic-adherent multipotent mesenchymal stromal cell population. *Cytotherapy* **2010**, *12*, 131-142.
(28) Eggeling, C.; Ringemann, C.; Medda, R.; Schwarzmann, G.; Sandhoff, K.; Polyakova, S.; Belov, V. N.; Hein, B.; von Middendorff, C.; Schonle, A.; Hell, S. W., Direct observation of the nanoscale dynamics of membrane lipids in a living cell. *Nature* **2009**, *457*, 1159-U121.

Chapter 6

Conclusions and perspective

The biological role of cell membranes has drawn attention in the last few decades. Proteins in plasma membranes regulate a wide range of biological processes, such as cell-cell interactions, cell signaling and adhesion, and virus infections. Some lipid molecules in the membranes also participate in cell regulating,[1] including fibroblast growth factor[2] and toxin binding[3]. Lipid rafts model[4] has been raised to describe the plasma membrane structures and functions. Since 1997, many techniques have been employed to verify the lipid rafts model in artificial and cell membranes, including the cutting edge FCCS, STORM, STED, and SIMS. Nonetheless, the direct evidence of lipid rafts in living cells still remains lacking, mainly because of the limitation of current available techniques to detect the microdomains form in cell membranes that have small size (20-200 nm) and short lifetimes (<1 s).[5] We have designed and synthesized a series of fluorinated ganglioside GM1 analogues (F-GM1s) to facilitate the lipid rafts detection using nanoSIMS, taking advantage of their almost identical properties to native version and high sensitivity in SIMS imaging.

We have achieved the synthesis of fluorinated GM1 by modification of natural GM1 that derived from bovine brain tissues using fluorinated fatty acid substitution on the lipid tails. (Chapter 2) Mono- and tri-fluorinated GM1 analogues[6] have been obtained with fluorine atoms at different positions of the lipid tail. Coupling of fluorinated fatty acid NHS ester exhibited good selectivity to the sphingosine amine group of DeAc-lysoGM1, compared to the other amine group on sialic acid residue, because of higher steric hindrance at the oligosaccharide moiety. Higher order fluorination (–C6F13) of GM1 has also been accomplished either on the fatty acid chain or both the fatty acid (C6F13-GM1) and the sphingosine chains (Di-C6F13-GM1). The C6F13 modification of

the fatty acid chain was achieved similarly by substitution with a new fatty acid containing the -C6F13 residue. The modification of sphingosine hydrocarbon chain has governed a cleavage of the double bond to form an aldehyde using ozonolysis at low temperature, followed by wittig coupling of the aldehyde with a ylide containing the –C6F13 residue. Peracetylation of hydroxyl groups on the GM1 analogue was required for the wittig coupling. Purification of the Di-C6F13-GM1 product was easily achieved by using a fluorous phase cartridge that can separate high fluorinated molecules from non-fluorinated ones. This is the first report of modification of the sphingosine chain on ganglioside analogues. Our previous trial of sphigosine modification by using olefin cross metathesis showed the desired product but also a by-product with different length of the hydrocarbon chain that could not be separated from the product.

We have evaluated the biophysical properties of F-GM1s using multiple techniques, including FACS, AFM and calcium signaling assay. In FACS analysis (Chapter 3, Section 3.1), mono- and tri-fluorinated GM1 were incubated in cell culture to incorporate on the cells and labeled with FITC-CTB for detection. All the F-GM1s exhibited concentration dependent incorporation on living cells, and their activities were at the same level as that of the native GM1.

AFM has been extensively used to study phase behaviors of supported lipid bilayers (SLBs). We have studied the phase properties of F-GM1s in SLBs by using the AFM imaging technique. (Chapter 3, Section 3.2) We have employed DPPC/POPC mixture to prepare SLBs than can form gel phase and liquid disordered (l_d) phase in the membrane. By addition of F-GM1s, a type of separated microdomains has been observed

in the gel phase and at the boundary between the two phases. By comparing with SLBs containing native GM1, it has been revealed that 18-F-GM1 has the most similar phase properties as the native version.

Ganglioside GM1 has been found to be related to calcium signaling in T cells and able to induce increase of cytosolic calcium ion concentrations by clustering on cell surfaces.[7] We have employed F-GM1s on Jurkat cells to study their activities in calcium signaling. (Chapter 3, Section 3.3) It has been observed that 18-F-GM1 exhibited very similar ability as the native GM1 to induce calcium ion influx. Therefore, based on all the biophysical property test results, we have concluded that the terminal mono-fluorinated version (18-F-GM1) best mimics the native GM1 and could be potentially used as a probe to study its behaviors in membranes.

SIMS is a light-free, secondary ion mass spec based technique that can scan and map the chemical compositions of sample surfaces.[8] Using the nanoSIMS imaging technique, we have observed phase separation and domain formation in a quaternary mixture of supported lipid bilayers (SPM/DOPC/cholesterol = 2:2:1 with 5% F-GM1). By isotopic labeling, the domains were revealed to be rich in F-GM1 and cholesterol, and other areas have higher composition of SPM and DOPC. Mono-fluorination enabled the high sensitivity of GM1 analogues in SIMS detection and generated the first chemical composition image of membrane domains formed by GM1 and cholesterol. Additionally, it has also been noticed that 18-F-GM1 formed much larger domains than 12-F-GM1 in SLBs. We attributed it to their phase property difference resulted from 12-F induced structural change. A DSC experiment verified the property difference by comparing their

phase transition temperatures (T_m) in aqueous solution. As a result, 18-F-GM1 exhibited a T_m very close to that of native GM1, whereas 12-F-GM1 showed a significant change of T_m. Therefore, the terminal mono-fluorinated GM1 mimics native GM1 as an almost "label-free" probe, thus provides us with a new tracking system for lipid rafts study by using high resolution SIMS imaging.

As the size of lipid rafts are in the range of 20-200 nm, current available nanoSIMS that has resolution of ~100 nm can theoretically detect the relatively larger rafts of 100-200 nm in size. However, nanoSIMS technically requires a thin layer of samples on a conductive support for secondary ion generation and detection,[8] which may hamper its application in living cell studies. TOF-SIMS requires milder working conditions and, in fact, has been used to image living cells[9-12] or tissue samples[13,14] by several research groups. Many efforts have been made to enhance the sensitivity and resolution of TOF-SIMS,[15] nonetheless, the lateral resolution of TOF-SIMS imaging remains at micrometer scale[16]. The short lifetime of lipid rafts might be another problem, because current scan rate of SIMS imaging is around 1 ms/pixel and to obtain a whole image usually takes seconds to minutes. Therefore, the direct visualization of lipid rafts in living cells using SIMS imaging technique might not be done today, but we believe that with the fast development of SIMS imaging technique, especially in the last few years, it will be achieved in the near future. It might be a long way but it is on the right direction.

Gangliosides play an important role in endocytosis and participate in vesicle formation in caevolae and lipid rafts induced endocytic pathways.[17] We have proposed to

use ganglioside GM1 as a carrier, taking advantage of its higher composition in endocytic vesicles, to efficiently deliver cargos to inside of the cells. For this purpose, we have designed a new fluorescently labeled GM1 marker to study the endocytic pathway of GM1 in mammalian cells. We chose NBD for the fluorescence label and the sialic residue as the modification site to minimize any influences during endocytic processes. The GM1 derivative linked with NBD was obtained by synthesis and applied to Hela cells for confocal fluorescence microscopy imaging. By comparing with localization of other dyes, the NBD labeled GM1 has been found accumulated in lysosomes, golgi complex, and ER. The observations suggested the endocytic pathway of GM1 in cells and provided us with theoretical basis for probe design and drug delivery studies in future.

Ganglioside GM1 is a common component of lipid rafts in cell membrans and potentially enhances the lipid rafts induced endocytosis, which the mechanism is unclear though. The carriers of GM1 derivatives can more efficiently deliver cargos into the cells via endocytic pathways, compared to other drug carriers that passively utilize endocytosis for delivery, such as lipids, peptides, and nanoparticles. Indeed, any component of lipid rafts has the potential to deliver cargos through the same route, and their different trafficking pathways can provide with more options to selectively deliver cargos to different targets. For example, if a drug or inhibitor targets an enzyme that resides in *trans*-golgi network, the carrier of GM1 derivative can efficiently transport the molecule to the organelles other than randomly distribute it in the cytosol. Or, if a ganglioside of lipid rafts component can selectively transport to ER via endocytic trafficking pathway, we can link inhibitors onto the ganglioside carrier to screen any potential targets in ER. In

any events, the lipid rafts based delivery system is promising to construct a new platform for drug delivery and functional studies.

References

(1) Gouy, H.; Cefai, D.; Christensen, S. B.; Debre, P.; Bismuth, G., Cyclic Amp-Independent and Inositol Phosphate-Independent Inhibition of Ca2+ Influx by Cholera-Toxin in Cd3-Stimulated Jurkat T-Cells - a Study with a Cholera Toxin-Resistant Cell Variant and the Ca2+ Endoplasmic Reticulum-Atpase Inhibitor Thapsigargin. *J. Immunol.* **1991**, *147*, 757-766.

(2) Rusnati, M.; Urbinati, C.; Tanghetti, E.; Dell'Era, P.; Lortat-Jacob, H.; Presta, M., Cell membrane GM1 ganglioside is a functional coreceptor for fibroblast growth factor 2. *Proc. Natl. Acad. Sci. U. S. A.* **2002**, *99*, 4367-72.

(3) Vanheyni.S, Cholera Toxin - Interaction of Subunits with Ganglioside Gm1. *Science* **1974**, *183*, 656-657.

(4) Simons, K.; Ikonen, E., Functional rafts in cell membranes. *Nature* **1997**, *387*, 569-572.

(5) Lingwood, D.; Simons, K., Lipid Rafts As a Membrane-Organizing Principle. *Science* **2010**, *327*, 46-50.

(6) Liu, Z.; Kumar, K., Trifluoromethyl Derivatization of the Ganglioside, G(M1). *Synthesis-Stuttgart* **2010**, 1905-1908.

(7) Zeyda, M.; Stulnig, T. M., Lipid Rafts & Co.: an integrated model of membrane organization in T cell activation. *Prog Lipid Res* **2006**, *45*, 187-202.

(8) Boxer, S. G.; Kraft, M. L.; Weber, P. K., Advances in Imaging Secondary Ion Mass Spectrometry for Biological Samples. *Annual Review of Biophysics* **2009**, *38*, 53-74.

(9) Winograd, N.; Parry, S., High-resolution TOF-SIMS imaging of eukaryotic cells preserved in a trehalose matrix. *Anal. Chem.* **2005**, *77*, 7950-7957.

(10) Ostrowski, S. G.; Van Bell, C. T.; Winograd, N.; Ewing, A. G., Mass spectrometric imaging of highly curved membranes during Tetrahymena mating. *Science* **2004**, *305*, 71-73.

(11) Kurczy, M. E.; Piehowski, P. D.; Van Bell, C. T.; Heien, M. L.; Winograd, N.; Ewing, A. G., Mass spectrometry imaging of mating Tetrahymena show that changes in cell morphology regulate lipid domain formation. *Proc. Natl. Acad. Sci. U. S. A.* **2010**, *107*, 2751-2756.

(12) Fletcher, J. S.; Rabbani, S.; Henderson, A.; Lockyer, N. P.; Vickerman, J. C., Three-dimensional mass spectral imaging of HeLa-M cells - sample preparation, data interpretation and visualisation. *Rapid Commun. Mass Spectrom.* **2011**, *25*, 925-932.

(13) Passarelli, M. K.; Winograd, N., Characterizing in situ Glycerophospholipids with SIMS and MALDI Methodologies. *Surf. Interface Anal.* **2011**, *43*, 269-271.

(14) Benabdellah, F.; Seyer, A.; Quinton, L.; Touboul, D.; Brunelle, A.; Laprevote, O., Mass spectrometry imaging of rat brain sections: nanomolar sensitivity with MALDI versus nanometer resolution by TOF-SIMS. *Anal. Bioanal. Chem.* **2010**, *396*, 151-162.

(15) Heile, A.; Muhmann, C.; Lipinsky, D.; Arlinghaus, H. F., Investigations of secondary ion yield-enhancing methods in combination. *Surf. Interface Anal.* **2011**, *43*, 20-23.

(16) Piehowski, P. D.; Davey, A. M.; Kurczy, M. E.; Sheets, E. D.; Winograd, N.; Ewing, A. G.; Heien, M. L., Time-of-Flight Secondary Ion Mass Spectrometry Imaging of Subcellular Lipid Heterogeneity: Poisson Counting and Spatial Resolution. *Anal. Chem.* **2009**, *81*, 5593-5602.

(17) Doherty, G. J.; McMahon, H. T., Mechanisms of endocytosis. *Annu. Rev. Biochem.* **2009**, *78*, 857-902.

Appendix

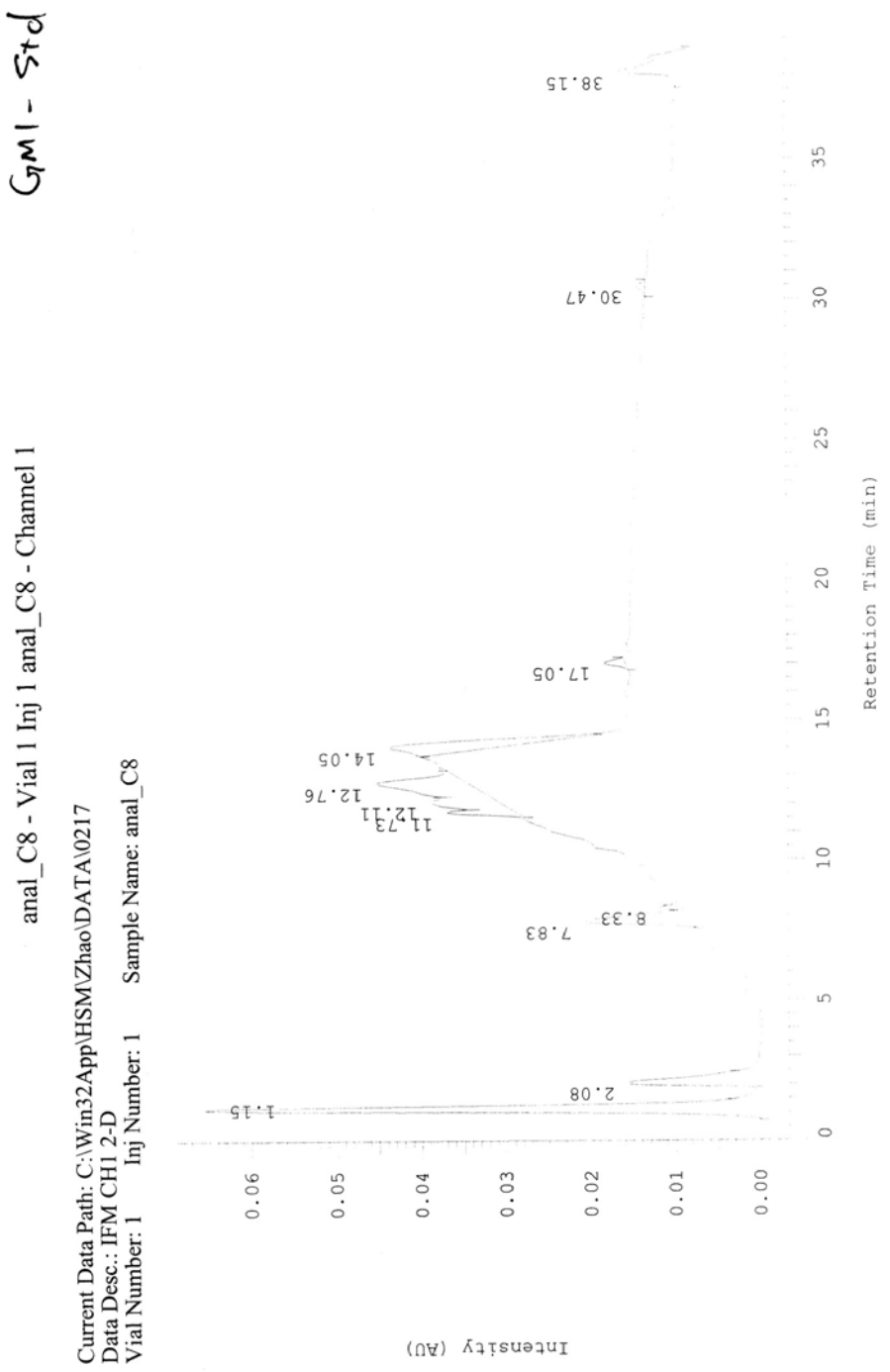

App 1. HPLC trace of ganglioside GM1 standard

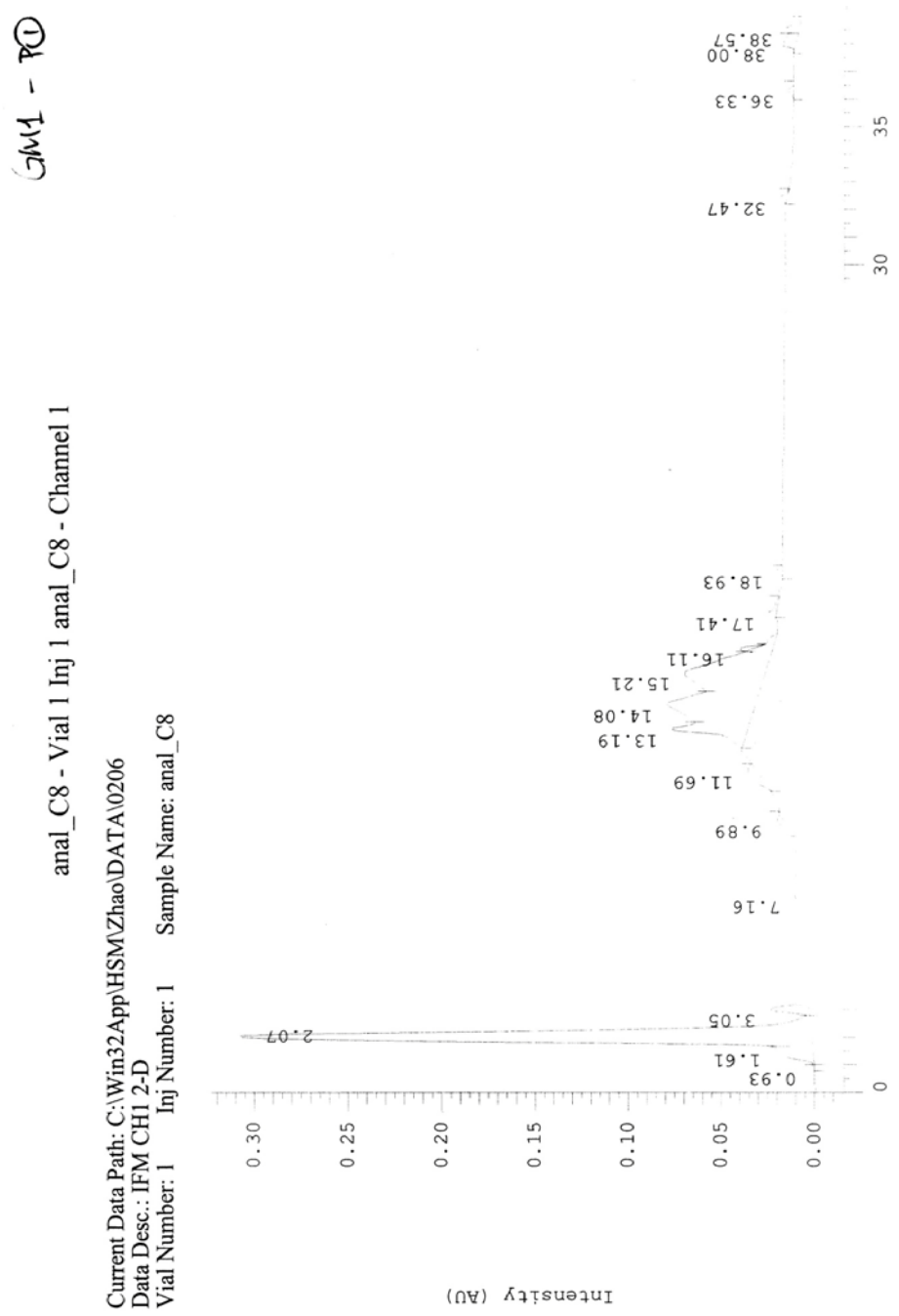

App 2. HPLC trace of isolated GM1 from bovine brain

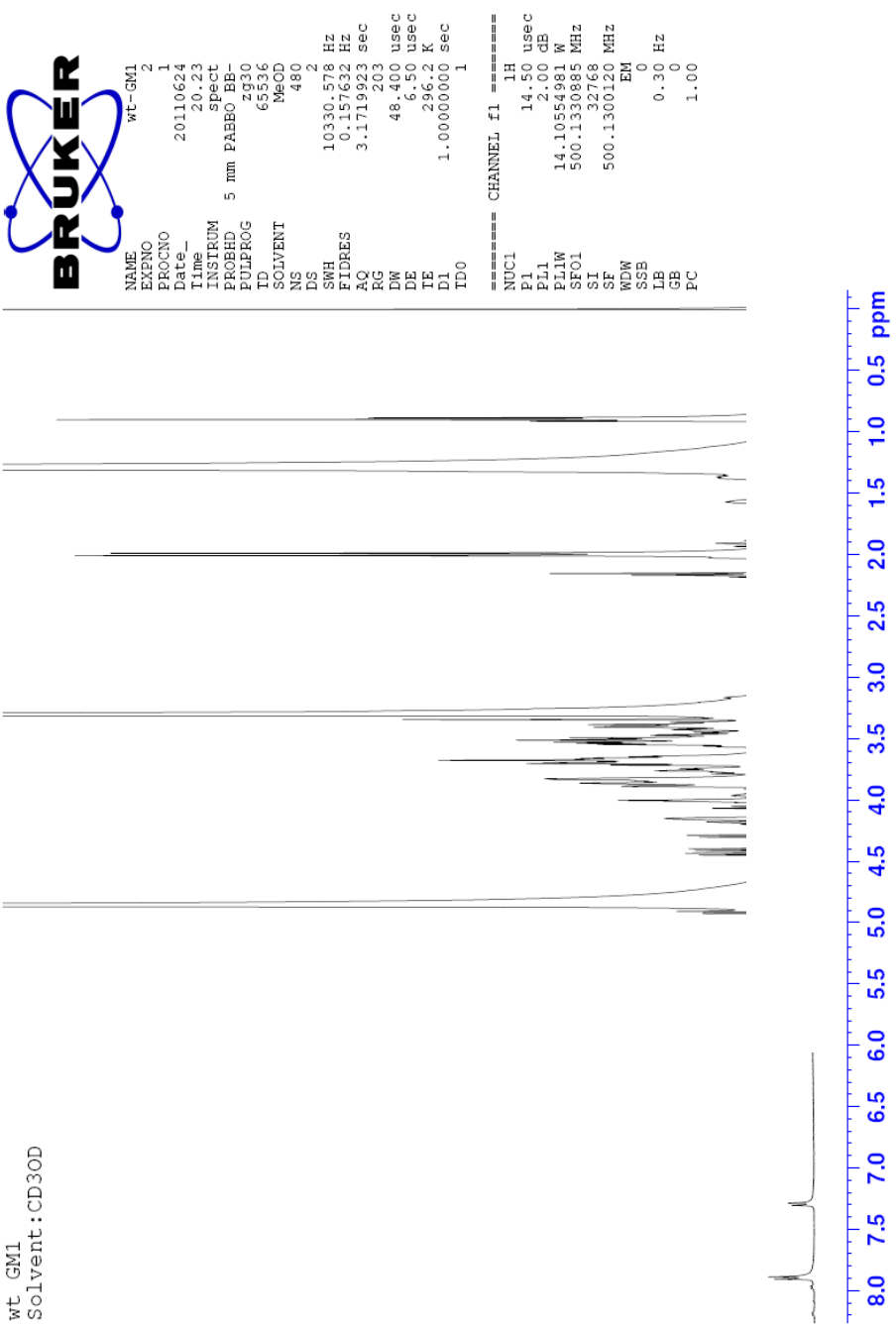

App 3. ^{1}H-NMR spectrum of wild type ganglioside GM1 from bovine brain

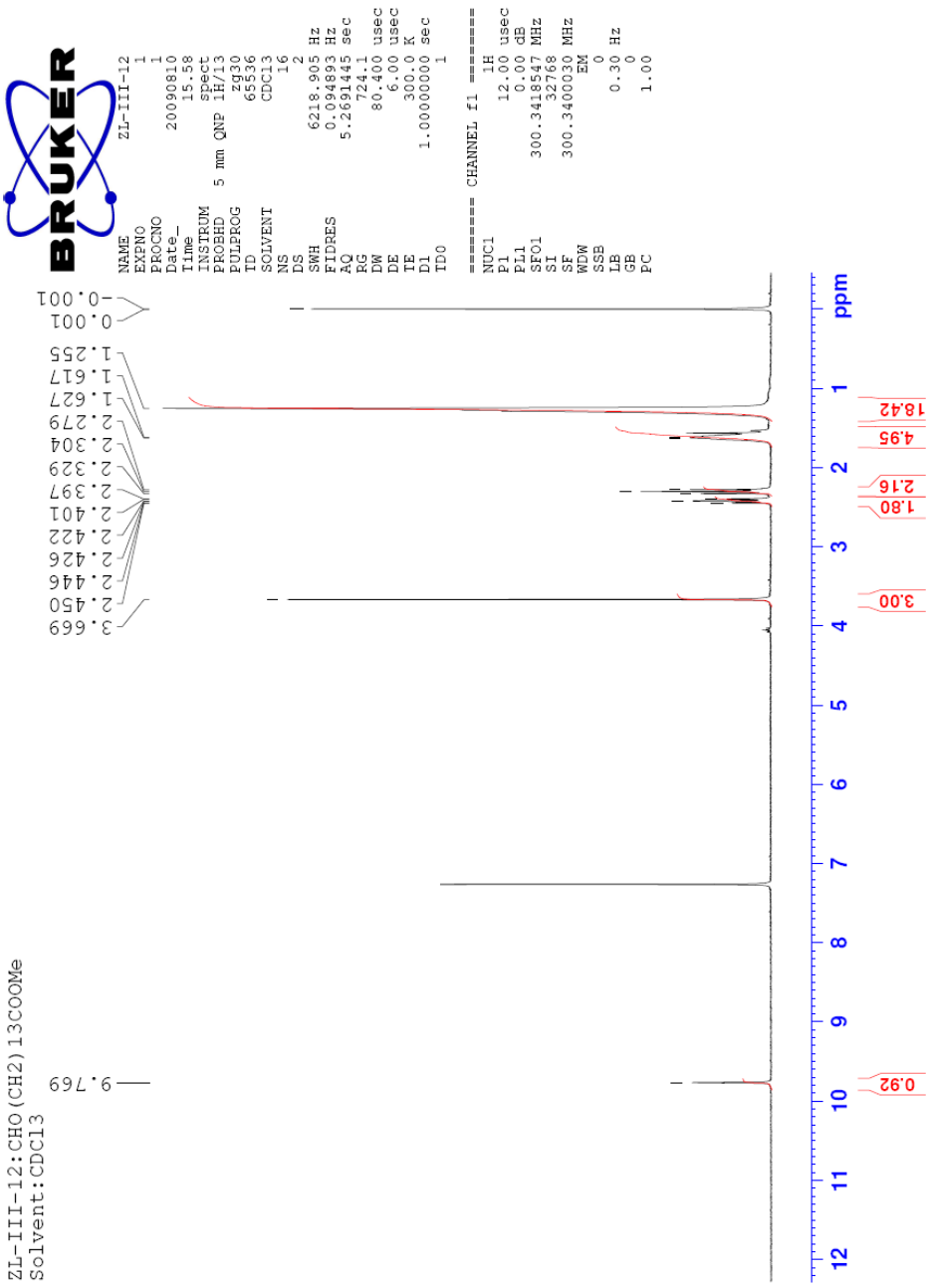

App 4. ^{1}H-NMR spectrum of methyl 15-Oxopentadecanoate (**6**)

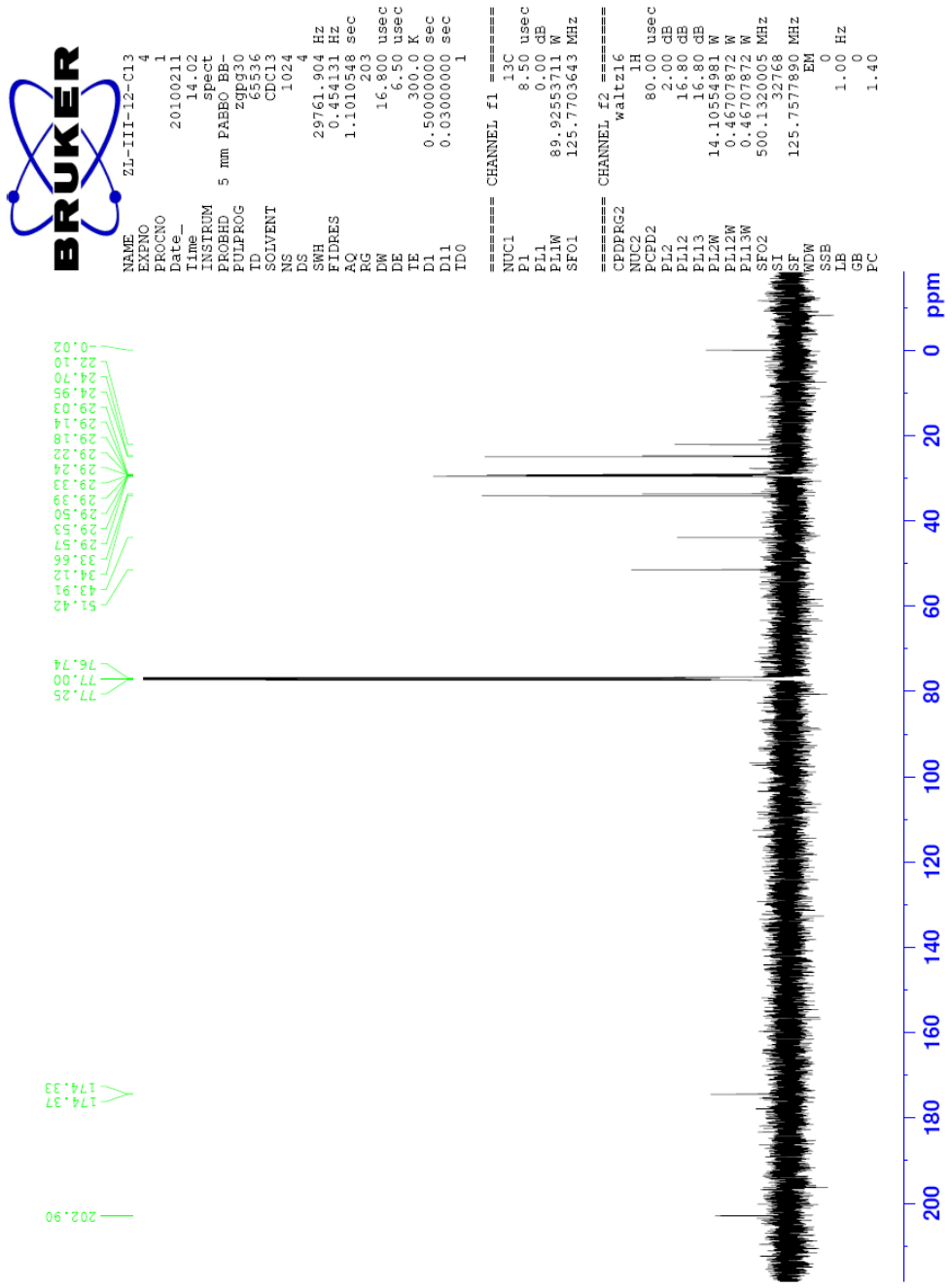

App 5. ^{13}C-NMR spectrum of methyl 15-Oxopentadecanoate (**6**)

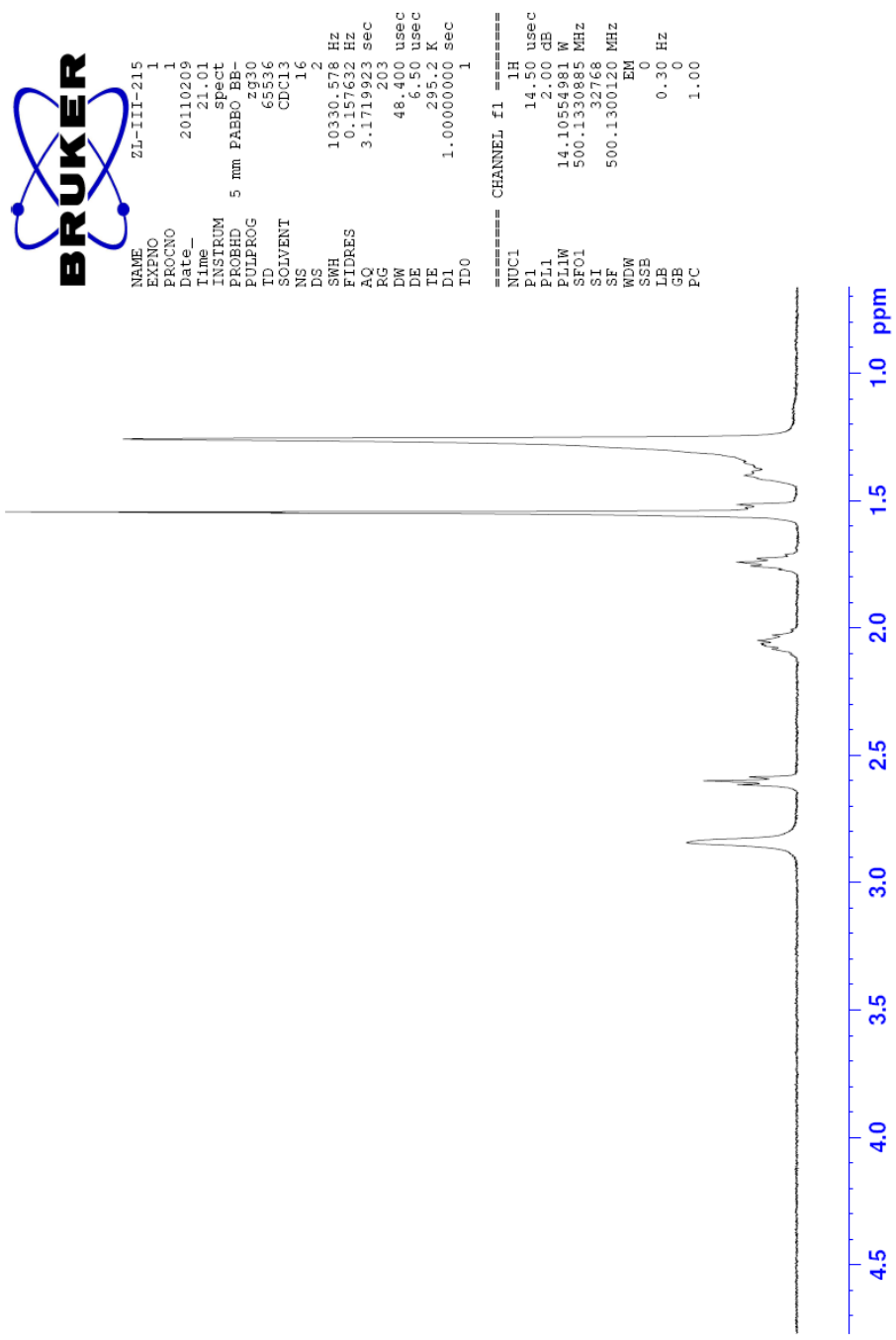

App 6. ^{1}H-NMR spectrum *N*-Succinimidyl 18,18,18-Trifluorostearate (**11**)

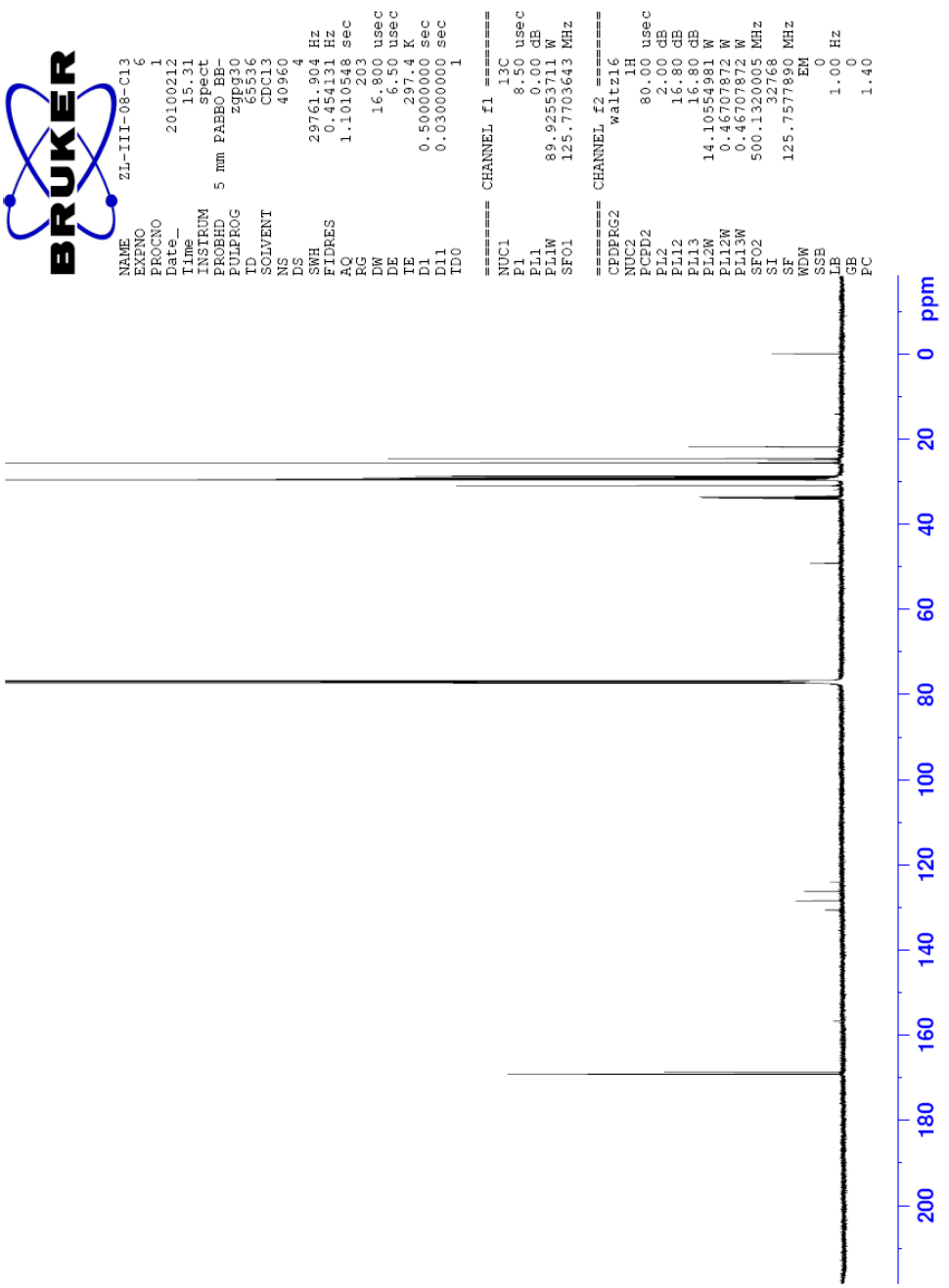

App 7. ^{13}C-NMR spectrum *N*-Succinimidyl 18,18,18-Trifluorostearate (**11**)

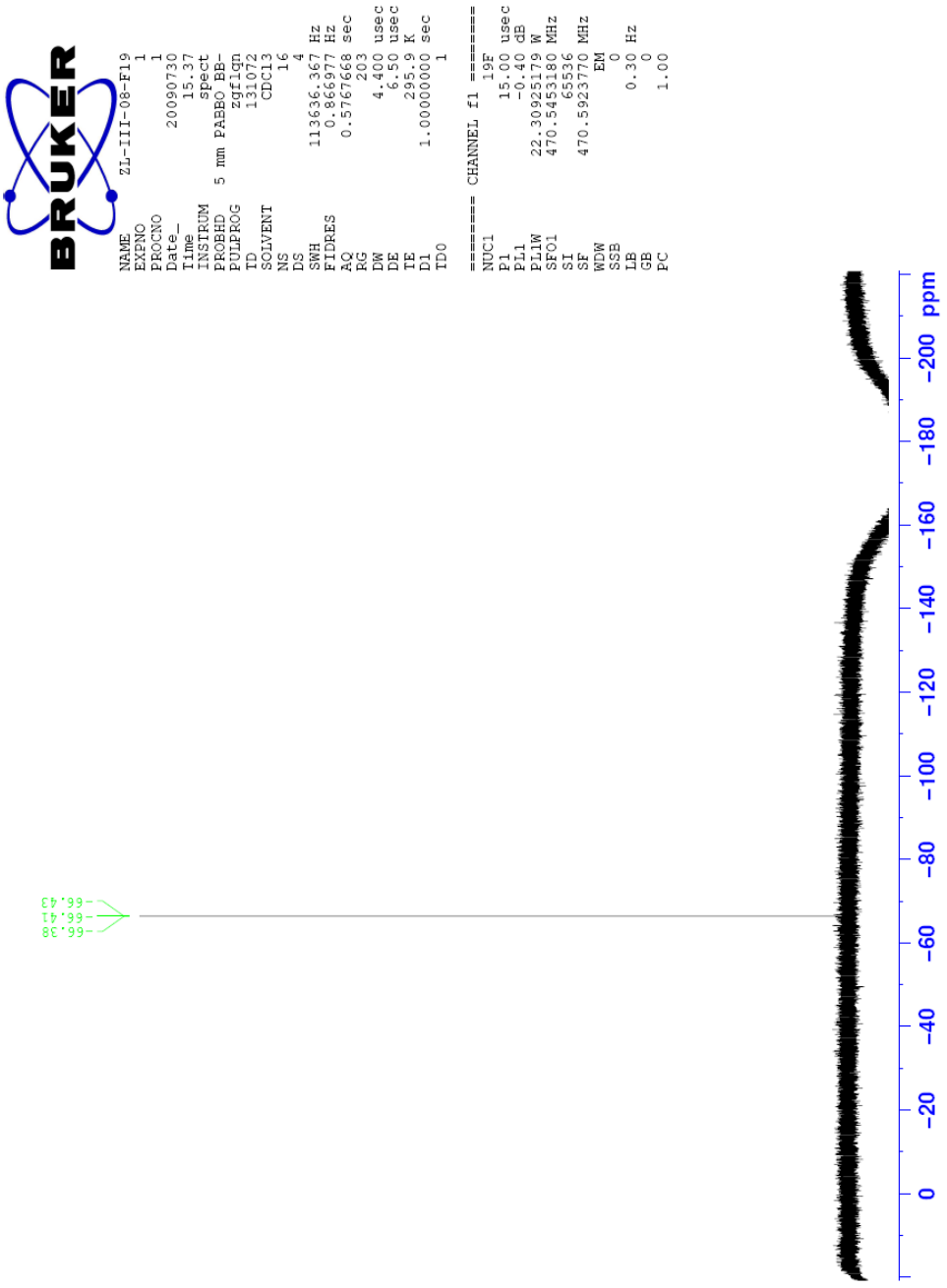

App 8. ^{19}F-NMR spectrum *N*-Succinimidyl 18,18,18-Trifluorostearate (**11**)

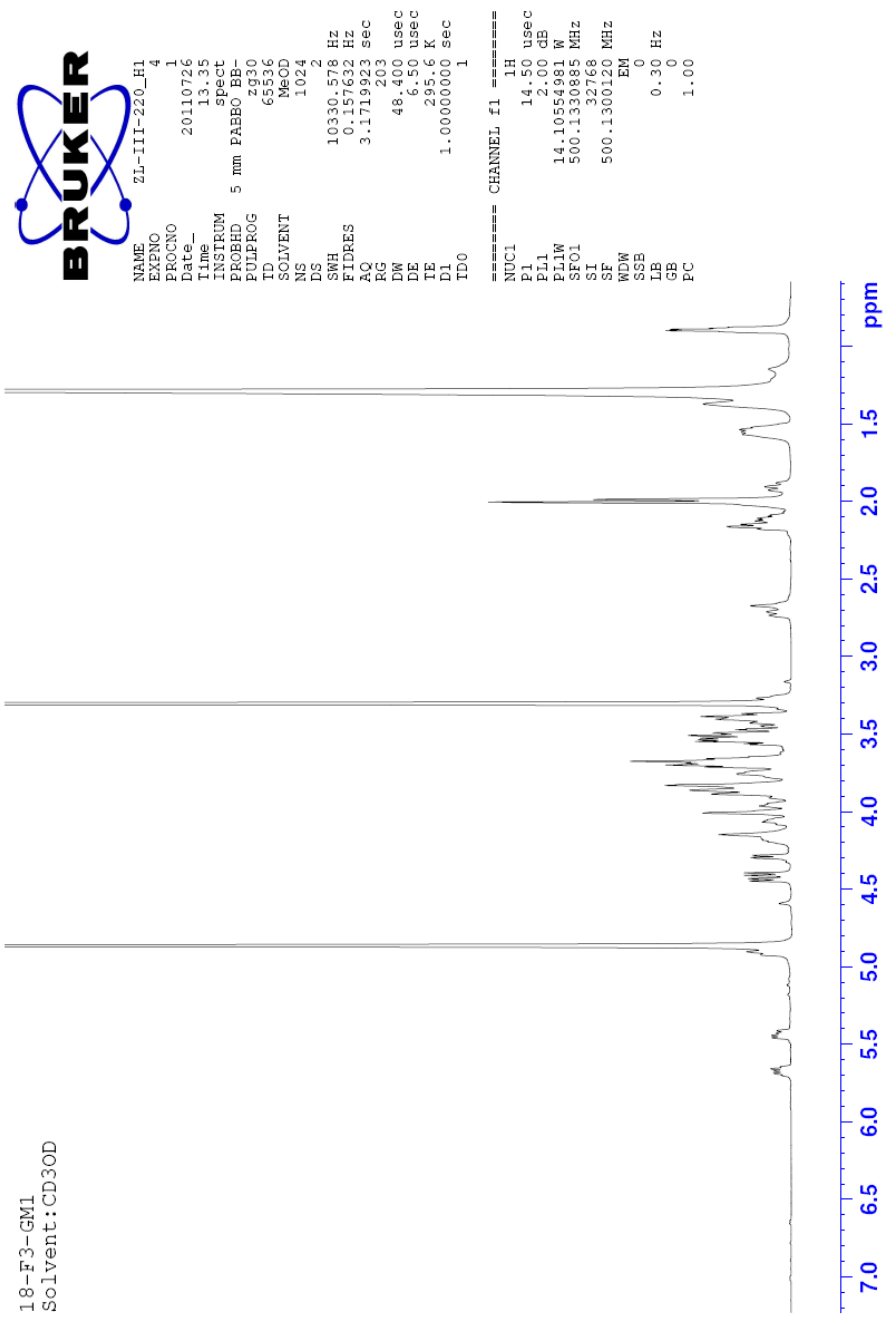

App 9. ^{1}H-NMR spectrum 18-F3-GM1 (**12**)

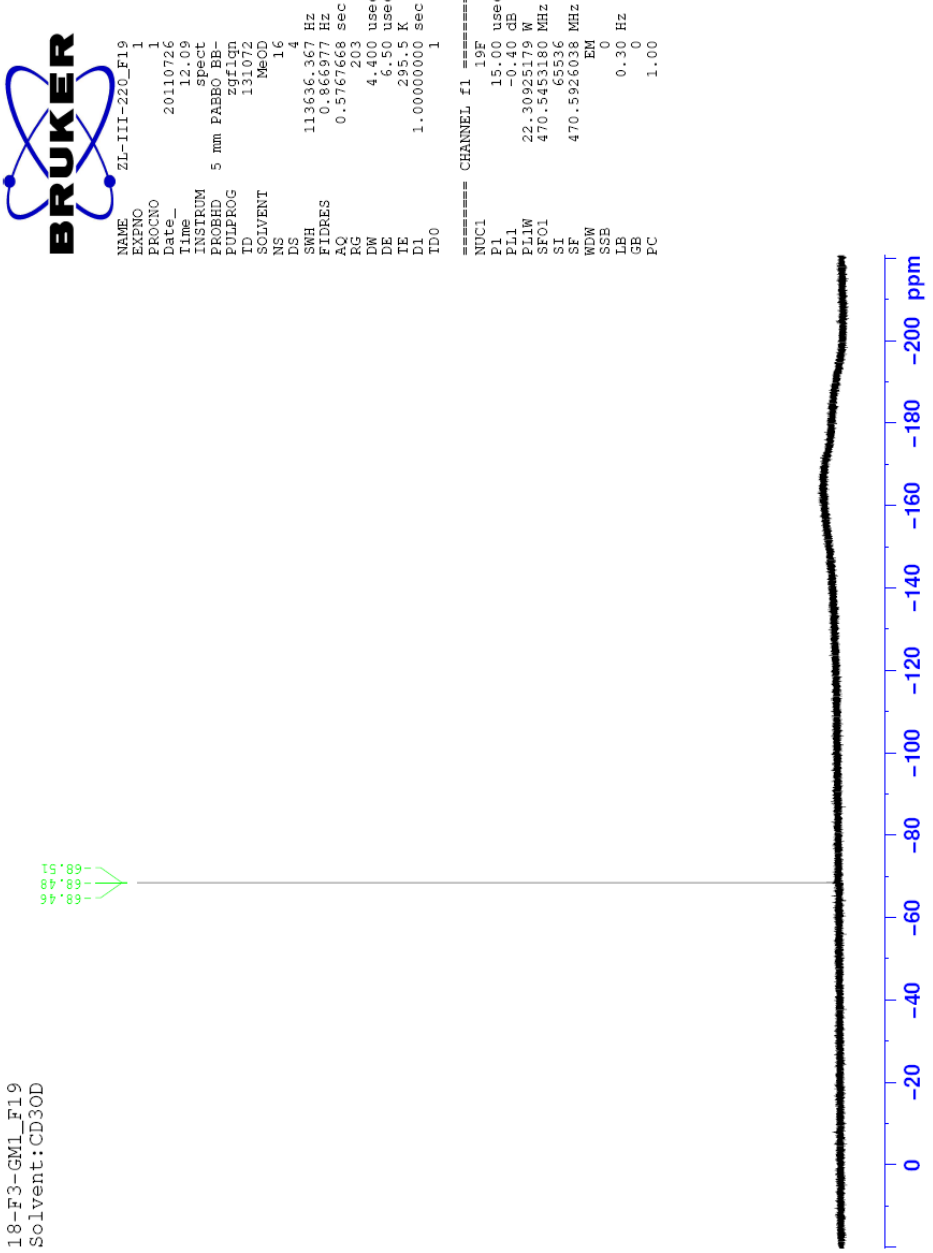

App 10. ^{19}F-NMR spectrum 18-F3-GM1 (**12**)

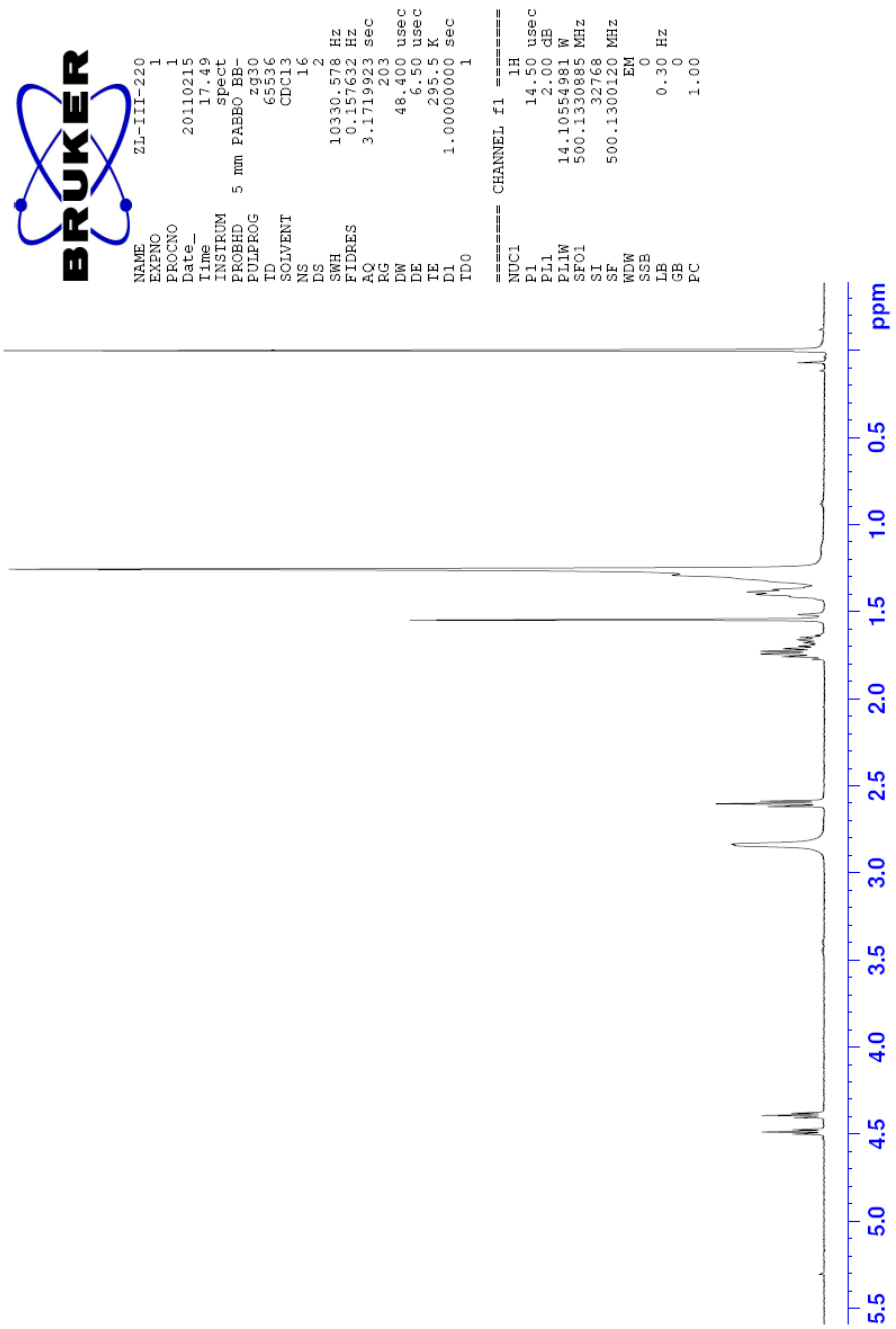

App 11. ^{1}H-NMR spectrum *N*-succinimidyl 18-fluorostearate (**17**)

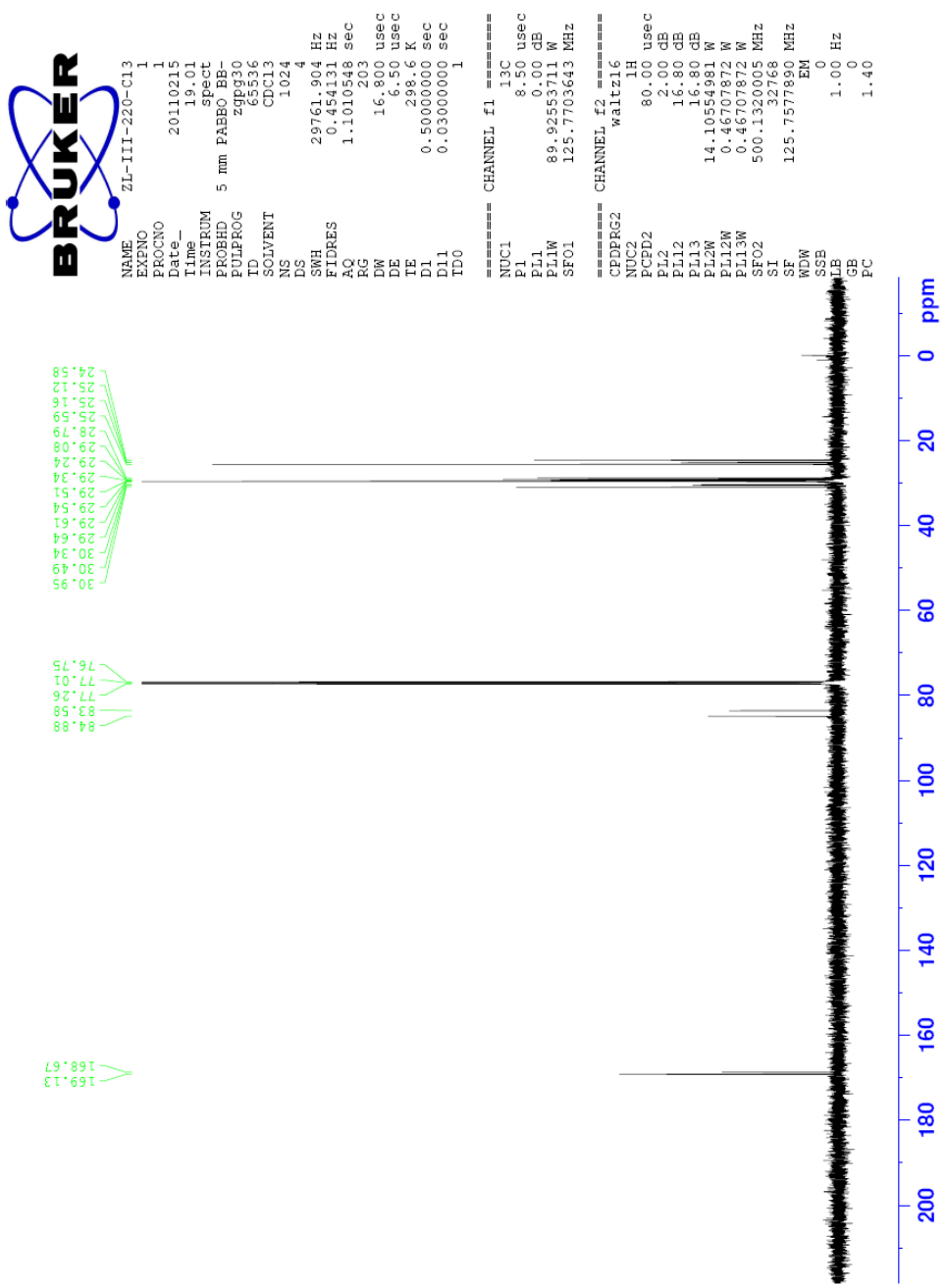

App 12. ^{13}C-NMR spectrum *N*-succinimidyl 18-fluorostearate (**17**)

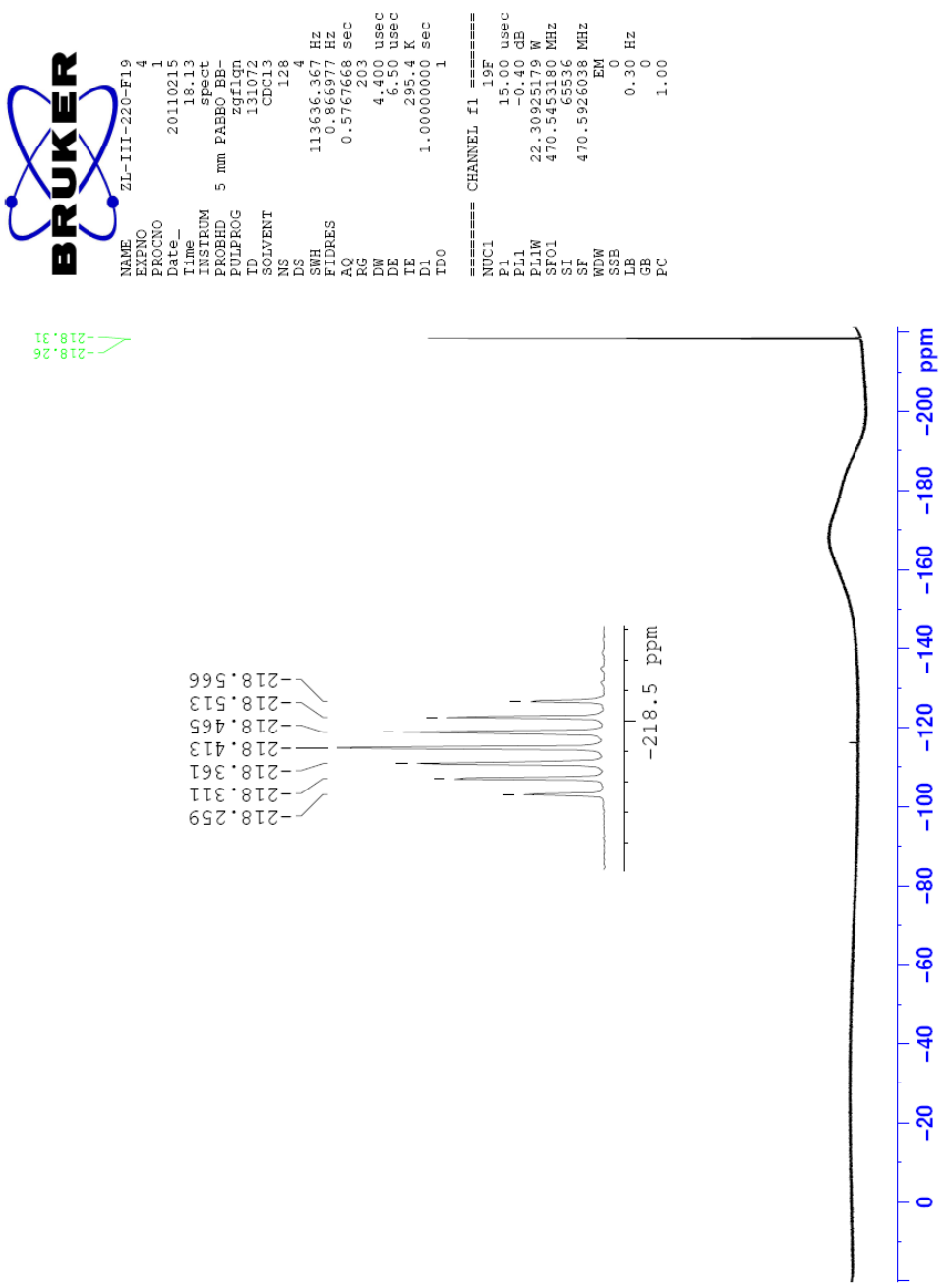

App 13. ^{19}F-NMR spectrum *N*-succinimidyl 18-fluorostearate (**17**)

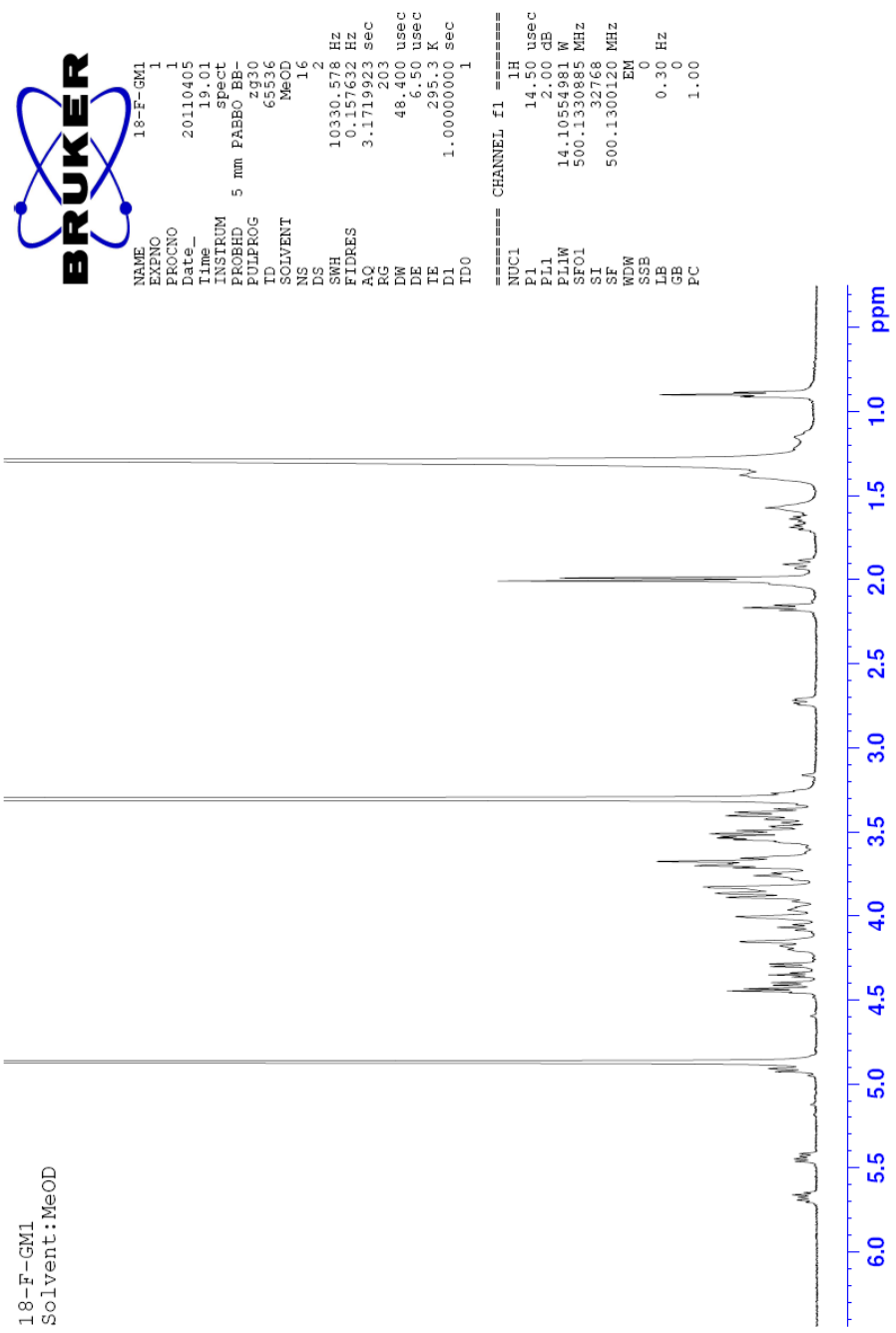

App 14. ^{1}H-NMR spectrum 18-F-GM1 (**18**)

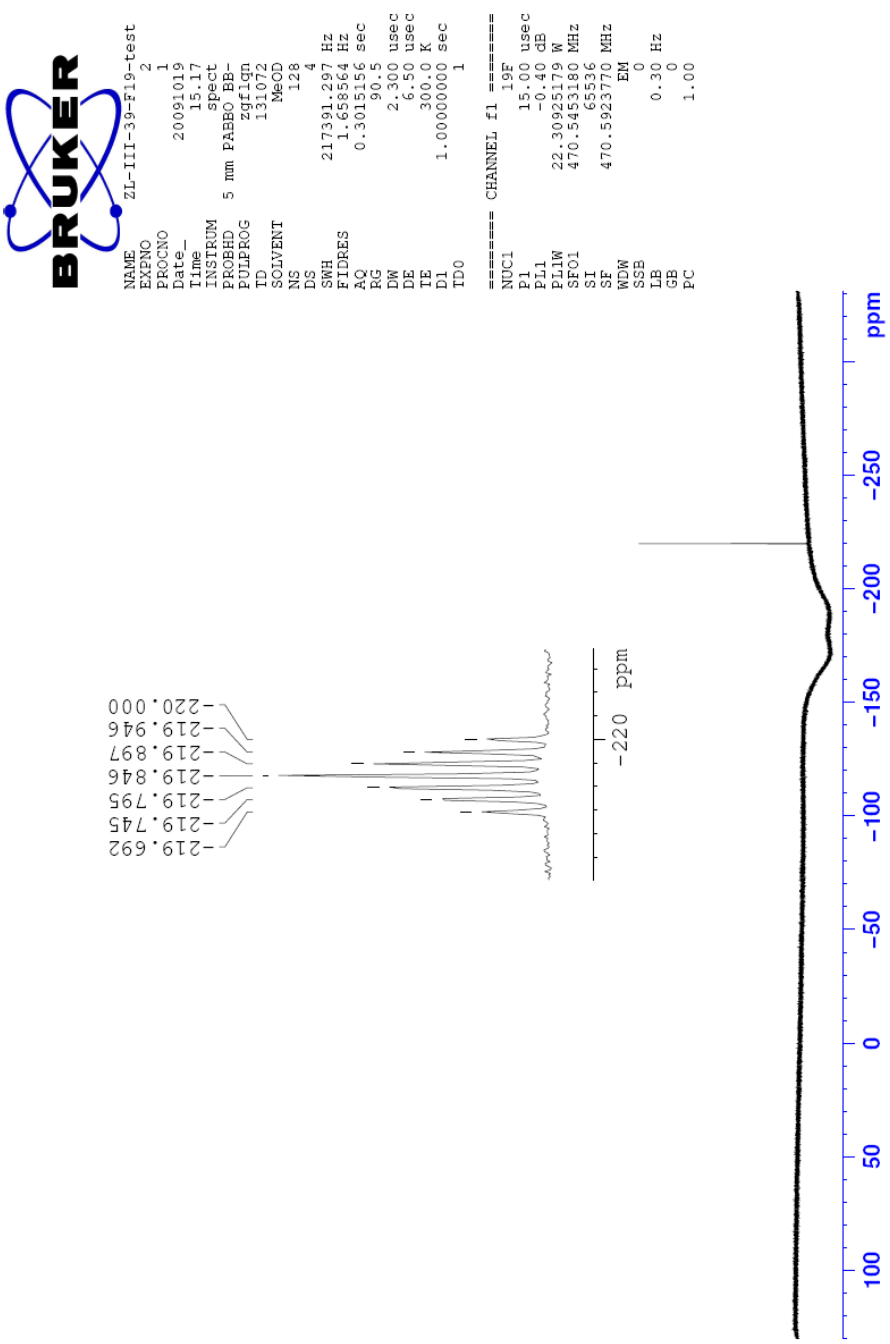

App 15. ^{19}F-NMR spectrum 18-F-GM1 (**18**)

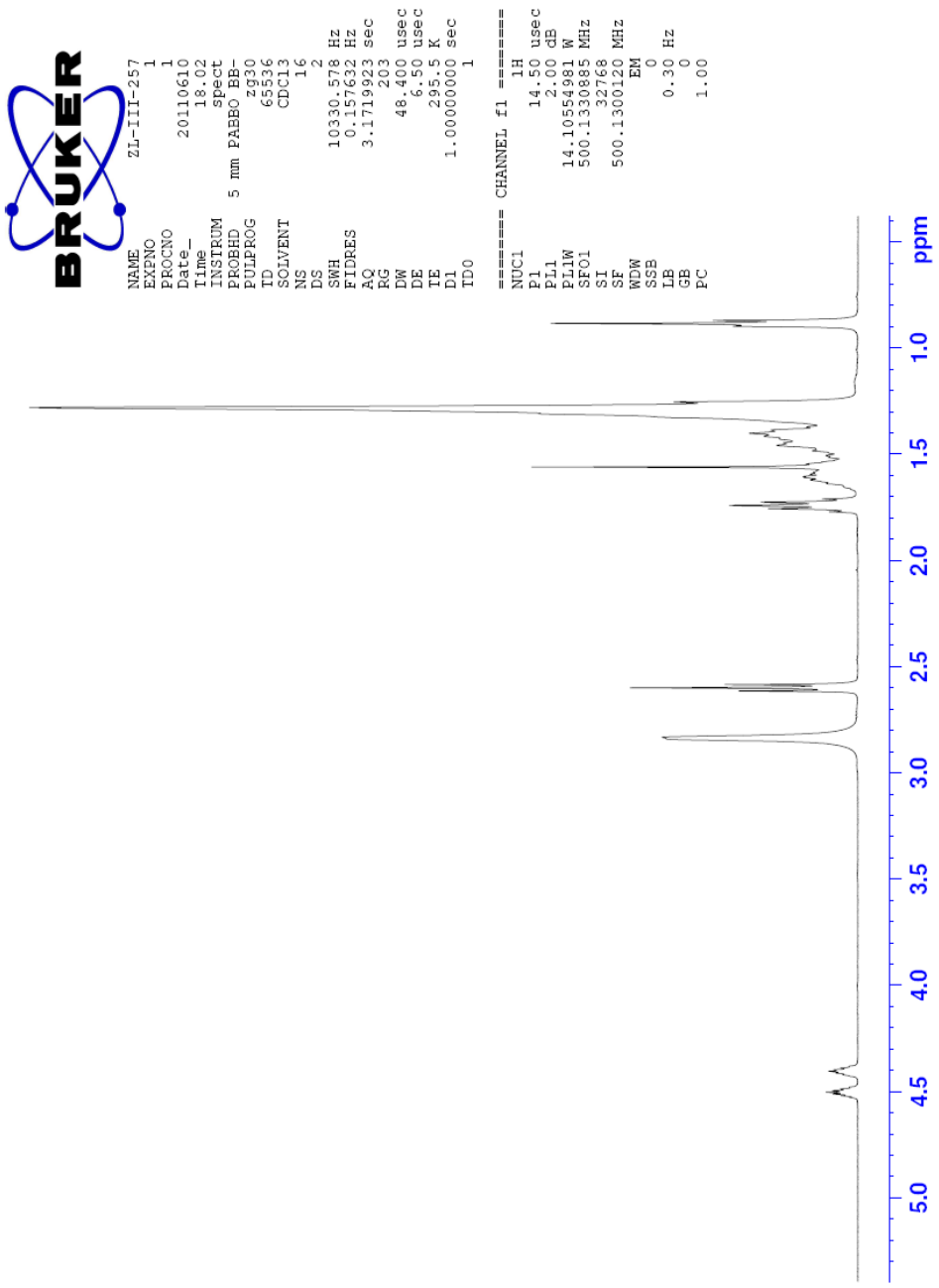

App 16. ^{1}H-NMR spectrum *N*-succinimidyl 12-fluorooctadecanoate (**22**)

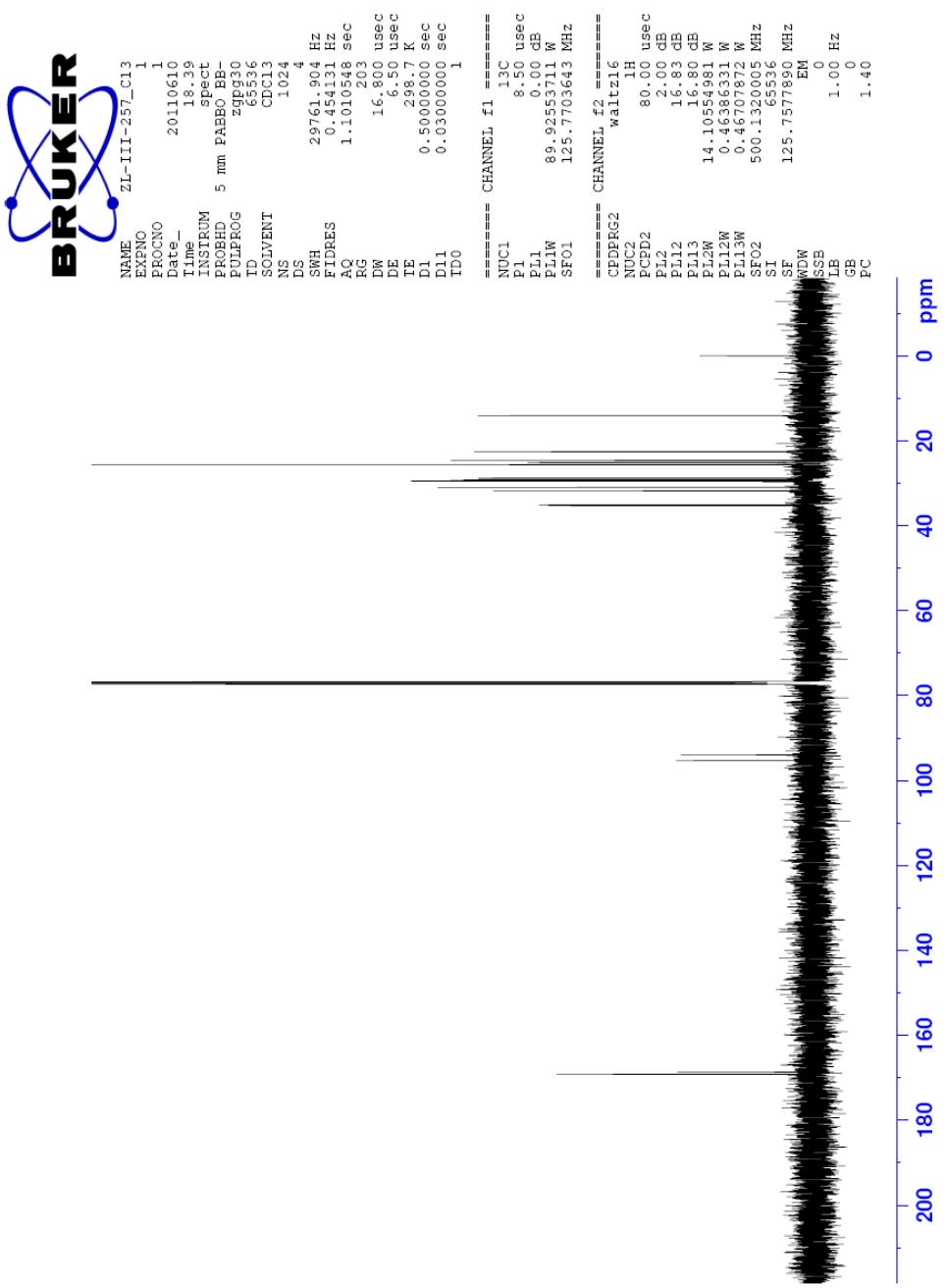

App 17. ^{13}C-NMR spectrum *N*-succinimidyl 12-fluorooctadecanoate (**22**)

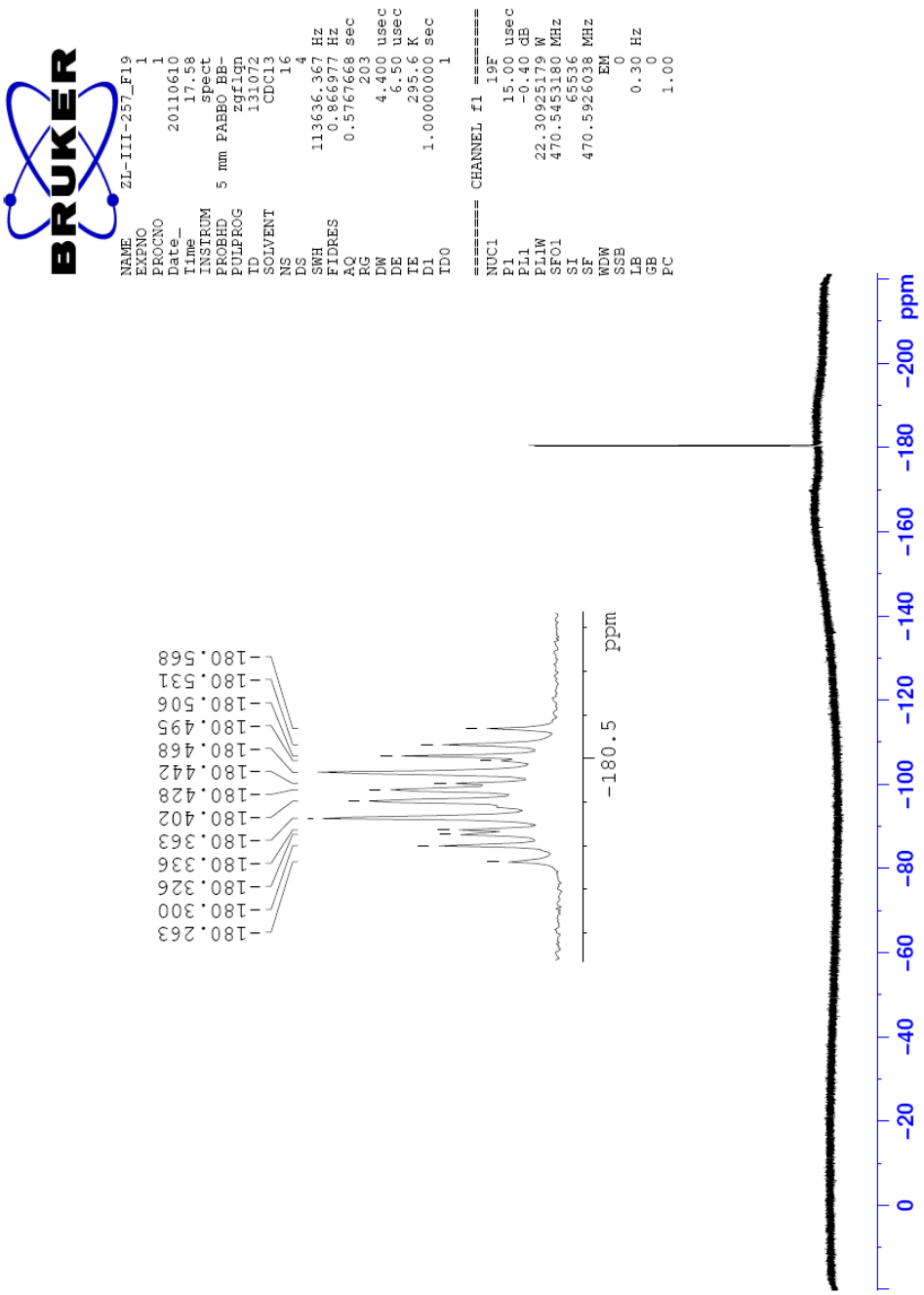

App 18. ^{19}F-NMR spectrum *N*-succinimidyl 12-fluorooctadecanoate (**22**)

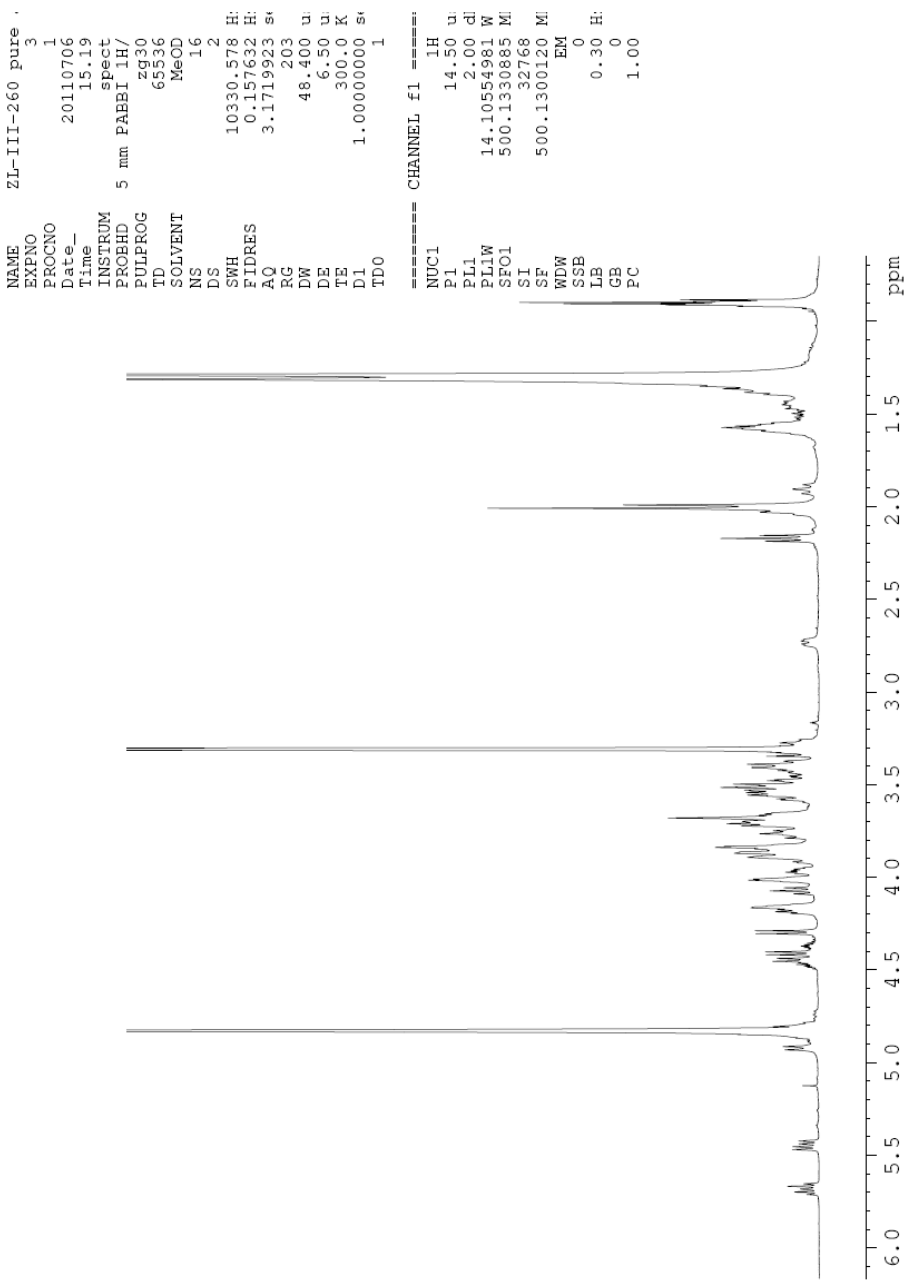

App 19. ^{1}H-NMR spectrum of 12-F-GM1 (**23**)

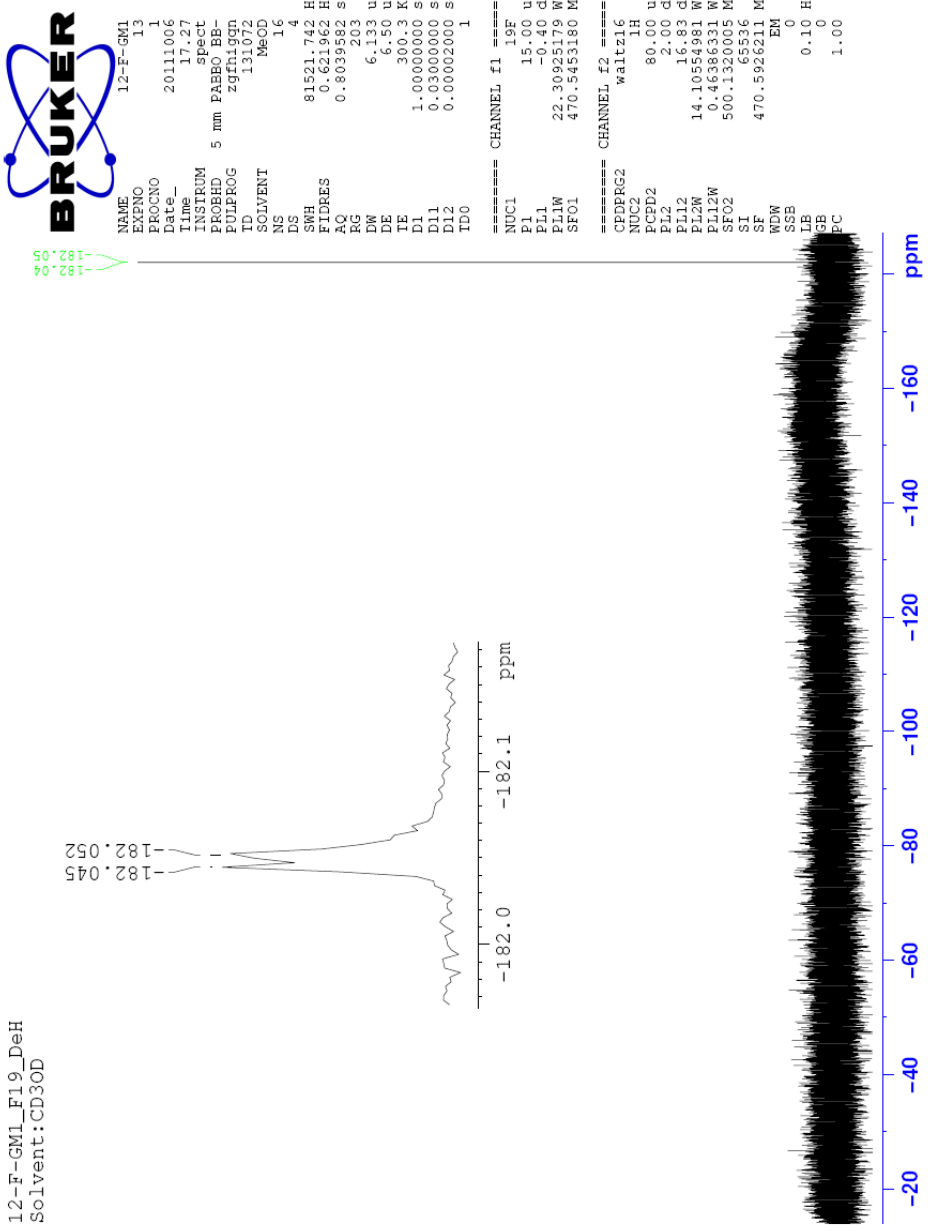

App 20. ^{1}H decoupled ^{19}F-NMR spectrum of 12-F-GM1 (**23**)

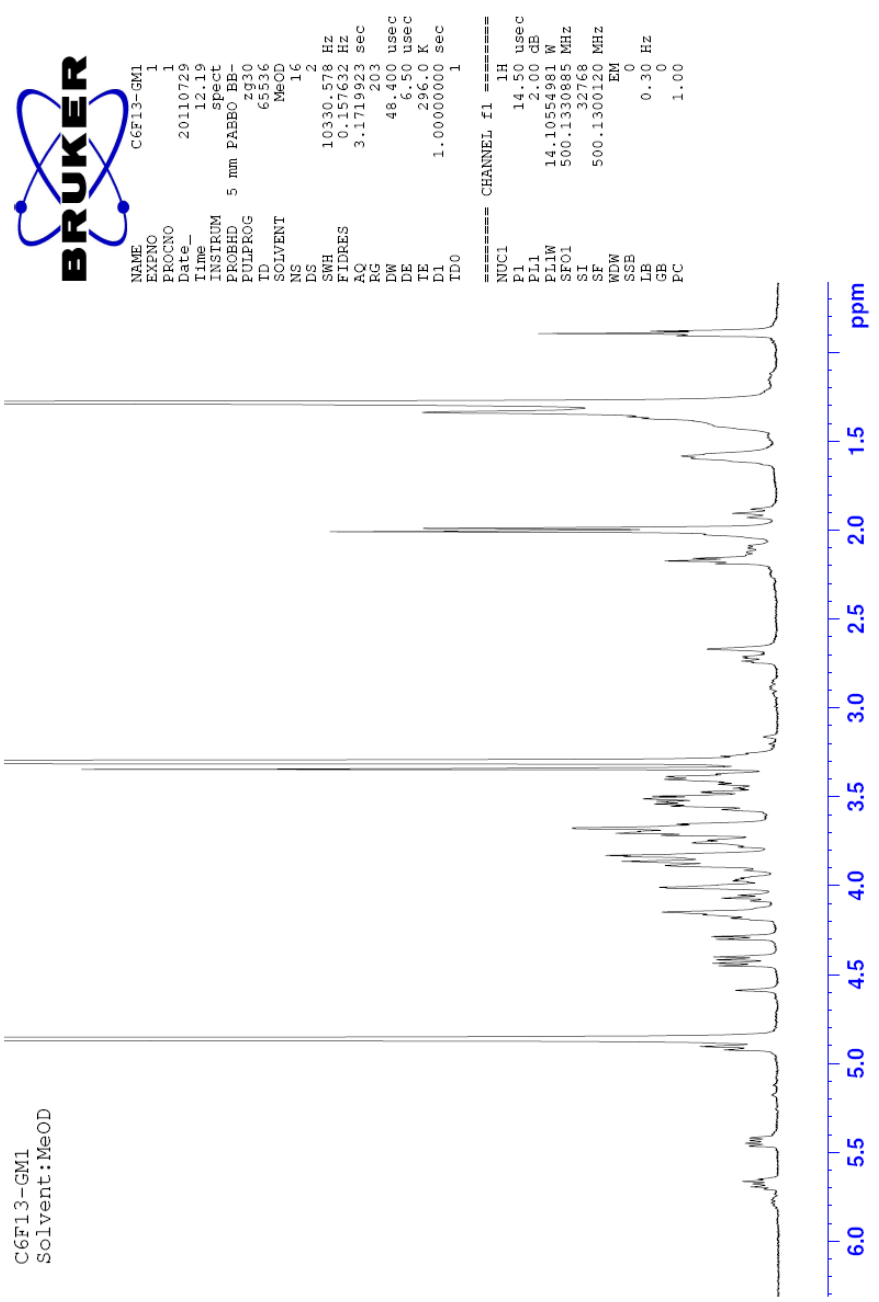

App 21. ^{1}H-NMR spectrum of C6F13-GM1 (**24**)

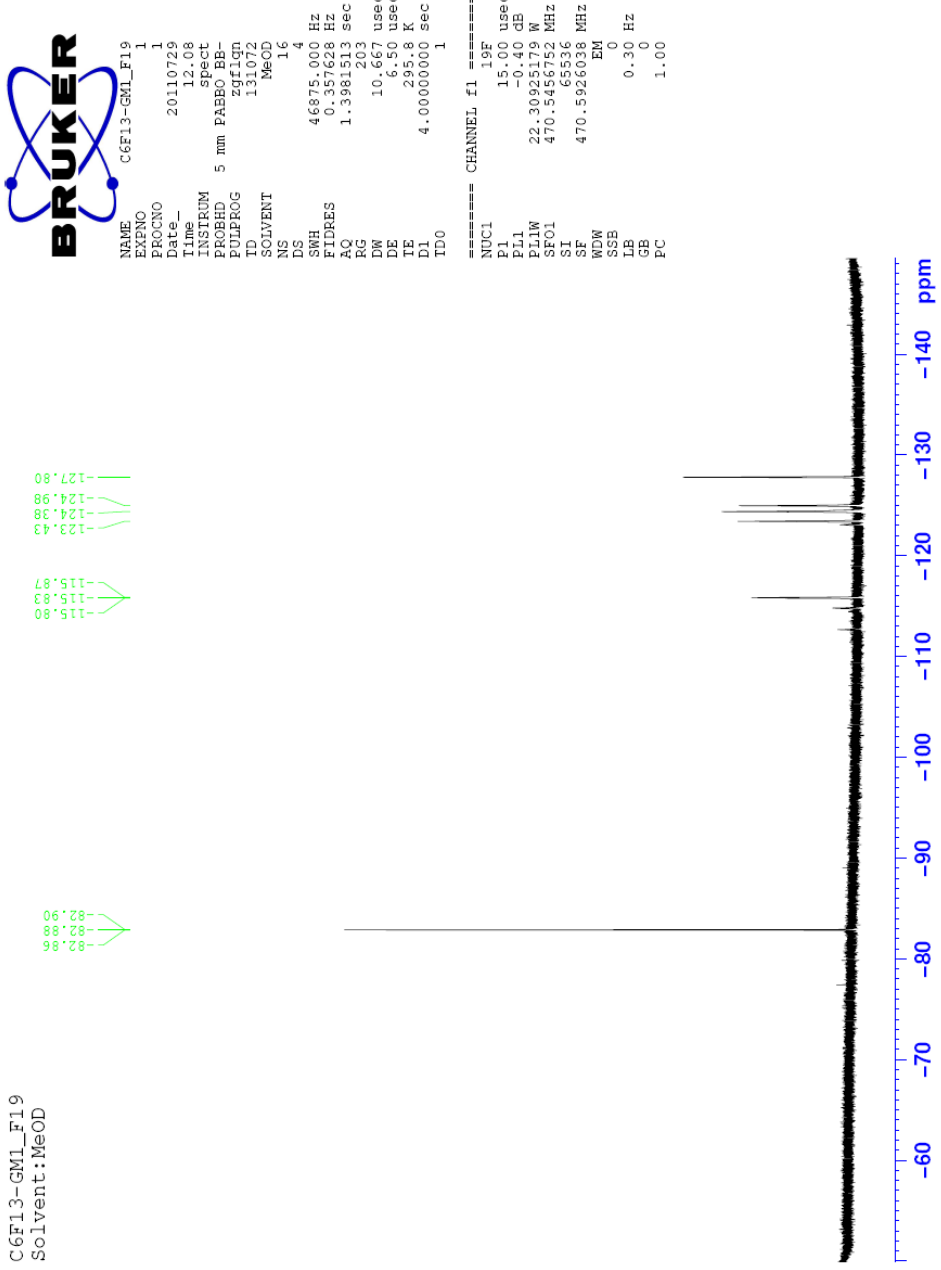

App 22. ^{19}F-NMR spectrum of C6F13-GM1 (**24**)

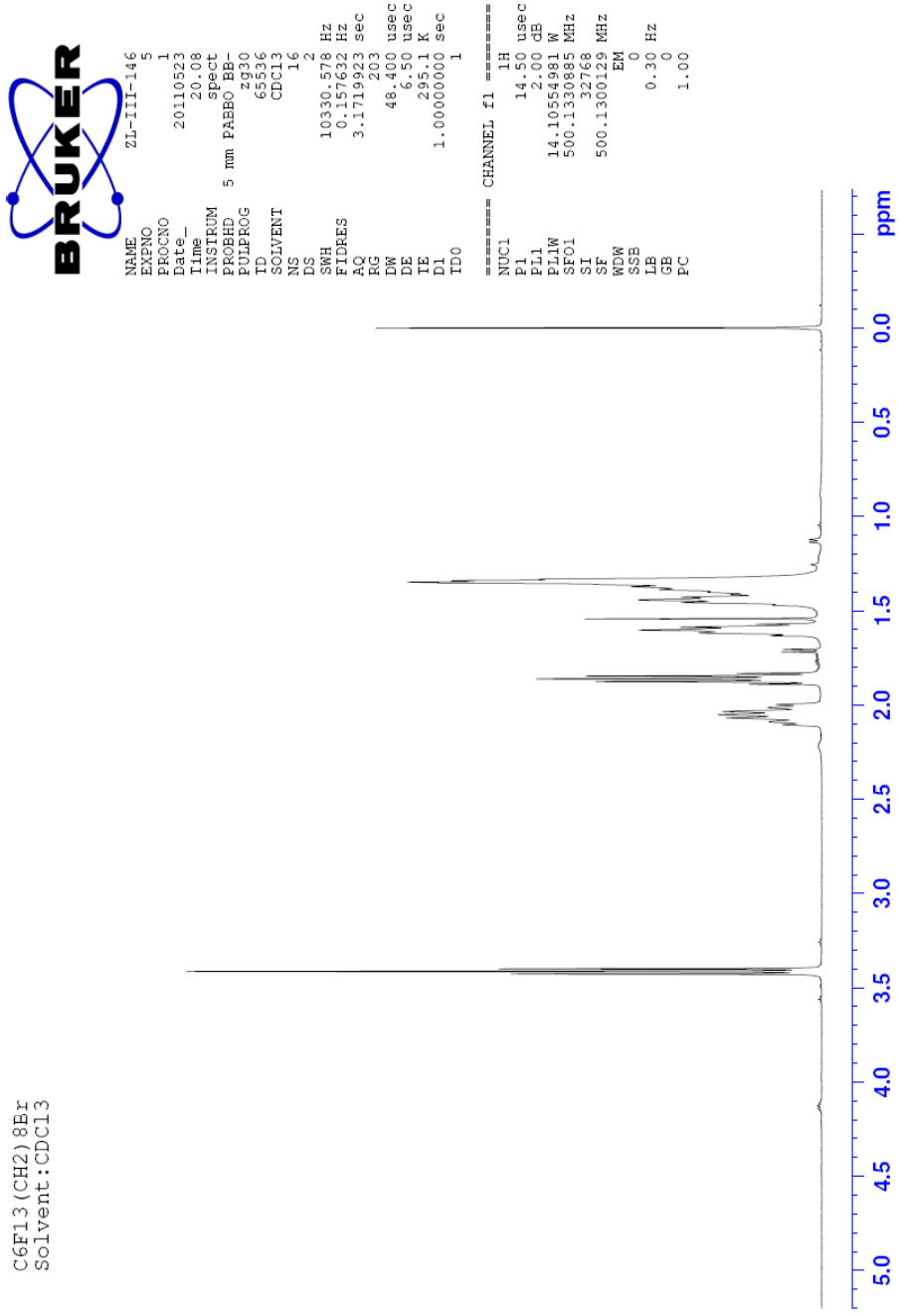

App 23. ^{1}H-NMR spectrum of 14-bromo-1,1,1,2,2,3,3,4,4,5,5,6,6-tridecafluorotetradecane (**27**)

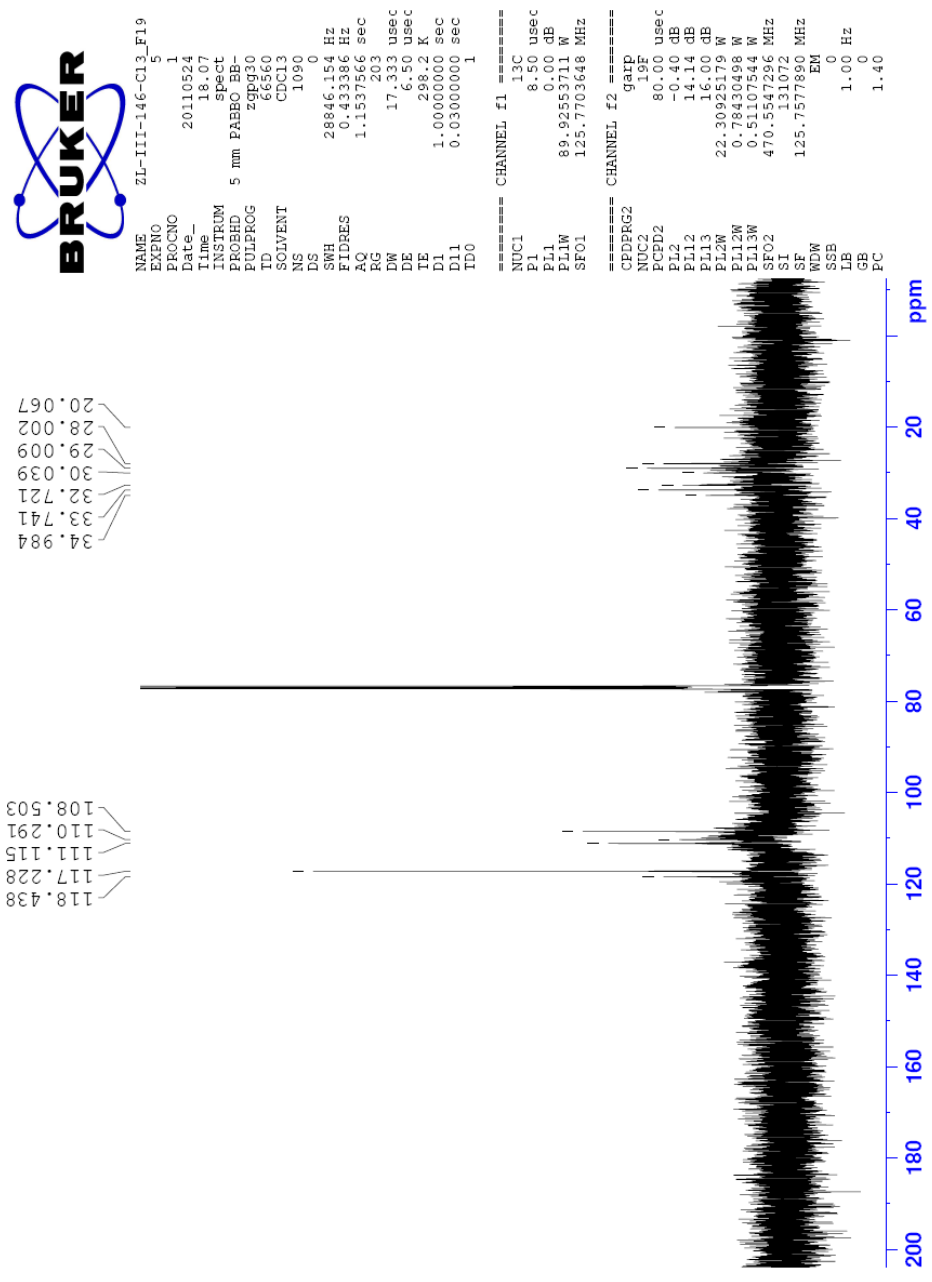

App 24. ^{19}F decoupled ^{13}C-NMR spectrum of 14-bromo-1,1,1,2,2,3,3,4,4,5,5,6,6-tridecafluorotetradecane (**27**)

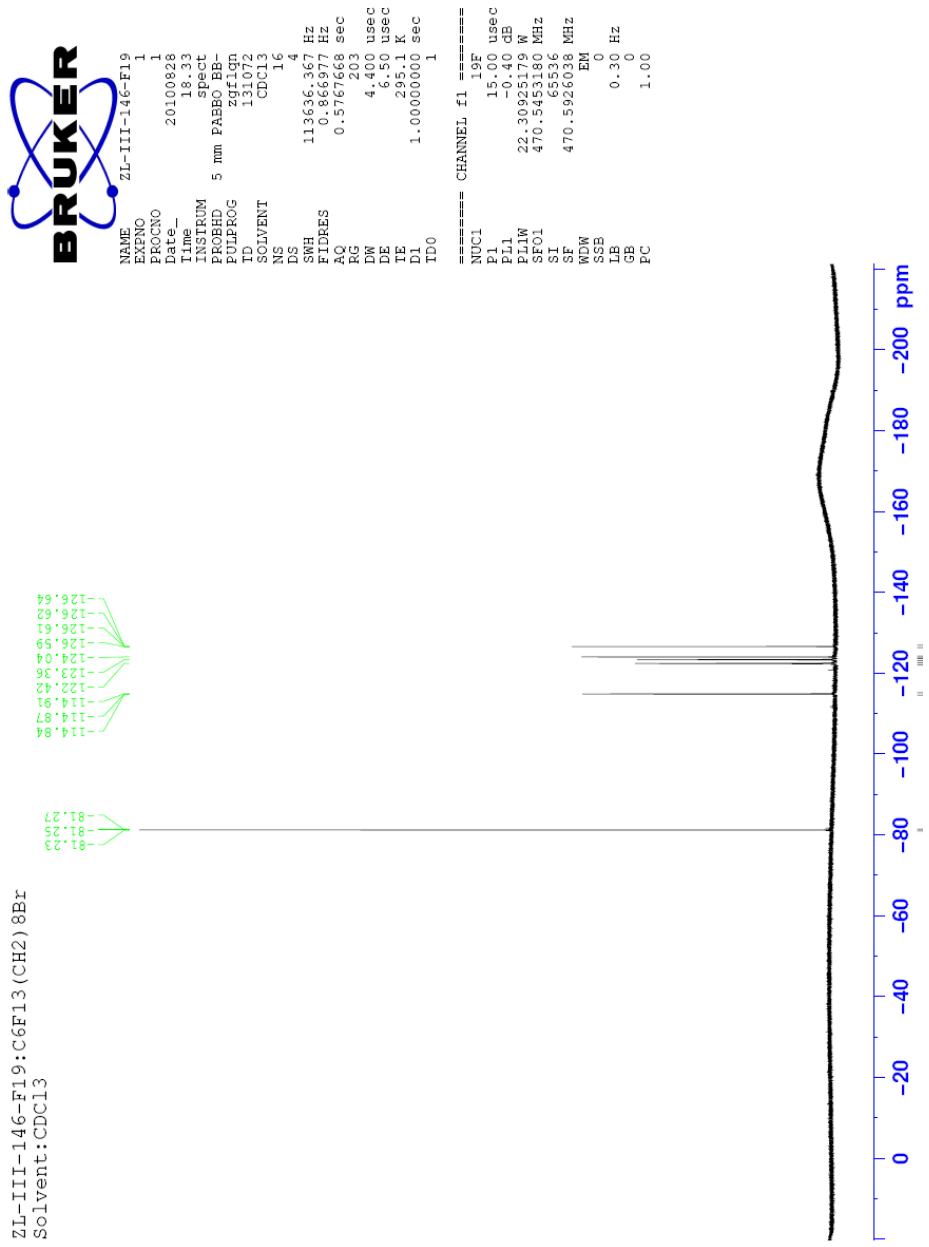

App 25. ^{19}F-NMR spectrum of 14-bromo-1,1,1,2,2,3,3,4,4,5,5,6,6-tridecafluorotetradecane (**27**)

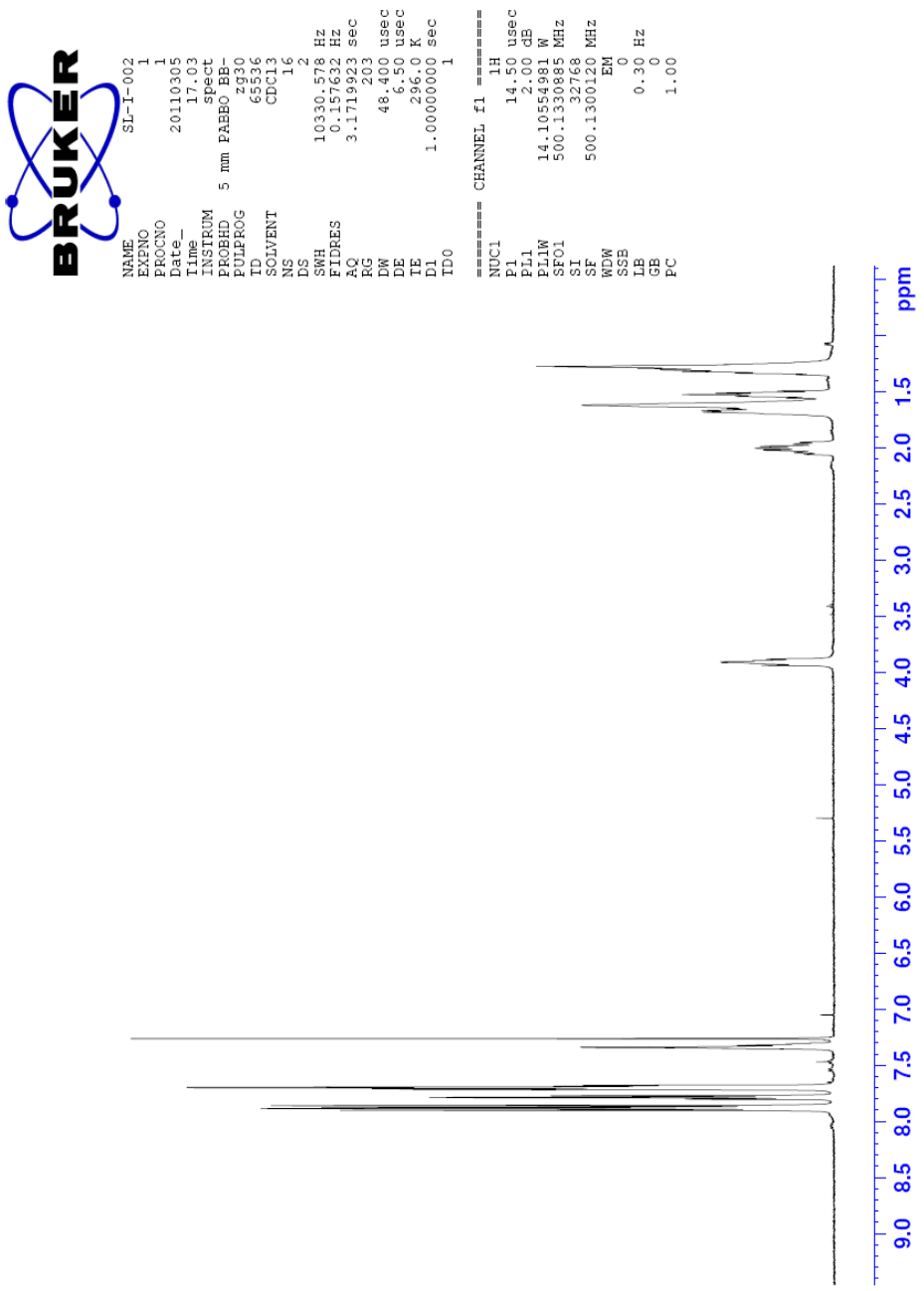

App 26. ^{1}H-NMR spectrum of 9,9,10,10,11,11,12,12,13,13,14,14,14-tridecafluorotetradecanyl triphenylphosphorium bromide (**28**)

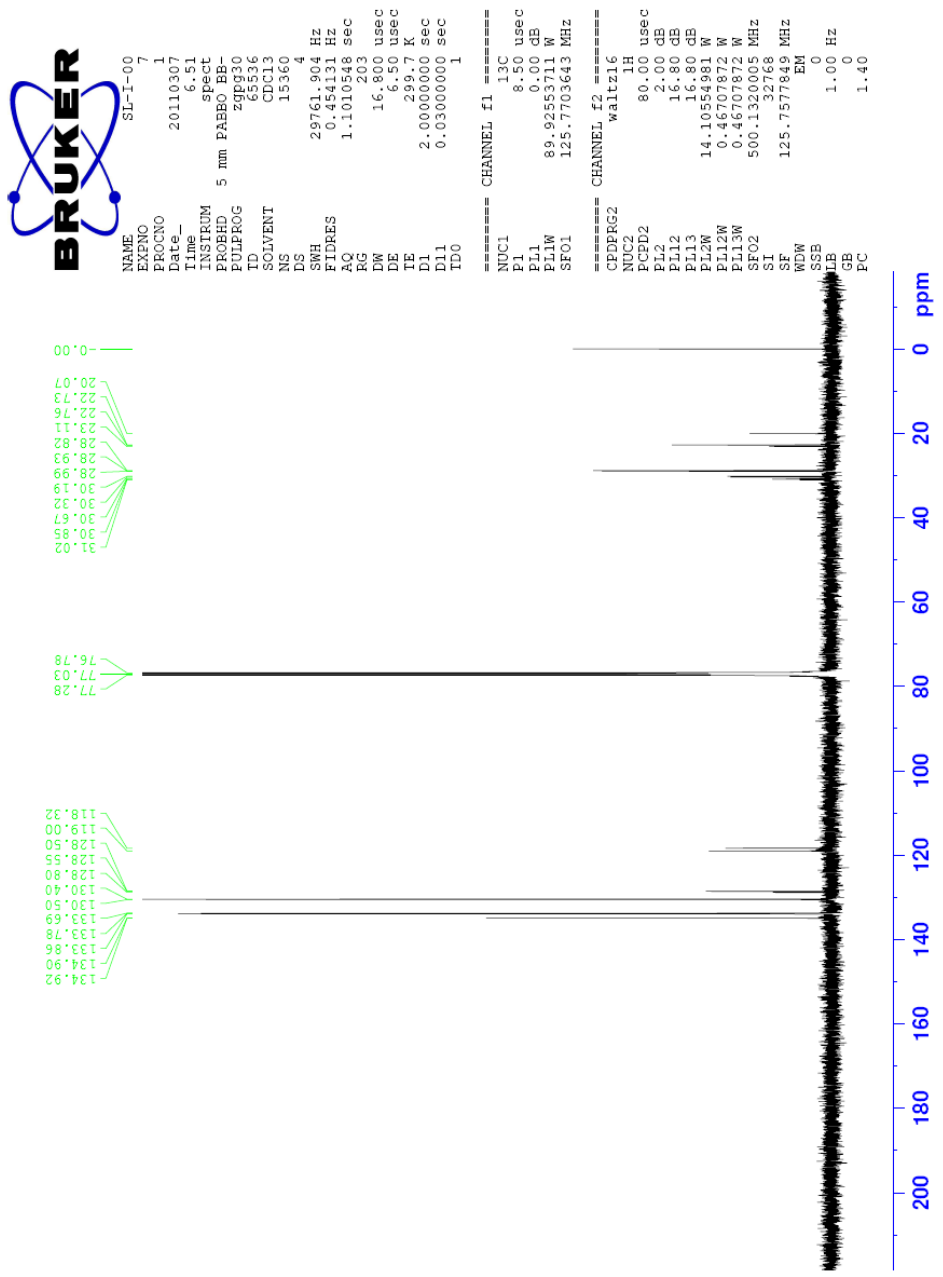

App 27. ^{19}F decoupled ^{13}C-NMR spectrum of 9,9,10,10,11,11,12,12,13,13,14,14,14-tridecafluorotetradecanyl triphenylphosphorium bromide (**28**)

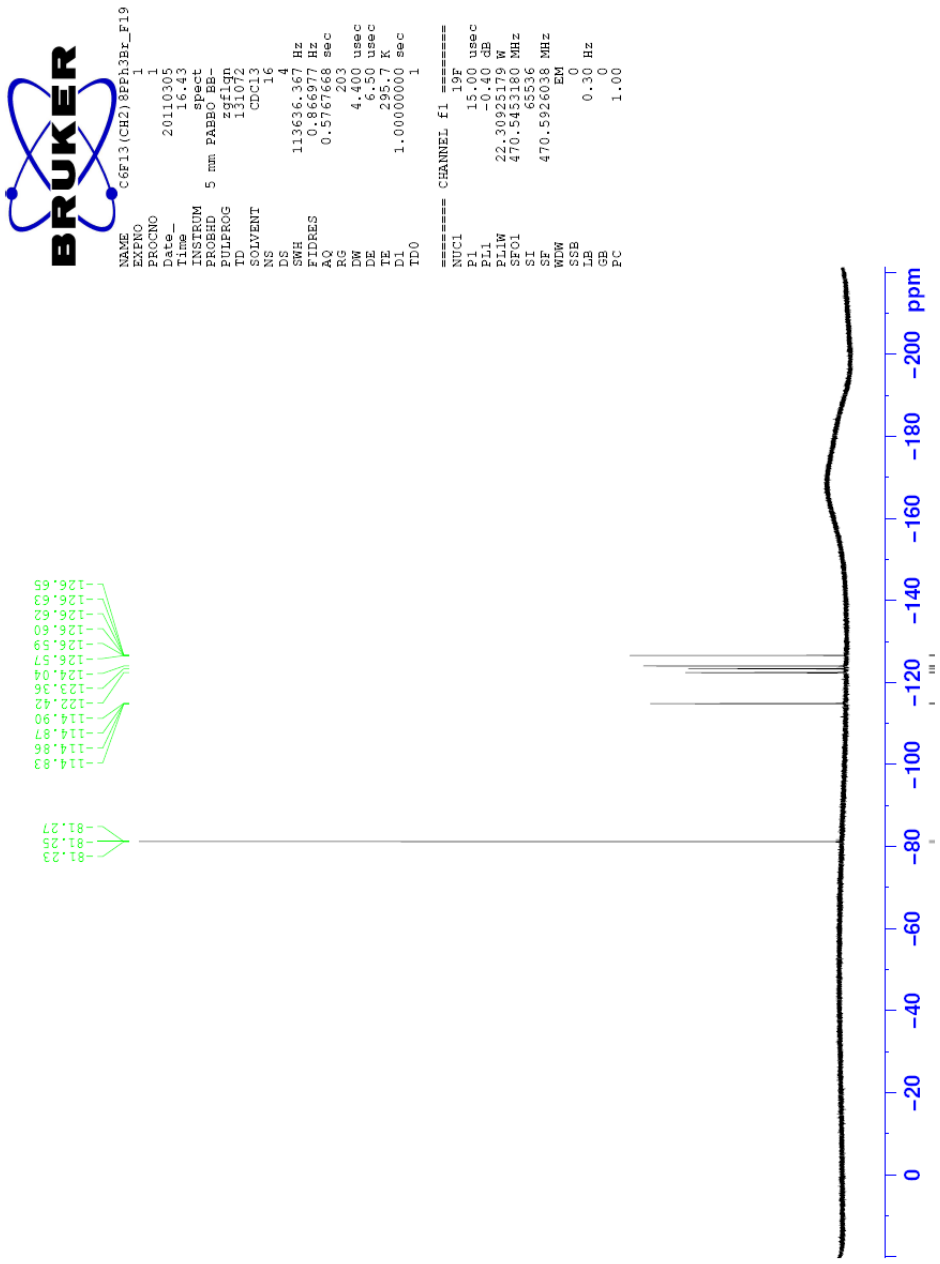

App 28. ^{19}F-NMR spectrum of 9,9,10,10,11,11,12,12,13,13,14,14,14-tridecafluorotetradecanyl triphenylphosphorium bromide (**28**)

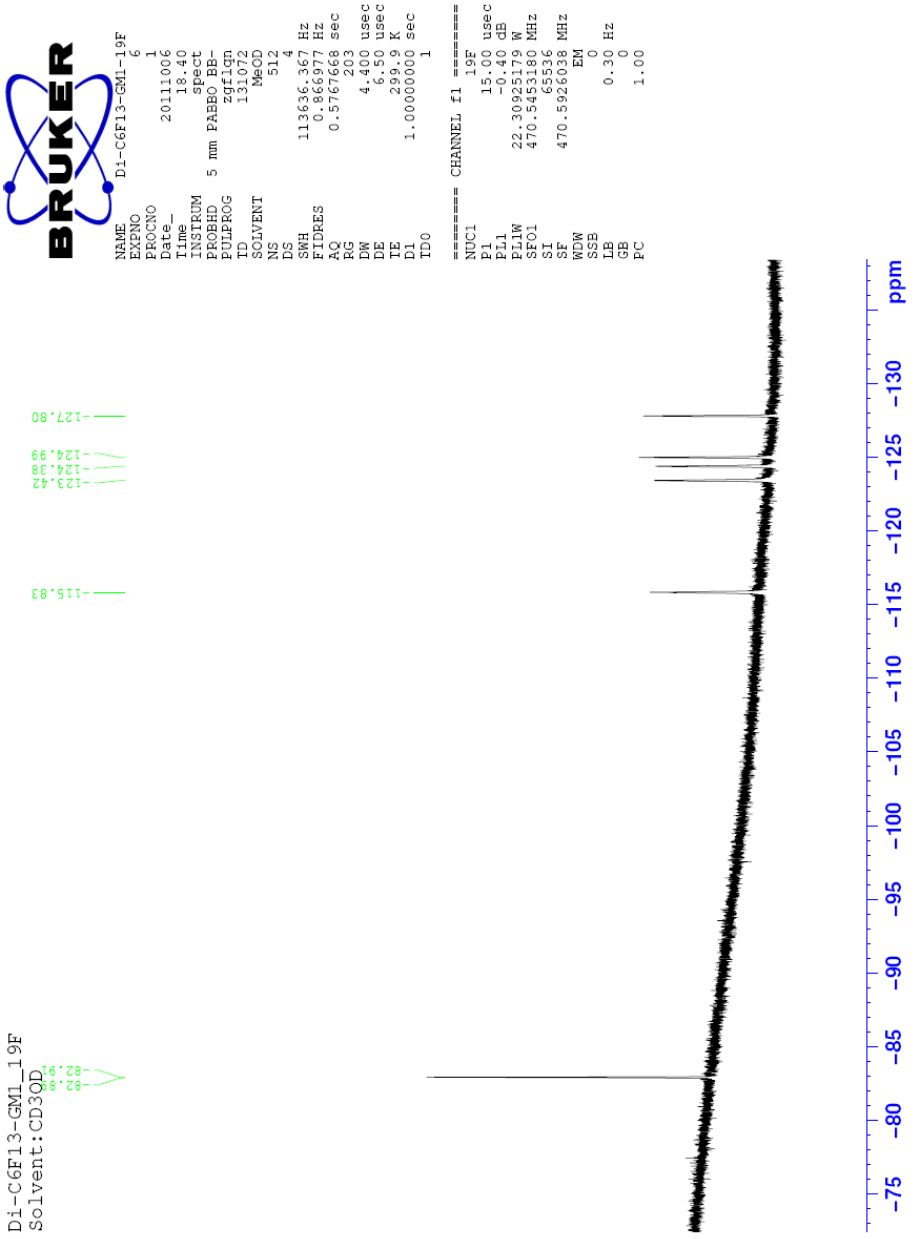

App 29. ^{19}F-NMR spectrum of Di-C6F13-GM1 (**31**)

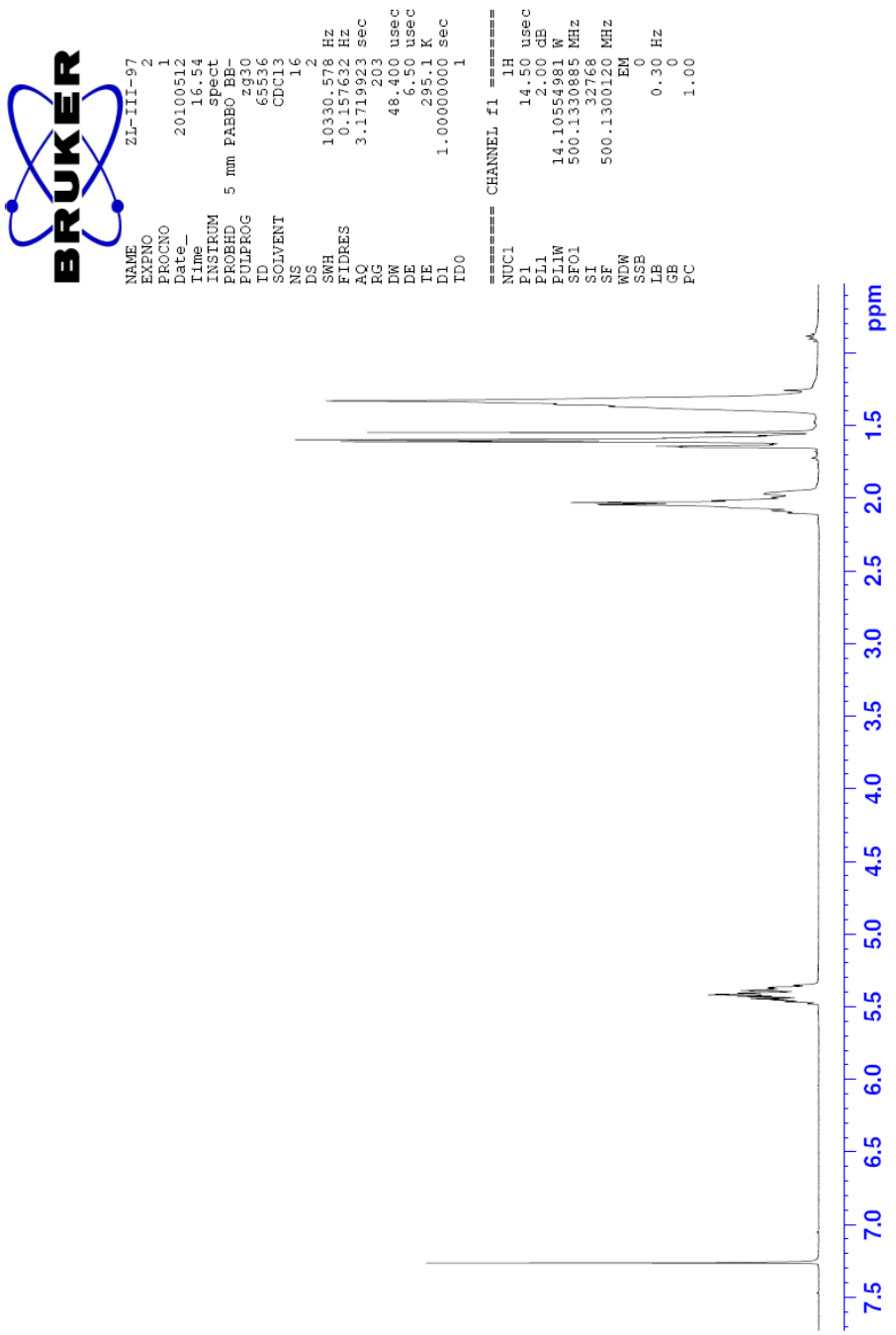

App 30. ^{1}H-NMR spectrum of (*E*)-11,11,12,12,13,13,14,14,15,15,16,16,16-tridecafluorohexadec-2-ene (**38**)

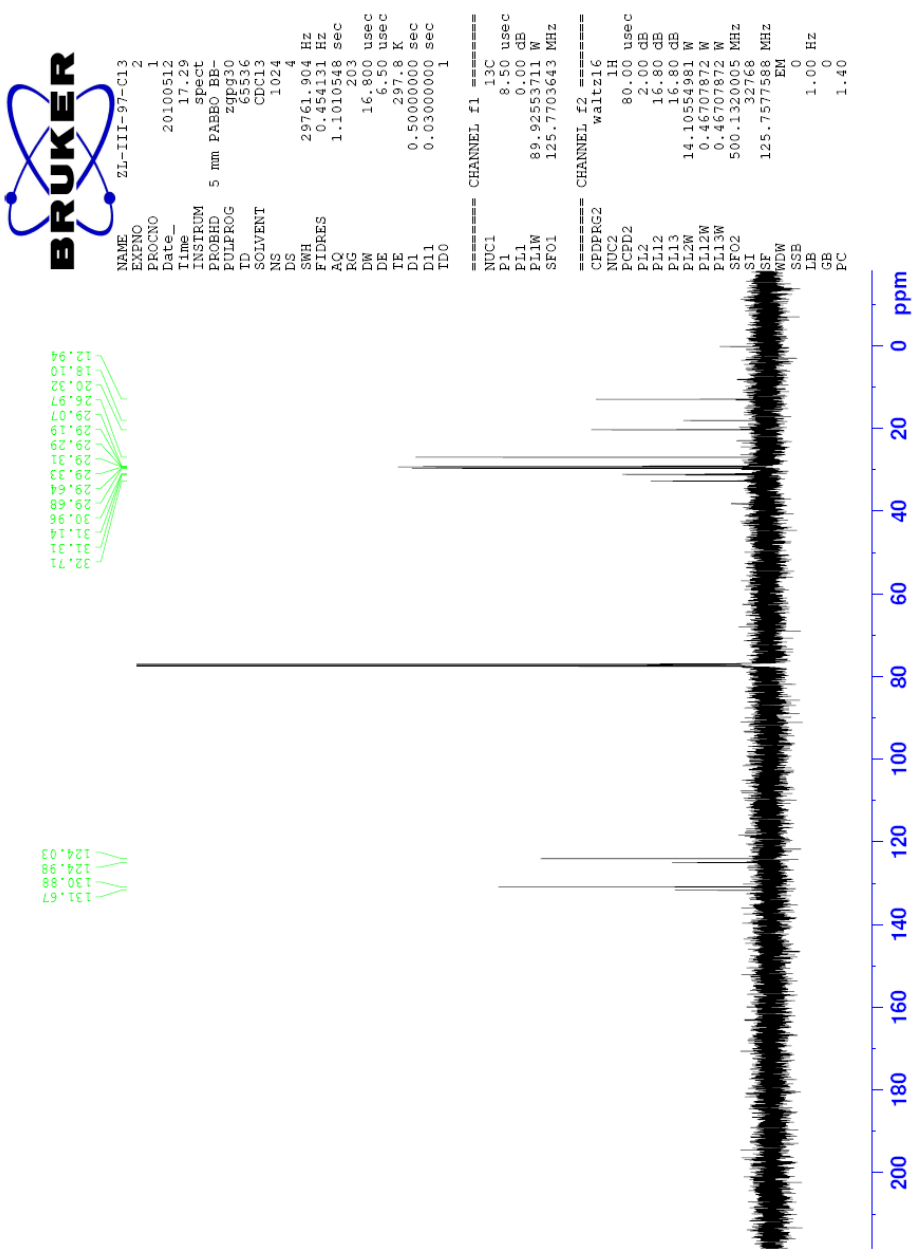

App 31. ^{13}C-NMR spectrum of (*E*)-11,11,12,12,13,13,14,14,15,15,16,16,16-tridecafluorohexadec-2-ene (**38**)

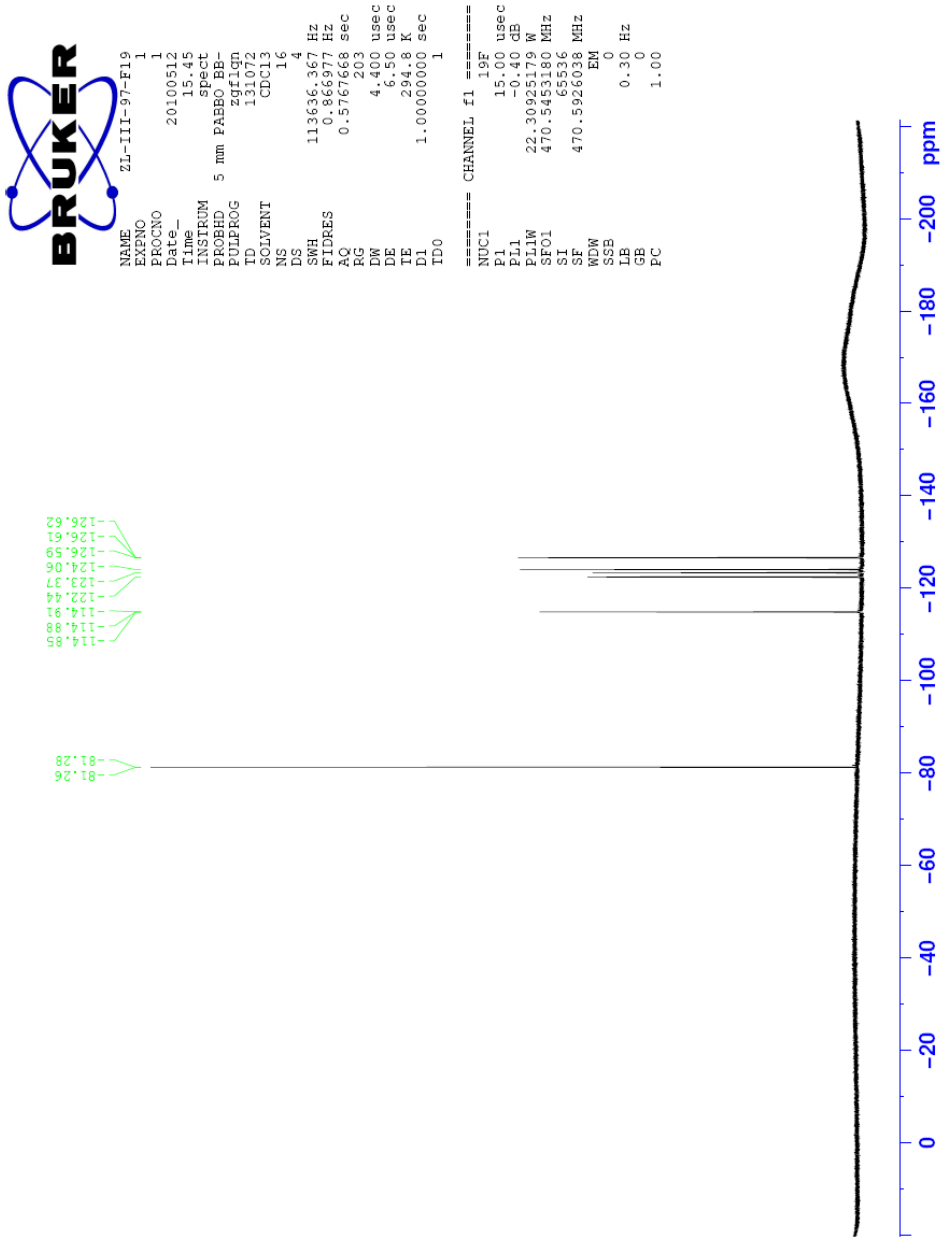

App 32. ^{19}F-NMR spectrum of (*E*)-11,11,12,12,13,13,14,14,15,15,16,16,16-tridecafluorohexadec-2-ene (**38**)

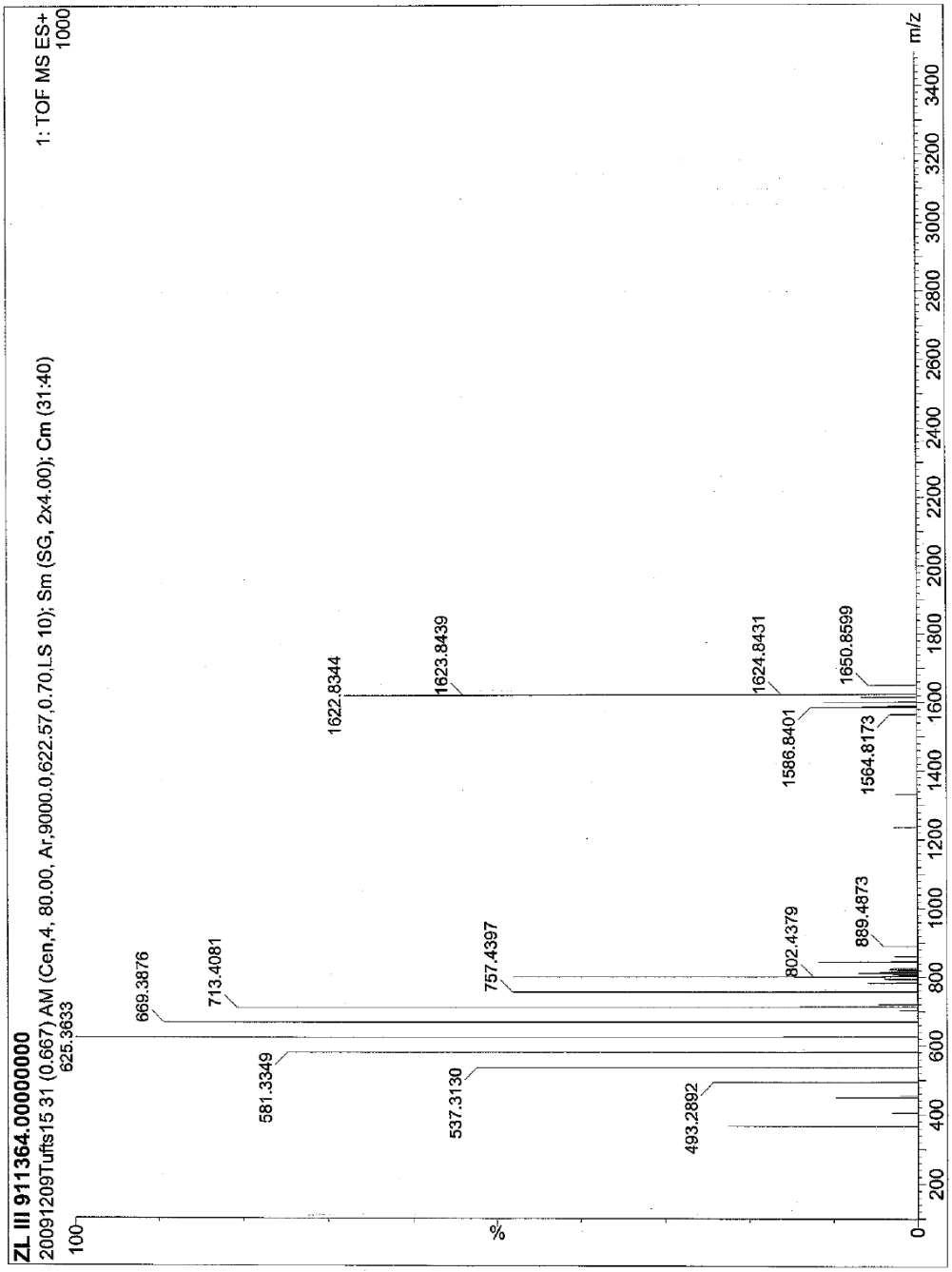

App 33. HRMS of 18-F3-GM1 (**12**)

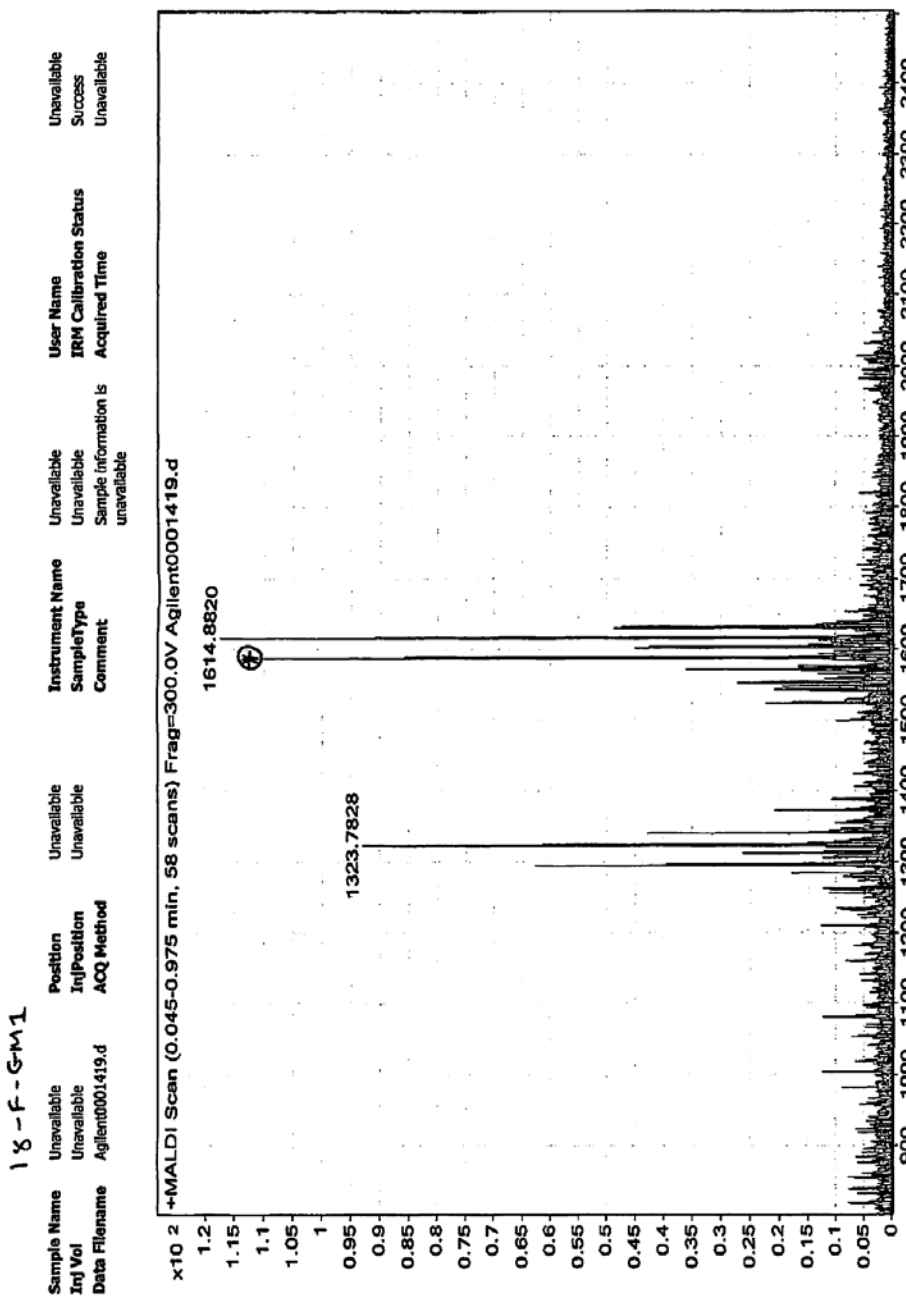

App 34. HRMS of 18-F-GM1 (**16**)

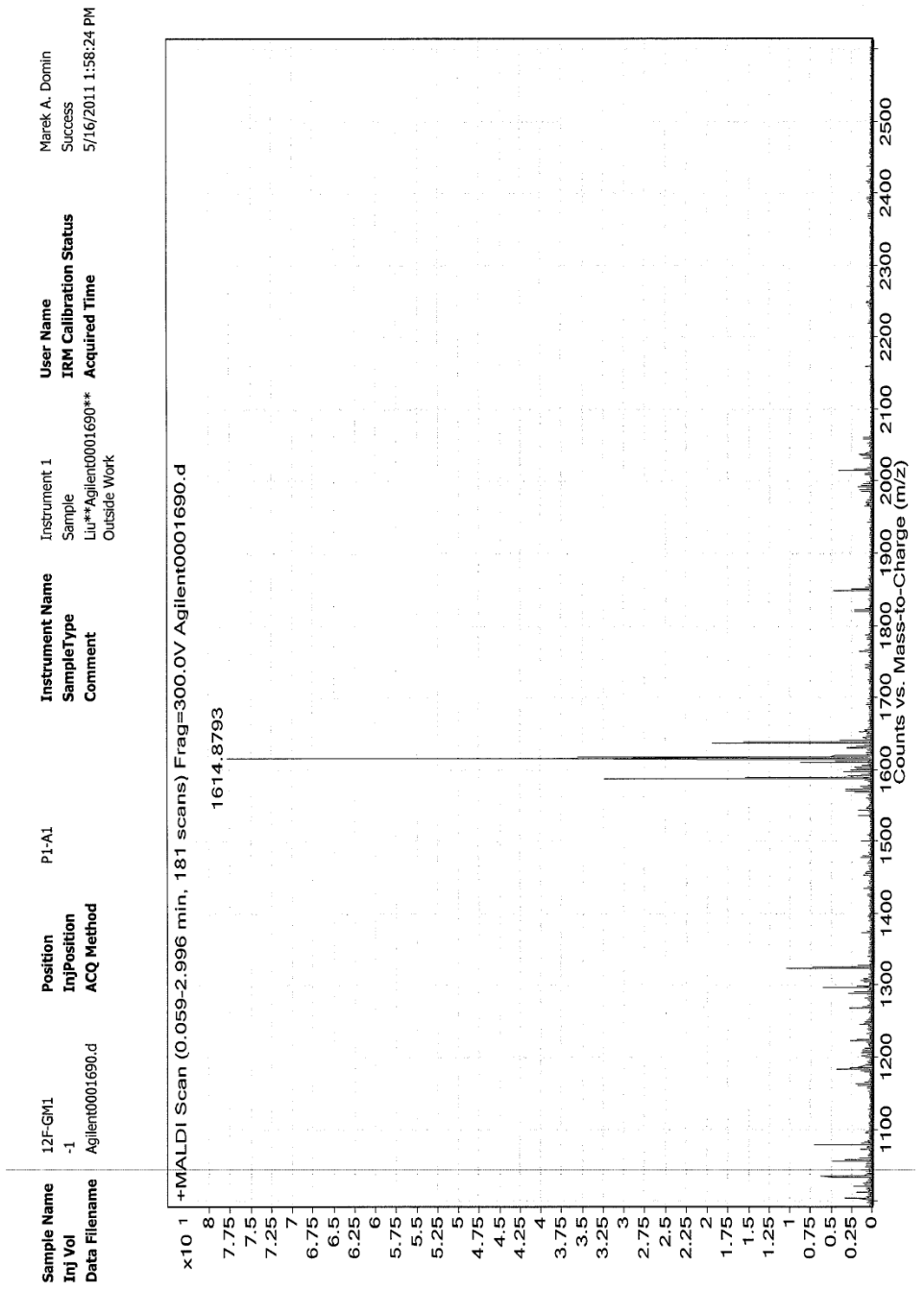

App 35. HRMS of 12-F-GM1 (**23**)

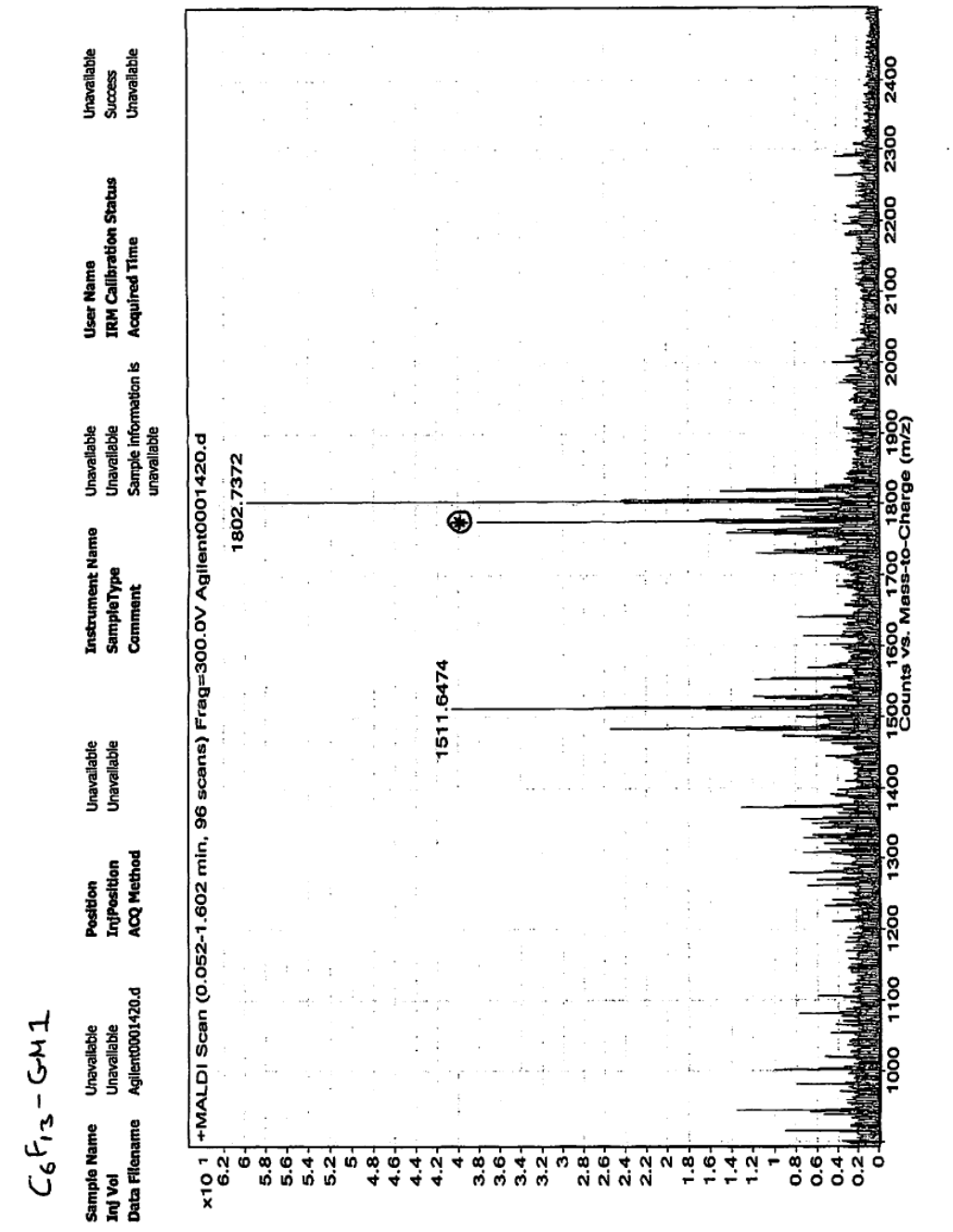

App 36. HRMS of C6F13-GM1 (**24**)

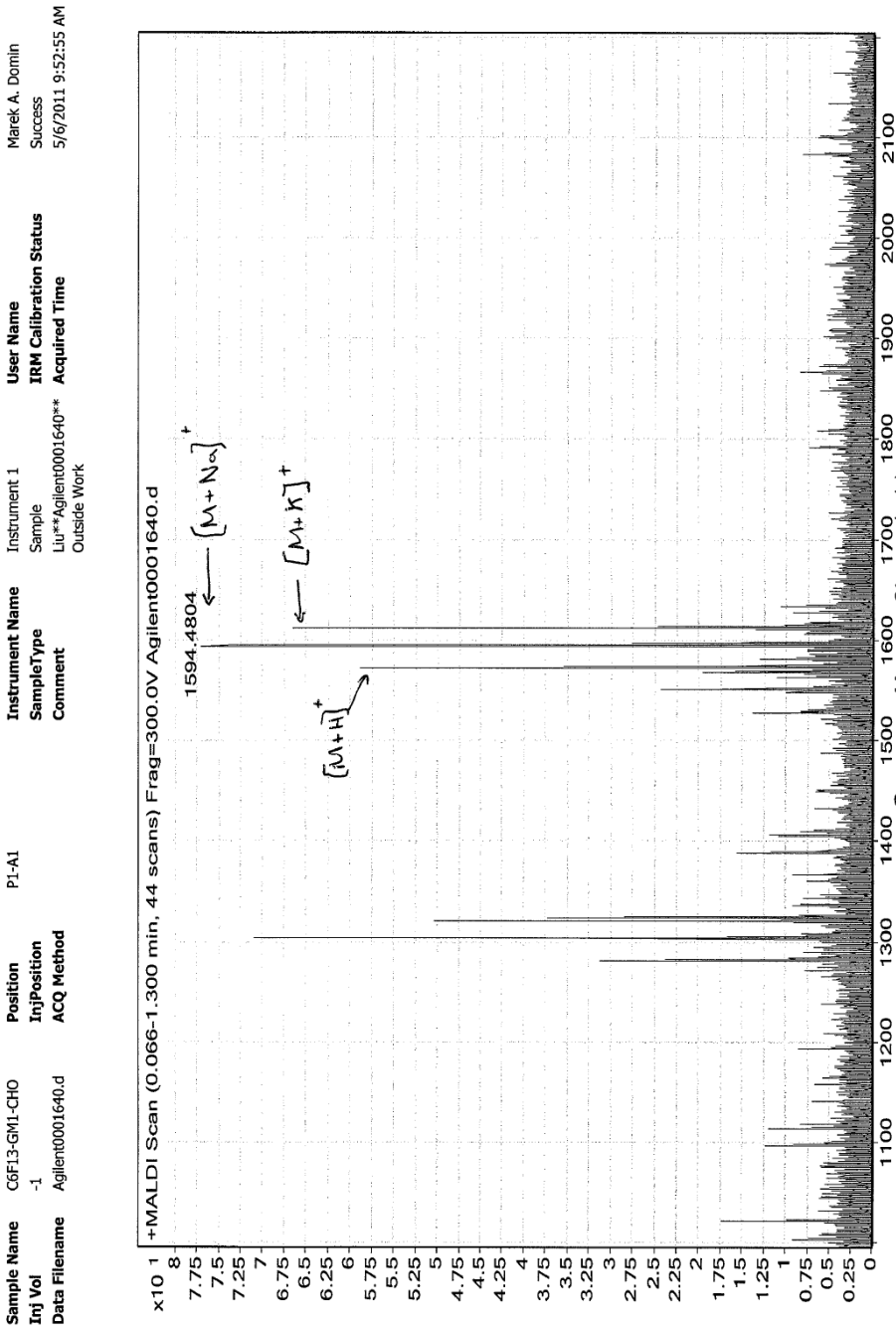

App 37. HRMS of C6F13-GM1-CHO (**29**)

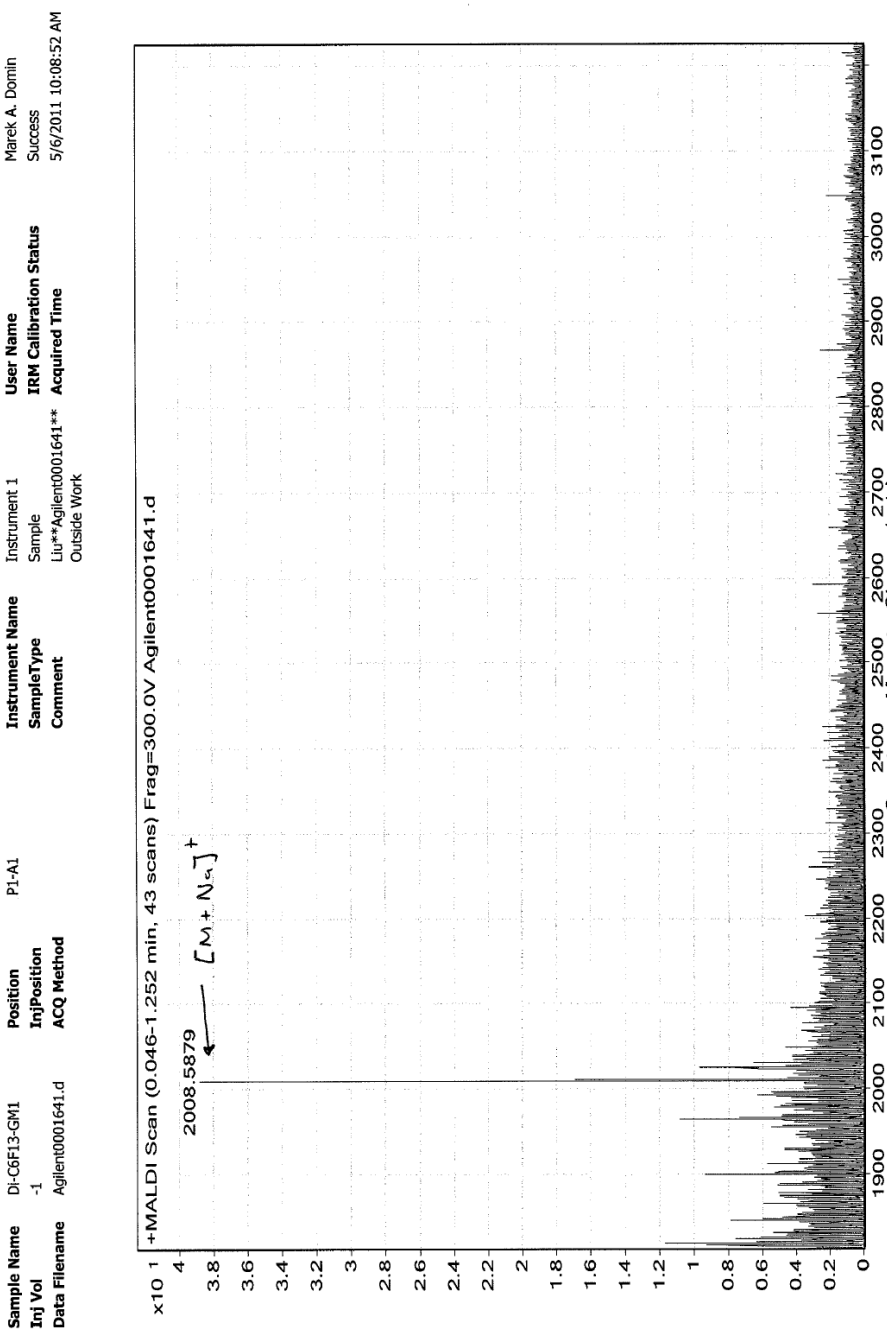

App 38. HRMS of Di-C6F13-GM1 (**31**)